Seasonal Climatology, Variability, Characteristics, and Prediction of the Caribbean Rainfall Cycle

Carlos Javier Martinez

Submitted in partial fulfillment of the
requirements for the degree of
Doctor of Philosophy
under the Executive Committee
of the Graduate School of Arts and Sciences

COLUMBIA UNIVERSITY

2021

Abstract

Seasonal Climatology, Variability, Characteristics, and Prediction of the

Caribbean Rainfall Cycle

Carlos Javier Martinez

The Caribbean is a complex region that heavily relies on its seasonal rainfall cycle for its economic and societal needs. This makes the Caribbean especially susceptible to hydro-meteorological disasters (e.g., droughts and floods), and other weather/climate risks. Therefore, effectively predicting the Caribbean rainfall cycle is valuable for the region. The efficacy of predicting the Caribbean rainfall cycle is largely dependent on effectively characterizing the climate dynamics of the region. However, the dynamical processes and climate drivers that shape the seasonal cycle are not fully understood, as previous observational studies show inconsistent findings as to what mechanisms influence the mean state and variability of the cycle. These inconsistencies can be attributed to the limitations previous studies have when investigating the Caribbean rainfall cycle, such as using monthly or longer resolutions in the data or analysis that often mask the seasonal transitions and regional differences of rainfall, and investigating the Caribbean under a basin-wide lens rather than a sub-regional lens. This inhibits the ability to accurately calculate and predict subseasonal-to-seasonal (S2S) rainfall characteristics in the region. To address these limitations and inconsistencies, the research in this thesis examines the seasonal climatology, variability, and characteristics of the Caribbean rainfall cycle under a sub-regional and temporally fine lens in order to investigate the prediction of the cycle.

Regional variations and dynamical processes of the Caribbean annual rainfall cycle are assessed using (1) a principal component analysis across Caribbean stations using daily observed

precipitation data; and, (2) a moisture budget analysis. The results show that the seasonal cycle of rainfall in the Caribbean hinges on three main facilitators of moisture convergence: the Atlantic Intertropical Convergence Zone (ITCZ), the Eastern Pacific ITCZ, and the North Atlantic Subtropical High (NASH). A warm body of sea-surface temperatures (SSTs) in the Caribbean basin known as the Atlantic Warm Pool (AWP) and a low-level jet centered at 925hPa over the Caribbean Sea known as the Caribbean Low-Level Jet (CLLJ) modify the extent of moisture provided by these main facilitators. The interactions of these dynamical processes are responsible for shaping the seasonal components of the annual rainfall cycle: The Winter Dry Season (WDS; mid-November to April); the Early-Rainy Season (ERS; mid-April to mid-June); an intermittent relatively dry period known as the mid-summer drought, (MSD; mid-June to late August), and the Late-Rainy Season (LRS; late August to late November). Five geographical sub-regions are identified in the Caribbean Islands, each with its unique set of dynamical processes, and consequently, its unique pattern of rainfall distribution throughout the rainy season: Northwestern Caribbean, the Western Caribbean, the Central Caribbean, the Central and Southern Lesser Antilles, and Trinidad and Tobago and Guianas. Convergence by sub-monthly transients contributes little to Caribbean rainfall.

The wettest and driest Caribbean ERS and LRS years' are then explored by conducting the following: (1) a spatial composite of rainfall using the daily rainfall data; and, (2) spatial composites of SSTs, sea-level pressure (SLP), and mean flow moisture convergence and transports using monthly data. The ERS and LRS are impacted in distinctly different ways by two different, and largely independent, large-scale phenomena, external to the region: a SLP dipole mode of variability in the North Atlantic known as the North Atlantic Oscillation (NAO), and the El Nino Southern Oscillation (ENSO). Dry ERS years are associated with a persistent dipole of cold and

warm SSTs over the Caribbean Sea and Gulf of Mexico, respectively, that are caused by a preceding positive NAO state. This setting involves a wind-evaporation-SST (WES) feedback expressed in enhanced trade winds and consequently, moisture transport divergence over all of the Caribbean, except in portions of the Northwestern Caribbean in May. A contribution from the preceding winter cold ENSO event is also discernible during dry ERS years. Dry LRS years are due to the summertime onset of an El Niño event, developing an inter-basin SLP pattern that moves moisture out of the Caribbean, except in portions of the Northwestern Caribbean in November. Both large-scale climate drivers would have the opposite effect during their opposite phases leading to wet years in both seasons.

Existing methodologies that calculate S2S rainfall characteristics were not found to be suitable for a region like the Caribbean, given its complex rainfall pattern; therefore, a novel and comprehensive method is devised and utilized to calculate onset, demise, and MSD characteristics in the Caribbean. When applying the method to calculate S2S characteristics in the Caribbean, meteorological onsets and demises, which are calculated via each year's ERS and LRS mean thresholds, effectively characterize the seasonal evolution of mean onsets and demises in the Caribbean. The year-to-year variability of MSD characteristics, and onsets and demises that are calculated by climatological ERS and LRS mean thresholds resemble the variability of seasonal rainfall totals in the Caribbean and are statistically significantly correlated with the identified dynamical processes that impact each seasonal component of the rainfall cycle.

Finally, the seasonal prediction of the Caribbean rainfall cycle is assessed using the identified variables that could provide predictive skill of S2S rainfall characteristics in the region. Canonical correlation analysis is used to predict seasonal rainfall characteristics of station-averaged sub-regional frequency and intensity of the ERS and LRS wet days, and magnitude of

the MSD. Predictor fields are based on observations from the ERA-Interim reanalysis and GCM output from the North America Multi-Model Ensemble (NMME). Spearman Correlation and Relative Operating Characteristics are applied to assess the forecast skill. The use of SLP, 850-hPa zonal winds (u850), vertically integrated zonal (UQ), and meridional (VQ) moisture fluxes show comparable, if not better, forecast skill than SSTs, which is the most common predictor field for regional statistical prediction. Generally, the highest ERS predictive skill is found for the frequency of wet days, and the highest LRS predictive skill is found for the intensity of wet days. Rainfall characteristics in the Central and Eastern Caribbean have statistically significant predictive skill. Forecast skill of rainfall characteristics in the Northwestern and Western Caribbean are lower and less consistent. The sub-regional differences and consistently significant skill across lead times up to at least two months can be attributed to persistent SST/SLP anomalies during the ERS that resemble the North Atlantic Oscillation pattern, and the summer-time onset of the El Niño-Southern Oscillation during the LRS. The spatial pattern of anomalies during the MSD bears resemblance to both the ERS and LRS spatial patterns.

The findings from this thesis provide a more comprehensive and complete understanding of the climate dynamics, variability, and annual mean state of the Caribbean rainfall cycle. These results have important implications for prediction, decision-making, modeling capabilities, understanding the genesis of hydro-meteorological disasters, investigating rainfall under other modes of variability, and Caribbean impact studies regarding weather risks and future climate.

Table of Contents

List of Figures

List of Tables

Acknowledgments

Completion of this thesis would not have been possible without the incredible support of advisors, colleagues, mentors, friends, and family, whom over the course of my PhD career have been instrumental in the success, guidance, and thrill of this thesis. I owe an enormous amount of gratitude to my PhD advisors to whom over the past five years have been nothing but joy to work with. Each of you brought a different but wonderful style of mentorship, forming a diverse advisory committee that was extremely valuable to my graduate career. To Dr. Lisa Goddard, my primary advisor, a special thank you. Since that first day at IRI, where you met me in my cubical at Monell 137, you have been an incredible mentor and friend. I am moved at the way you genuinely desire to see me excel and pursue my passions. Thank you for your wisdom, knowledge, and sacrifices that you have made over these years. Cheers to our Friday meetings. To Dr. Yochanan Kushnir, who I met in Boulder, Colorado at NOAA ESRL as an aspiring scientist, thank you for taking the time in getting to know me all those years ago and being a wonderful mentor. You helped me navigate various complex research problems while also providing many words of encouragement. To Mingfang Ting, thank you for the invaluable advice relating to my research, or future career plans, etc. Your constructive feedback was always appreciative.

To my research brother, Ángel Muñoz, I cannot thank you enough for your guidance throughout my graduate career and giving me numerous connections and sound advice that is brought out in this thesis.

To Cédric Van Meerbeeck, Teddy Allen, and the Caribbean Institute for Meteorology and Hydrology, thank you for your support, guidance, constructive conversations, and providing me with valuable datasets that were paramount for the findings and implications of this thesis.

I would also like to thank the broader OCP and IRI community for their support and help. Thank you to Richard Seager for the constructive qualifying exam 101 sessions. To Elizabeth Gawthrop for introducing me to Adobe Illustrator, which is why the end of every Chapter has an illustrative schematic. To Andy Robertson, Naomi Henderson, Diego Pons, Göran Ekström, Arnold Gordon, Lorenzo Polvani, Alessandra Giannini, Rémi Cousin, and Simon Mason, thank you for your assistance and guidance on the OCP Server, IRI Data Library, and various topics related to my research.

To my friends in the DEES program over the years: Arianna, Una, Weston, Dan, Catherine, Yuxin, Nathan, and Kevin, thank you all for the wonderful memories and support over the years.

To Aaron Piña and Joseph Trujillo, thank you for walking with me. In many ways your support and love has guided me through this incredible journey.

To Ford Hall, my beloved home throughout my graduate career. To Trevor, Audrey, Rebecca R., Kathy, Isi, Rosie, Haohan, Joe, Natalie, Peter F. Walker, Kenneth, Rebecca D., Sarah M., Kemi, Guillame, Raquel, Sarah C., Stan, Oscar, Peter A., Giovanna, Justin, Miguel, Arjun, Elvira, Elizabeth, Katrina, thank you for your prayers, memories, and for being incredible housemates.

Finally, to all of my hometown/abroad friends and family. Drew, Michael, Taylor, Sarahi, Justin T., and Shannon, and Chris H., your unbounded love, prayers, and support over these years have been a real gift to me. Thank you all so much for inspiring me to be who I am today. To Cristina, my sister, thank you for the many laughs and joys when I come home, and endless support. To my parents, your love and support brought me here today. I love you both dearly. Finally, to almighty God for the opportunity to unearth science under His Glory.

Dedication

To my nightly 9 hours of sleep.

Introduction

Chapter 1: Introduction

Rainfall in the Caribbean (5°N to 27°N and 58°W to 90°W; Fig. 1) is imperative for the region's socioeconomic well-being. Industries such as rain-fed agriculture, tourism, water management, and health, all rely on the Caribbean rainfall cycle for food production, water consumption, preventing water-borne diseases, and healthy livestock (OCHA 2015; FAO 2016). Recent hydro-meteorological disasters such as multi-year droughts and floods (e.g., 2013-2016 Pan-Caribbean Drought) have cost Caribbean countries hundreds of millions of dollars from water shortages and contamination which result in agricultural and energy production losses that hamper economic growth and exacerbate the concurrent social issues (NOAA 2005; ODPEM 2010; FAO 2016; OCHA 2015, 2016).

Figure 1.1: Map of the Caribbean

In addition to having densely populated coastal low-lying areas, complex topography, and limited human/natural resources, its socioeconomic sensitivity to precipitation changes and extremes is why the Caribbean is identified as a highly-vulnerable region to climate variability and change (Lewsey 2004; Simpson et al. 2010; Taylor et al. 2012). As multiple stakeholders rely on their local weather and climate services for forecasts on Caribbean rainfall and its characteristics (Vaughan and Dessai, 2014), effectively characterizing and predicting the Caribbean rainfall cycle is critical for the societal and economic stability of the region.

The dynamical context of the Caribbean rainfall cycle is highly complex. Tropical islands and large land masses surrounded by the Gulf of Mexico, the Caribbean Sea, and the Tropical North Atlantic (TNA) (Fig 1). As a result, the Caribbean is at the intersection of competing mid-latitude, tropical, and inter-basin forcings across spatial-scales.

One of the large-scale features that impact the rainfall seasonal cycle in the Caribbean is the semi-permanent subtropical anticyclone known as the North Atlantic Subtropical High (NASH). NASH follows an annual variability pattern with its peak intensity during the boreal summer as a maritime single-maximum pattern and a boreal winter feature with dual-maxima with one center over the subtropical Atlantic and another center over the North American continent (Davis et al. 1997). During the summer and winter NASH induces strong easterly trade winds and subsidence across the Caribbean region (Giannini et al. 2000; Wang and Lee 2007). The boreal Spring and Fall are characterized as transitional periods of NASH that result in weaker easterlies and weaker subsidence (Davis et al. 1997; Wang and Lee 2007).

Two important sources of rainfall in the Caribbean are the Intertropical Convergence Zone (ITCZ) and the South American Monsoon System (SAMS). The ITCZ is a zonally elongated tropical band of deep convection associated with confluent trade winds, high rainfall rates, and

low pressures (Henderson-Sellers and Robinson 1986; Zhang 2001; Hastenrath 2002). Two branches of the ITCZ affect the Caribbean: the Atlantic ITCZ and the Eastern Pacific ITCZ. Their seasonal migrations follow the meridional movement of maximum solar radiation with a lag of 1–2 months (Mitchell and Wallace 1992; Waliser and Gautier 1993). Their northernmost extent occurs during early September and southernmost extent during early March. Unlike the Atlantic ITCZ and Eastern Pacific ITCZ, the land-based SAMS migrates in sync with the solar insolation cycle and is characterized by interactions between South American topography and ocean–atmosphere dynamics (Silva and Kousky 2012).

Additionally, the convection in the Caribbean is influenced by the location of the Western Hemisphere Warm Pool (WHWP) (Weisberg 1996; Wang and Enfield 2001). The WHWP, an area of regional sea-surface temperatures (SSTs) warmer than 28.5C, consists of two branches: The Eastern North Pacific Warm Pool and the Atlantic Warm Pool (AWP), the latter of which affects the Caribbean Basin (Wang et al. 2008). The AWP is absent during the winter. It appears off of the Northwestern Caribbean in June. It then expands into the Gulf of Mexico in July, the western Caribbean Sea in August and the eastern Caribbean Sea in September. It begins to contract by October (Wang and Lee 2007). The onset and duration of the AWP is in sync with the onset and duration of the Caribbean rainfall season (Misra et al. 2014). Its emergence and expansion weaken NASH and its southwestern flank, and weakens upper-level westerlies over the Caribbean (Wang and Lee 2007). The regional warming of the AWP also enhances precipitable water in the Eastern Pacific ITCZ and western flank of the Atlantic ITCZ (Wang et al. 2008).

The NASH, ITCZ, and AWP and their interactions broadly shape the climatological rainfall pattern in the Caribbean (Giannini et al. 2000; Taylor and Alfaro 2005). The Caribbean is at its driest during the winter, when strong trade winds, subsidence, and cool SSTs, influence the

region, and the ITCZ migrates southward (Taylor and Alfaro 2005). Hence, these large-scale features are consistent with responsible for the region's classification as "dry-winter tropical" (Rudloff 1981). During the summer rainfall season, on the other hand, these large-scale features compete, due to their interactions with regional-scale features and associated feedback mechanisms.

One such regional scale features is the Caribbean Low-Level Jet (CLLJ) (Amador 1998; Amador et al. 2000). Located between Northern South America and the Greater Antilles and extending across the western Caribbean, the CLLJ is a major transporter of moisture for the Caribbean and Central America (Durán-Quesada et al. 2010). The CLLJ is also an important component of circulation associated with the mid-summer drought, which is a short period of relatively dry conditions between two rainy intervals (MSD, Magaña et al. 1999; Herrera et al. 2015). Studies have attributed the genesis of the CLLJ to the intensification of easterly winds by NASH (e.g. Wang 2007; Cook and Vizy 2010) and its strength and orientation to be influenced by the AWP (Wang and Lee 2007), NASH (Cook and Vizy 2010), and topography (Muñoz et al. 2008).

Two important summertime transient circulation features that influence rainfall in the Caribbean are African Easterly Waves (AEW) and tropical cyclones (TCs). AEWs are synoptic-scale perturbations, associated with the mid-tropospheric sub-Saharan jet, that propagate across the Atlantic Basin from mid-June to early October (Burpee 1972). These waves are a source of precipitation for the Caribbean and, also account for more than half of all Atlantic TCs, and ~ 85% of major hurricanes (Agudelo et al. 2011). TCs have a similar seasonal timeframe as AEWs; however, TCs peak in June and September, and have a minimum in July. In addition to AEWs, TCs can form from interactions with the Eastern Pacific ITCZ (Toma and Webster 2010), and the

emergence of the AWP (Wang et al. 2008). TCs can weaken under large vertical wind shear (Angeles et al. 2010), ocean upwelling in the southwestern Caribbean (Inoue et al. 2002) and interactions with the CLLJ (Wang et al. 2008). There are also other regional influences on Caribbean rainfall, such as a cyclonic sea-land circulation in Central America that displaces moist air into the Caribbean Sea (Poveda and Mesa 2000; Allen and Mapes 2017), mid-latitude troughs that provide confluence from barotropic moist vs. baroclinic cold air masses (Reding 1992; Schultz et al. 1998; Giannini et al. 2000; Sáenz and Durán-Quesada 2015; Allen and Mapes 2017), and large incursions of warm, dry dusty air in the mid-troposphere – the Sahara Air Layer – that suppresses moisture (Carlson and Prospero 1972; Dunion 2011; Mote et al. 2017).

More localized mechanisms affect the magnitude of rainfall across various regions of the Caribbean. Sea breezes associated with strong easterly winds by NASH, together with orographic lifting, bring about rainfall on the leeward side of Caribbean islands and the Caribbean coast of Central America (Taylor and Alfaro 2005; Giannini et al. 2000; Hidalgo et al. 2015; Maldonado et al. 2018). Diurnal heating accompanied by warm SSTs also enhance convection in the Caribbean (Taylor and Alfaro 2005).

In addition to the small-to-large scale dynamical processes, there are also large-scale climate drivers that influence the climate dynamics of the Caribbean rainfall cycle. The El Niño–Southern Oscillation, a coupled ocean-atmosphere phenomenon in the Equatorial Pacific, and the North Atlantic Oscillation (NAO), the meridional dipole pattern of anomalous SLP in the North Atlantic, have been found to influence the variability of the rainfall seasons in the Caribbean (Malmgren et al. 1998; Giannini et al. 2000; Giannini et al. 2001c; Rodriguez-Vera et al. 2019).

Only a handful of studies have investigated the climate dynamics of Caribbean rainfall, and show inconsistent findings on its behavior and influence. Of the recent observational studies

that have investigated the observed spatial and temporal rainfall patterns in the Caribbean, most studies only investigate one or a subset of the various dynamical mechanisms and climate drivers that are hypothesized to influence Caribbean rainfall (Giannini et al. 2000; Chen and Taylor 2002; Taylor 2002; Taylor and Alfaro 2005; Jury et al. 2007; Wang et al. 2008; Gamble et al. 2007; Curtis and Gamble 2007; Stephenson et al. 2014). Some studies only focused on a specific sub-region of the Caribbean (Gouirand et al. 2012; Mote et al. 2017; Torres-Valcárcel 2018; Hernández Ayala 2019). There are inconsistent findings as to the temporal structure of the Caribbean rainfall cycle, such as its modality, and classifying regions of the Caribbean based on characteristics of their annual cycle. These inconsistencies are in large part due to the spatial and temporal scales used in either the analyses or data that can mask the seasonal transitions and regional differences of the rainfall cycle. In addition, publicly available precipitation data at finer temporal resolutions in the Caribbean is sparse. As a result, longer time-scale averaged datasets are typically used to investigate the climatology of the Caribbean.

The inconsistencies and limitations from previous studies pose challenges when characterizing agronomically-dependent subseasonal-to-seasonal (S2S) rainfall characteristics and investigating the capability of current models to simulate rainfall in the region. Rainfall characteristics such as onset and demise of the wet season(s), the frequency of seasonal wet days, and the intensity of seasonal wet days are useful for farmers for agricultural planning (Marengo et al. 2001; Alfaro et al. 2018; Fernandes et al. 2020), but most have yet to be characterized in the Caribbean as a result of their rapid transitions between dry and wet seasons which would be masked using monthly or longer temporal resolutions. The detection of modeling biases on the simulation of Caribbean rainfall and its associated mechanisms depends on accurately depicting and understanding the observed rainfall cycle (Ryu and Hayhoe 2013; Eichhorn and Bader 2017).

These challenges are significant for rainfall prediction; the ability to predict the rainfall cycle depends on effectively characterizing its observed spatial and temporal behavior. A full and comprehensive understanding of the Caribbean rainfall cycle, its variability, and associated climate dynamics is lacking.

An effective way to enhance the prediction of the Caribbean rainfall cycle is a comprehensive and observational study on Caribbean rainfall under a temporally and sub-regionally fine lens. The goal of this thesis is to better understand the observed characteristics, climatology, and variability of the Caribbean rainfall cycle in order to improve our ability to make predictions for the region. The following important questions are addressed in this study:

1. What is the seasonal rainfall cycle across the Caribbean and what are the small-to-large scale dynamical mechanisms and processes that influence rainfall in the region?

2. What are the large-scale climate drivers that govern the interannual variability of Caribbean rainfall and influence the associated dynamical mechanisms that impact the seasonal rainfall cycle?

3. What is the relationship between the timing of the Caribbean rainfall cycle and the magnitude of the Caribbean rainfall cycle?

4. How predictable are characteristics of Caribbean rainfall under observations and the latest operational models using dynamical processes from (1) and (2)?

To address these questions, daily rain gauge station data were employed from across the Caribbean in collaboration with the Caribbean Institute for Meteorology and Hydrology (CIMH), the National Oceanic and Atmospheric Administration (NOAA) Global Historical Climatological Network (GHCN), and the Guatemalan National Meteorological Service (INSIVUMEH). Utilizing daily observational data ensures accurate representation of the spatial and temporal

behavior of the Caribbean rainfall cycle and its variability. In addition, several reanalysis and modeling datasets are utilized to either complement the observed station daily data, or investigate the relationship between rainfall and several important local and remote atmospheric and oceanic processes.

Each chapter addresses one of the four questions. In Chapter 2, regional variations of the Caribbean climatological rainfall cycle and the dynamical processes associated with the annual march of the hydrological cycle are studied using pentad climatologies of the station rainfall data, a principal component analysis, and a moisture budget (Martinez et al. 2019). The pentad climatologies and principal component analysis provide a better understanding of the regional differences of the seasonal hydrological cycle using a higher temporal resolution than what previous studies have used. A total moisture budget analysis delineates the role small-to-large scale dynamical processes that influence precipitation variability with its mean and transient moisture convergence terms and circulation flows (Seager et al. 2010). In addition to the mean and transient moisture budget terms, a decomposition of the mean flow into its mass convergence and advection of specific humidity is calculated. The analysis found five sub-regions, each with unique climatological annual rainfall cycles that are influenced differently in space and time by three main facilitators of moisture convergence: The Eastern Pacific ITCZ, the Atlantic ITCZ, and the western flank of convergence from NASH; and two modifiers of moisture convergence: the AWP, and the CLLJ.

The findings from Chapter 2 are expanded in Chapter 3, by investigating how the rainfall cycle and its dynamical processes change during particularly wet vs. dry years in the Caribbean (Martinez et al 2020). A composite analysis considers sea-surface temperature (SST), sea-level pressure (SLP), and the mean flow of the moisture budget over two important seasonal components

of the rainfall cycle: The Early-Rainy Season (ERS; mid-April to mid-June), and the Late-Rainy Season (LRS; mid-August to November), in order to investigate their variabilities. Results show that the interannual variability of the ERS is dominated by persistent anomalous SSTs due to a wind-evaporation-SST (WES) feedback, initiated by the preceding winter NAO. The interannual variability of the LRS is dominated by ENSO and the associated seasonal SLP see-saw between the Eastern Pacific and Caribbean basin/tropical Atlantic. As the main climate drivers for each rainfall season are distinctly different and largely independent from one another, the variability of the ERS and LRS are independent of each other.

Existing methodologies that calculate S2S characteristics of rainfall were not found to be suitable to utilize for a region like the Caribbean, given its complex rainfall pattern as found in Chapters 2 and 3. In Chapter 4, a new and comprehensive method is presented that calculates important and not-yet investigated S2S Caribbean rainfall characteristics on a sub-regional scale (Martinez et al. 2021a). The method can be utilized under a meteorological or agronomical lens, and is used in this chapter to compare onsets and demises and characteristics of the Mid-Summer Drought (MSD; mid-June to mid-August). Results show a relationship between Caribbean seasonal rainfall amounts / dynamical processes and the timing of onsets and demises when the temporal characteristics are configured based on the climatological seasonal rainfall mean, rather than yearly seasonal rainfall means. Furthermore, a relationship is found between the strength and duration of the MSD and the ERS and LRS rainfall totals / the dynamical processes affecting the ERS and LRS, respectively.

With a complete observational understanding of the climate dynamics and rainfall patterns in the Caribbean (Chapters 2 and 3), and the ability to calculate S2S Caribbean rainfall characteristics (Chapter 4), the seasonal prediction of the relevant characteristic Caribbean rainfall

cycle is investigated (Chapter 5; Martinez et al. 2021b). This chapter investigates whether seasonal Caribbean rainfall characteristics are predictable using observed and model derived atmospheric and oceanic variables (e.g., North Atlantic SST, SLP, zonal winds) that pertain to the dynamical processes that influence Caribbean rainfall. The main findings show the use of several atmospheric variables have similar or improved forecast skill of the S2S rainfall characteristics than SSTs, which is generally the commonly-used predictor in a given region's climate forecasts. The identified sub-regional differences and consistent skill are attributed to the dynamical processes and climate drivers that shape the ERS, MSD, and the LRS. Finally, conclusions from this study are provided in Chapter 6.

Overall, the findings from this thesis establish a more comprehensive and complete observational understanding of the seasonal climatology, variability, and dynamics of Caribbean rainfall. The thesis demonstrates the importance of using greater temporal resolution in order to distinguish rainfall characteristics in the Caribbean and the value of investigating the Caribbean through each of its sub-regions. The results of this thesis provide an observational framework for the Caribbean rainfall cycle that can be utilized to investigate other important research topics such as the cause and evolution of hydro-meteorological disasters, the variability of rainfall at intraseasonal, decadal, and multi-decadal timescales, modeling diagnostics on characterizing rainfall, and future projections of the Caribbean rainfall cycle and its dynamics. In addition, other regions of the world that are influenced by mechanisms similar to those seen in the Caribbean, such as precipitation in the Southeastern United States (Cook and Vizy, 2010), benefit from the findings of this thesis. Outside of the scientific community, the findings from this thesis will be beneficial for operational forecasting to enhance subseasonal-to-seasonal forecasts of rainfall, and consequently, for the stakeholders who rely on forecasts for decision making.

Part I

Seasonal Climatology and Variability of the Caribbean Rainfall Cycle

Chapter 2: Seasonal Climatology and Dynamical Mechanisms of Rainfall in the Caribbean

Note: A modified version of this chapter has been published in Climate Dynamics (2019)[1]

2.1 Introduction

The Caribbean is identified as a susceptible region to climate variability and change (Taylor et al. 2012). The region's vulnerability to climate is a result of a variety of factors including: limited human/natural resources; topography; densely populated coastal, low-lying urban areas; and, high-risk industries, such as tourism and agriculture (Taylor et al. 2012; Simpson et al. 2010; Lewsey et al. 2004; FAO 2016; OCHA 2015). In addition, hydrometeorological extremes (e.g., droughts and floods), have historically impacted the societal and economic welfare in the Caribbean (NOAA 2005; ODPEM 2010; FAO 2016; OCHA 2015, 2016). Numerous modeling studies have found systematic biases in the simulation of Caribbean rainfall (Ryu and Hayhoe 2013; Eichhorn and Bader 2017). These biases are attributed to an insufficient understanding of how small and large-scale atmospheric and oceanic processes interact to shape the seasonal rainfall pattern in the Caribbean.

A handful of studies have investigated the observed spatial and temporal rainfall patterns in the Caribbean and identified large differences across different parts of the region (Giannini et al. 2000; Chen and Taylor 2002; Taylor and Alfaro 2005; Jury et al. 2007; Gamble et al. 2007; Curtis and Gamble 2007; Stephenson et al. 2014). Although most of these studies describe the seasonal rainfall cycle of the Caribbean as having a bimodal temporal pattern, many of these studies are inconsistent with each other when explaining regional differences. Some studies

[1]Martinez C., Goddard L., Kushnir Y., Ting M., 2019: Seasonal climatology and dynamical mechanisms of rainfall in the Caribbean. Clim Dyn. https://doi.org/10.1007/s00382-019-04616-4

describe the seasonal rainfall as bimodal in the northwestern portion of the Caribbean and unimodal in the eastern Caribbean (e.g., Taylor and Alfaro 2005); others describe the opposite (e.g., Jury et al. 2007). Giannini et al. (2000) found the MSD to exist only in the central and eastern Caribbean, whereas Curtis and Gamble (2007) and Gamble et al. (2007) found the MSD to progress from the eastern Caribbean in May to Central America by July. The inconsistencies in explaining regional differences are a result of spatial and temporal scales in either their analysis or data that can mask the seasonal evolution and regional differences of the Caribbean rainfall cycle. As publicly available precipitation data at sub-monthly temporal resolutions in the Caribbean are sparse, longer-time scale averaged datasets are used to investigate the climatology of the Caribbean.

Furthermore, the relative influence dynamical mechanisms have on rainfall in the Caribbean is relatively unknown. As described in Chapter 1, the climate dynamics of the Caribbean rainfall cycle includes large-scale features such as NASH and the ITCZ, regional features such as the AWP and CLLJ, and small-scale features such as frontal passages, sea-breezes, and orographic lifting. However, of the studies that have investigated the climate dynamics of the Caribbean rainfall cycle, most have investigated only one or a few of the small-to-large scale dynamical features. Most studies have only investigated either SST, SLP, or wind-fields to investigate the influence small-to-large scale dynamical features have on influencing rainfall in the Caribbean (Giannini et al. 2000; Chen and Taylor 2002; Taylor 2002; Taylor and Alfaro 2005; Jury et al. 2007; Wang et al. 2008; Gamble et al. 2007; Curtis and Gamble 2007; Stephenson et al. 2014). However, to date there has not been a detailed moisture budget analysis for the Caribbean. Moisture budgets have been widely used to investigate sources and inhibitors of moisture globally (Trenberth and Guillemot 1995; Seager et al. 2010) and regionally (Huang et al. 2005; Jin and

Zangvil 2010; Pomposi et al. 2015). Given that precipitation, evaporation, and net moisture transport into or out of an atmospheric column balance on timescales greater than 10 days (Brubaker et al. 1993), moisture budgets are useful in determining the hydrological cycle on a seasonal scale.

Here, we study the observational seasonal cycle of rainfall in the Caribbean using daily data and conducting a principal component analysis (PCA) to identify spatial and temporal variabilities. In addition, we study the total moisture budget of the Caribbean using the ERA-Interim Reanalysis (Seager and Henderson 2013). This analysis allows us to answer the following questions:

1. What are the regional differences of the seasonal cycle of rainfall across the Caribbean?
2. What are the local and remote dynamical processes that shape the spatial and temporal patterns of the seasonal cycle in the Caribbean?

Chapter 2 is structured as follows. Section 2.2 and 2.3 describes the data and methods used, respectively. Section 2.4.1 looks at the observed rainfall patterns of the Caribbean using the Principal Component Analysis. Section 2.4.2 details the results of a total moisture budget of the Caribbean. Section 2.4.3 breaks down the Caribbean into its climatological rainfall sub-regions based on the findings from 2.4.1 to 2.4.2. A summary and proposed schematic of the dynamical mechanisms that influence rainfall in the Caribbean are found in Sect. 2.5. Finally, a discussion comparing this study with other studies, its significance, and future work are also found in Sect. 2.5.

2.2 Data

This Chapter uses the CIMH 1969–2017 daily station rainfall. Given that some countries in the Caribbean are not member states of the Caribbean Meteorological Organization (CMO) from

whom the CIMH's data originates, NOAA's GHCN 1960–2017 daily station rainfall dataset is also used. Stations are data-stitched across the two observational datasets: station's missing data in one dataset is patched by the other dataset. This process is done only when the stations' coordinates between each dataset are within a 0.05° margin from each other. The data are also checked for uniformity by analyzing overlapping years from each dataset. The combined CIMH/GHCN metadataset provides temporally finite historical precipitation data. A total of 38 stations are found, shown in Table 2.1, satisfying the requirements. In order to supplement the station data and validate the proposed regional classifications in the Caribbean, NASA's Tropical Rainfall Measuring Mission (TRMM) version 7 with 0.25° by 0.25° gridded daily precipitation estimate dataset (Huffman et al. 2007) is used.

For understanding the dynamical context of the seasonal hydrological cycle, the European Centre for Medium-Range Weather Forecasts Interim Re-Analysis (ERA-Interim) (Dee et al. 2011) is used to calculate the climatological moisture budget. The ERA-Interim is available at several resolutions. For this study, we used a spatial resolution of 1.5° by 1.5°, a 6-hourly temporal resolution from 1979 to 2012 (2016 for SST), and 26 pressure levels. In the Caribbean, ERA-Interim bias with respect to the Global Precipitation Climatology Project estimate of precipitation amounts up to $\sim +2$ mm/day, which presents a reduction of excess precipitation over evaporation compared to ERA-40 (Dee et al. 2011). We note however that the reanalysis precipitation is only used in a consistent context with the entire ERA-Interim based moisture budget analysis (see below).

Table 2.1: List of rainfall stations used in the study. Station ID, station name, location in latitude and longitude, number of valid years from 1960 – 2017 that have valid pentad data, the total number of years available, and missing data. Missing data shows the percentage of pentads missing two or more days during total number of years.

Station ID	Station	Location Lat/Lon		Data Valid Years (Total Years)	Missing Data %
1	BC B. In. AP. Antigua & Barbuda	17.135	-61.791	46 (57)	0.79%
2	Nassau Intl. AP., Bahamas	25	-77.5	43 (48)	5.89%
3	CIMH, Barbados	13.148	-59.624	48 (48)	0.00%
4	Grantley Intl AP., Barbados	13.08	-59.485	45 (45)	0.00%
5	Cfarm, Belize	17.2	-89	40 (48)	2.45%
6	Intl. AP., Belize	17.53	-88.3	52 (57)	0.33%
7	Georgetown, Cayman	19.3	-81.3	45 (50)	0.41%
8	Camaguey, Cuba	21.24	-77.51	50 (56)	0.80%
9	La Habana, Cuba	23.1	-82.21	51 (55)	0.79%
10	DCAP, Dominica	15.547	-61.2993	39 (42)	0.61%
11	Santo Domingo, D.R.	18.25	-69.58	25 (57)	26.33%
12	Guadeloupe	16.2	-61.66	44 (57)	2.16%
13	Georgetown, Guyana	6.8	-58.133	47 (48)	0.45%
14	Time H.R.I, Guyana	6.483	-58.25	45 (46)	0.02%
15	Worthy Park, Jamaica	18.143	-77.149	39 (42)	1.35%
16	Intl. AP., Martinique	14.59	-60.99	56 (57)	0.14%
17	Hewanorra Intl. AP., St. Lucia	13.737	-60.952	39 (43)	0.15%
18	Dumbarton, St. Vincent	13.18	-61.17	43 (48)	3.17%
19	Corantjinpolder, Suriname	5.96	-57.04	31 (45)	3.47%
20	Zanderji, Suriname	5.45	-55.2	35 (57)	1.37%
21	Piarco Intl AP, T&T	10.59	-61.34	44 (57)	0.00%
22	Crown Point, T&T	11.15	-60.84	44 (57)	0.14%
23	Sunset/Ft. Lauderdale, USA	26.1	-80.28	54 (57)	1.61%
24	Key West, USA	24.55	-81.75	56 (57)	0.02%
25	Miami Intl AP, USA	25.82	-80.28	57 (57)	0.00%
26	Palm Beach AP, USA	26.68	-80.08	56 (57)	0.05%
27	Henry E. Rohlsen AP, St. Croix	17.7	-64.81	39 (44)	2.55%
28	Cyril E. King AP, St. Thomas	18.33	-64.97	25 (43)	9.65%
29	Coloso, USPR	18.381	-67.157	38 (57)	2.61%
30	Dora Bora, USPR	18.336	-66.667	42 (57)	6.68%
31	Ensenda, USPR	17.973	-66.946	49 (57)	2.96%
32	Guaynama, USPR	17.978	-66.087	35 (57)	9.61%
33	Jajome Alto, USPR	18.072	-66.143	47 (57)	1.49%
34	Mora Camp, USPR	18.474	-67.029	44 (57)	2.31%
35	Paraiso, USPR	18.265	-65.721	44 (57)	3.34%
36	Morovis N, USPR	18.334	-66.408	54 (57)	1.25%
37	San Andrés, Columbia	12.583	-81.717	31 (55)	15.89%
38	Felipe, Mexico	19.7	-87.9	32 (57)	12.73%

2.3 Methods

2.3.1 Pentad Climatologies and PC Analysis

Given the noise in daily data, pentad (5-day) averages of daily rainfall observations are calculated for each station. Using similar criteria from Hamada et al. (2002), if a pentad has two or more days of missing data, the pentad is omitted. If a pentad is missing or omitted within an analysis year, the entire analysis year is omitted for that station. Valid years for the analysis are given in Table 2.1. The rainfall pentad climatology for each station is calculated by averaging all valid years. After normalizing the pentad climatologies for each station, a Principal Component Analysis (PCA) is conducted, where the space dimension is the station number and the time dimension are the 73 pentads. The first three PCs are preserved and passed through a binomial filter for smoothing. The correlation coefficients between each stations' climatological seasonal rainfall cycle and PC are also calculated. A caveat is that the PCA analysis privileges more densely sampled areas, which is why the station pentad climatologies are shown in the analysis when distinguishing the regional classifications in the Caribbean. In addition, TRMM pentad climatologies for each of the regional classifications are calculated and compared with the station pentad climatologies in order to determine the authenticity of the classified regions.

2.3.2 Moisture Budget Analysis

The atmospheric moisture budget equation can be expressed as:

$$P - E = -\frac{1}{g\rho_w} \nabla \cdot \int_0^{p_s} q\boldsymbol{V}\, dp \qquad (1)$$

In this equation, precipitation (P) minus evaporation (E) is equal to the convergence of the column integrated moisture flux (q$\boldsymbol{V}$, where q is specific humidity and $\boldsymbol{V}$ is the horizontal wind vector) multiplied by the scaling factor of gravity (g) and density of water (ρ_w). Following Seager and

Henderson (2013), Eq. 1 is rewritten by taking its monthly time mean from 6-hourly intervals and put in K model pressure levels

$$\bar{P} - \bar{E} = -\frac{1}{g\rho_w} \nabla \cdot \sum_{k=1}^{K} \overline{\boldsymbol{V}_{(6,k)} q_{(6,k)}}\, \overline{dp_k} \tag{2}$$

where the overbars denote the monthly means. The right-hand side of Eq. 2 denotes the convergence of the total moisture flux (TMF), or the net amount of convergence in the atmospheric column vertically integrated in K pressure levels. One can further break down the TMF into its two components: moisture convergence associated with the monthly mean circulation and moisture convergence associated with the submonthly transient eddies:

$$\bar{P} - \bar{E} = -\frac{1}{g\rho_w} \nabla \cdot \sum_{k=1}^{K} \left(\overline{\boldsymbol{V}_k}\, \overline{q_k} + \overline{\boldsymbol{V}'_{(6,k)} q'_{(6,k)}} \right) \overline{dp_k} \tag{3}$$

where the first term in the summation on the right-hand side represents convergence by the mean flow, and the second term in the summation on the right-hand side represents convergence by 6-hourly transient flow. The primes on the second term denote daily departures from the monthly mean. Next, the divergence operator is moved to inside the summation in Eq. 3 in order to break down the mean flow convergence into its components. After calculating the climatological monthly and/or seasonal means, Eq. 3 can be rewritten as:

$$\bar{\bar{P}} - \bar{\bar{E}} = -\frac{1}{g\rho_w} \left[\sum_{k=1}^{K} \overline{\left(\overline{q_k} (\nabla \cdot \overline{\boldsymbol{V}_k}) + \overline{\boldsymbol{V}_k} \cdot (\nabla \cdot \overline{q_k}) \right) \overline{dp_k}} + \nabla \cdot \sum_{k=1}^{K} \overline{\overline{\boldsymbol{V}'_{(6,k)} q'_{(6,k)}}\, \overline{dp_k}} \right] - \overline{\overline{-q \boldsymbol{V}_s \nabla p_s}} \tag{4}$$

where the double bar represents the climatological monthly or seasonal mean. The first two terms on the right-hand side of Eq. 4 represents the mean moisture convergence due to mass convergence and mean moisture advection. The third term represents the climatological mean transient moisture convergence, and the last term is the surface term, which is related to the surface topography and

the resulting surface pressure gradient. For this analysis the surface term is relatively small compared to other terms and is thus ignored.

2.4 Results

2.4.1 Principal Component Analysis of the Seasonal Cycle of Rainfall in the Caribbean

The first three principal components (PCs) explain 78% of the total variance (54%, 16%, 8%, respectively) of the pentad rainfall climatological seasonal cycle (Fig. 2.1a–c). The first principal component (Fig. 2.1a) displays the known seasonal characteristics dominant in the Caribbean: the Early-Rainy Season beginning in mid-April and lasting through June, the MSD from June through August, the Late-Rainy Season (LRS) from August through November, and the Winter Dry Season (WDS) from mid-November to April. In addition, the maximum rainfall occurs during the LRS and the MSD is not necessarily a dry season but rather a period of less intense rainfall than the ERS and LRS. Nearly all stations in the Caribbean have high positive correlation coefficients with PC1 (Fig. 2.1d; Table 2.2), with the exception of the four Guiana stations. With its negative peak in June and positive peak in November, PC2 indicates a modification of the intensity of the ERS compared to the LRS rainfall (Fig. 2.1b). PC2 also shows a gradual ascent of rainfall towards the LRS in positively correlated stations. A notable contrast in spatial correlation pattern (Fig. 2.1e; Table 2.2) is seen with PC2 from NW to the SE portion of the Caribbean stations. Stations in the southeast, from the mid to upper portion of the Lesser Antilles, the U.S. Virgin Islands, and some in Puerto Rico have positive correlations with PC2, while stations in Florida, Cuba, and the Bahamas have negative correlations. This implies that the ERS peaking in June has a stronger signature in the Northwestern Caribbean than in the Southeastern Caribbean while the

opposite is seen

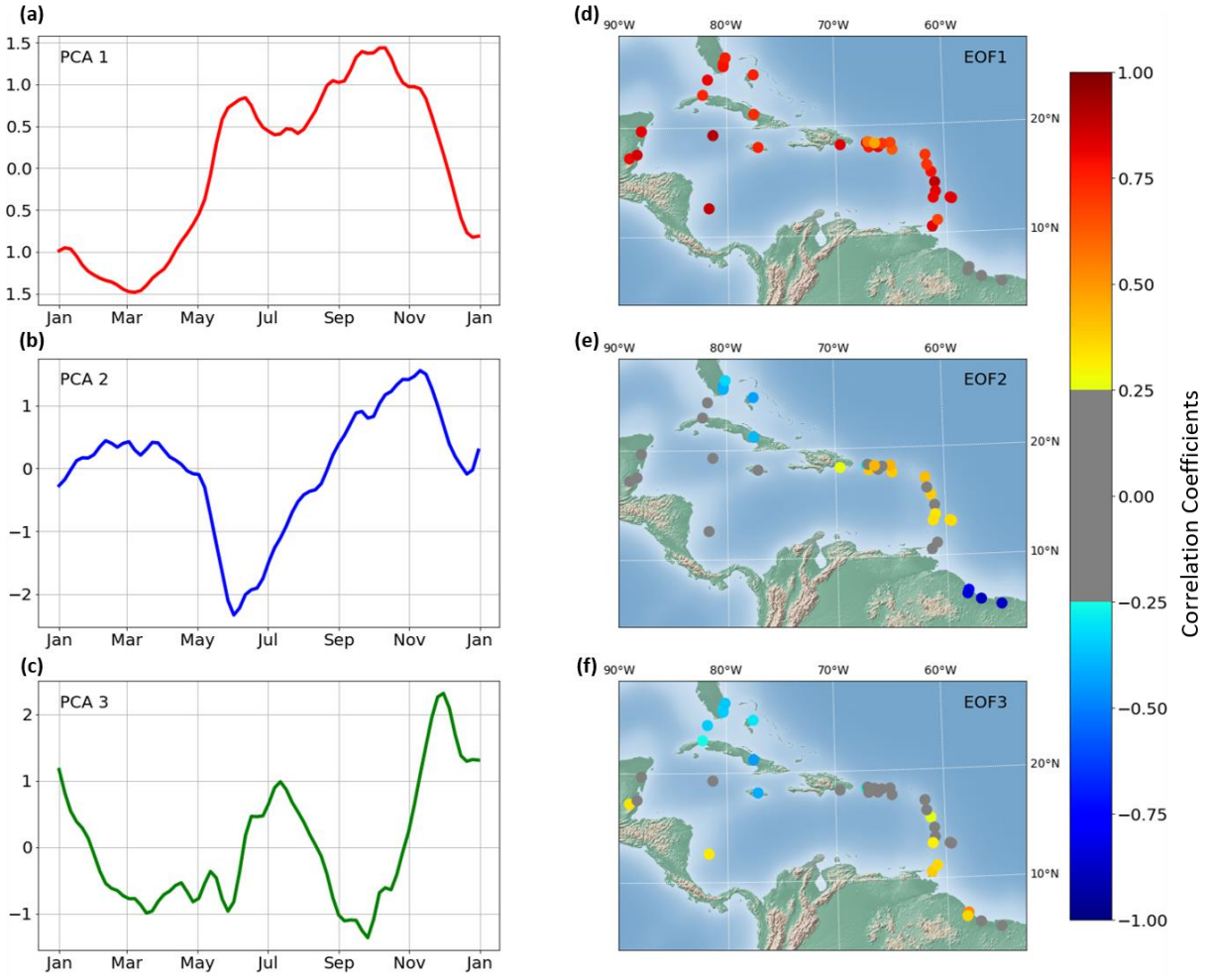

Figure 2.1: Principal Component Analysis (a–c) and spatial correlation coefficients (d–f) of the climatological Caribbean pentad rainfall at 38 CIMH/GHCN stations. Coefficients > 0.25 or < − 0.25 are colored for significance at the 95th confidence level.

during the climatological LRS. Meanwhile, stations in the Guianas have high negative correlation coefficients, indicating a complete inverse of PC2: a dominant ERS and little to no rainfall during the climatological LRS. Finally, PC3 denotes, in stations positively correlated with it, the absence of the MSD and a late-LRS peaking in late November and extending into the WDS (Fig. 2.1c). The correlation coefficients in PC3 show a notable meridional contrast (Fig. 2.1f; Table 2.2). Stations in the Northwestern Caribbean (e.g. Cuba, Jamaica, Bahamas, and Florida) have negative

correlations whereas some stations in Central America, the lower tier of the Lesser Antilles, and Guyana, have positive correlations. Given the negative correlations seen in PC2 in the Northwestern Caribbean, and a later peak of the LRS seen in PC3, the negative correlations in PC3 in the Northwestern Caribbean suggest this region has a stronger signature of the MSD and an earlier LRS in comparison to the eastern Caribbean. Meanwhile, the positive correlations in Guyana are a combination of the absence of the climatological MSD and a late-LRS given their inverted relationship seen in PC2.

Table 2.2: Correlation coefficients between the station annual cycle of rainfall and PC1, 2, and 3. Values bolded and italicized denote significance at the 95th confidence level.

Region	(ID) Station Name	*r*PC1	*r*PC2	*r*PC3
Northwest Caribbean	(2) Nassau, Bahamas	***0.751***	***-0.432***	***-0.290***
	(7) Georgetown, Cayman	***0.910***	0.025	-0.127
	(8) Camaguey, Cuba	***0.728***	***-0.387***	***-0.440***
	(9) La Habana, Cuba	***0.746***	-0.214	***-0.254***
	(15) Worthy Park, Jamaica	***0.752***	-0.029	***-0.410***
	(23) Ft. Lauderdale, USA	***0.770***	***-0.418***	***-0.314***
	(24) Key West, USA	***0.811***	-0.130	***-0.347***
	(25) Miami Intl. AP., USA	***0.784***	***-0.402***	***-0.348***
	(26) Palm Beach, USA	***0.763***	***-0.321***	***-0.352***
Western Caribbean	(5) CFarm, Belize	***0.799***	-0.103	***0.330***
	(6) Intl. AP., Belize	***0.850***	-0.021	0.162
	(37) San Andrés, Columbia	***0.879***	-0.080	***0.327***
	(38) Felipe, Mexico	***0.817***	-0.111	-0.164
Central Caribbean / Northern Lesser Antilles	(1) BC Bird Intl. AP., Antigua/Barbuda	***0.703***	***0.420***	0.093
	(11) Santo Domingo, DR	***0.822***	0.262	-0.216
	(27) Henry E. Rohlsen AP., St. Croix	***0.628***	***0.385***	0.166
	(28) Cyril E. King, St. Thomas	***0.673***	***0.444***	0.047
	(29) Coloso, USPR	***0.830***	-0.275	***-0.287***
	(30) Dora Bora, USPR	***0.641***	0.140	***-0.318***
	(31) Ensenda, USPR	***0.766***	***0.394***	-0.175
	(32) Guaynama, USPR	***0.873***	0.026	-0.101
	(33) Jajome Alto, USPR	***0.812***	0.224	0.070
	(34) Mora Camp, USPR	***0.584***	-0.123	-0.094
	(35) Paraiso, USPR	***0.708***	0.197	0.116

	(36) Morovis N., USPR	***0.463***	***0.431***	-0.086
Central and Southern Lesser Antilles	(3) CIMH, Barbados	***0.820***	***0.345***	0.160
	(4) Grantley A. Intl. AP., Barbados	***0.826***	***0.346***	0.225
	(10) DCAP, Dominica	***0.781***	***0.384***	0.251
	(12) Guadeloupe	***0.716***	0.131	-0.029
	(16) Intl. AP., Martinique	***0.884***	0.245	0.215
	(17) Hewanorra, St. Lucia	***0.822***	***0.334***	0.165
	(18) Dumbarton, St. Vincent	***0.811***	***0.340***	***0.312***
T&T / Guianas	(13) Georgetown, Guyana	0.078	***-0.780***	***0.530***
	(14) Time HRI, Guyana	0.185	***-0.843***	***0.362***
	(19) Corantjinpolder, Suriname	-0.001	***-0.895***	0.194
	(20) Zanderji, Suriname	-0.067	***-0.881***	0.064
	(21) Piarco, T&T	***0.824***	-0.193	***0.389***
	(22) Crown Pt. T&T	***0.676***	-0.204	***0.356***

Overall, the PCA suggests three distinct sub-regions of the rainfall cycle in the Caribbean: the Northwestern Caribbean, the Central and Eastern Caribbean (Puerto Rico and the Lesser Antilles), and the Guianas. However, this rough division of the Caribbean regions paints an incomplete picture. Findings from the total moisture budget provide important insights on the regional precipitation patterns across the Caribbean.

2.4.2 Seasonal Moisture Budget of the Caribbean

The reanalysis' spatial moisture budget climatology (1979–2012) for the Caribbean is divided into the four climatological precipitation seasons: the WDS (Fig. 2.2), ERS (Fig. 2.3), MSD (Fig. 2.4), and LRS (Fig. 2.5).

2.4.2.1 Winter Dry Season (December-April)

Given P-E (Fig. 2.2a) equals the TMF (Fig. 2.2b) in the moisture budget equation, both terms resemble each other well in the WDS. In the TMF, convergence is found over the continental United States and south of the Caribbean domain (except Guianas) where the ITCZ is situated. Divergence is seen throughout nearly all of the Caribbean, and the tropical North Atlantic coinciding with NASH. In addition, SSTs in the Caribbean have values between 24 and 27 °C

(Fig. 2.2b). When the convergence of the TMF is broken down into its mean (Fig. 2.2c) and transient (Fig. 2.2d) components, the latter is seen to dominate the TMF convergence north of 20 N, and the mean flow dominates the TMF south of 20 N. Therefore, the convergence band in the continental

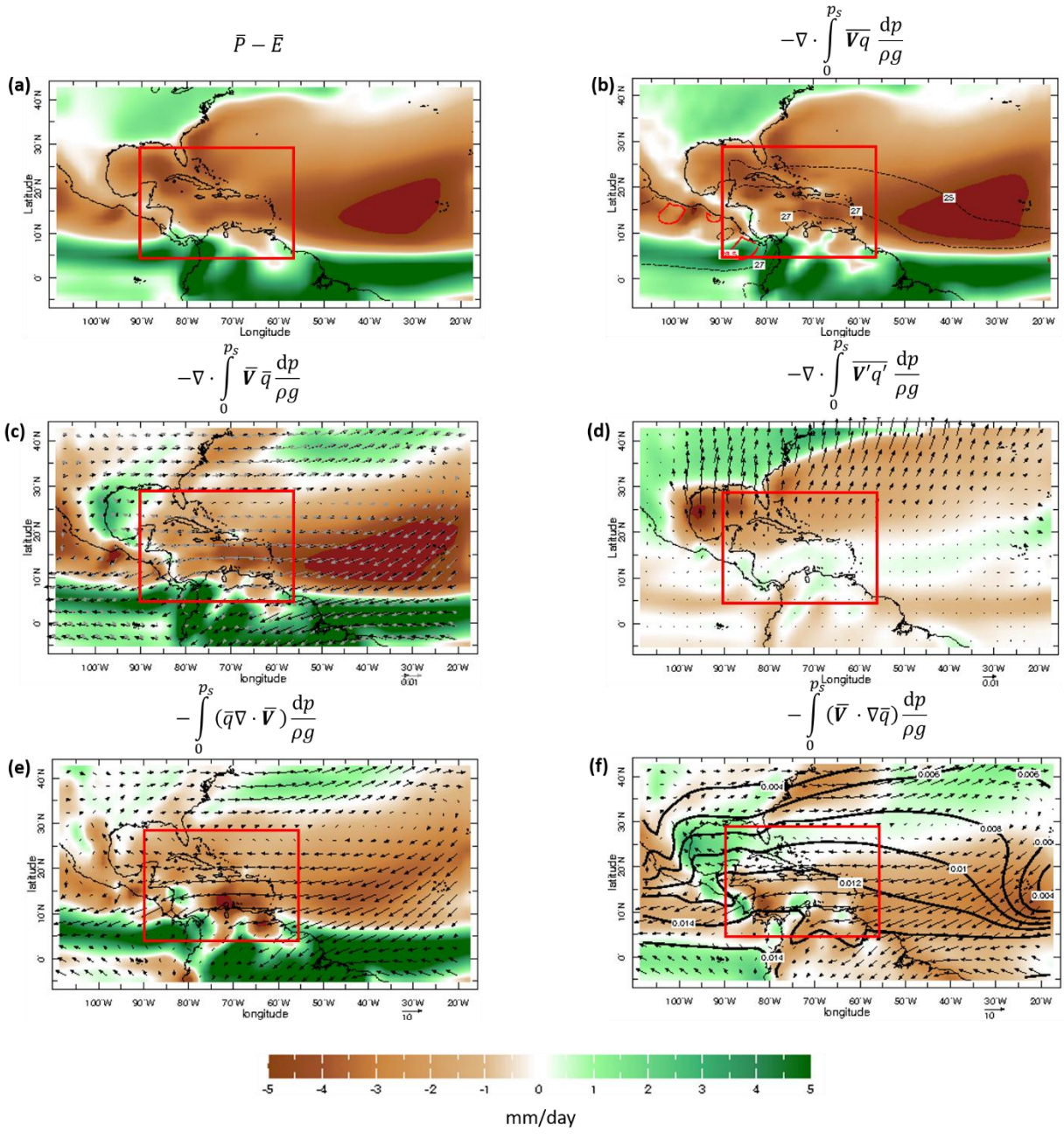

Figure 2.2: Winter Dry Season (Dec-Apr) climatological seasonal mean moisture budget in mm/day. (a) Precipitation minus evaporation. Shaded in green (convergence) and

brown (divergence) are (b) total moisture flux convergence, (c) convergence by the mean flow, (f) convergence by the transient flow, (e) mass convergence, and (f) mean flow moisture advection. The contours in (b) are SSTs. The black vectors in (c) and (d) are the vertically integrated mean and transient moisture transport vectors, respectively. The grey vectors in (c) are the 925hPa wind vectors. The black vectors in (e) and (f) are the 925hPa wind vectors. The solid black contours in (f) are specific humidity at 925hPa

U.S. and divergence bands in the Gulf of Mexico and Northwestern Caribbean are due primarily to the transient flow. The divergence across the tropical north Atlantic, SE Caribbean, and convergence bands in the Guianas/ITCZ regions are due to the mean flow. As for the transient flow, the transient mean moisture transport vectors are meridional, that is the land–ocean convergence and divergence couplet are a result of high-frequency transient eddies that transport moisture poleward.

The breakdown of the mean flow into its mass convergence (Fig. 2.2e) and moisture advection components (Fig. 2.2f) show that mass convergence is the dominant term of the mean flow impact on the moisture budget while moisture advection acts as a modifier. For instance, mean flow divergence in the tropical North Atlantic is due to mass divergence by northeasterly winds carrying lower values of specific humidity (q) into the region. This is associated with the circulation imposed by the NASH along its southern flank. In addition, strong 925hPa easterly winds are seen across the central Caribbean Sea, these are associated with the wintertime CLLJ (Wang 2007). The Gulf of Mexico is the only region where moisture advection dominates by acting to overcome the effect of weak mean mass divergence. Here, strong moisture advection by southeasterly winds carries higher q from the Caribbean Sea into the Gulf of Mexico.

2.4.2.2 Early-Rainy Season (May-June)

During the ERS, the mean flow (Fig. 2.3e, f) is the dominant contributor of the TMF (Fig. 2.3c, d). In May, two bands of convergence in the Caribbean appear in the TMF (Fig. 2.3c): one in the western flank of NASH from the Dominican Republic/Puerto Rico to the mid-latitudes, and

the other across western portion of the Caribbean Sea. Convergence also appears in the Guianas as the Atlantic ITCZ convergence band moved northward.

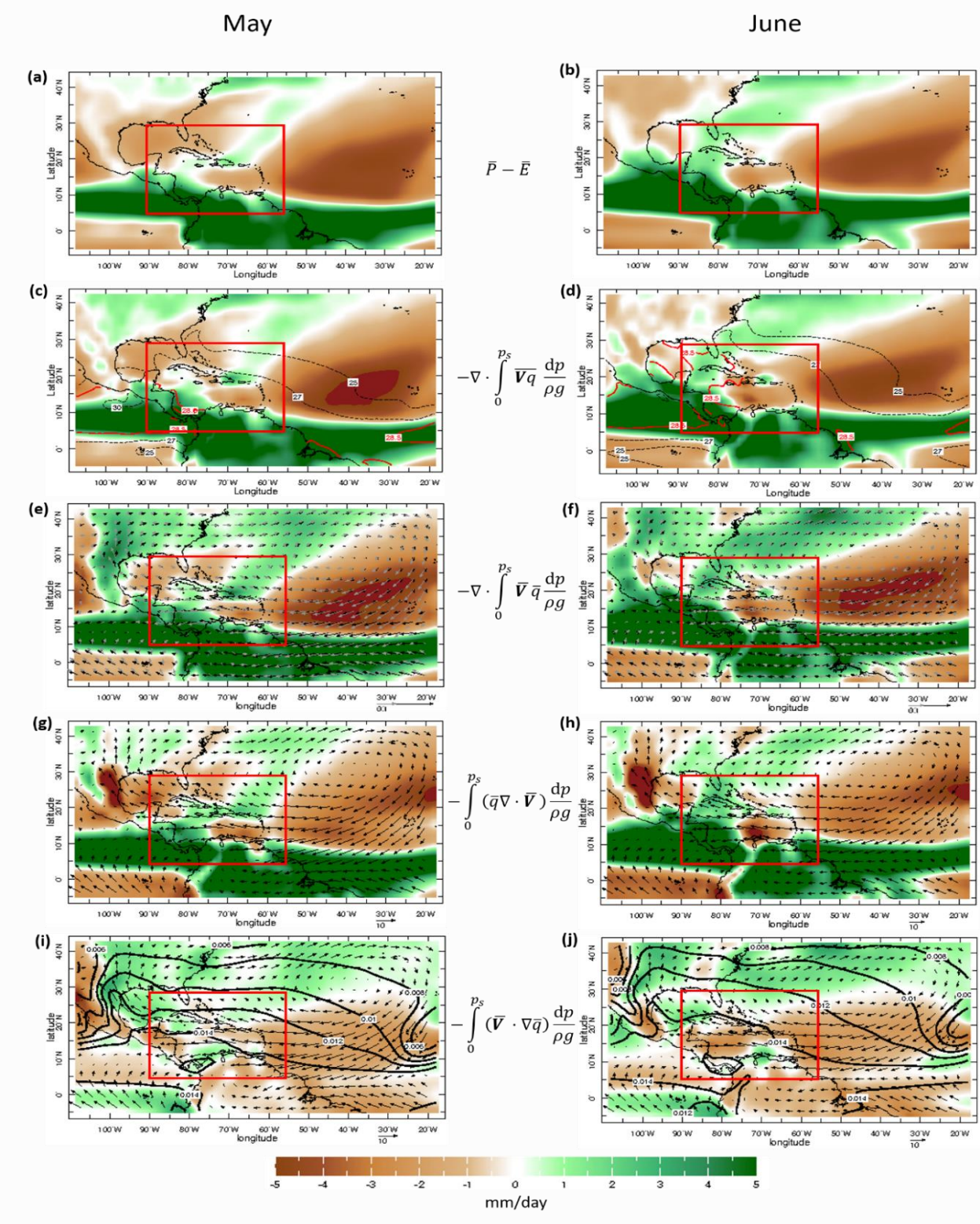

Figure 2.3: Early Rainy Season (May-Jun) climatological monthly mean moisture budget for May (a, c, e, g, i) and June (b, d, f, h, j). (a, b) Precipitation minus evaporation. Shaded in green (convergence) and brown (divergence) are (c, d) total moisture flux, (e, f) convergence by the mean flow, (g, h) mass convergence, and (i, j) advection of specific humidity. The contours in (c) and (d) are SSTs. The black vectors in (e) and (f) are the vertically integrated mean moisture transport vectors. The grey vectors in (e) and (f) are the 925hPa wind vectors. The black vectors in (g–j) are the 925hPa wind vectors. The solid black contours in (i) and (j) are specific humidity at 925hPa

Convergence is also seen where the northward migrating Eastern Pacific ITCZ and SAMS are located. Three zones of divergence are found: one in the Gulf of Mexico and Northwestern Caribbean, the southern flank of NASH, and a divergence tongue from the Lesser Antilles to the Central Caribbean Sea. SSTs in the Caribbean Sea are between 27 °C-28 °C and the Gulf of Mexico is at or below 27 °C (Fig. 2.3c). Areas such as the Eastern Pacific ITCZ and the Caribbean shoreline of Central America have SSTs at or above 28.5 °C, denoting the warm pool and its Caribbean branch. The regional maximum of warm waters coincides with the largest values of convergence seen in the Caribbean, which is indicative of the WHWP enhancing the Eastern Pacific ITCZ and the convection in the western Caribbean Sea.

In the convergence band in the western flank of NASH, mass convergence (Fig. 2.3g) and advection of moister air (Fig. 2.3i) are found. The 925hPa wind and mean moisture transport vectors in this convergence band have a stronger southerly component than during the WDS. Therefore, the convergence band in the western flank of NASH is a result of weakened trade winds and their associated mass divergence and higher values of q from the tropics being advected into the subtropics. The convergence band in the western Caribbean Sea is mainly associated with mass convergence that connects with the Eastern Pacific ITCZ. In addition, the 925hPa winds in the Caribbean Sea have a stronger southerly component than during the WDS. Mass divergence in the central Caribbean Sea is weaker than during the WDS. This implies that the western Caribbean Sea band is receiving moisture from the Eastern Pacific ITCZ as a result of enhanced southerly

flow which weakens the divergent trade winds in the Caribbean Sea. The Gulf of Mexico and far Northwestern Caribbean mean flow divergence is due to mass divergence; however, positive advection of moisture via southeasterly winds in the region modifies the magnitude of the overall mean flow moisture flux divergence. Finally, the ITCZ convergent bands are a result of mass convergence by the trade winds that converge towards the ITCZ.

In June, the TMF and mean flow convergence bands associated with the western flank of NASH shift westward to the eastern U.S. coastline and to portions of the Gulf of Mexico/Northwestern Caribbean (Fig. 2.3d, f). This observation is consistent with recent studies that investigate the ERS (e.g., WT5 in Moron et al. 2015; Allen and Mapes 2017). The westward shift of the western flank of NASH, mean flow convergence band is due to the westward shift of mass convergence (Fig. 2.3h) and northwestward shift of positive moisture advection (Fig. 2.3j). In addition, the 925hPa southeasterly winds shift westward as southeasterly winds in the Gulf of Mexico and Northwestern Caribbean have strengthened while the southeasterly winds north of the Dominican Republic/Puerto Rico have become easterly. SSTs warm throughout the Caribbean domain and the AWP (28.5 °C) expands to regions where convergence across the western Caribbean Sea and Gulf of Mexico is found (Fig. 2.3d). The convergence band in the western Caribbean Sea shifts slightly northwestward as mass convergence from the Eastern Pacific ITCZ migrated further northward. The Atlantic ITCZ convergence band also shifts northward, but the SAMS convergence band is stagnant. For the TMF/mean flow divergence, the divergence band in the Gulf of Mexico disappears, the divergence band in the southern flank of NASH shifts northward, and the divergence tongue in the Caribbean Sea extends westward as negative moisture advection (Fig. 2.3j) is enhanced across the Caribbean Sea. In addition, the 925hPa easterly winds and mean moisture divergence vectors in the Caribbean Sea strengthen (Fig. 2.3f), similarly to

what is found during the WDS. The Caribbean Sea mass convergence-negative moisture advection couplet found in the WDS also returns (Fig. 2.3h, j).

2.4.2.3 Mid-Summer Drought (July-August)

The MSD TMF shows three convergent bands and one large divergent band in the Caribbean domain (Fig. 2.4b).

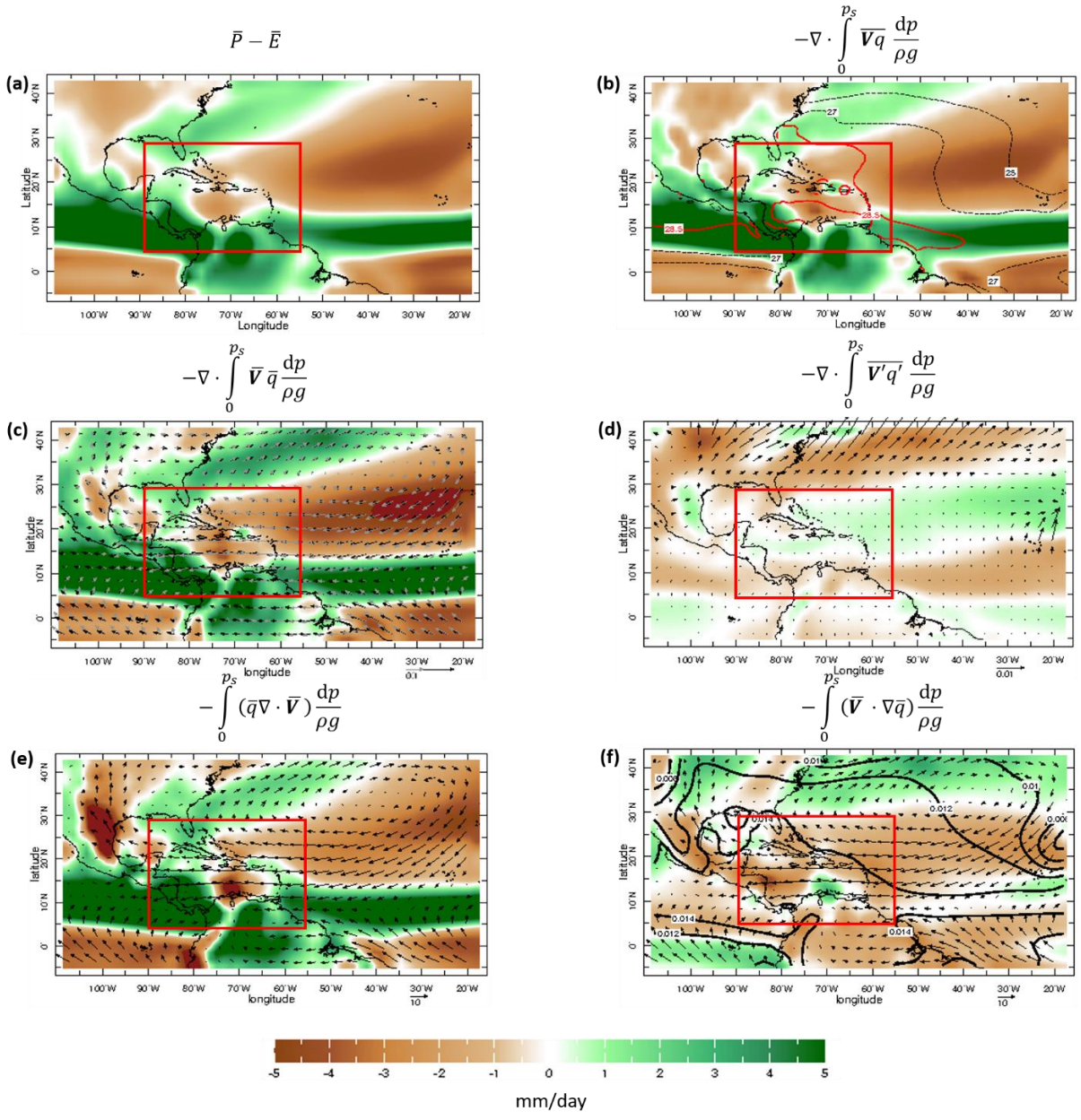

Figure 2.4: Same from Fig. 2.2 but for the Mid-Summer Drought season (Jul-Aug)

The convergence bands coincide where precipitation exceeds evaporation the most (Fig. 2.4a) and vice versa with the seen divergence bands. The first convergence band is associated with the northwestern flank of NASH and is seen from Florida to the mid-latitude Atlantic Ocean. The second convergence band is seen in the western Caribbean Sea, south of the Eastern Pacific ITCZ convergence band. The third convergence band is seen in the Lesser Antilles in association with the Atlantic ITCZ. The divergence band is seen in the southern flank of NASH, portions of the Greater and Lesser Antilles, and central Caribbean Sea. In comparison to the ERS, the NASH convergence band shifts northwestward and the Eastern Pacific ITCZ/Atlantic ITCZ bands move northward. The mean flow is responsible for these convergent and divergent bands (Fig. 2.4c). Upon the breakdown of the mean flow into its mass convergence (Fig. 2.4e) and moisture advection (Fig. 2.4f) components, mass convergence is largely responsible for the convergence bands, whereas mass divergence and negative advection of specific humidity are largely responsible for the divergent band. The enhanced negative advection across most of the Caribbean is due to marginally lower values of q across the southern flank of NASH being zonally advected into the Caribbean. Mean flow convergence in the ITCZ regions and northwestern flank of NASH are a consequence of converging winds associated with the trade winds, and converging southeasterlies on the western flank of NASH which advect lower values of q into the mid-latitudes, respectively. Similarly, to the WDS and ERS-June, a large convergence-divergence couplet is seen between mass convergence and moisture advection in the Caribbean Sea.

The western Caribbean Sea alongside the Nicaragua shoreline has mass convergence and advection of drier air, whereas the central Caribbean Sea north of the Bay of Venezuela has mass divergence and positive moisture advection. Similarly, during the WDS, a pocket of lower q and strong divergent winds are seen north of the Bay of Venezuela, whereas larger values of q and

strong convergent winds are seen to its east and west. The SSTs at and around the Caribbean Sea divergence pocket are cooler than the surrounding region (Fig. 2.4b), which is likely a result of coastal upwelling (Inoue et al. 2002). This upwelling is forced by the low-level easterly winds, or CLLJ, that are parallel to the South American coastline (Fig. 2.4c, e). In addition, the AWP (28.5C) extends eastward into the Lesser Antilles but does not reach the North South American coastline (Fig. 2.4b). This induces an inverted meridional SST gradient from the northern South American coast to the Greater Antilles. Based on thermal wind balance, the negative meridional temperature gradient enhances low-level winds from the east (Angeles et al. 2010; Wang 2007) in a positive feedback loop. Given that the CLLJ peaks during the MSD, it drives the moisture convergence-divergence couplet, an observation that is consistent with previous studies (Muñoz et al. 2008; Hidalgo et al. 2015; Herrera et al. 2015).

Finally, transient flow impact on the moisture budget is relatively weak across the Caribbean (Fig. 2.4d). That said, transient convergence modifies the extent of mean flow divergence as values of transient convergence are seen off the coast of West Africa and the Caribbean. The mean transient transport vectors over the tropical North Atlantic and off of West Africa are meridional; therefore, the transient convergence is a response to easterly moving high-frequency eddies (e.g., AEWs). However, the negligible transient convergence values seen in the Caribbean suggests their influence is marginal.

2.4.2.4 Late-Rainy Season (September-November)

The LRS TMF in September shows convergence throughout most of the Caribbean domain (Fig. 2.5a) as precipitation well exceeds evaporation (not shown). Convergence is seen throughout the Northwestern Caribbean, eastern Central America, the Greater Antilles, and the Lesser Antilles. Some divergence is seen in the central Caribbean Sea and in the Guianas. The AWP

covers the entire Caribbean domain (Fig. 2.5a). When breaking down the TMF into its mean (Fig. 2.5d) and transient (Fig. 2.5g) components, it is found that TMF convergence is due to convergence from the mean flow. Mass convergence (not shown) is the dominant component of the LRS mean flow as moisture advection (not shown) is negative but negligible across the Caribbean.

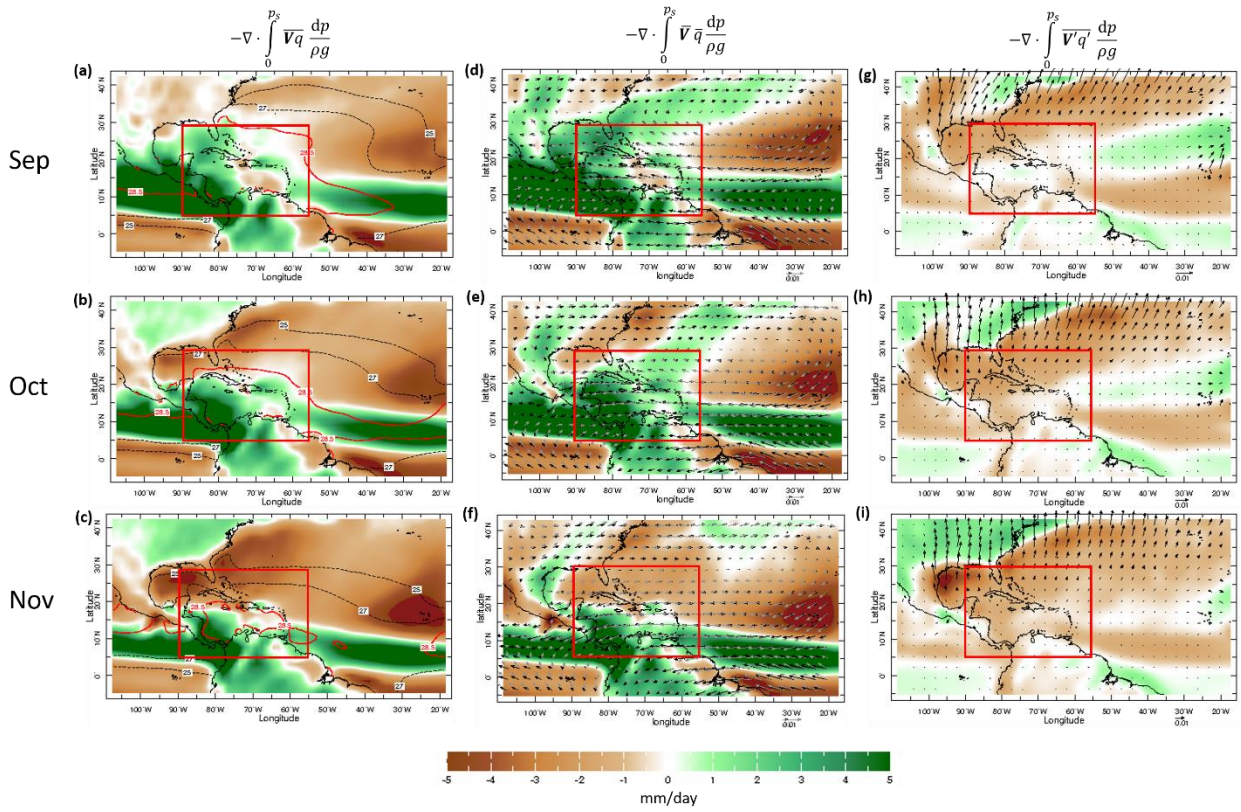

Figure 2.5: Late rainy season climatological monthly mean moisture budgets for September (a, d, g), October (b, e, h), and November (c, f, i) (LRS). Shaded in green and brown are (a), (b), (c) total moisture flux, (d), (e), (f) convergence by the mean flow, and (g), (h), (i) convergence by the transient flow. The contours in (a), (b), (c) are SSTs. The black vectors in (d–f) and (g–i) are the integrated mean and transient moisture transport vectors, respectively. The grey vectors in (d–f) are the 925hPa wind vectors

In the mean flow, three bands of convergence are found: one located on the climatological Atlantic ITCZ, one located on the climatological Eastern Pacific ITCZ, and one located on the western flank of NASH. Both ITCZ convergence bands are seen in the TMF and only the southern portion of the western flank of the NASH convergence band is seen in the TMF. Transient divergence is

found across the Gulf of Mexico and where the northwestern flank of NASH is located. Therefore, transient divergence overtakes the mean flow convergence northeast of Florida, which results in TMF divergence. The mean transient transport vectors are mainly meridional and increasing in magnitude poleward; thus, extratropical high-frequency transient eddies are likely responsible for transient divergence seen in the Gulf of Mexico and U.S. eastern coastline.

When comparing the LRS-September to the seasonal MSD, it is found that the mean flow NASH convergence band migrates southward as the Eastern Pacific and Atlantic ITCZ convergence bands migrate northward. SAMS mean flow convergence band weakens and remains stagnant. The mean flow divergence pocket seen in the central Caribbean Sea is diminished. The southern flank of the NASH divergence band is also diminished. Low-level winds shift from easterly to southeasterly across most of the Caribbean domain. Therefore, the migration of large-scale convergence bands alongside winds that favor mass convergence may explain the enhanced convergence across the entire Caribbean. As for transience, the convergence seen in the Caribbean and off of West Africa is diminished as divergence from the mid-latitudes extends southward into the Gulf of Mexico and portions of the Northwestern Caribbean. This suggests mid-latitude high-frequency transient eddies extending southward as tropical easterly high-frequency transient eddies, e.g., AEWs, diminish.

In October, TMF convergence moves southward in the Caribbean (Fig. 2.5b) Convergence is seen across the Lesser Antilles, Central America, and Puerto Rico/Dominican Republic. Divergence infiltrates the Northwestern Caribbean and Gulf of Mexico, as evaporation strengthens and exceeds precipitation (not shown) across the Northwestern Caribbean and Gulf of Mexico. The mean flow (Fig. 2.5e) shows Atlantic ITCZ and Eastern Pacific ITCZ bands shifting slightly southward. The NASH mean flow convergence band shifts southeastward and is at similar position

seen during the ERS-May. However, most of the NASH convergence band vanishes. Transient divergence by U.S. mainland high-frequency mid-latitude eddies (Fig. 2.5h) shifts southward and strengthens; therefore, the transient divergence overtakes the NASH convergence band. Also, seen in the TMF is the contraction of the AWP (Fig. 2.5b). SSTs at or below 27 °C in the Gulf of Mexico and portions of the Northwestern Caribbean while the rest of the Caribbean is at or above 28.5C. Notably, areas in the Caribbean that have larger mean flow convergence than transient divergence, have SSTs at or greater than 28.5 °C, whereas the opposite is true where transient divergence is greater. Finally, low-level winds remain southeasterly across the eastern half of the Caribbean domain, whereas the western half sees an easterly shift. The easterly shift in the western half of the Caribbean is also on the southern flank of an emerging anticyclonic feature seen in the SE United States, which is likely the continental High.

TMF convergence zone moves further southward in November (Fig. 2.5c) as evaporation strengthens (not shown) and precipitation weakens (not shown) across most of the Caribbean. Convergence is seen across the Caribbean coast of Central America and the southern half of the Lesser Antilles in correspondence to the southward shift of the Atlantic ITCZ and Eastern Pacific ITCZ convergence bands (Fig. 2.5f). The Atlantic ITCZ shift results in moisture convergence to return to the Guianas. SAMS shifts southward. A pocket of convergence is seen in Dominican Republic/Puerto Rico and is a result of enhanced surface term convergence on top of mass convergence (not shown). The Caribbean is now under the influence of the southern flank of a broad anticyclonic circulation consisting of NASH and the continental U.S. anticyclone. The shift of low-level winds to easterly across the entire Caribbean is likely responsible for the pocket of convergence via orographic lifting/zonal convergence across the Caribbean side of Central America. The mean flow NASH convergence band disappears and is replaced by mean flow

divergence. Mean flow divergence is also seen in the Northwestern Caribbean and Gulf of Mexico. Therefore, mean flow divergence enhances TMF divergence in the Gulf of Mexico and Northwestern Caribbean that is dominated by transient divergence (Fig. 2.5i). SSTs continue to cool across the Caribbean (Fig. 2.5c) and the AWP contracts further and is concentrated in the Caribbean Sea.

2.4.3 Caribbean Climate Regions and Pentad Climatologies

Based on the findings from the PCA, three sub-regions are seen in the Caribbean. However, with the results of the moisture budget analysis, five distinct regions are found, each with unique rainfall cycle characteristics (Fig. 2.6): Central Caribbean (Region 1: Dominican Republic, Puerto Rico, the Virgin Islands, and Northern Lesser Antilles), the Western Caribbean (Region 2: Caribbean coast of Central America), the Northwest Caribbean (Region 3: Florida, Bahamas, Cuba, Cayman Islands, and Jamaica), the Central and Southern Lesser Antilles (Region 4), and Trinidad & Tobago (T&T) / Guianas (Region 5). Furthermore, the TRMM-based results support the multi-seasonality of the different regions based on the station data (Fig. 2.7). Although most of the regional pentad climatologies in TRMM have lower magnitudes than the station data, this is possibly due to TRMM containing some ocean grids in its pentad calculations. Another possible source of difference could be due to the different temporal coverage of the station vs. TRMM data as shown in Fig. 2.7. However, when the station data temporal range matches with TRMM the station pentad climatologies' from 1969 to 2017 vs. 1998–2014 matched well; therefore, there are no systematic differences between the two different sets of climatological periods. In sum, the station dataset is robust to represent the regional climatology.

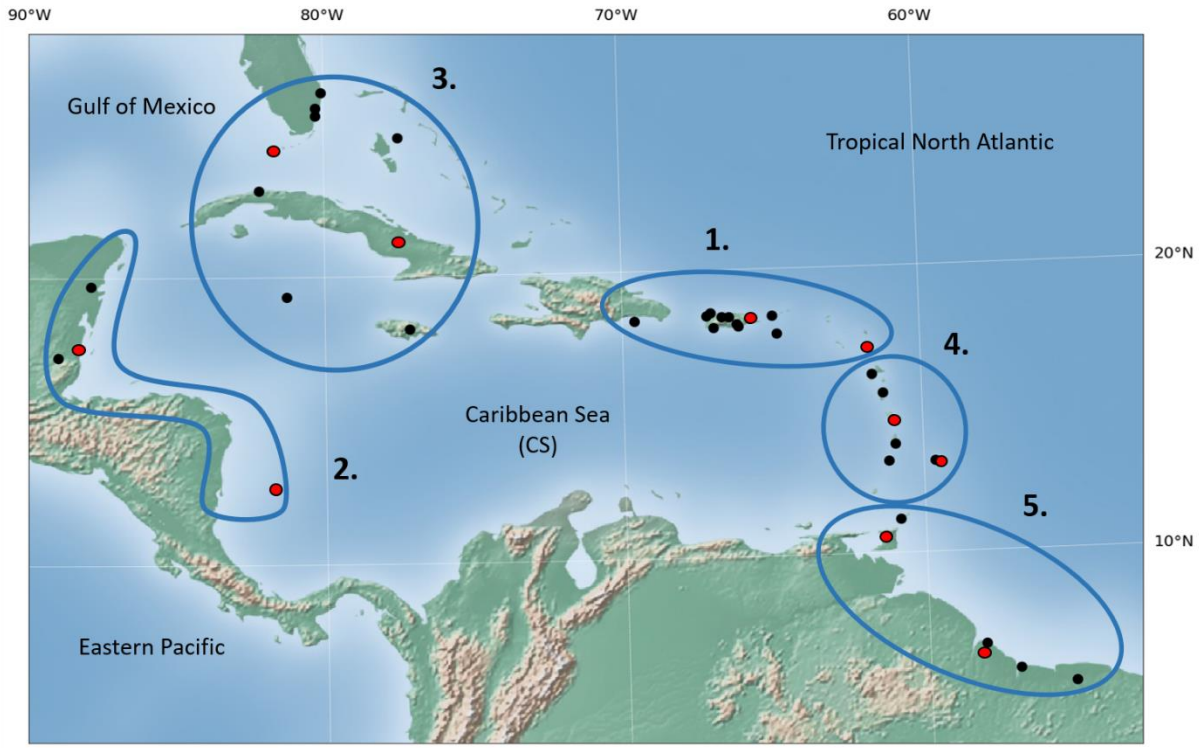

Figure 2.6: Regional Classifications for the Caribbean. (1) Central Caribbean; (2) Western Caribbean; (3) Northwest Caribbean; (4) Central and Southern Lesser Antilles; (5) Trinidad and Tobago (T&T) and Guianas. Red dots indicate stations shown in Fig. 2.7

2.4.3.1 Central Caribbean

The Central Caribbean rainfall cycle is influenced by moisture convergence associated with the expansion and contraction of the western flank of the NASH. At the beginning of the ERS (late-April/early May) convergence from the western flank of NASH emerges anywhere from the northern Lesser Antilles to Puerto Rico, and progresses northwestward into the Northwestern Caribbean as NASH expands westward. The pentad climatologies (Fig. 2.7a, b) show an ERS in the Northern Lesser Antilles, and its magnitude increases over the U.S. Virgin Islands and Puerto Rico. However, their ERS peaks in May and diminishes in June, hence the positive correlations seen in PC2 (absence of ERS in June) in this region. Moisture divergence from the southern flank of NASH returns in the Central Caribbean, which causes the MSD. During the LRS, NASH contracts eastward and its western flank moves back into the Central Caribbean on a similar path

to what is seen during the ERS. The western flank stalls and dissipates in the Central Caribbean as NASH merges with the continental U.S. High; therefore, convergence remains in the region and is why the Central Caribbean LRS has a longer duration than its ERS (Fig. 2.7a, b).

2.4.3.2 Western Caribbean

The Western Caribbean rainfall cycle is dominated by the Eastern Pacific ITCZ with some interactions between ITCZ and NASH and regional modifications by the AWP and the CLLJ. The ERS peaks later than the Central Caribbean, starting in late May through early July (Fig. 2.7c, d). The northward migration of the Eastern Pacific ITCZ provides moisture for the Western Caribbean during the ERS to LRS. During the ERS, P-E is enhanced in this region from two convergence bands in the western Caribbean Sea: one on the Nicaraguan to Costa Rican Caribbean coast, and the other extending from Jamaica to the Yucatan/Belize Caribbean coast. Both are enhanced by the AWP; however, the former receives convergence from orographic lifting and zonal convergence by easterly winds, and the latter receives convergence from the transport of moisture from NASH induced southeasterly winds. During the MSD easterly winds are enhanced by the expansion of NASH, which (1) enhances orographic lifting and zonal convergence by the CLLJ and (2) cuts off penetration of the Eastern Pacific ITCZ into the Caribbean. Therefore, most of the Western Caribbean experiences an MSD but not to the extent seen in other regions. The pentad climatologies and PC3 support these findings. Stations in the western Caribbean (Fig. 2.7c, d) have a less prominent MSD and no significant correlation with PC3. The exception is the Nicaraguan to Costa Rican Caribbean coastlines where a lack of the MSD is observed due to enhanced convergence by the CLLJ (Herrera et al. 2015; Hidalgo et al. 2015). During the LRS, the easterly winds weaken as NASH contracts, and the moisture regime and processes described during the ERS return. The slow southward migrating Eastern Pacific ITCZ stays in the Western Caribbean.

which is likely why the pentad climatologies and PC3 show a late-end and start to the LRS and WDS, respectively.

2.4.3.3 Northwestern Caribbean

The Northwestern Caribbean rainfall cycle is similar to the Western Caribbean, except it is influenced more by the expansion–contraction of the western flank of NASH, and migration patterns of U.S. mainland mid-latitude features. During the second half of the ERS, the convergence band associated with the western flank of NASH migrates from the Central Caribbean to the Northwestern Caribbean. This is consistent with the negative correlation between PC2 and rain gauge stations on the eastern half of the Northwestern Caribbean. In addition, the NASH southeasterly winds in the Caribbean Sea provide moisture to extend the Eastern Pacific ITCZ into the southern portion of the Northwestern Caribbean. During the MSD, this ITCZ penetration is marginal as divergence associated with trade winds on the southern flank of NASH infiltrates the Caribbean Sea. The pentad climatologies (Fig. 2.7e, f) and the phase of PC3 support these findings in the moisture budget. The Northwestern Caribbean has negative correlations with PC3, which is largest in its southern half, consistent with the absence of the MSD. During the LRS, NASH contracts and its western flank moves southeast on a similar path seen during the ERS. However, transient divergence from U.S. mainland mid-latitude features quickly strengthens in the continental U.S. and propagates into the Gulf of Mexico and eastern Atlantic. Simultaneously, the AWP begins its contraction in the Caribbean over the Northwestern Caribbean first. Therefore, convergence from the western flank of the NASH dissipates as a result of transient divergence overtaking mean flow convergence in the Northwestern Caribbean and the disappearance of the AWP. This supports what is seen in the pentad climatologies (Fig. 2.7e, f) and in PC3 in the Northwestern Caribbean. PC3 shows that these stations have negative correlations to a late-LRS,

and the pentad climatologies show these stations have the earliest demise of the LRS than any other region in the Caribbean.

2.4.3.4 Central and Southern Lesser Antilles/T&T/Guianas

The Central and Southern Lesser Antilles and the Trinidad and Tobago (T&T)/Guianas rainfall cycles are affected by competing influences from the Atlantic ITCZ and the diverging trade winds on the southern flank of NASH.

During its northward migration, Atlantic ITCZ convergence moves through the Guianas and T&T during the late-ERS and into MSD and slows down while reaching its northern most extent at the central Lesser Antilles by the mid LRS. While the Atlantic ITCZ migrates north from the southern to central Lesser Antilles during the MSD to mid LRS, divergence is seen across the Guianas. During the late-LRS, convergence returns in T&T and the Guianas as the Atlantic ITCZ migrates south and divergence associated with the trade winds returns in the central and southern Lesser Antilles. The Atlantic ITCZ and its migration pattern explains what is seen in the Lesser Antilles and Guianas in the PCA analysis and pentad climatologies (Fig. 2.7g–j). This is consistent with numerous rainfall studies in the Guianas (e.g. Shaw 1987; Bovolo et al. 2012; Durán-Quesada et al. 2012); however, no study has mentioned the Atlantic ITCZ as the major source of moisture convergence for the Lesser Antilles. The lack of an ERS seen in the Lesser Antilles (Fig. 2.7g, h) is in response to not only divergence by NASH (Gamble et al. 2007) and trade winds, but also due to the absence of the Atlantic ITCZ in the region during the ERS. This also explains the Guianas' negative correlations in PC1, and the positive correlations with PC3 across T&T and Guianas. The bimodal rainfall pattern in the T&T and Guianas (Fig. 2.7i, j) is distinct from the climatological bimodal pattern seen in most of the Caribbean.

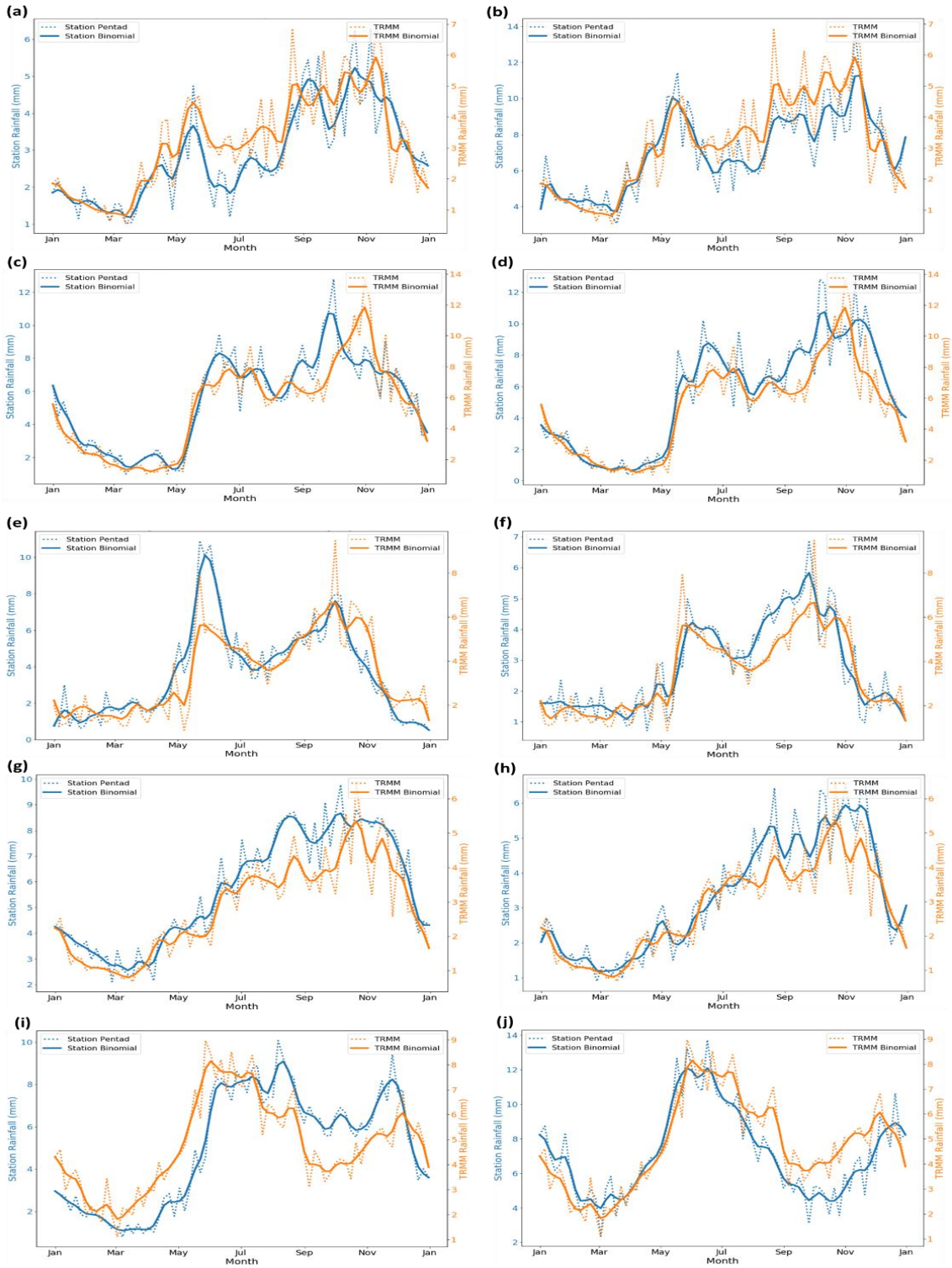

Figure 2.7: Pentad rainfall climatologies in millimeters/day in the Central Caribbean: (a) Antigua and Barbuda, (b) Paraiso, Puerto Rico; the Western Caribbean: (c) Belize City, Belize, (d) San Andrés, Colombia; the Northwest Caribbean: (e) Camaguey, Cuba, (f) Key West, USA; the Central and Southern Lesser Antilles: (g) Martinique, (h) Grantley, Barbados; and

the T&T and Guianas: (i) Piarco, Trinidad and Tobago, (j) Time HRI, Guyana. The blue dotted and solid lines represent the pentad and binomial filtered station precipitation climatology (respectively) averaged over the specified stations for the period 1969–2017. The orange dotted and solid lines represent (respectively) the area-averaged pentad and binomial filtered TRMM precipitation climatologies in the station-based classified regions, for the period 1998–2014

2.5 Summary and Discussion

Chapter 2 analyzed the seasonal cycle of rainfall in the Caribbean using a PCA of station data from the Caribbean Institute for Climatology and Hydrology and NOAA Global Historical Climatological Network between 1960 and 2017. The first principal component (PC1) shows high positive correlations across the entire Caribbean as it details the well-known bimodal rainfall structure of the Caribbean: the Winter Dry Season, Early-Rainy Season, Mid-Summer Drought, and Late-Rainy Season. When the ERS and LRS are modified (PC2), a northwestern to southeastern contrast is seen where stations in the Northwestern Caribbean show positive correlations to a strong ERS and weak LRS while stations in the Eastern Caribbean show positive correlations to a weak ERS and strong LRS. A meridional contrast for stations in PC3 is found as Northwestern Caribbean stations show positive correlations to an enhanced MSD and early-peaking LRS, while stations in lower latitudes show positive correlations to an absent MSD and late-peaking LRS.

This chapter then presents a detailed total moisture budget for the Caribbean by using the ERA-Interim Reanalysis from 1979 to 2012. The results in this chapter suggest three facilitators of moisture convergence that influence the seasonal cycle of rainfall in the Caribbean: the western flank of North Atlantic Subtropical High (NASH), the Eastern Pacific ITCZ, and the Atlantic ITCZ. In addition, two inhibitors of moisture are found to influence the seasonal cycle of rainfall in the Caribbean: mid-latitude transients from the continental United States, and the trade winds along the southern flank of NASH. The Atlantic Warm Pool (AWP) branch of the Western

Hemispheric Warm Pool (WHWP) and Caribbean Low-Level Jet (CLLJ) act as regional modifiers of moisture convergence in the Caribbean.

The Caribbean is categorized into five climate sub-regions based on the findings from the PCA and moisture budget analysis: Central Caribbean, Western Caribbean, Northwestern Caribbean, Central and Southern Lesser Antilles, and the Trinidad and Tobago and Guianas. A schematic (Fig. 2.8) is proposed to demonstrate the interactions of the main climatological features across these regions throughout the seasonal cycle evolution.

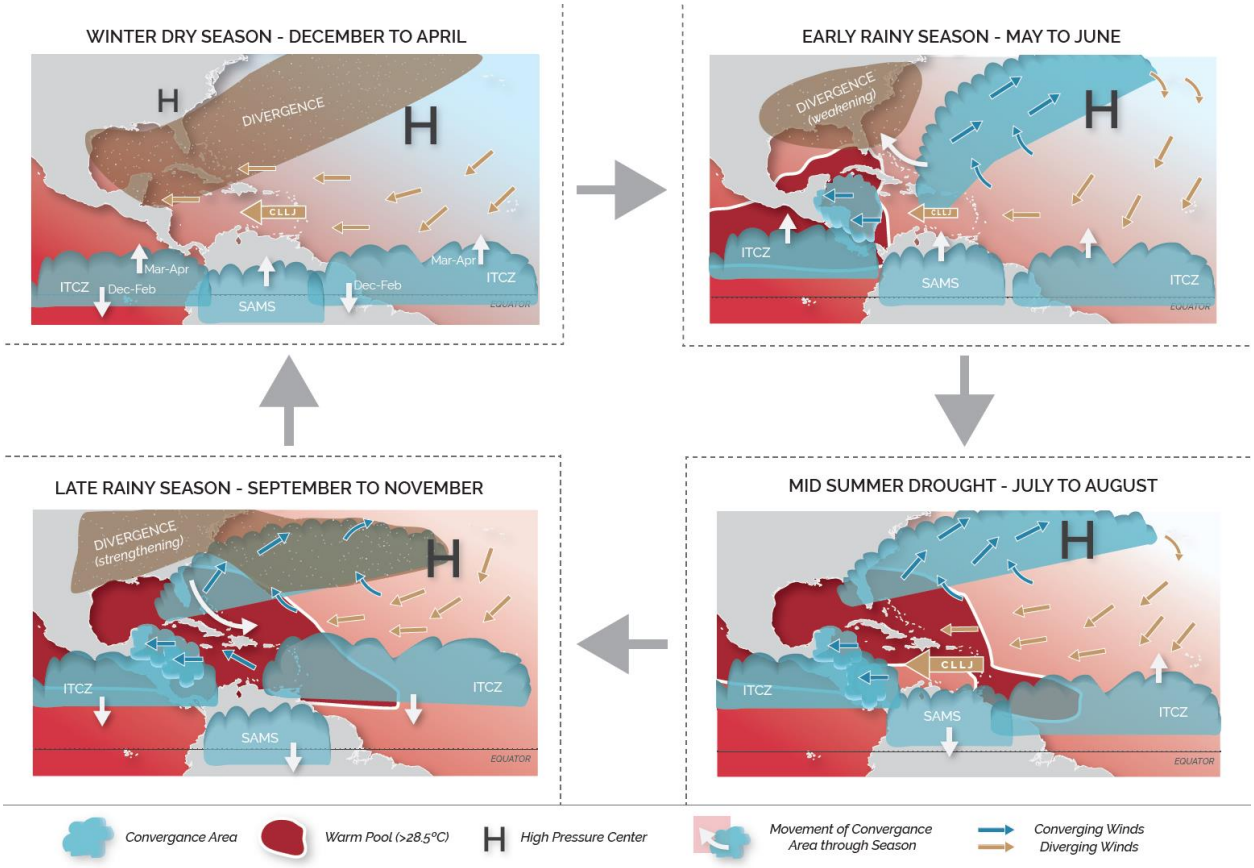

Figure 2.8: Schematic of the features associated with the seasonal cycle of rainfall over the Caribbean. Areas shaded in blue are the convergence bands. Areas in brown denote transient divergence. White arrows denote their movement during a given season. Shaded blue and brown arrows denote the convergent and divergent wind vectors, respectively. The large "H" denotes the North Atlantic Subtropical High. The small "H" denotes the continental High. The warm pool denotes SSTs greater than 28.5 °C is highlighted in maroon.

1. During the WDS, NASH influence on the Caribbean is strong. The North Atlantic anticyclone connects with the continental North American High and provides strong diverging trade winds and subsidence in the Caribbean. The WDS-CLLJ, an absence of the AWP, and strong mid-latitude features from the U.S. mainland enhance divergence in the Caribbean Sea, Caribbean, and Northwestern Caribbean, respectively. The southern flank of NASH expands southward as the ITCZ migrates southward. The southward migration of the Atlantic ITCZ draws moisture to South America (e.g., to the Guianas) during the beginning of the WDS.

2. During the transition into the ERS, the NASH breaks off from the dissipating continental High. As a result, the western flank of the high-pressure cell emerges and induces converging low-level southeasterly winds from the Caribbean Sea to the mid-latitudes which breaks the influence of the diverging trade winds and wintertime CLLJ and produces uplifting and rainfall. In addition, the Atlantic and Eastern Pacific ITCZ begins its northward migration. During the ERS, the western flank of NASH expands westward and brings excess rainfall over evaporation to the central and Northwestern Caribbean. The mid-latitude features over the continental U.S. and their divergence retreat northward. The Eastern Pacific ITCZ migrates northward and affects the Western Caribbean. The expanding western flank of NASH interacts with the northward migrating Eastern Pacific ITCZ to transport moisture to the Northwestern Caribbean through its shifting easterly to southeasterly winds. Simultaneously, the AWP emerges across the western Caribbean Sea and Gulf of Mexico and enhances the moisture convergence provided by the Eastern Pacific ITCZ and the western flank of NASH. The Atlantic ITCZ migrates into the Guianas and its absence, which is accompanied by strong divergent low-level trade winds from the

northward shifting southern flank of NASH, inhibits the ERS in the Lesser Antilles. The low-level trade winds re-intensify and re-infiltrate the Caribbean as NASH strengthens, which results in the MSD.

3. During the MSD, NASH expands westward and shifts northwestward. This cuts off moisture transport into the Caribbean as mass divergence and subsidence associated with the trade winds return. This causes an enhanced MSD in the Northwestern Caribbean. The Eastern Pacific ITCZ migrates northward into Central America and buffers the extent of the MSD in the Western Caribbean. The Atlantic ITCZ migrates into the Lesser Antilles. The U.S. mid-latitude features are absent. The AWP expands to all but the colder ocean waters of the North South American coastline, causes a strong meridional SST gradient in the Caribbean Sea, and enhances the NASH-SST feedback loop and resultant MSD-CLLJ. The CLLJ enhances divergence across the central and eastern Caribbean Sea and convergence in the Nicaraguan to Costa Rican coastlines of the Western Caribbean. The MSD transitions into the LRS as NASH begins its western flank contraction.

4. During the LRS, NASH contracts and its western flank migrates southeast. The Eastern Pacific ITCZ begins its southward migration and its interaction with the western flank of NASH returns as low-level southeasterly winds return across the Caribbean Sea. However, U.S. mainland mid-latitude features and its divergence rapidly shift southward and weaken the convergence on the western flank of NASH and its confluent interactions with the Eastern Pacific ITCZ. The Atlantic ITCZ reaches its northern most extent in the Lesser Antilles and begins its southward migration. The AWP, which is at its largest spatial coverage, begins to contract and enhances moisture convergence across the Caribbean. The CLLJ disappears as the combination of returning southeasterlies and warmer SSTs in the

central Caribbean Sea reduces the NASH-SST feedback loop. NASH continues to contract until the continental High emerges, which results in the dissipation of its western flank, intensification of the trade winds in the Caribbean Sea, and the beginning of the WDS.

The schematic provides several important insights addressing previous literature on the dynamical mechanisms of Caribbean rainfall. First, the structure of the ERS Caribbean Rain Belt (CRB) theorized by Allen and Mapes (2017), is similar to the ERS in Chapter 2 and appears to return during the LRS. Second, the pattern of the U.S transient divergence suggests the migration pattern of mid-latitude troughs in the Caribbean and continental U.S: gradual decline in its frequency during the ERS, and abrupt incline in its frequency during the LRS (DiMego et al. 1976). DiMego et al. (1976) also suggests that during the spring these features stall in the Caribbean, whereas in the fall they quickly pass through; therefore, the convergence bands in the Northwestern and Western Caribbean may be influenced by the stalling of convergence by the right flank of mid-latitude troughs, a notion similarly suggested in Allen and Mapes (2017). The greater frequency of mid-latitude features in the Caribbean during the LRS and WDS may explain why transient divergence infiltrates the Caribbean quickly, which is synonymous with subsidence behind cold surges (Reding 1992; Schultz et al. 1998; Giannini et al. 2000; Sáenz and Durán-Quesada 2015). Finally, tropical cyclones and easterly waves have marginal influences in the climatological Caribbean rainfall cycle, which is in contrast with several studies (Taylor et al. 2002; Herrera et al. 2015), and are not shown in the schematic.

The results from this chapter finds several distinctive characteristics in the Caribbean and Caribbean climate regions that are not seen in earlier Caribbean regional classification studies that use monthly or longer averaged datasets. For instance, the results find the Northwestern Caribbean to have a bimodal pattern with portions of the region having a prominent MSD, and most of the

Lesser Antilles to have a unimodal rainfall pattern. This differs from Jury et al. (2007) where they describe the Northwestern Caribbean as unimodal with bimodality increasing in magnitude from the Northwestern Caribbean to the Lesser Antilles. This also differs from Chen and Taylor (2002) and Giannini et al. (2000) who describe the entire Caribbean as having a bimodal rainfall pattern. Hence, the differences are likely due to longer time averages in previous studies which mask the sub-monthly rainfall transitions that this chapter finds. Overall, this chapter demonstrates the importance of using greater temporal resolution in order to distinguish rainfall characteristics in the Caribbean. Although it is apparent regional and large-scale dynamics are the major contributors of the rainfall cycle in the Caribbean, given the limited station data available in the region we cannot fully evaluate the role that the local forcings may play in the higher-resolution spatial detail of seasonal rainfall.

Finally, this chapter provides a framework for investigating the variability, change, and consequently, prediction of the rainfall cycle in the Caribbean. For example, the interannual variability of the Caribbean rainfall cycle is important for understanding the genesis of seasonal hydrometeorological disasters such as droughts and floods and how large-scale interannual phenomena, such as ENSO, influence rainfall in the region. Hence, the subsequent chapter applies the understanding of the seasonal climatology and dynamical mechanisms in the Caribbean in order to investigate the interannual variability of the rainfall cycle. Recent studies have found large-scale phenomena such as the Madden Julian Oscillation (MJO), a natural coupled ocean–atmosphere wave with a cycle of 30–90 days (Madden and Julian 1971), and the Atlantic Multidecadal Oscillation (AMO) to influence rainfall in the Caribbean at intraseasonal and multi-decadal timescales, respectively (Martin and Schumacher, 2011; Stephenson et al. 2014). The work from this chapter could be utilized to investigate the behavior of the Caribbean rainfall cycle

under intraseasonal, decadal, and multi-decadal time scales, and the role large-scale phenomena such as the MJO and AMO influence the cycle. Understanding how the observed dynamical mechanisms and regional rainfall characteristics change under future climate is significant for future climate mitigation and adaptation practices, agricultural planning, and decision making. Modeling studies that investigate rainfall and climate dynamics in the Caribbean would benefit from this work, by understanding how well models simulate the underlying regional characteristics and dynamical mechanisms of the climatological rainfall cycle, and deduce the extent natural precipitation variability versus climate change are affecting rainfall in the region. Consequently, the benefits of utilizing this chapter to improve the understanding of the variability and change of rainfall in the Caribbean, advances the overarching goal of better predicting the Caribbean rainfall cycle.

Chapter 3: Interannual Variability of the Early and Late-Rainy Seasons in the Caribbean

Note: A modified version of this chapter has been published in Climate Dynamics (2020)[2]

3.1 Introduction

The contributions from the large-scale atmospheric circulation are documented for the annual cycle of rainfall in the Caribbean (Chapter 2). A natural assumption may be that the year-to-year variability of Caribbean rainfall is governed by variability in those same elements. But what are the large-scale climate modes of variability that may have a significant impact on the SSTs, NASH, the CLLJ, and the regional ITCZ? One can also ask whether the dominant modes of variability impacting the Caribbean change with season, and if so if the interannual variability of the ERS is linked to that of the LRS? While climatologically, the local influences of the NASH, the trade winds, and the ITCZ vary by region, their interannual variability occurs largely in concert, such that a strengthened NASH and enhanced trade winds are connected and both are associated with a southern displacement of the ITCZ, and vice versa (Giannini et al. 2001b; Wang 2007; Hidalgo et al. 2015). It stands to reason that although the Caribbean rainfall regions do experience different governing mechanisms, climatologically, the interannual variations of the mechanisms affecting interannual variability are in sync and that nearly the entire Caribbean experiences anomalous wetness or dryness during each rainy season. An important exception may be the Northwestern Caribbean, as a recent study found that in many years when droughts were pervasive throughout most of the Caribbean, drought was not experienced in Southern Florida, the Bahamas, and Cuba; a similar spatial pattern of impact was found in Caribbean pluvial years (Herrera and

[2]Martinez, C., Kushnir, Y., Goddard, L., Ting M., 2020: Interannual variability of the early and late-rainy seasons in the Caribbean. Clim Dyn 55, 1563–1583 https://doi.org/10.1007/s00382-020-05341-z

Ault 2017). Hence, one may ask how uniform is the interannual variability of the ERS and LRS over the Caribbean?

Several studies have attributed the interannual variability of the Caribbean to two large-scale climate modes of variability: The El Niño–Southern Oscillation (ENSO) and the North Atlantic Oscillation (NAO). In the Caribbean, ENSO was found to affect both the ERS (Giannini et al. 2000, 2001c; Chen and Taylor 2002; Taylor et al. 2002; Gouirand et al. 2012), during boreal spring, when ENSO events end, and the LRS during boreal fall when events are mature (Giannini et al. 2000, 2001c; Taylor et al. 2002; Spence et al. 2004; Wang et al. 2008; Rodriguez-Vera et al. 2019)., Other studies found no significant correlation between ENSO and rainfall in the Central and Eastern Caribbean (Chen and Taylor 2002; Malmgren et al. 1998; Torres-Valcárcel, 2018; Hernández Ayala 2019) and showed instead that in those regions, rainfall is highly correlated with the NAO (Malmgren et al. 1998; Giannini et al. 2001c; Gouirand et al. 2012; Mote et al. 2017). The NAO, which exhibits peak variability in the boreal winter months, affects the Hadley Circulation and corresponding NASH (Wang 2001), SSTs in the tropical North Atlantic region (TNA) (Bjerknes 1964; Kushnir 1994; Seager et al. 2000; Hurrell et al. 2003; Kushnir et al. 2006) and consequently rainfall, during the Caribbean ERS (George and Saunders 2001; Giannini et al. 2001c; Rodriguez-Vera et al. 2019).

The literature varies on how and what large-scale climate drivers affect the Caribbean, because most Caribbean-wide papers looked only at ENSO (Giannini et al. 2000; Chen and Taylor 2002; Taylor et al. 2002; Spence et al. 2004 Wang et al. 2008) or NAO (George and Saunders 2001). Recent papers that have considered both ENSO and NAO only focused on a specific region of the Caribbean (Gouirand et al. 2012; Mote et al. 2017; Torres-Valcárcel 2018; Hernández Ayala 2019). Only a handful of studies investigated both ENSO and NAO across the entire Caribbean

(Giannini et al. 2001a, b, c; Rodriguez-Vera et al. 2019), yet they stop short of translating how these large-scale drivers affect the dynamical processes that affect each Caribbean sub-region found in Chapter 2. In addition, numerous studies investigating the interannual variability of rainfall in the Caribbean use less-resolved temporal resolutions of the ERS and LRS (e.g., bi-monthly or seasonal averages) that can mask their temporal and spatial evolutions (Malmgren et al. 1998; Giannini et al. 2000, 2001a, b, c; Chen and Taylor 2002; Spence et al. 2004; Taylor et al. 2002; Wang et al. 2008; Gouirand et al. 2012; Torres-Valcárcel 2018; Hernández Ayala 2019). In Chapter 2, the temporal resolutions used were pentad and monthly averages, and the results show that the ERS and LRS have within-season temporal and spatial evolutions between their early and late phases.

Chapter 3 seeks to identify the processes governing the interannual variability of rainfall during the different phases of the annual cycle across the Caribbean. Temporal and spatial composites of wet and dry years in the Caribbean provide insight towards answering the following questions:

1. What large-scale climate drivers govern the interannual variability of Caribbean rainfall, how do they change throughout the rainy seasons, and how do they relate to the large-scale drivers that govern the climatology?
2. Is there a dependency between the variability experienced in the ERS and LRS that may impart longer lead-time for prediction?

Chapter 3 is framed such that the interannual variability of rainfall is investigated for the Caribbean as a whole, but sub-regional deviations are also examined.

Chapter 3 is structured as follows. Section 3.2 and 3.3 describes the data and methods used, respectively. Section 3.4.1 looks at and discusses the homogeneity of the interannual variability of

the ERS and LRS in the Caribbean. Sections 3.4.2 and 3.4.3 look at and discuss the spatial composites of climate variables pertinent to interannual variability in the Caribbean rainfall cycle during the ERS and LRS, respectively. Section 3.4.3 investigates the independence of the ERS and LRS variability. The summary of the results and its implications and concluding remarks are found in Section 3.5.

3.2 Data

The daily station rainfall dataset described in Chapter 2, Section 2, is utilized here to investigate the interannual rainfall cycle. A total of 38 stations are found; however, only 34 stations are used for this study as stations in the Guianas have a lagged rainfall cycle from the rest of the Caribbean (Chapter 2) that would skew the analysis. Station information can be found in Table 2.1.

To document the dynamically-relevant background state of the seasonal rainfall cycle and its variability, the 1854–2018 2° gridded NOAA v5 Extended Reconstructed Sea Surface Temperature (Huang et al. 2017) and 1949–2018 2.5° NCEP/NCAR reanalysis (Kalnay et al. 1996) datasets are used for gridded SST, and sea level pressure (SLP), respectively. For this study we use a monthly temporal resolution from 1960–2016.

Indices for NAO and ENSO are obtained from the NOAA Climate Prediction Center. The NAO Index is derived from a rotated principal component analysis of monthly SLP anomalies (Barnston and Livezey 1987). The index can be found here: https://www.cpc.ncep.noaa.gov/products/precip/CWlink/pna/nao.shtml. The ENSO Index is the Extended NINO3.4 Index (Huang et al. 2017). The index can be found here: https://www.cpc.ncep.noaa.gov/data/indices/. For both indices a monthly temporal resolution is used from 1960–2016.

For moisture budget analysis, this study uses the European Centre for Medium-Range Weather Forecasts Interim Re-Analysis (ERA-Interim; Dee et al. 2011) to examine interannual changes in the regional moisture budget. The ERA-Interim is used at a 6-hourly temporal resolution from 1979 to 2016, at 26-pressure levels, and a 1.5° by 1.5° spatial resolution. For further details on the moisture budget calculation please refer to Seager and Henderson (2013) and to Section 2.3.2 of Chapter 2.

3.3 Methods

3.3.1 Quantifying Rainy Seasons

Given the high-frequency noise in daily data, pentad (5-day) averages of daily rainfall observations were calculated for each station. Using similar criteria as Hamada et al. (2002), if a pentad has two or more days of missing data, the pentad was omitted. If a pentad was missing or omitted within the rainfall season, the entire analysis year was omitted for that station. A general definition of the rainfall season is used: from the 17th pentad of the year (centered on March 24th) to the 67th (centered on November 30th). This is done in order to address the different temporal characteristics found in each sub-region (Chapter 2). For each station, averages of the ERS precipitation are calculated for every year (from the 21st pentad of the year—centered on April 13th—to the 34th or June 17th). For every year, each station's seasonal-averaged ERS is subtracted from their long-term climatology. The same procedure is done to calculate the seasonal-averaged LRS anomalies (pentads numbered 46 or August 16th to 64 or November 14th relative to the first pentad of the year). Yearly Caribbean-wide ERS and LRS anomalies are calculated by averaging the 34 station's ERS and LRS anomalies.

3.3.2 Uniformity of Caribbean and Dynamical Spatial Composites

Caribbean-wide composites are determined as the theorized large-scale phenomena that influence the dynamical mechanisms in the Caribbean encompass the entire region. Each station's ERS pentads and LRS pentads were summed for each year to obtain the total ERS and LRS rainfall for that year. The data for each station's ERS and LRS totals were ranked from driest to wettest. The years with rainfall below the 33rd percentile and above the 66th percentile for a given ERS or LRS are designated as the stations' dry ERS/LRS and wet ERS/LRS year, respectively. If a year is designated as a dry ERS or LRS for at least 15 of the 34 stations, regardless of the station's location, the year was designated as a Caribbean ERS or LRS dry year. A similar procedure was applied for classifying Caribbean ERS and LRS wet years. Using the regional classifications from Chapter 2 a cross check was done to make sure that a dense station network in a specific part of the Caribbean was not dominating the rainy season variability analysis. Only two years were omitted from the data filtering (dry LRS, 1986; wet ERS, 1992) as they did not satisfy the cross check. Anomalies of rainfall for the Caribbean ERS and LRS dry and wet years were calculated as percent-normal. The Caribbean-wide composite years are shown in Table 3.1.

Table 3.1: Dry and Wet ERS, and LRS years. Years only in bold denote years where the ERS and LRS are the same. Years bolded, italicized and underlined denote years where the ERS and LRS are opposite. Years with asterisk are years not in the mean flow moisture budget ERA-Interim reanalysis.

Dry		Wet	
ERS	LRS	ERS	LRS
1967*	1976*	1969*	**1979**
1973*	***1981***	**1979**	1984
1974*	***1983***	***1981***	***1985***
1975*	1987	***1983***	1988
1985	**1991**	***1986***	1996
1989	1992	2004	1998
1991	**1997**	**2005**	***1999***
1994	2002	***2009***	**2005**
1997	***2009***	**2010**	***2008***

1999 2001 ***2008*** 2014 **2015**	***2012*** **2015**	**2011** ***2012*** 2013	**2010** **2011**

Using the years designated for composting (Table 3.1), spatial composites from detrended (over 1960–2016) ERS and LRS wet and dry years were created for SST and SLP over the 180°W to 15°E; 20°S to 75°N domain. The ERS and LRS wet and dry years were also calculated for moisture transport and convergence over the 120°W to 15°W; 4.5°S to 75°N domain. Anomalies between the composite and the climatology were calculated. A two-sample t test is conducted in order to investigate statistical significance at the 90th confidence level.

3.4 Results and Discussion

3.4.1 Uniformity of Caribbean Interannual Variability

Most of the Caribbean experiences anomalous dry or wet conditions at the same time, as evidenced in the rainfall anomalies in percent-normal for the composite dry and wet ERS (Fig. 3.1a, b) and dry and wet LRS (Fig. 3.1c, d). In Fig. 3.1, the composites during both dry and wet ERS and LRS, respectively, show the magnitude of the anomalies in the Northwestern Caribbean to be weaker than the rest of the Caribbean. In particular, during some years of the composite (not shown) certain stations in the Northwestern Caribbean experienced the opposite signal to the rest of the Caribbean. This is expected, as several studies found similar results in their analyses (Giannini et al. 2001b; Chen and Taylor 2002; Spence et al. 2004; Herrera and Ault 2017). Finally, the Central and Lesser Antilles have the largest percent anomalies in comparison to the rest of the Caribbean in the ERS (Fig. 3.1a, b). As a whole, the composites capture the largely uniform dryness or wetness across the Caribbean well. However, the differences seen between the Northwestern Caribbean and the rest of the Caribbean, and the large rainfall anomalies in the

Central and Lesser Antilles hint that the set of dynamical processes that correspond to each sub-region are being affected differently than each other.

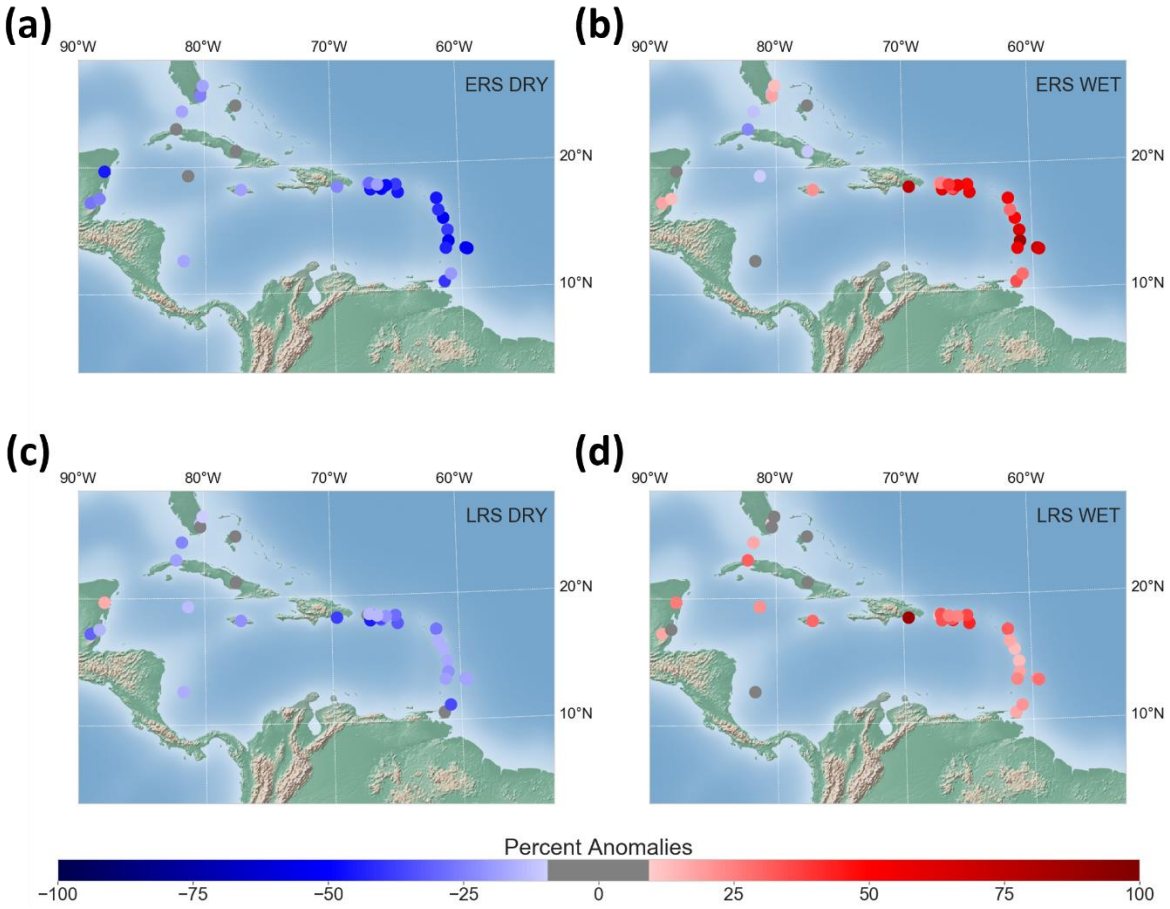

Figure 3.1: Wet and Dry ERS (top) and LRS (bottom) composite mean percent anomalies for each station. Blues denote negative departures from each station's climatological ERS and LRS. Reds denote positive departures from each station's climatological ERS and LRS. Grey denotes percent anomalies between −10 to 10% of the mean seasonal value

3.4.2 Relationship between ERS and ENSO/NAO

There is a tripolar SST pattern in the North Atlantic Basin, including the Caribbean Sea, in the dry minus wet ERS years during the Winter Dry Season (WDS; December to April; Fig. 3.2a). The SST tripole exhibits a large tongue of colder than normal SSTs across the southern flank of the TNA and Caribbean Sea. To the north, there is a warm tongue across portions of the

Northwestern Caribbean, Gulf of Mexico, and northern edge of the TNA. The northern part of the tripole consists of another cold SST center in the subpolar gyre region. Centered over the North Atlantic subtropical region and extending into the TNA and Caribbean Sea during the WDS is a large anomalous, positive SLP region (Fig. 3.2f). Meanwhile areas across Greenland and Iceland show large anomalous negative SLPs (Fig. 3.2f). In the equatorial Eastern Pacific, anomalous negative SSTs and positive SLPs are seen during the preceding WDS, but these weaken and become non-significant by May and throughout the rest of the year. In May, the southern TNA and Caribbean Sea cold SSTs intensify and the warm, northern TNA SST tongue shrinks and weakens (Fig. 3.2b). Warm SSTs emerge over the Gulf of Guinea and the Benguela Current region along the coast of South Africa. Of the SLP WDS dipole, the only significant remnant by May is a region of anomalously positive SLP in the southwestern TNA and the Caribbean (Fig. 3.2g). This anomalous SLP center roughly overlaps the region of negative SST anomalies of this month. By June, the warm SST signal in the northern flank of the TNA diminishes and is no longer significant, while the cold SST signal in the southern TNA/Caribbean Sea and warm SST signal along western South Africa persists (Fig. 3.2c). In addition, the region of significant positive SLP anomalies contracts further into the western and Northwestern Caribbean while the rest of the North Atlantic does not display any large, coherent significant anomalies. The South Atlantic shows some anomalous negative SLP anomalies. Following the ERS, the Caribbean Sea cold SSTs weaken but remain significant for the MSD (Fig. 3,2d; July–August) and LRS (Fig. 3.2e; September–November). The South African coast warm SST signal weakens by the MSD and becomes non-significant by the LRS.

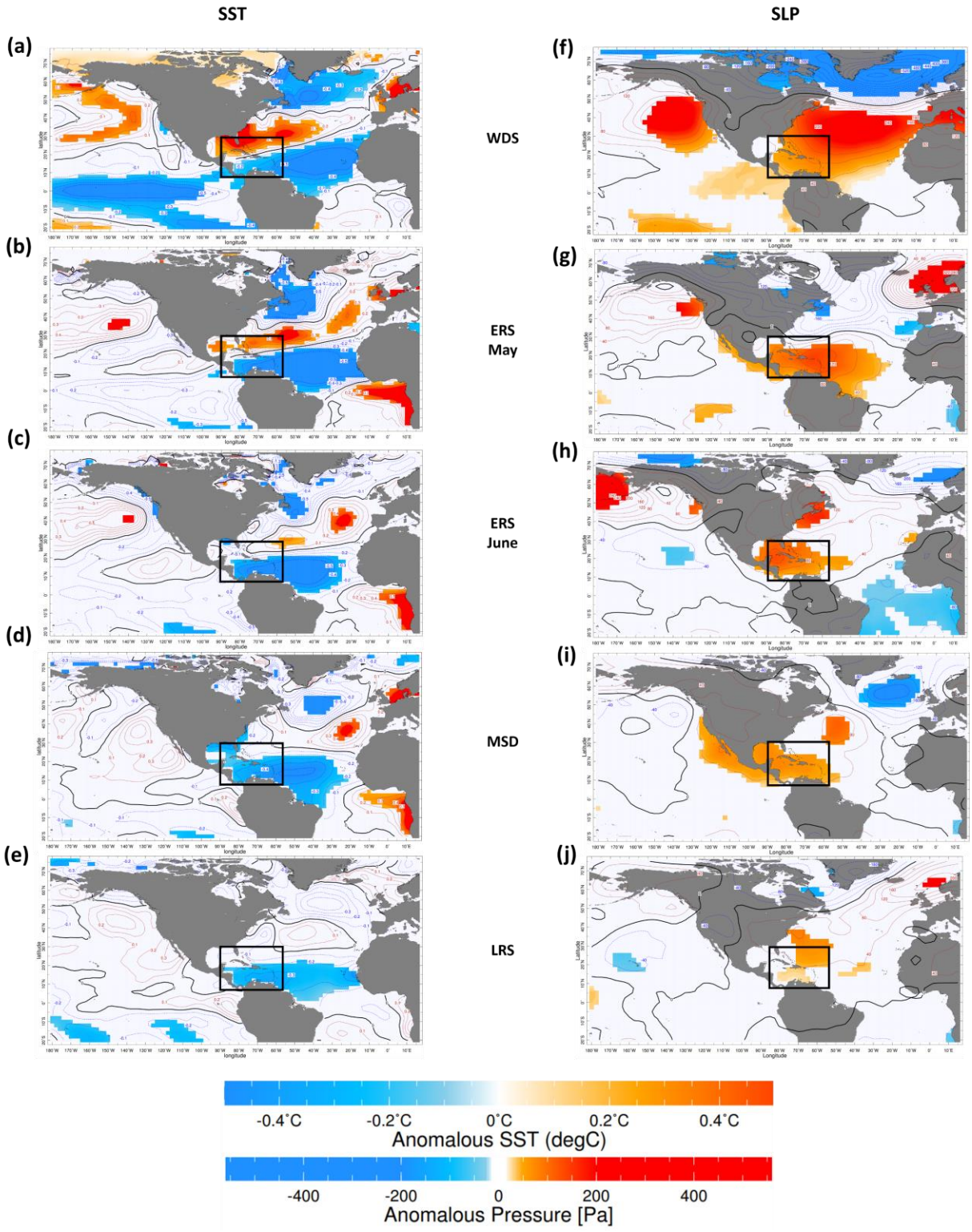

Figure 3.2: Early rainy season dry-year minus wet-year SST (left) and SLP (right) composite anomalies for Dec-Apr WDS (a, f), ERS (b, c, g, h), Jul–Aug MSD (d, i), and Sep–

Nov LRS (e, j). Black box indicates the Caribbean domain. Contours are the anomalous SSTs and SLPs with colors denoting significance at 90% according to a two-sample t-test

Anomalously positive SLPs (Fig. 3.2i) remain in the Caribbean during the MSD; however, the magnitude of anomalous SLP decreases as significant values are seen only in the Caribbean Sea and the Gulf of Mexico and along the Central American, Eastern Pacific coastlines. By the LRS there are little to no statistically significant SLP anomalies in the Caribbean (Fig. 3.2j) or the rest of the North Atlantic.

The spatial patterns of both the SST and SLP anomalies during the WDS implicates the WDS NAO in affecting dry and wet ERS anomalies in the Caribbean region. To quantify the relationship, lagged-correlations between the NAO index with the Caribbean averaged ERS rainfall anomalies are calculated, with the NAO index moving through every overlapping three-month season, starting from the November of the previous year and ending in the following year's February. There is a moderate, negative correlation between the preceding winter NAO and the ERS rainfall (Fig. 3.3a), with the DJF and JFM correlations at -0.316 and -0.342, respectively, and significant at the 1% level (assuming that yearly values are independent of one another). A similar calculation is performed using an index for ENSO (Fig. 3.3a) and with the exception of MAM (-0.287 at 95th significance), ENSO exhibits elevated, but not significant, correlations during the WDS and early spring. Therefore, of the two phenomena being examined, the NAO seems to be the most relevant climate mode that impacts the ERS rainfall variability. We will return to discuss the possible role of ENSO in the ERS below.

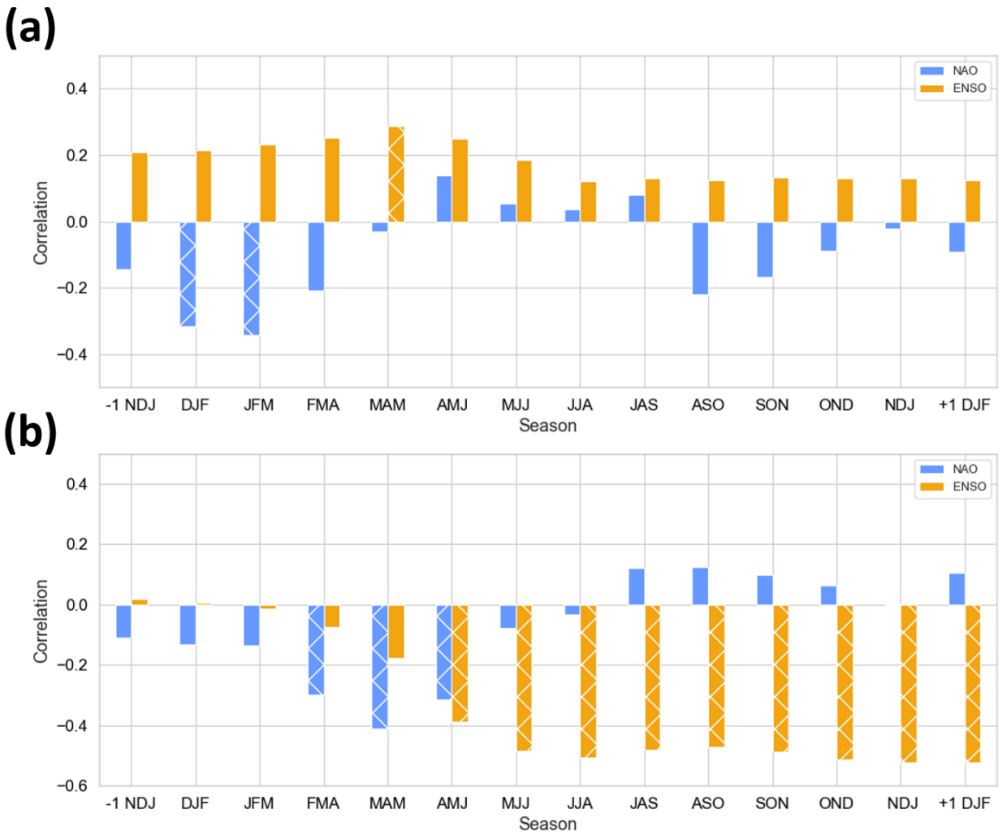

Figure 3.3: Correlations between seasonal means of NAO (blue) and ENSO (orange) and Caribbean-wide anomalous ERS (top) and LRS (bottom). Hatching denotes significance at the 95th confidence interval level

During the WDS with a positive NAO phase, the Hadley Circulation (Wang 2001) and NASH intensify and cause enhanced trade winds and westerlies, south and north of the anticyclone center, respectively. The observed (Fig. 3.2) ocean surface temperature response to the positive winter NAO phase is consistent with numerous previous studies (e.g., Cayan 1992; Seager et al. 2000; Chiang and Vimont 2004; Czaja et al. 2002; Kushnir et al. 2002; Marshall et al. 2001; Gouirand et al. 2012). In the Gulf of Mexico and Northwestern Caribbean the warm SST signal falls within a region where, in the climatology, westerlies are found during the WDS (Chapter 2). The intensified NASH blocks the intrusion of cold, dry continental air from North America into the northwest Caribbean during the WDS and the SST there respond with anomalous warming

(Reding 1992; Schultz et al. 1998; Giannini et al. 2000; Seager et al. 2000; Sáenz and Durán-Quesada 2015; Chapter 2).

By the time of ERS, the NAO is typically not very strong (Kushnir et al. 2006), and there are no significant correlations between spring-time SLP or the NAO indices and ERS anomalies (Fig. 3.3a). However, it is evident that the previous winter NAO induces a SST signal in the Caribbean, which persists during the ERS. This is similarly suggested in previous studies (Giannini et al. 2000, 2001a; Hu et al. 2011), and can be explained by the wind, evaporation, and SST feedback (WES; Xie and Philander 1994; Chang et al. 1997). Under a positive NAO phase, the SST gradient between the cold SST signal in the Caribbean Sea and the warm SST signal across the Northwestern Caribbean and central TNA produces a localized meridional SLP gradient that intensifies the trades across the Caribbean Sea, enhancing the release of latent heat thus continuing the cold SST signal. The northern Caribbean warm SST signal does not persist as long as its cold SST counterpart, which seems to explain the rainfall suppression in the region (see more below). In the climatology, the westerlies seen in the Gulf of Mexico/Northwestern Caribbean and central TNA during the WDS migrate northward during the ERS (Chapter 2); therefore, the enhanced easterlies would weaken the westerly-induced warm SST signals in both the Gulf of Mexico/Northwestern Caribbean, and the central TNA. The climatological AWP, which initializes during the ERS, strengthens in the Gulf of Mexico and Northwestern Caribbean due to the persistence of the anomalous warm SSTs created in the earlier season. However, in the Caribbean Sea, the AWP would weaken as a consequence of enhanced coastal upwelling and the SST cold signal in the Caribbean Sea. The SST and SLP patterns demonstrate that the NAO-SST/SLP persistent signal decays by the MSD and disappears by the LRS.

The NAO-SST/SLP persistent signal affects the moisture flow and convergence pattern in the Caribbean during the ERS. The mean flow component of the moisture budget dominates the climatology of the Caribbean rainfall cycle (Chapter 2). The mean flow component further breaks down into its mass convergence and moisture advection sub-components. Following Chapter 2, where mass convergence was shown to dominate the total mean moisture convergence, we examine here only the mass convergence term (Fig. 3.4).

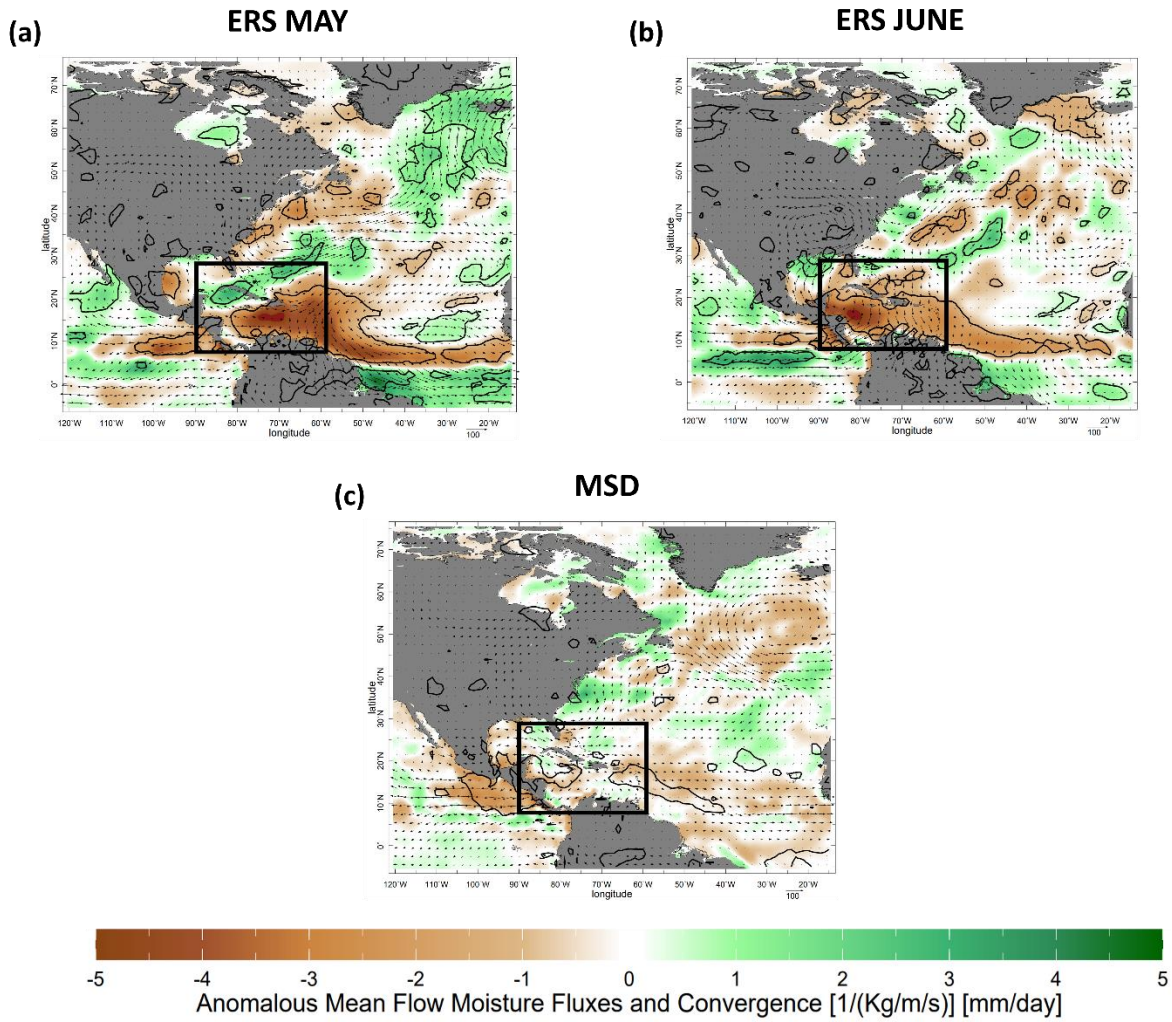

Figure 3.4: Early rainy season dry-year minus wet-year mass convergence (colors) and fluxes (vectors) composite anomalies for ERS (a, b) and Jul–Aug MSD (c). Black box indicates the Caribbean domain. Contours denote significance at the 90% according to a two-sample t-test

The mass convergence composites are mostly consistent with the anomalous SLP composites and support what has been suggested about the changing wind-field across the Caribbean during the dry–wet ERS year. There appears to be some discrepancy between the mean flow transport composite (Fig. 3.4) and SLP composite (Fig. 3.2); however, the corresponding surface winds composites (not shown) justify the anomalous circulation patterns implied in the SLP composites. The dry minus wet composites show an anomalous anticyclonic circulation in the TNA with enhanced easterlies across the Caribbean during the WDS (not shown). In May, the anomalous anticyclonic flow in the composite dry–wet year differences is centered over the western TNA and Caribbean Sea (Fig. 3.4a). On the southeastern flank of the anomalous anticyclonic circulation, anomalous moisture divergence is found with anomalous, northerly flow, across the Caribbean Sea and southern TNA. In the May climatology, an anticyclonic circulation dominates over the southwestern TNA associated with the western flank of NASH. This, in turn, is associated with moisture divergence west of the Lesser Antilles and a convergence band over the Central Caribbean (Fig. 2.3e). The anomalous circulation in dry–wet Mays expands NASH, stretching its western flank further into the Caribbean Sea and enhancing the climatological divergence seen in the Caribbean Sea. This would weaken the climatological southeasterlies in the Caribbean Sea and along the Central American coast, and as a result enhance the CLLJ. The enhancement of the CLLJ would enhance divergence in all but the Nicaragua to Costa Rican coastline, as this coastline climatologically experiences zonal convergence from the CLLJ (Hidalgo et al. 2015; Chapter 2). This explains why there is little to no anomalous divergence across this portion of the Western Caribbean (Fig. 3.4). Simultaneously, the band of climatological convergence in the Central Caribbean shifts to the northwest, causing the Northwestern Caribbean and Central Caribbean to receive anomalous convergence and divergence, respectively. The resulting shift in the

convergence band explains how this analysis (Fig. 3.1a) and others (e.g., Jury et al. 2007; Allen and Mapes 2017; Herrera and Ault 2017) find a weakened dry signal or in some cases an anomalous wet signal in the Northwestern Caribbean while the rest of the Caribbean experienced dryness during the ERS.

In June (Fig. 3.4b), the dry–wet year anomalous anticyclonic circulation cell shifts westward and northwestward to affect the entire Caribbean Island chain. As a result, anomalous northerly flow and divergence is seen across the entire Caribbean. The anomalous flow is associated with a weakened western flank of NASH convergence band and a more easterly flow across the Caribbean Sea and Northwestern Caribbean, where southeasterlies are seen in the June mean-flow climatology (Fig. 2.3f). The anomalous northerly-northeasterly flow over the Caribbean Sea and southern Central America turns easterly in the Eastern Pacific and a weak divergence-convergence dipole in the Eastern Pacific marks the southern displacement of the ITCZ convergence band there, as is the case in the equatorial Atlantic. This is consistent with how a strengthened CLLJ has been associated with a southward displacement of the Eastern Pacific ITCZ (Hidalgo et al. 2015). The southern displacement of the Atlantic ITCZ explains why the Central and Southern Lesser Antilles have the largest change in percent rainfall anomalies during dry ERS years than any other region (Fig. 3.1a). Unlike other regions, the Central and Southern Lesser Antilles have only one main facilitator of moisture convergence, the Atlantic ITCZ (Chapter 2); therefore, any changes with the Atlantic ITCZ would significantly affect rainfall in the region. The advection of specific humidity enhances dryness across the Caribbean Sea especially in dry minus wet June's and over the Western Caribbean and Central America (not shown) as a result of the Caribbean Sea to Eastern Pacific anomalous flow. The changes described in the paragraph above

occur following a winter with a positive NAO anomaly. The opposite changes occur after a winter with a negative NAO phase and the consequent WES feedback.

The anomalous patterns weaken in the Caribbean by the MSD (Fig. 3.4c) as the anomalous circulations shift unto Central America, weakly impacting convergence in the Western Caribbean. Some significant anomalous divergence is found across portions of the Lesser Antilles. By the LRS non-significant anomalous flow and convergence are found in the Caribbean (not shown). The lack of changes in the moisture budget and transport in the MSD and LRS further support the suggestion that the NAO-SST persistence signal only weakly affects the MSD and LRS.

As indicated above, this study finds (Fig. 3.3a) a weak connection between the ERS and the mature/post-mature phase of ENSO during the winter preceding the ERS. This connection is consistent with previous studies (Giannini et al. 2000, 2001c; Chen and Taylor, 2002; Taylor et al. 2002; Hu et al. 2011; Gouirand et al. 2012), however, as we describe below, the role of ENSO appears secondary to that of the NAO. The SST and SLP signal in the Eastern Pacific are reminiscent of the winter footprint of a mature ENSO phase from the previous calendar year (Fig. 3.2a, f) and are indicating the presence of a La-Niña state in the winter preceding a dry ERS. The relationship is weak given the weak ENSO-ERS correlations, similarly to that found in some previous studies (Malmgren et al. 1998; Jury et al. 2007; Torres-Valcárcel 2018). A simple way to evaluate the relative roles of the NAO and ENSO in the ERS is by using Kendall's Tau (τ), a non-parametric rank correlation coefficient, which takes into consideration issues such as outliers, and the non-gaussian distribution of rainfall. Here, Kendall τ is used to determine the association between the indices of each climate driver and the ERS anomalies in the Caribbean. DJF and JFM NAO with ERS anomalies produce a Kendall τ of 0.182 and 0.201, respectively, which indicates a constructive non-trivial role for the NAO. DJF and JFM ENSO with ERS anomalies produce a

Kendall τ of 0.155 and 0.170, respectively, also indicative of a constructive, albeit weaker role. When DJF NAO and DJF ENSO are combined, they produce a Kendall τ of 0.208, indicating that there is added value in accounting for the state of ENSO in ERS variability. However, JFM NAO and JFM ENSO combined produce a value of 0.195, less than the association with NAO alone, signifying that JFM ENSO does not play a supporting role to the NAO in the late winter. This ENSO supporting role is likely due to the effects post-mature ENSOs have on springtime SSTs in the tropical Atlantic. In this case, the aftermath of a cold phase of ENSO is linked with a wintertime negative Pacific-North-American (PNA) teleconnection pattern, with a high-pressure anomaly over the TNA, which enhances the trade winds, and consequently decreases TNA SSTs. (Wang 2001). Under a positive NAO phase, this enhances the local NAO impact on TNA SSTs and its persistence onto the ERS. Under a negative NAO phase, this dampens the local NAO impact on TNA SSTs and its persistence onto the ERS.

Finally, the weak to moderate correlations of NAO/ENSO and ERS variability may suggest that other climate drivers are affecting ERS variability. However, there are no other regions outside of the Eastern Pacific and Atlantic basins in the global spatial composites of the ERS (not shown) that show significant SST or SLP anomalies, which suggests there are no other climate drivers inducing the SST or SLP signal over the Atlantic. The weaker correlations between the climate drivers and ERS variability is likely due to the existing incoherence seen between the Northwestern Caribbean and the rest of the Caribbean. Although the entire Caribbean experiences the same climate driver, its effects on the Northwestern Caribbean during portions of the ERS are opposite to the rest of the Caribbean. Therefore, the ERS regional average may reflect this, and result in lower correlations. Furthermore, the SST and SLP composites (Fig. 3.2a–d, f–i) in the equatorial Atlantic is similar to the Atlantic Meridional Mode (AMM) a non-ENSO coupled

ocean/atmosphere variability in the Atlantic basin (Servain 1991), of which has been found to be forced by the NAO (Chiang and Vimont 2004). This further suggests that the TNA SST signal is induced by the NAO.

3.4.3 Relationship between LRS and ENSO/NAO

Unlike dry minus wet composite ERS years, dry minus wet composite LRS years (Fig. 3.5a–f) display a strong SST signal in the Eastern Pacific and a less pronounced signal in the Atlantic. During the preceding WDS, a weak SST tripole is found in the North Atlantic, somewhat reminiscent of the tripole found during the WDS during dry minus wet ERS years (compare Fig. 3.5a to Fig. 3.2a). SLPs during the WDS show an anomalous dipole pattern in the extratropical North Atlantic. Specifically, there are anomalous positive SLPs centered between 45°N and 50°N and anomalous negative SLPs over Greenland and Iceland (Fig. 3.5g). There are negative SSTs and positive SLPs over the South Atlantic, and in the Equatorial Pacific the opposite is found. Although there is little significance in the anomalous SSTs or SLPs in the Caribbean during the WDS, and there are no significant correlations between wintertime ENSO and NAO with anomalies of the LRS (Fig. 3.3b), the spatial pattern in the North Atlantic looks somewhat reminiscent of the NAO. This may be due to how some wet and dry LRS years coincide with wet and dry ERS years (Table 3.1).

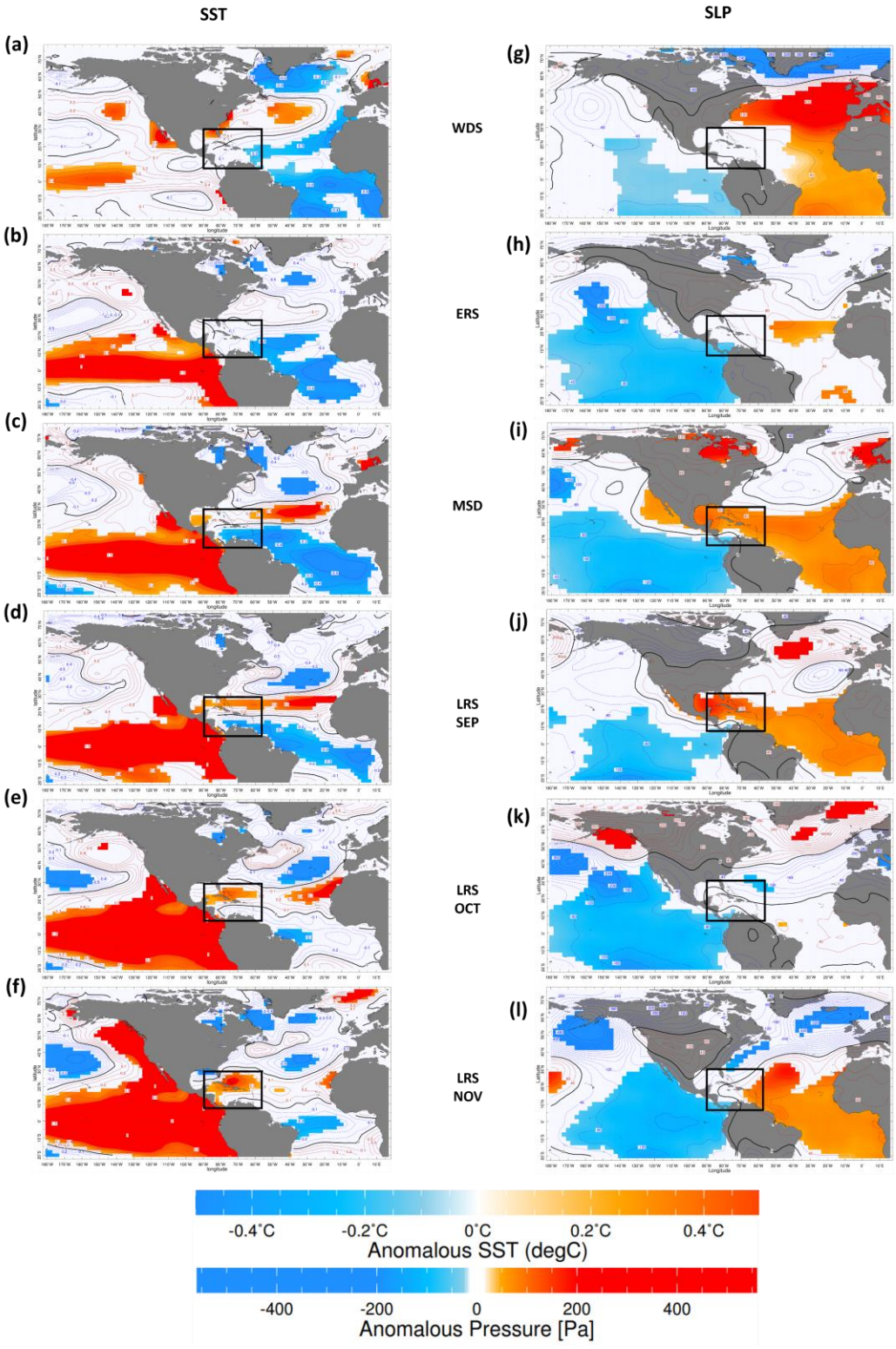

Figure 3.5: Late rainy season dry-year minus wet-year SST composite anomalies for Dec-Apr WDS (a, g), May–June ERS (b, h), Jul–Aug MSD (c, i), and LRS (d–f, j–l). Black box

indicates the Caribbean domain. Contours are the anomalous SSTs with colors denoting significance at 90% according to a two-sample t-test

During the ERS for dry minus wet LRS years, the North Atlantic SST (Fig. 3.5b) and SLP (Fig. 3.5h) pattern disappears. The sole significant residual in the North Atlantic is an anomalous cold SST band in the equatorial Atlantic. In the Eastern Pacific, anomalous and significant warm SSTs (Fig. 3.5b) and a negative SLP anomaly (Fig. 3.5h) emerge. During the preceding MSD (Fig. 3.5c), the Eastern Pacific SST anomalous signal strengthens as does the equatorial Atlantic anomalous cold SST signal, which now extends into the Caribbean Sea. In the northern TNA, a significant signal of warm SSTs emerges. A tongue of positive SLP stretching from the South Atlantic to the Gulf of Mexico is seen while in the Eastern Pacific a negative SLP anomaly persists (Fig. 3.5i). The spatial Eastern Pacific-Caribbean dipole of SLPs and SSTs during the ERS and MSD in the Eastern Pacific are consistent with an El Niño state. ENSO indices during the late-spring and summertime are significantly and negatively correlated with Caribbean-averaged LRS anomalies (Fig. 3.3b) at the 99% confidence level, suggesting that El Niño (La Niña) is associated with the LRS dry (wet) conditions. In response to the emerging El Niño, a cold SST anomaly and an anomalous high-pressure anomaly form over the Tropical Atlantic (Curtis and Hastenrath 1995; Poveda and Mesa 1997) through an ENSO atmospheric bridge (Giannini et al. 2000). In the early summer, during warm events, the anomalous anticyclonic circulation across the Caribbean Basin results in enhanced trade winds across the southern TNA and Caribbean Sea and weakened trade winds across the northern TNA and north of the Caribbean Sea. The latter results in a warm SST band via weakened air-sea fluxes. The anomalous wind flow in the southern TNA funnels through Central America and onto the Eastern Pacific Basin as a result of the SLP seesaw pattern between the Eastern Pacific and Caribbean basins (Giannini et al. 2000). The opposite occurs during the initialization of a cold ENSO event.

It is important to note however that there are also some significant and negative correlations between spring-time NAO indices and the LRS anomalies (Fig. 3.3b). FMA, MAM, and AMJ NAO indices have correlations of − 0.297, − 0.416, and − 0.315, respectively. The FMA and AMJ correlations are significant at the 95% confidence level and during the MAM they are significant at the 99% confidence level. The findings are inconsistent with the composites in Fig. 3.5, as there is no indication of the characteristic SST and SLP patterns that are associated with the NAO during the ERS. This remains a subject for further investigation.

The SLP and SST pattern seen in the MSD persists into the LRS. The warm SST signal in the TNA, now extends into the Northwestern Caribbean (Fig. 3.5d–f). The cold SST signal in the Eastern Pacific continues (Fig. 3.5d–f). Although the Eastern Pacific negative SLP anomalies continue (Fig. 3.5d–f), some notable SLP changes are seen in the Atlantic Basin. The high-pressure Caribbean anomaly diminishes in October (Fig. 3.5k). In November, a dipole of anomalous SLPs emerges with negative SLPs in the Northwestern Caribbean and Eastern U.S. Seaboard, and positive anomalous SLPs in the Eastern Caribbean and Equatorial Atlantic (Fig. 3.5l). It is evident from the spatial composite months coinciding with the LRS that ENSO and its atmospheric bridge effect during the MSD continue into the LRS. ENSO indices during the boreal Fall and + 1 Winter are significantly and negatively correlated with LRS anomalies (Fig. 3.3b). The SLP spatial composite during anomalous LRS Novembers is similar to numerous ENSO composite studies which found warm ENSO composites to show anomalous high SLPs over the TNA and anomalous low SLPs over Greenland in November, and vice versa for cold ENSO composites (Moron and Gouirand 2003; Fereday et al. 2008; King et al. 2018; Ayarzagüena et al. 2018). In addition, warm ENSO composites in (+ 1) January thru March have Atlantic SLP anomalies that are opposite to what are found in November and December, and vice versa for cold ENSO composites, suggesting

SLPs in the Atlantic with respect to ENSO are inverted between the early and late halves of the WDS (Moron and Gouirand 2003; Fereday et al. 2008; King et al. 2018; Ayarzagüena et al. 2018).

It is understandable that ENSO and its associated Eastern Pacific and Caribbean Sea SLP seesaw pattern would affect moisture flow in the Caribbean during the LRS. It would be important to determine whether or not the differences seen in the early and late phases of the LRS from the SST/SLP composites are also seen in how moisture is fluxed in the Caribbean and how the dynamical processes that drive the climatological LRS are affected. We begin with the MSD during anomalous LRS years as the WDS and ERS moisture transports do not directly affect the LRS rainfall.

The mean flow moisture transport anomalies (Fig. 3.6) are, as anticipated, consistent with anomalous SLP composites. The LRS dry minus wet composite during the MSD through most of the LRS show anomalous easterlies and divergence over the Caribbean with an anticyclonic circulation over the Gulf of Mexico (Fig. 3.6a–c). North of the Caribbean are anomalous westerlies associated with an anomalous cyclonic circulation seen across the northern subtropical Atlantic. In addition, a strong convergence band over the Eastern Pacific with anomalous easterlies north of ~ 10°N are found (Fig. 3.6a–d). From the climatological MSD and LRS moisture budget in Chapter 2, the anomalous easterlies and convergence in the Eastern Pacific shown during dry years is consistent with the enhanced northeasterly flow on the northern flank of the climatological Eastern Pacific ITCZ convergence band and reduces the southeasterly flow on its southern flank. This means that the climatological convergence band is displaced southward. In addition, the Atlantic ITCZ band weakens with anomalous divergence over the region during dry years. The climatological, western flank of NASH convergence band begins its southeasterly movement from the Northwestern Caribbean in September to the Central Caribbean by October (Chapter 2, Fig.

2.5e, f). Therefore, the resulting pattern in dry years suggests that convergence on the western flank of NASH is (1) relatively normal across the Northwestern Caribbean and (2) weaker across the Central Caribbean.

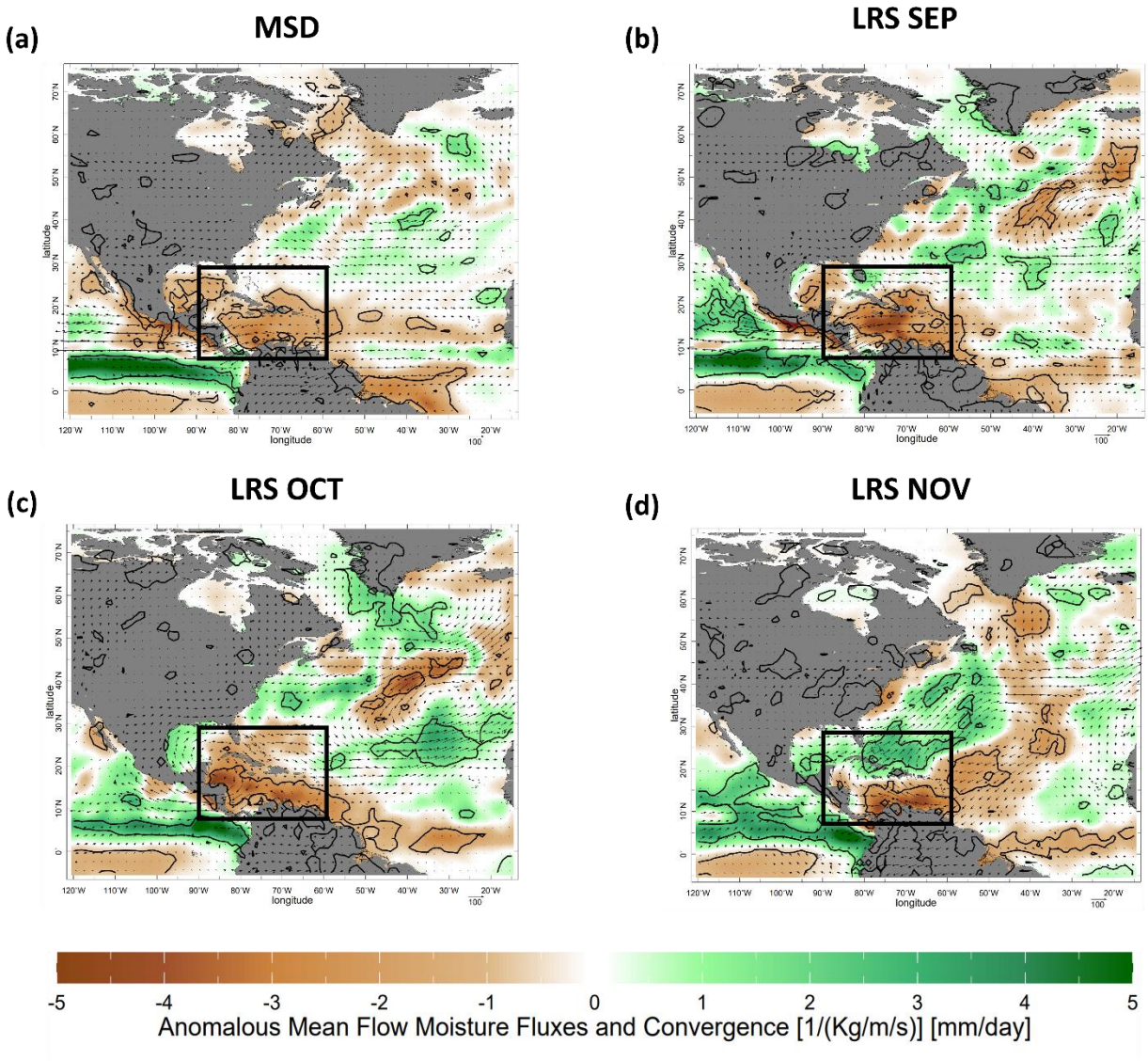

Figure 3.6: Late rainy season dry-year minus wet-year mass convergence (colors) and fluxes (vectors) composite anomalies for Jul-Aug MSD (a), and LRS (b-d). Black box indicates the Caribbean domain. Contours denote significance at the 90% according to a two-sample t-test

Although the anomalous pattern continues in the Eastern Pacific and Atlantic basins in November, several changes are found in the Caribbean basin. Dry minus wet Novembers show an

anomalous anticyclonic circulation over the TNA (Fig. 3.6d). On the southeastern flank of the anomalous circulation are anomalous divergence and southeasterlies across the Caribbean Sea, On the northwestern flank of the anomalous circulation are southwesterlies and convergence over the Greater Antilles and Northwestern Caribbean. The anomalous convergence from the advection of specific humidity enhances the anomalous convergence band from mass convergence onto the mean flow (not shown). Based on the climatological November pattern (Chapter 2, Fig. 2.5c, f), in dry years Caribbean regions on the southeastern flank of the anomalous pattern would experience strengthened divergence and easterlies while Caribbean regions on the northwestern flank of the anomalous pattern would experience weakened divergence and easterlies. The opposite would be seen in wet Novembers, where an anomalous cyclonic circulation appears over the TNA. Clearly, the ENSO induced SLP signal can impact the demise of the LRS across the Caribbean. This finding may explain how this study and others (Giannini et al. 2001b; Chen and Taylor 2002; Spence et al. 2004; Herrera and Ault 2017) find weakened dryness or anomalous wetness in the Northwestern Caribbean while the rest of the Caribbean experiences dryness during Caribbean LRS dry years, and the opposite during Caribbean LRS wet years. This finding also suggests that the displacement of the subtropical jet as a result of ENSO during the winter (Giannini et al. 2001b; Spence et al. 2004; Kushnir et al. 2006) is not the sole reason for the difference in the anomalous signal between the Northwestern Caribbean and the rest of the Caribbean, as the November divergence-convergence couplet is seen in the mean flow of the moisture budget. Although there is not a definitive conclusion as to how ENSO produces the Atlantic SLP signal in November (Bladé et al. 2008; Ineson and Scaife 2009; King et al. 2018; Ayarzagüena et al. 2018), this study is in congruence with Ayarzagüena et al. (2018) suggestion

that ENSO-related perturbations to precipitation anomalies over the Caribbean basin are responsible for the teleconnection to the North Atlantic.

Finally, changes with the AWP and CLLJ, regional modifiers of the LRS (Chapter 2), would be seen. With a warm ENSO event, the anomalous easterlies strengthen the CLLJ which would enhance dryness across most of the Western Caribbean and Central Caribbean. The exception is across the Nicaraguan to Costa Rican coastlines where, climatologically, it receives zonal convergence by the CLLJ (Hidalgo et al. 2015; Chapter 2). An enhancement of the CLLJ enhances zonal convergence in this region and explains the anomalous convergence seen there (Fig. 3.6). The cold SSTs over the southern TNA would weaken the AWP that is climatologically seen in the southern TNA (Chapter 2, Fig. 2.5). The climatological AWP in the southern TNA is located where the Atlantic ITCZ is (Chapter 2); therefore, the weakening of the AWP would contribute to the drying of the southern edge of the Caribbean Island chain associated with the southern displacement of the Atlantic ITCZ. In the Northwestern Caribbean and Gulf of Mexico, the AWP would be normal or strengthened, which weakens the extent of anomalous divergence in the region. Given the linear relationship seen in the composites, the changes of the dynamical processes during dry years would be opposite during wet years during the initialization of cold ENSO events.

3.4.4 Independency of the ERS and LRS

The findings of the dynamical spatial composites give reason to suggest that the ERS and LRS are independent of each other. To quantify the independence of the ERS and LRS, the Caribbean-averaged ERS and LRS anomalies are correlated. The 1960–2016 time series of ERS and LRS anomalies (Fig. 3.7) have a correlation of 0.0634, indicating that the ERS and LRS are uncorrelated. To determine if this is uniform across the entire Caribbean, each station's ERS and

LRS anomalies are correlated. 32 of the 34 stations show their anomalous ERS and LRS to be uncorrelated (Table 3.2). A closer look into the years that are determined for the composites provides further evidence that the ERS and LRS are independent of each other. Of the 57 years in this study, there are 33 years identified (Table 3.1). Of those, only 7 years had both the ERS and the LRS as both wet or both dry.

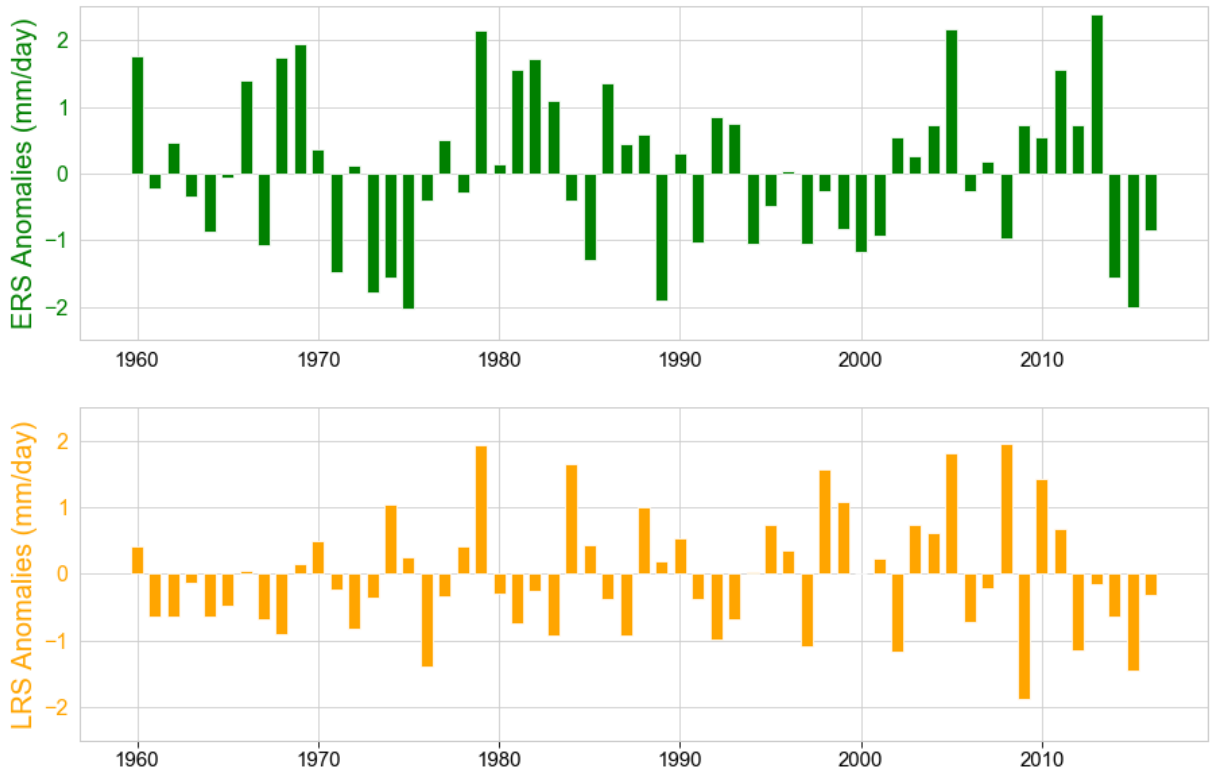

Figure 3.7: Year-by-year anomalies of the 34-station averaged ERS (top) and LRS (bottom) from 1960–2016

In contrast, there are 8 years where the ERS and LRS anomalies were opposite to each other (e.g., wet ERS and dry LRS), and 18 years where one portion of the rainfall season experiences anomalous wetness or dryness while the other portion experiences normal conditions (between the 33rd and 66th percentiles). Hence, the variability of the ERS and LRS are independent of each other, as each season has a different dominating large-scale climate driver affecting its interannual variability. The processes that lead to the ERS and LRS anomalies are different. The NAO-SST

persistence pattern alone does not persist by the LRS during dry and wet LRS years, suggesting that the LRS is relatively normal during dry and wet ERS years. The onset of ENSO and its associated SLP-seesaw pattern does not materialize during the ERS across the Caribbean; therefore, the ERS is relatively normal during dry and wet LRS years.

Table 3.2: Correlation coefficients between seasonal-averaged ERS anomalies and seasonal-averaged LRS anomalies for each station. Values in bold denote significance at the 95th confidence level.

Region	(ID) Station Name	ERS-LRS Correlations
Northwest Caribbean	(2) Nassau, Bahamas	0.085
	(7) Georgetown, Cayman	0.132
	(8) Camaguey, Cuba	0.108
	(9) La Habana, Cuba	0.028
	(13) Worthy Park, Jamaica	-.011
	(19) Ft. Lauderdale, USA	0.225
	(20) Key West, USA	-0.097
	(21) Miami Intl. AP., USA	-0.071
	(22) Palm Beach, USA	0.041
Central Caribbean / Northern Lesser Antilles	(1) BC Bird Intl. AP, Antigua/ Barbuda	-0.113
	(11) Santo Domingo, DR	**0.495**
	(23) Henry E. Rohlsen AP., St. Croix	-0.094
	(24) Cyril E. King, St. Thomas	-0.131
	(25) Coloso, USPR	-0.600
	(26) Dora Bora, USPR	-0.095
	(27) Ensenda, USPR	0.092
	(28) Guaynama, USPR	0.0193
	(29) Jajome Alto, USPR	-0.033
	(30) Mora Camp, USPR	0.266
	(31) Paraiso, USPR	0.201

	(32) Morovis N., USPR	0.164
Eastern Caribbean	(3) CIMH, Barbados	0.015
	(4) Grantley A. Intl. AP., Barbados	-0.064
	(10) DCAP, Dominica	-.218
	(12) Guadeloupe	0.045
	(14) Intl. AP., Martinique	-0.169
	(15) Hewanorra, St. Lucia	-.0168
	(16) Dumbarton, St. Vincent	0.144
	(17) Piarco Intl AP, T&T	-0.071
	(18) Crown Point, T&T	**-0.623**
Western Caribbean	(5) CFarm, Belize	0.104
	(6) Intl. AP., Belize	-0.044
	(33) San Andrés, Columbia	0.075
	(34) Felipe, Mexico	0.093

3.5 Summary and Conclusions

This chapter studies the interannual variability of the seasonal cycle of rainfall in the Caribbean based on precipitation station data from the CIMH and GHCN between 1960–2016. The results show that the year-to-year variabilities of the ERS and LRS are relatively uniform across the Caribbean, with exception in the Northwestern Caribbean. Eastern Pacific and Atlantic-wide spatial composites of wet and dry ERS and LRS years for SST, SLP, mean flow moisture convergence and moisture transports are analyzed. The two wet seasons are impacted in distinctly different ways by two different, and largely independent, large-scale phenomena: ENSO and the NAO. The interannual variability of the ERS is dominated by persistent anomalous SSTs due to a WES feedback, initiated by the preceding winter NAO. The interannual variability of the LRS is dominated by ENSO and an associated seasonal SLP see-saw between the Eastern Pacific and Caribbean basin/tropical Atlantic. Schematics illustrate the summarized effects of each large-scale

climate driver on the climatological rainfall pattern and dynamical mechanisms in the Caribbean (Fig. 3.8).

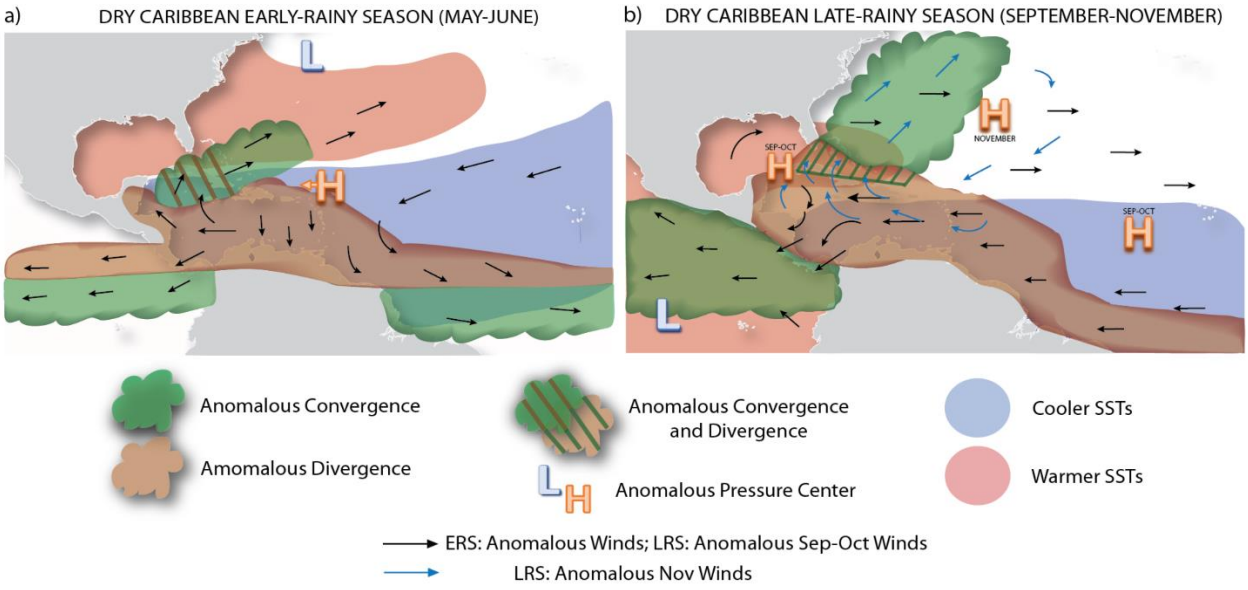

Figure 3.8: (a) Schematic of the anomalous pattern during dry Caribbean early-rainy seasons as a result of preceding winter dry season positive NAO-SST persistence and WES feedback. (b) Schematic of the anomalous pattern during dry Caribbean late-rainy seasons as a result of the summertime onset of warm ENSO and associated inter-basin see-saw sea-level pressure pattern. Areas shaded in green denote anomalous convergence. Areas shaded in brown denote anomalous divergence. Areas shaded in blue and red denote cooler and warmer sea-surface temperatures, respectively. Black arrows denote the anomalous surface wind pattern. Blue arrows denote the anomalous surface wind pattern in November. Large "H" denotes an anomalous high. Large "L" denotes an anomalous low. The ERS area with hatched convergence is due to divergence moving into the area as the anomalous High propagates west during the season. The LRS area of hatched divergence is due to the circulation change between September/October and November, producing convergence.

As suggested in Sect. 3.4.2 and Fig. 3.8a, when a positive NAO phase precedes the WDS, the NAO-SST TNA pattern that persists into spring and early summer through the WES feedback would cause the following changes to the ERS climatological pattern (Fig. 2.8): a strengthening and expansion of NASH during the ERS, more easterly flow across the Caribbean Sea, more westerlies across the Northwestern Caribbean, a northwestward shift of the NASH convergence band with a larger SW-NE tilt, weakening of the AWP in the Caribbean Sea but strengthening in

the Gulf of Mexico and Northwestern Caribbean, a strengthened CLLJ, and a southern displacement of the ITCZ convergence bands. These changes induce dryness across the entire Caribbean, with a lesser dry (or slightly wet) signal in the Northwestern Caribbean and a weaker dry signal along the Nicaraguan and Costa Rican coastlines. The opposite would occur when the WDS is preceded by a negative NAO phase. Preceding winter mature/post-mature ENSO phases play a secondary role on ERS variability by modifying the NAO induced SST-persistence signal.

El Niño, the warm phase of ENSO, and its associated seasonal SLP see-saw pattern between the Eastern Pacific and Caribbean basins (description in Section. 3.4.3; Fig. 3.8b) would cause the following changes to the LRS climatological pattern (Fig. 2.8): a strengthening of the southwestern flank of NASH during the LRS, strengthened easterlies across the Caribbean Sea and southern TNA, weakened easterlies north of the Caribbean Sea and northern TNA, enhanced CLLJ, southern displacement of the Eastern Pacific ITCZ, weakened Atlantic ITCZ across the Lesser Antilles, weakened AWP across the eastern Caribbean Sea and southern TNA, and strengthened AWP across the northern TNA, and Northwestern Caribbean. These changes would induce dryness across the entire Caribbean, with a lesser dry signal or wet signal in the Northwestern Caribbean, and along the Nicaraguan and Costa Rican Caribbean coastlines.

Similar to the findings from Chapter 2, the findings from this chapter are possible when utilizing pentad and monthly resolutions in order to avoid masking the evolution of the variability of rainfall in the Caribbean throughout the rainy season. For instance, a seasonal composite of the LRS would likely mask the November signal seen in this work, which is important in determining how the Caribbean experiences some differences in its anomalous LRS precipitation signal. In the ERS, composites of the entire season during the ERS would likely dampen the May signal which

is important in explaining the differences in anomalous precipitation seen between the Northwestern Caribbean and the rest of the Caribbean.

This chapter provides several implications and considerations when investigating the predictability of rainfall in the Caribbean. First, it is important to consider whether the predictability of these large-scale climate drivers is uniform across the Caribbean, as each sub-region has distinct sets of dynamical mechanisms which are impacted differently by each climate driver in both space and time. Hence, the predictive skill of the large-scale climate drivers and dynamical mechanisms (e.g., NASH, CLLJ, AWP, ITCZ) should be investigated for each sub-region. Second, it is valuable to assess what spatial domain of the large-scale fields would maximize the predictive skill of the ERS and LRS across each sub-region, as the climate drivers that influence each rainfall season encompass different spatial domains. For instance, an SST index consisting of TNA and Caribbean Sea SSTs may be beneficial for predicting ERS characteristics across the Caribbean, whereas an inter-basin SST index between the Tropical Eastern Pacific and Atlantic basins would better inform predictive skill for LRS characteristics in the region. Third, both the pre-ERS SST-persistence signal that the winter NAO induces and the persistent inter-basin SLP signal that ENSO induces span over the course of several months. This implies that the predictability of characteristics of the ERS and LRS could be investigated under S2S timescales. This could impart better lead-time prediction for S2S characteristics such as the onset and demise of the rainfall cycle. Parts II and III incorporate these implications and considerations when investigating the characteristics and prediction of the Caribbean rainfall cycle.

Models have been found to misrepresent some of the dynamical mechanisms in the Caribbean, and may be responsible for their biases in simulating Caribbean rainfall (Ryu and Hayhoe 2013; Eichhorn and Bader 2017). A likely reason for these systematic biases may be that

the models misrepresent the seasonal and temporal evolutions of the climate drivers that affect the dynamical mechanisms within the ERS and LRS. Assessing how current climate models simulate the mean state and variability of the NAO, the NAO-induced SST persistence signal, ENSO, the ENSO induced SLP see-saw effect, may provide insight on these systematic biases and improve the predictability of the rainfall cycle in models.

This chapter has several implications for investigating climate change impact on rainfall in the Caribbean. Previous studies have shown that there is no observed trend on the annual precipitation of rainfall in the Caribbean. Given that the main drivers of ERS and LRS variability are independent, it would be valuable to assess whether this is because the trends of the climate drivers (Dong et al. 2011; Cai et al. 2014) and processes that respond to them have ERS and LRS trends that negate each other. Future projections in NAO and ENSO from climate change can also be used to assess how they translate to changes in the ERS and LRS, respectively. Overall, the better understanding of the interannual variability of the Caribbean rainfall cycle presented in this Chapter could be used to better predict the seasonal rainfall cycle, advance modeling capabilities, understand future climate in the region, and the regional climate effects stemming from large-scale climate drivers.

Part II

Quantifying Subseasonal-to-Seasonal Characteristics of Caribbean Rainfall

Chapter 4: An Adaptive Approach to Quantify Weather-within-Climate Rainfall Characteristics: Assessment of Temporal and Mid-Summer Drought Characteristics in the Caribbean Basin

Note: A modified version of this chapter is under review in Climate Dynamics (2021)[3]

4.1 Introduction

Across the globe, S2S rainfall characteristics such as onset, demise, and strength and duration of intermittent dry periods, or relative dry periods between rainfall seasons, provide important insight for the agriculture, health, disaster, and energy industries. These characteristics are classified as S2S because they exhibit S2S variation in their interannual variability, or the characteristic is within a rainfall season that spans a few weeks to a few months. These characteristics are examples of what are known as "weather within climate", or characteristics of weather that lead to climate anomalies such as floods and agricultural droughts (Moron et al. 2019). Generally speaking, temporal characteristics (e.g., onset and demise) of the annual rainfall cycle are more useful than rainfall amounts for farmers (Marengo et al. 2001; Ingram et al. 2002). The onset and demise of the annual rainfall cycle is significant for rainfed agriculture. In this case agricultural planning, and consequently food production are heavily affected by changes to the start and end of the rainfall season (Camberlin and Diop 2003; Boyard-Micheau et al. 2013; Diaconescu et al. 2014; Obarein and Amanambu 2019). The timing of the annual rainfall cycle also impacts water consumption, human health via water-borne diseases, and energy generation (Li and Fu 2002; Bombardi et al. 2020, hereafter B20). Changes in the duration and magnitude of

[3]Martinez C., Muñoz Á., Goddard L., Kushnir Y., Ting M., 2021: An Adaptive Approach to Quantify Weather-within-Climate Rainfall Characteristics. Clim Dyn. *Under Review*

intermittent dry periods impact planting dates and crop yields that are important for growing and harvesting seasons (Hastenrath 1966, Magaña et al 1999, Van der Zee Arias et al 2012, Pons et al. 2016). These S2S rainfall characteristics are especially important for complex rainfall regimes, or regions that have one or more of the following: (1) multiple rainfall seasons in a given year, (2) a relatively wet dry season, (3) unclear transitions between wet and dry seasons. However, forecasts on the temporal and intermittent dry period characteristics of the annual rainfall cycle are not readily available from local weather or climate services to which a majority of stakeholders turn for forecasts on the annual rainfall cycle (Vaughan and Dessai 2014).

S2S characteristics of the annual rainfall cycle are valuable for investigating atmospheric dynamics and simulating rainfall in models. In most regions, monsoon and large-scale patterns are responsible for the wet and dry seasons. Temporal variations in the monsoonal or large-scale patterns affect the timing of the annual rainfall cycle (Marengo et al. 2001; Bombardi et al. 2017), and intermittent dry periods (Anderson et al. 2019). In some regions, the interannual variability of the onset and demise is related to the interannual variability of the total seasonal rainfall (Marengo et al. 2001; Li and Fu 2001). Hence, accurately characterizing temporal and intermittent dry period characteristics of rainfall can enhance the understanding of what dynamical mechanisms contribute to the annual rainfall cycle and how they affect its variability. In addition, research on temporal and intermittent dry period characteristics can improve the detection of biases that models have in simulating the annual rainfall cycle and its interannual variability (Liebmann et al. 2007; Anderson et al. 2019).

The asymmetry of the annual rainfall cycle, variations in modality across sub-regions, an intermittent dry period, and unclear transitions between wet and dry seasons make the Caribbean annual rainfall cycle a prime example of a region with a complex rainfall regime. The rainfall

pattern in the Caribbean is not uniform; there are five sub-regions, all of which have complex rainfall regimes (Chapter 2). The Northwestern, Western, and Central Caribbean regions have non-homogenous and subtle bimodal rainfall regimes with a short duration ERS and a longer duration LRS. The MSD which separates the ERS and LRS is an intermittent dry period. Each sub-region has a different set of regional to large-scale dynamical mechanisms that are responsible for their distinct rainfall characteristics (Chapter 2). In addition, the interannual variabilities of the ERS and LRS are independent of each other due to differences in large-scale climate drivers that affect each subset of dynamics mechanisms corresponding to each seasonal component (Chapter 3). Therefore, the temporal characteristics associated with the ERS are independent of those of the LRS.

Although the onset, demise and MSD characteristics are important for numerous industries in the Caribbean, temporal and MSD rainfall characteristics in the Caribbean have been largely unexplored, particularly on a sub-regional scale. Previous studies that have investigated rainfall characteristics in the Caribbean have only focused on precipitation amount, frequency of wet or dry days, or wet and dry extremes (Stephenson et al. 2014; Moron et al 2015; Maldonado et al. 2017; Vigaud and Robertson 2018; Alfaro et al. 2017). Gouirand et al. 2020 calculated onsets and demises using weather-types of low-level winds, but only treated the Caribbean as one homogenous region when calculating onsets and demises. And only recently have there been investigations into MSD characteristics, given the importance of understanding the magnitude and duration of the MSD for agricultural planning and transitions from ERS to LRS, but these investigations have been focused only in Central America (Karnauskas et al. 2013; Maldonado et al. 2016a; Maldonado et al. 2016b; Alfaro et al. 2016; Alfaro et al. 2017; Anderson et al. 2019)

There are also no publicly available datasets on Caribbean MSD and temporal rainfall characteristics.

Given the absence of datasets and investigations into sub-regional temporal and MSD rainfall characteristics in the Caribbean, a natural step would be to look at other regional and global studies with methods on S2S rainfall characteristics, and apply them to the Caribbean. Meteorological methods are one of two types of methods for calculating temporal characteristics of rainfall. Meteorological methods typically use a geographically-fixed observation from one variable such as rainfall, outgoing long wave radiation, or moisture fluxes to detect the timing of the rainfall season. A commonly-used method is from Liebmann and Marengo (2001) which defines the onset and demise dates based on accumulated rainfall anomalies relative to the climatological annual mean. Several studies adapt the Liebmann and Marengo (2001) method for their region (Camberlin and Diop 2003; Liebmann et al. 2007; Bombardi and Carvalho 2008, 2009; Dunning et al. 2016, hereafter D16; Misra et al. 2017; Bombardi et al. 2017; B20). The other type of method for calculating temporal characteristics of rainfall are agronomical methods. Agronomical methods use a set of criteria or threshold(s) to determine the timing of the rainfall season relative to some crop (Moron and Robinson 2014; Nieto-Ferreira and Rickenbach 2011; Marengo et al. 2001, Li and Fu 2004; Obarein and Amanambu 2019; B20).

However, the existing meteorological and agronomical methods are not suitable to use for regions with complex rainfall patterns like those in the Caribbean. The main limitation in the Liebmann and Marengo (2001) method is that the method has to have consistent above normal precipitation in order to show an identifiable change in the accumulated precipitation anomaly. Any intermittent or light rainfall before or after the main portion of the wet season is given a negative daily rainfall anomaly, potentially reducing the length of the wet season. Adaptations of

the Liebmann and Marengo (2001) method experience this limitation; however, since most of these studies worked with regions that have unimodal rainfall patterns with distinct transitions between their dry and wet season (Camberlin and Diop 2003; Bombardi and Carvalho, 2008; 2009; Bombardi et al. 2017; Misra et al. 2017), the limitation is not pertinent for them. However, for regions that have gradual transitions into and out of the wet season, this can skew the timing of the onset and demise. Studies that adapt the Liebmann and Marengo (2001) method to investigate regions with multi-modal rainfall regimes acknowledge this (Dunning et al. 2016, hereafter D16; Bombardi et al. 2020, hereafter B20). A common limitation seen in several meteorological methods is using a climatological annual mean to determine the onset and demise of the rainfall cycle (Liebmann and Marengo 2001; Camberlin and Diop 2003; Cook and Buckley 2009; Moron and Robertson 2014; Carvalho et al. 2016; D16; Bombardi et al. 2017; Obarein and Amanambu 2019; B20). A climatological annual mean works well for unimodal or multi-modal regimes with clear wet and dry seasons. However, using a climatological annual mean for regions with asymmetrical rainfall seasons (e.g., B20) can skew the timing of the onset(s) and demise(s) in these regions because the annual mean can be biased towards the season within the annual rainfall cycle with the largest amount of rainfall. Agronomical methods commonly use a mm threshold and a criterion for persistence of rainfall in order to determine the timing of the rainfall onset and demise (B20). However, the threshold values and criteria are different for each agronomical study as the values are specific to their region or commodity of interest. Therefore, it would likely be unsuitable to apply the same values for a different sub-region or crop in the Caribbean. In addition, many agronomical studies have fixed dates to their rainfall season that may not be applicable for other regions

Furthermore, agronomical and meteorological methods have different purposes and benefits. Agronomical methods are advantageous for farmers and decision makers as it relates to the physical needs of their crops or livestock. In addition, agronomical methods can be applied for real-time monitoring and forecasting (Moron and Robertson 2014). However, agronomical methods do not focus on large-scale or monsoonal features, as pre-monsoon or transient activity may be enough to satisfy the required criteria or thresholds pertaining to the crop. If a researcher desires to investigate the variability and timing of monsoonal or large-scale features, a meteorological method is used. Meteorological methods are advantageous for diagnostic studies: they focus on monsoonal or regional to large-scale dynamical patterns that typically separate wet and dry seasons (B20) to assess what dynamical mechanisms affect the timing of the annual rainfall cycle. It would be beneficial to develop an agronomical/meteorological hybrid method given their respective benefits.

Most agronomical or meteorological methods do not detect intermittent dry periods, calculate its characteristics, use them to categorize rainfall modalities, and consequently, determine whether multiple onsets and demises can be calculated for a given region. Some studies classify rainfall modalities by defining rainfall seasons. For example, Seregina et al. (2018) defined a rainy season when at least five consecutive pentads exceed their pre-defined rainfall threshold. D16 used a ratio between the first and second peak amplitudes to determine whether or not a season is bimodal. Studies that classify rainfall modalities based solely on the rainfall season; however, can oversimplify complex rainfall patterns. There are regions with neither a classic unimodal or bimodal rainfall pattern (e.g., southeast Asia, Africa, Central America, and Caribbean) (Hermann and Mohr, 2011; B20; Chapter 2 and 3). Instead, these regions experience patterns that are referred to as single wet season bimodal (Herrmann and Mohr, 2011), or, as stated in previous Chapters, a

bimodal cycle that is subtle. In this Chapter, we will term regions with these patterns as unimodal dual maxima, in order to distinguish them from classic bimodal patterns. Their distinction comes from their subtle intermittent dry period, which prevents multiple onsets and demises from being calculated. However, unlike unimodal patterns, the onset and demise of unimodal dual maxima patterns are likely influenced by two separate sets of dynamical mechanisms that are associated with each rainfall maximum. Subtle intermittent dry periods are difficult to predict and are highly variable (Hellin et al 2017, Bellante 2019). As a consequence, methods that use dry periods to determine the modality of rainfall cycles in order to calculate onsets and demises classify rainfall patterns with subtle intermittent dry periods as unimodal (e.g., B20). Yet subtle intermittent dry periods and their characteristics are important for farmers and water management as the period can impact the end of the preceding rainfall season and start of the subsequential rainfall season (Anderson et al. 2019). There has yet to be a method that 1) utilizes intermittent dry periods to classify rainfall modalities and determine whether multiple onsets and demises can be calculated and 2) distinguishes unimodal dual maxima patterns and calculates its temporal and intermittent dry period characteristics.

This chapter presents a new and comprehensive method for calculating S2S rainfall characteristics, and uses the method to investigate temporal and MSD characteristics of rainfall in the Caribbean. The new method aims to 1) include both meteorological and agronomical considerations 2) classify common and uncommon rainfall modalities (e.g., unimodal dual maxima), and 3) frame characteristics based on the modality of the annual rainfall cycle. Chapter 4 is structured as follows. Section 4.2 addresses the datasets used for the analysis. Section 4.3 discusses, step-by-step, the methodology on calculating temporal and intermittent dry period characteristics under a meteorological context. Section 4.4 compares the mean and variability of

Caribbean temporal rainfall characteristics calculated using the present method versus previous methods. In addition, Section 4.4 investigates the relationships between dynamical mechanisms that influence the Caribbean rainfall cycle (Chapter 2; Chapter 3), and temporal/MSD rainfall characteristics. Section 4.5 discusses how the method can be adapted for an agronomical context. Discussion and concluding remarks can be found in section 4.6 and 4.7, respectively.

4.2 Data

There are a few important considerations on what data to use in order to effectively utilize the method. This method requires daily data, in order to accurately capture the timing of the rainfall characteristics. Spatially, the method can be applied to local- or regionally-averaged time series. Both have their advantages and disadvantages. For example, use of individual stations or grid points allows one to investigate local forcings and transient activity, but missing values can cause issues when smoothing or filtering the data. Grouping stations or grid-points reduces rainfall 'noise' and missing values, but that averaging can dampen 'transient' features and local forcings. If a region does have sub-regional rainfall heterogeneity, it may be beneficial to further subset the data into smaller, but more homogenous regions. For the Caribbean region example that will be employed to demonstrate the method, the daily station rainfall dataset described in Chapter 2, Section 2, is used. Several stations from Guatemala are also included in this Chapter, provided by the INSIVUMEH. In total, the daily rainfall from 41 stations is used in this study. Stations are grouped by sub-region based on the classified Caribbean sub-regions from Chapter 2. A summary of the stations used to showcase this method can be found in Table 4.1.

Table 4.1: List of rainfall regions, and their corresponding stations used in Chapter 4. Station ID, station name, and location in latitude and longitude.

Region	(ID) Station Name	Latitude	Longitude
Northwest Caribbean Mode: Unimodal Dual Maxima Start Date: April 1st End Date: November 30th	(1) Nassau, Bahamas	25	− 77.5
	(2) Georgetown, Cayman	19.3	− 81.3
	(3) Camaguey, Cuba	21.24	− 77.51
	(4) La Habana, Cuba	23.1	− 82.21
	(5) Worthy Park, Jamaica	18.143	− 77.149
	(6) Ft. Lauderdale, USA	26.1	− 80.28
	(7) Key West, USA	24.55	− 81.75
	(8) Miami Intl. AP., USA	25.82	− 80.28
	(9) Palm Beach, USA	26.68	− 80.08
Central Caribbean / Northern Lesser Antilles Mode: Unimodal Dual Maxima Start Date: March 1st End Date: December 31st	(10) BC Bird Intl. AP, Antigua/	17.135	− 61.791
	(11) Santo Domingo, DR	18.25	− 69.58
	(12) Henry E. Rohlsen AP., St. Croix	17.7	− 64.81
	(13) Cyril E. King, St. Thomas	18.33	− 64.97
	(14) Coloso, USPR	18.381	− 67.157
	(15) Dora Bora, USPR	18.336	− 66.667
	(16) Ensenada, USPR	17.973	− 66.946
	(17) Guaynama, USPR	17.978	− 66.087
	(18) Jajome Alto, USPR	18.072	− 66.143
	(19) Mora Camp, USPR	18.474	− 67.029
	(20) Paraiso, USPR	18.265	− 65.721
	(21) Morovis N., USPR	18.334	− 66.408
Central and Southern Lesser Antilles (or Eastern Caribbean) Mode: Unimodal Start Date: March 1st End Date: +1 January 30th	(22) CIMH, Barbados	13.148	− 59.624
	(23) Grantley A. Intl. AP., Barbados	13.08	− 59.485
	(24) DCAP, Dominica	15.547	− 61.2993
	(25) Guadeloupe	16.2	− 61.66
	(26) Intl. AP., Martinique	14.59	− 60.99
	(27) Hewanorra, St. Lucia	13.737	− 60.952

	(28) Dumbarton, St. Vincent	13.18	− 61.17
Western Caribbean Mode: Unimodal Dual Maxima Start Date: April 1st End Date: +1 January 30th	(29) CFarm, Belize	17.2	− 89
	(30) Intl. AP., Belize	17.53	− 88.3
	(31) San Andrés, Columbia	12.583	-81.717
	(32) Felipe, Mexico	19.7	-87.9
	(33) Flores, Guatemala	16.915	-89.865
	(34) Las Vegas, Guatemala	15.600	-88.967
	(35) Puerto Barrios, Guatemala	15.737	-88.591
	(36) San Augustin Chixoy, Guatemala	16.067	-90.439
	(37) San Pedro Mactun, Guatemala	17.260	-90.949
Guianas Mode: Bimodal Start Date: March 1st End Date: +1 March 5th	(38) Georgetown, Guyana	6.8	-58.133
	(39) Time H.R.I., Guyana	6.483	-58.25
	(40) Corantjipolder, Suriname	5.96	-57.04
	(41) Zanderji, Suriname	5.45	-55.2

Additional steps are suggested to prepare the daily data ahead of the analysis. A smoothing filter on the daily data is also recommended in order to reduce noise. Gaussian windows are used here, as they simplify delineation of transient vs. non-transient activity, and have been used in other similar studies (e.g., B20). A 10-day Gaussian window was found to best suit the Caribbean: it reduced noise but did not substantially modify signals seen in the daily data.

4.3 Methods

The methodology comprises three parts: creating the annual cycle climatology of rainfall and determining intermittent dry periods, identifying seasonal windows, and calculating temporal and intermittent dry period rainfall characteristics for each year. For temporal characteristics, one context is examined in this section and a summary of the methodology in this context can be found in Fig. 4.1. In addition, Fig. 4.1 includes a summary of the adaptations of the methodology in other

contexts (e.g., Absolute Meteorological Characteristics, and Agronomical Characteristics), which can be found in Sections 4.4 and 4.5, respectively.

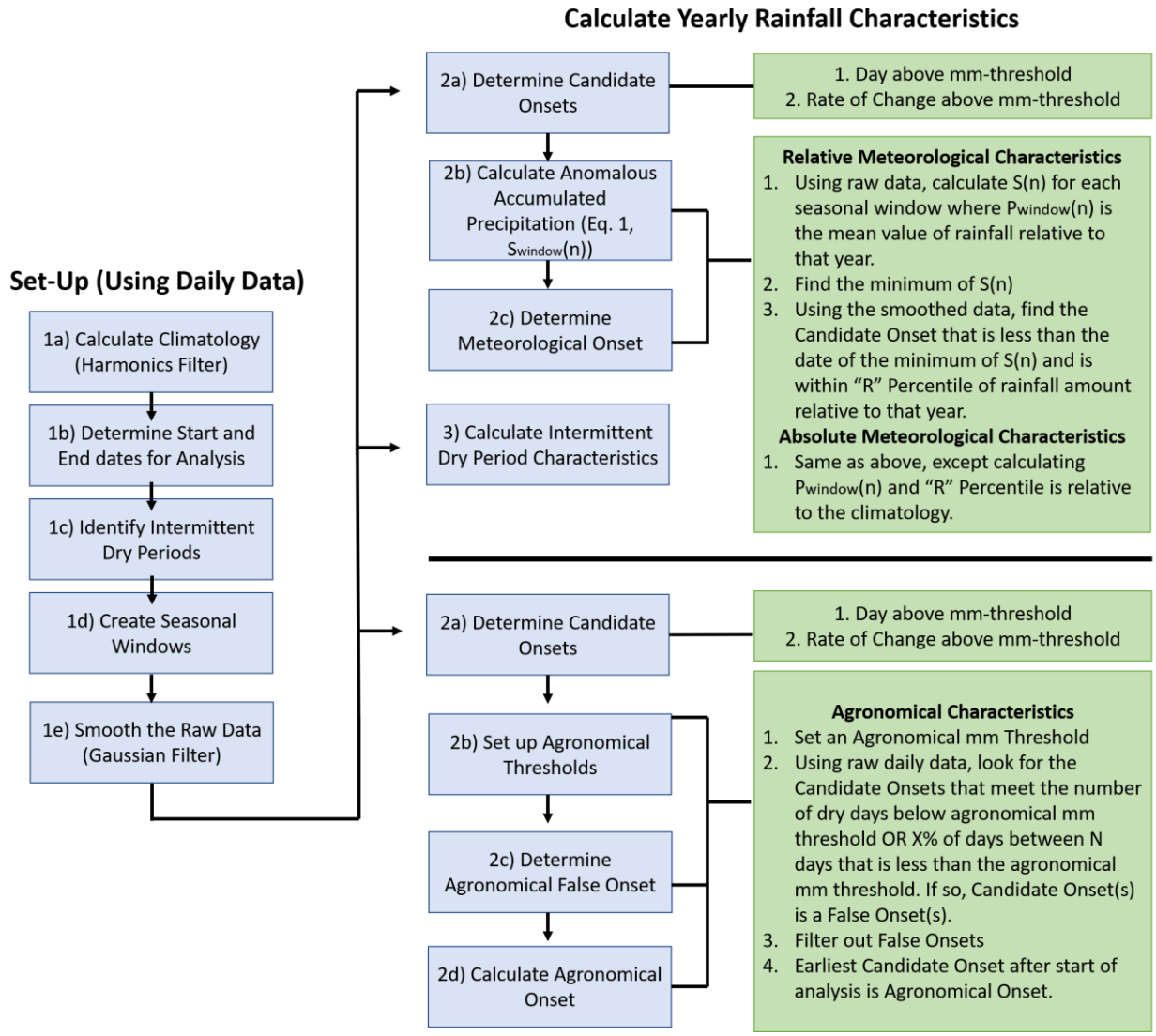

Figure 4.1: Summary of methodology under various contexts to calculate onset. Blue boxes highlight the steps. Green boxes are details of the blue boxes. The upper-half of the calculation of yearly rainfall characteristics are steps to calculate meteorological characteristics. The lower-half of the calculation of yearly rainfall characteristics are steps to calculate agronomical characteristics. Demises follow the same steps except in (2a) the candidate demise is only determined if the day is below the mm threshold. For Meteorological Demises, in (2b, c) the maximum of S(n) is found and the Candidate Demise is greater than the time of the maximum of S(n). For Agronomical Demises, in (2b-d) number of wet days, and above agronomical mm threshold are used.

4.3.1 Create Annual Cycle Climatology of Rainfall

The annual climatology of rainfall is calculated from the raw daily data, excluding leap days. A harmonic filter then smooths the climatological annual cycle. Harmonic filters have been used to investigate the number of wet seasons over a given region (e.g., Wang 1994; Wang and LinHo 2002; Liebmann et al. 2012). The number of harmonics used depends on the region under study. Previous studies suggest the use of the first 4 to 12 Fourier harmonics (Wang 1994; Wang and LinHo 2002; Liebmann et al. 2012). Here, a five harmonic (5-term Fourier) filter is used to smooth the climatology.

For the purposes of the analysis, the calendar year should be shifted also, to better capture the full cycle of annual rainfall cycle and all transition between wet and dry seasons (e.g., Bombardi et al. 2017; B20), particularly for regions where a rainfall season bridges two calendar years. The shift is determined by the peaks and troughs of the rainfall cycle that are identified in the smoothed climatology. In the smoothed climatology, the minima that separates the dry and wet seasons, and the final peak of the rainfall season are identified. The former denotes the beginning of the climatological rainfall cycle. Next, the start and end dates of the analysis are determined. Selecting the start and end dates are subjective choices. Recent studies used 20-50 days before the beginning of the climatological rainfall cycle as their start date (D16; B20). However, some determine the start date from tradition (e.g., Allen and Mapes 2017; CIMH deems the start of the Caribbean rainfall season as April 1st). The same steps are applied to determine the end date for the analysis; the end date must be some days after the final climatological peak of the rainfall cycle. Recent studies use 20-50 days after the final climatological peak of the rainfall cycle to determine the end date (D16; B20), or use a traditional date that is commonly used to describe the end of the rainfall cycle (e.g., Chapter 2, Chapter 3). These dates will also be used in the year-to-

year analysis. For the Caribbean, the data is shifted such that Day 1 is March 1st and Day 365 is February 28th of the following year. For the Guianas, the data is shifted such that Day 1 is February 1st and Day 365 is January 30th of the following year. Daily data for each sub-region was calculated by averaging their stations' daily data. The start date for the Northwestern and Western Caribbean is April 1st. Since the transition from less-wet to wet rainfall season begins in late March/early April for the Central and Eastern Caribbean (Chapter 2), the start date is March 1st. The start and end date in the Guianas is the day of the climatological minima prior to the first rainfall season, or March 1st through March 5th of the following year. The end date is November 30th in the Northwestern Caribbean. The Central Caribbean end date is December 30th and the Eastern and Western Caribbean is January 30th of the following year, as the demise of their rainfall cycles is later in the year than in the Northwestern Caribbean (Chapter 2). A summary of the start and end dates for each sub-region can be found in Table 4.1.

Intermittent dry periods in the smoothed climatology are identified in order to determine the modality of the rainfall cycle. Between the start and end dates, an intermittent dry period is identified if the difference between either rainfall peak and the minima between peaks is greater than 1 mm, following similar steps from B20. Next, any identified intermittent dry period is classified as subtle or distinct. If the intermittent dry period minimum is 1 mm less than the climatological annual mean, the intermittent dry period is distinct. Otherwise, the intermittent dry period is subtle. A step-by-step example of the process for identifying and classifying intermittent dry periods using the smoothed climatology is given for the Northwestern Caribbean (Fig. 4.2a) and Guianas (Fig. 4.2b). In the Northwestern Caribbean there are two rainfall peaks with a minimum between peaks. The difference between the minimum and either rainfall peak is greater than 1 mm; therefore, the Northwestern Caribbean experiences one intermittent dry period. The

intermittent dry period is not 1 mm less than the climatological annual mean (~3.8mm/day); therefore, the intermittent dry period is subtle. Similarly, the Guianas has two rainfall peaks with an intermittent dry period. However, the intermittent dry period minimum in the Guianas is 1 mm less than its climatological annual mean (~6mm); therefore, the intermittent dry period is distinct. The number of intermittent dry periods and their classification determines the modality of the rainfall cycle. The Northwestern Caribbean experiences one subtle intermittent dry period; therefore, the modality of the rainfall cycle is unimodal dual maxima, or a subtle bimodal rainfall cycle. The Guianas experiences one distinct intermittent dry period; therefore, the modality of the rainfall cycle is bimodal. Whether or not an intermittent dry period is subtle or distinct determines whether one is able to calculate multiple onsets and demises between the start and end dates of the analysis. For example, in the Northwestern Caribbean, only one onset and demise can be determined in the yearly analysis because the intermittent dry period is7 subtle. In the Guianas, two onsets and two demises can be determined in the yearly analysis because the intermittent dry period is distinct. A summary of the classified modalities for each sub-region can be found in Table 4.1.

4.3.2 Identify Seasonal Windows

Using the smoothed climatology, seasonal windows are introduced for the calculation of characteristics associated with each rainy season of the annual rainfall cycle for each year. For unimodal regimes, the seasonal window is the rainfall start-to-end date. For bimodal regimes, the first window is set between the start date to the date of the rainfall minimum within the first valid intermittent dry period. The second window is set between the rainfall minimum within the first valid intermittent dry period and the end date. A few regions yield trimodal patterns (B20); hence, for a trimodal regime, the first window is set between start date and the date of the rainfall

minimum within the first valid intermittent dry period. The second window is set between the rainfall minimums within the first and second valid intermittent dry periods. The third window is set between the rainfall minimum within the second valid intermittent dry period and the end date. Intermittent dry period windows are set by determining the midpoints between the rainfall peaks and the minima of the intermittent dry period.

To demonstrate the construction of the smoothed climatology and creation of seasonal windows, a step-by-step illustration of the process is given for the Northwestern Caribbean region. For the Caribbean, the data is shifted such that Day 1 is March 1st and Day 365 is February 28th of the following year. Daily data was averaged across stations in the Northwestern Caribbean to investigate the region. For the Northwestern Caribbean, the rainfall minimum that is associated with the start of the rainfall cycle is on day 50 (April 19th) (Fig. 4.2), and we choose to take the start date as defined from tradition: day 30 (April 1st). The time that is associated with the peak of the hydrological cycle is on day 215 (October 1st) (Fig. 4.2), but there can be rainfall long after. Hence the end date is defined from tradition: day 274 (November 30th).

The Northwestern Caribbean follows a bimodal rainfall cycle (Fig. 4.2a) as it experiences one valid intermittent dry period. Two seasonal windows are set: the 'Early Rainfall Season' window, which is between the start date and the minimum location of its intermittent dry period, or Day 141 (July 18th), and the 'Late Rainfall Season' window, which is between the minimum location of the intermittent dry period to the end date (Fig. 4.2a). The intermittent dry period window is Day 117 (June 26th) to Day 164 (August 12th) (Fig. 4.2a).

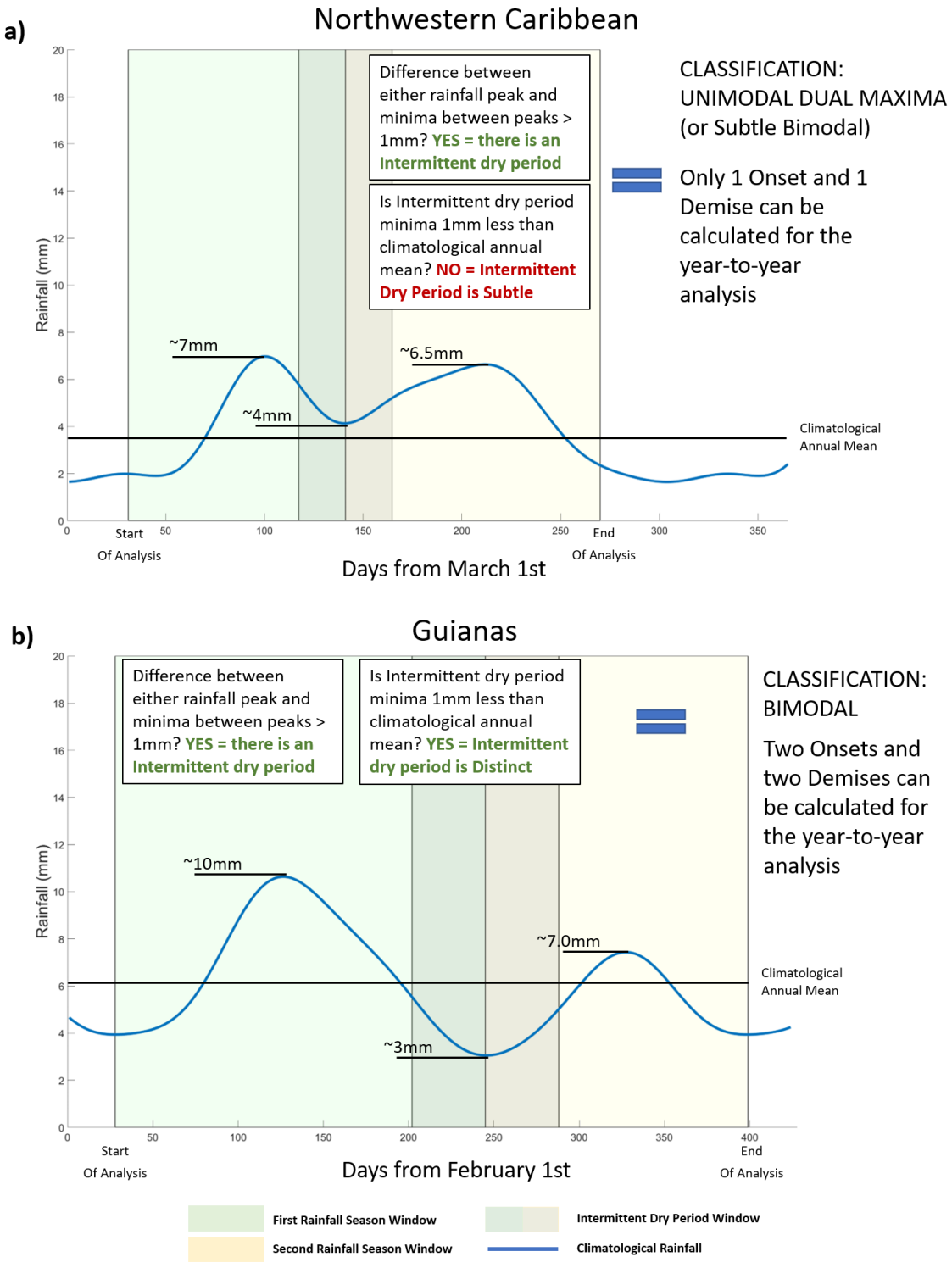

Figure 4.2: Calculating the climatological rainfall cycle, classifying intermittent dry period, and setting seasonal windows for the Northwestern Caribbean (a) and the Guianas (b), where Day 1 is March 1st and February 1st, respectively. Blue line denotes the smoothed climatology averaged over all stations for each region. Seasonal windows are shaded: first

rainfall season (green), and second rainfall season (yellow). The darkened green/yellow window is the intermittent dry period window, or mid-summer drought (MSD)for the Northwestern Caribbean.

4.3.3 Calculate Rainfall Characteristics for Each Year

First, the temporal location, amplitude, and width of every peak and trough in the gaussian-filtered daily data for each year is calculated. Second, inflection points are determined in the year-to-year smoothed data, and are classified as candidate meteorological onset or demise dates. For candidate onsets, the method considers every trough-to-peak within the smoothed daily data, and finds the minimum day, if any, that has both of the following user-input conditions: (1) the day is above an inflection point mm threshold, and (2) the rate of change between the inflection point and X days exceeds a given mm/day threshold. The latter is done to avoid inflection points in which no clear changes in slope above the mm threshold exist in subsequent days. For candidate demises, the method inspects every peak-to-trough and finds the minimum day, if any, that has its value below the inflection point mm threshold. To define a wet vs. non-wet day, most studies use a threshold value from 0.85mm (Stern et al. 1981) to 1 mm (Moron and Roberstson, 2014), but in some regions with unclear dry seasons, values as high as 2.5 mm are used (Nandargi and Mulye 2012). Therefore, it is recommended to set the inflection point mm threshold between .85mm and 2.5mm. For the onset calculation, the rate of change requirement is similar to methods that use a criterion to check for persistence of rainfall, and typically check approximately 10 days out. However, those methods do not check for slope and only ask how many days after the date are also at or above the mm threshold. Onsets are associated with a change in intensity of rainfall; hence they should also depend on the change in slope. This method is the first to put a mm/day tendency threshold. In the application of this method, the tendency is calculated as the average

change in daily rainfall amount between the climatological trough and peak that is associated with the onset.

To demonstrate the calculation of the accumulated precipitation anomalies, onsets, and demises, a step-by-step illustration of the method using the 2011 rainfall cycle in the Northwestern Caribbean (Fig. 4.3) and the 1985 rainfall cycle in the Guianas (Fig. 4.4), are shown. In the Northwestern Caribbean, a candidate onset is determined between any trough to peak if the inflection point is above 1 mm and if there is a rate of change of .102 mm/day between the date of the inflection point and 10 days out (Fig. 4.3a). The latter was determined by taking the difference between the climatological peak (7mm) and trough (1.9mm) that is associated with onset divided by the number of days between the climatological trough to peak associated with onset (50 days). A demise inflection point is determined between any peak to trough if the inflection point is below 1 mm (Fig. 4.3a). A similar procedure is done for the Guianas (Fig. 4.4a), except 1) the inflection point threshold is 1.5 mm because it is common for the region to not have consistent rainfall values below 1mm, and 2) determining candidate onsets are different between the first and second rainfall seasons, as the second rainfall season has a separate mm tendency threshold.

The context that is examined using the present method in this section is an adaptation of the approach used in Liebmann and Marengo (2001) and Bombardi et al. (2017) to onsets and demises that do not use a mean threshold based on the climatology of the rainfall cycle, or referred in this study as the Relative Meteorological Onset (RMO) and Demise (RMD). Using the raw daily data, the same equation from Bombardi et al. (2017) is applied with some modifications to calculate RMOs and RMDs:

$$(1) \qquad S_{\text{window}}(n) = \sum_{i=t_{\text{window}}}^{n} P(i) - P_{\text{window}}$$

Where $S_{window}(n)$ is the anomalous accumulated precipitation at precipitation day "i" to day "n". P(i) is the daily precipitation at day "i". P_{window} is the mean daily value of the rainfall in that year calculated over the particular seasonal window; this differs from other methods that use P_{window} as the annual climatological daily precipitation rate (Liebmann and Marengo 2001; Bombardi et al. 2017; D16; B20). Finally, t_{window} is the date related to the start, or before the start, of the seasonal window being used. Similar to Bombardi et al. 2017, for onsets it is recommended to place t_{window} in the dry season that precedes the rainfall season in order to accurately depict the transition from dry to wet seasons. Depending on the modality of the climatological rainfall pattern, one or multiple S_{window} (n) are used. For unimodal patterns, only one $S_{window}(n)$ is used and is used for calculating both onset and demise. For unimodal dual maxima patterns, two $S_{window}(n)$ are used: one is used for the onset, and the other is used for the demise. For bimodal patterns, four $S_{window}(n)$ are used: each for each onset and each demise calculation. For onset, the minimum of $S_{window}(n)$ is identified. Next, the candidate onsets from the smoothed data are utilized by finding the candidate onset that relates to the date of the minimum of $S_{window}(n)$. This is done by finding the latest date of a candidate onset that is (1) less than the date of the minimum of $S_{window}(n)$, and (2) the magnitude of the rainfall on the candidate onset day is within the R^{th} percentile of the rainfall amount, relative to that year, over the window. The latter is done in case the smoothing filter has several "kinks" between the date of the minimum of $S_{window}(n)$ to the actual onset. A recommended value for the onset R^{th} percentile is the 33^{rd} to 50^{th} percentile. The candidate onset that satisfies both criteria is deemed the RMO.

The approach to find the RMDs follows that for the RMOs, with a few key differences. The maximum of $S_{window}(n)$ is found. Using the candidate demises, the timing of the RMD is determined by finding the minimum candidate demise that: (1) is greater than the date of the

maximum of $S_{window}(n)$, and (2) the candidate demise value is within the R^{th} percentile of the rainfall amount, relative to that year, over the window. The latter is done in case the smoothing filter has several "kinks" from the date of the maximum of $S_{window}(n)$ to the actual demise. A recommended value for the demise R^{th} percentile is the 10^{th} to 33^{rd} percentile.

In the Northwestern Caribbean, two Swindow(n) are determined:

$$(2) \qquad S_{\mathrm{ERS}}(n) = \sum_{i=t_{\mathrm{ERS}}}^{n} P(i) - P_{\mathrm{ERS}}$$

$$(3) \qquad S_{\mathrm{LRS}}(n) = \sum_{i=t_{\mathrm{LRS}}}^{n} P(i) - P_{\mathrm{LRS}}$$

t_{ERS} is Day 1 (March 1^{st}) and t_{LRS} is the date of the climatological intermittent dry period minima, or Day 141 (July 18^{th}). Since the Northwestern Caribbean has a unimodal dual maxima pattern, only the first window is used to determine onset, and the second window is used to determine demise. The date of the minimum of $S_{ERS}(n)$ is calculated, and is on day 85 (May 30^{th}) (Fig. 4.3b). The date of the minimum of $S_{ERS}(n)$ is used as a reference date to determine the timing of the RMO (Fig. 4.3c). There is one candidate onset that is before the date of the minimum of $S_{ERS}(n)$ and its value is within the 33^{rd} percentile of the rainfall amount, relative to the year, over the ERS window. Therefore, the RMO is on day 80 (May 20^{th}). The date of the maximum of $S_{LRS}(n)$ is calculated, and is on day 248 (November 4^{th}) (Fig. 4.3b). There are two candidate demises that are after the date of the maximum of $S_{LRS}(n)$ and its value is within the 1

0^{th} percentile of the rainfall amount, relative to the year, over the LRS window (Fig. 3c). Therefore, the RMD is the earlier of the two candidate demises, or day 255 (November 11^{th}).

The Guianas experience a bimodal pattern; therefore, four $S_{window}(n)$ are determined (Fig 4.4b). For finding the onset of the first rainfall season and demise of the second rainfall season, Equation 1 is used. For finding the demise of the first rainfall season and onset of the second rainfall season, Equation 1 is altered, such that the mean daily value of the rainfall in that year calculated over the intermittent dry period window, or $P_{IDP}(n)$, is used. For bimodal patterns the demise of the first rainfall season (RFS1) and onset of the second rainfall season (RFS2) fall under the intermittent dry period window, where using $P_{IDP}(n)$ better characterizes the transition between each rainfall season. The minimums of $S_{RFS1}(n)$ and $S_{RFS2}(n)$ are calculated and RMOs for each season are determined (Fig. 4.4c). The maximums of $S_{RFS1}(n)$ and $S_{RFS2}(n)$ are calculated and RMDs for each season are determined.

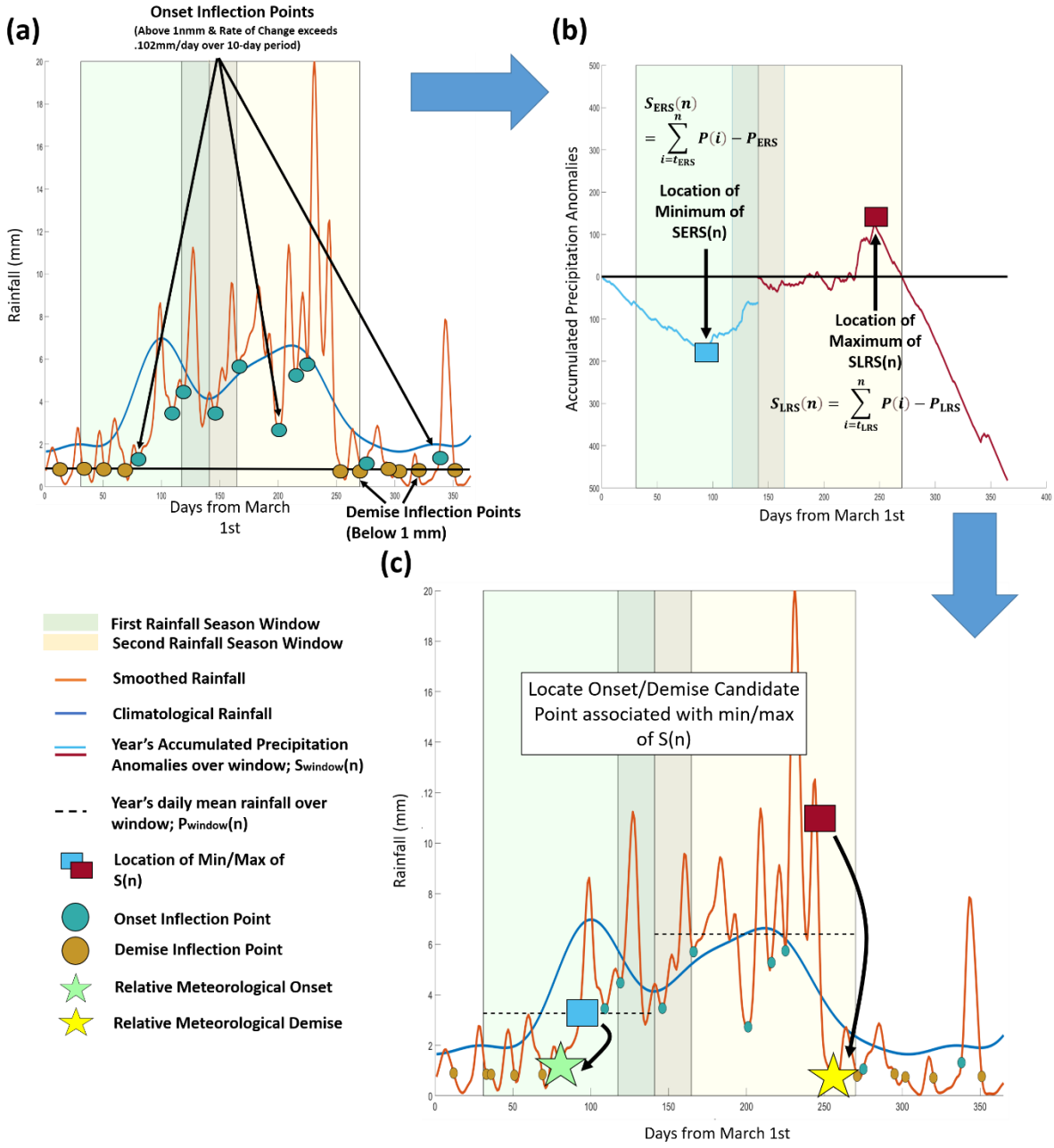

Figure 4.3: Schematic summary of using the method to calculate Relative Meteorological Onsets and Demises for the 2011 Northwestern Caribbean rainfall cycle using smoothed daily data (orange line). (a) Determining onset and demise candidates using the mm threshold and rate of change threshold. (b) the minimum and maximum of the accumulated precipitation anomalies using raw daily data (light blue and maroon lines) for each seasonal window (green and yellow boxes) are calculated. (c) locate the nearest candidate onset and demise from min/max S(n) (light blue and maroon squares) that satisfy conditions for Relative Meteorological Onset (green star) and Demise (yellow star).

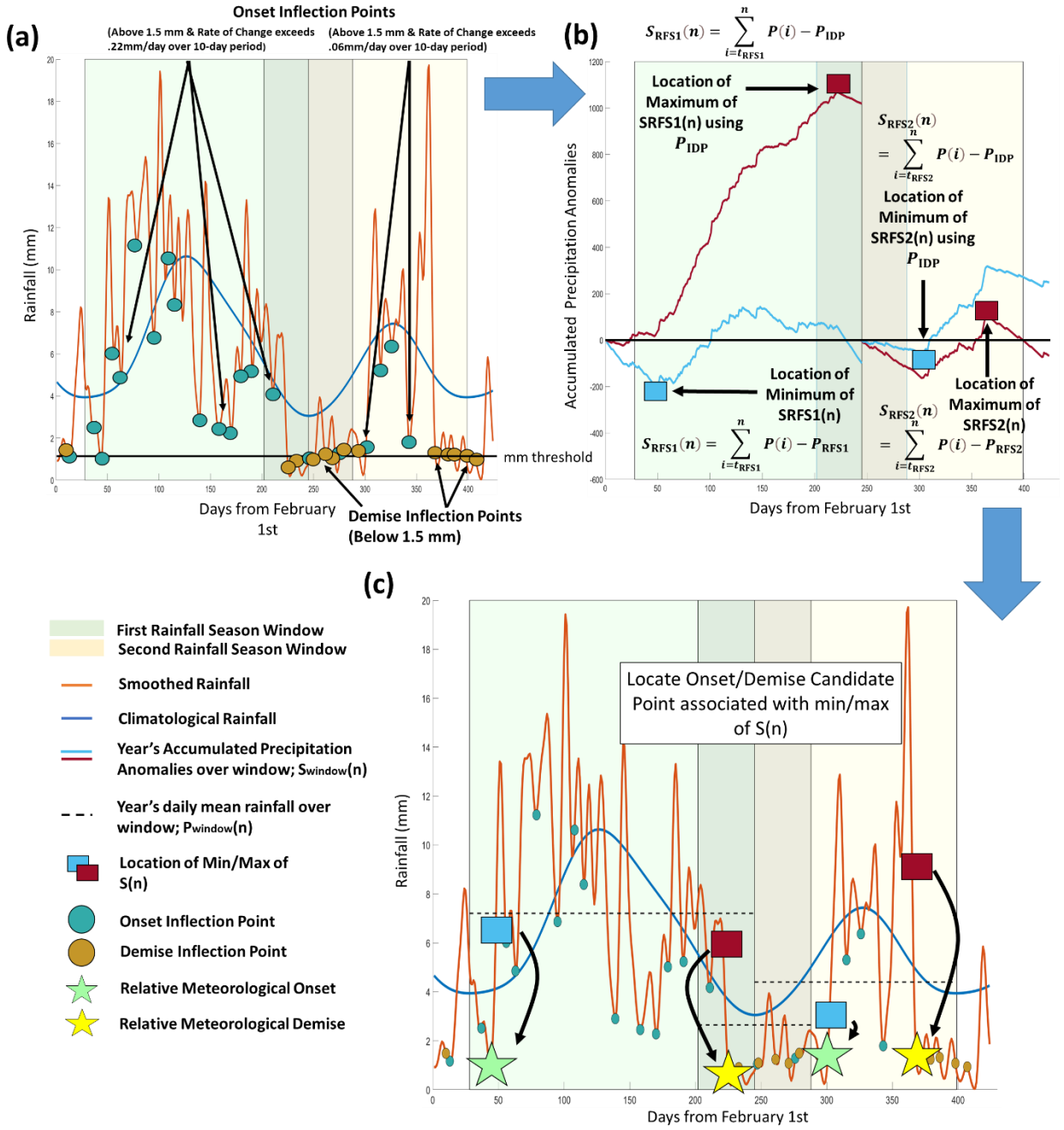

Figure 4.4: Schematic summary of using the method to calculate Relative Meteorological Onsets and Demises for the 1985 Guianas rainfall cycle using smoothed daily data (orange line). (a) Determining onset and demise candidates using the mm threshold and rate of change threshold. (b) the minimum and maximum of the accumulated precipitation anomalies using raw daily data (light blue and maroon lines) for each seasonal window (green and yellow boxes) are calculated. (c) locate the nearest candidate onset and demise

from min/max S(n) (light blue and maroon boxes) that satisfy conditions for Relative Meteorological Onset (green star) and Demise (yellow star).

4.3.4 Characteristics related to the Intermittent Dry Period

The intermittent dry period window is used to calculate the magnitude and duration of intermittent dry periods. The magnitude of the intermittent dry period is estimated from the raw daily data as the mm/day average within the intermittent dry period window. The duration of the intermittent dry period is the total number of raw daily data days within the intermittent dry period window that has a mm value less than the 66^{th} percentile of the raw daily climatological intermittent dry period magnitude. For the Northwestern Caribbean, the climatological magnitude of the intermittent dry period is 4.70mm, and the dates categorized as less than the 66^{th} percentile of the raw daily climatological intermittent dry period magnitude would be those with amounts less than 5.60mm.

4.4 Results

The mean and variability of temporal characteristics have been used to investigate their relationship with other characteristics of rainfall in order to determine its predictability with other characteristics or dynamical phenomena (e.g., Liebmann and Marengo, 2001; Moron and Robertson 2014; D16; B20). Some examples are, but not limited to, rainfall amount, frequency of wet days, and intensity of rainfall. One relationship that varies with region is the relationship between temporal rainfall characteristics and seasonal or annual rainfall totals. Some regions have little to no correlation between seasonal rainfall totals and onset/demise (Drosdowsky 1996; Nicholls et al. 1982; Marengo et al. 2001), while other regions have strong correlations (Liebmann and Marengo, 2001; Moron et al. 2009; Camberlin et al. 2009; Mugo et al. 2016). A factor in determining whether a relationship exists between onset/demise and rainfall amount is whether a sizable amount of rainfall in the seasonal or annual totals are attributed to pre or post rainfall season

activity. However, whether or not the relationship is attributed to how an onset and demise is defined has yet to be determined. For example, would onsets and demises that are based on the climatological mean, as D16 and B20 use, have a different relationship with rainfall amount than those that are based on means relative to a particular year's rainfall season, as this study uses? Below this method and other methods are applied to the Caribbean data to investigate the climatology and variability of temporal characteristics of rainfall. Additionally, the present method is examined to understand relationships between temporal/intermittent dry period characteristics and select dynamical mechanisms that shape the regional climate of the Caribbean, which are determined from the results from Chapters 2 and 3. Information on the atmospheric/oceanic indices used in the analysis can be found in Table 4.2.

Table 4.2: Atmospheric/oceanic indices and rainfall characteristics used to correlate with temporal and intermittent dry period characteristics for the Caribbean/Guianas. All indices/characteristics are from 1979-2015. For indices, seasonal means are created using the selected time period. Seasonal Rainfall totals are the rainfall totals within the time period.

NAME (ACRONYM/REFERENCE)	DATASET	TIME PERIOD(s)	LAT/LON
North Atlantic Oscillation (NAO) (Barnston and Livezey 1987)	NOAA Climate Prediction Center NAO Index	January-March (JFM)	(Barnston and Livezey 1987)
El Nino Southern Oscillation Extended NINO3.4 Index (ENSO) (Huang et al. 2017)	Extended Reconstructed Sea Surface Temperature version 5	July-August (JJA) September-November (SON)	5°N-5°S, 150°W-90°W
Southern Tropical North Atlantic (STNA) SST and SLP	European Centre for Medium-Range Weather Forecasts	First Rainfall Season: startdate until the date of the climatological minima of the intermittent dry period for each region. For the Eastern Caribbean, startdate until enddate.	9.5°N-19.5°N;75.5°W-39.5°W
East Eastern Pacific (EEP) SST and SLP			0°N-12°N 100°W-80°W
925hPa Caribbean Sea Zonal (CLLJ), Meridional (CSv925),			

and direction (CSV925dir) wind components	Interim Re-Analysis (ERA-Interim; Dee et al. 2011)	Second Rainfall Season: the date of the climatological minima of the intermittent dry period until November 30th for Northwestern, Central, and Western Caribbean and enddate for Guianas. Intermittent Dry Period: Intermittent Dry Period window	12.5°N-17.5°N; 80°W-70°W
North South America 925hPa Zonal and Meridional Wind Components (NSAM u925) (NSAM v925)			4°N-13°N 64°W-40°W
Seasonal Rainfall Totals	Station data from study		Varies by sub-region

4.4.1 Onset Climatology and Variability

There is a large spread in dates determined by the methods for the mean of the onset for all years across each of the four sub-regions in the Caribbean and Guianas (Table 4.3). The onset means from this study show that the RMOs progress from east-to-west, starting earliest in the Central Caribbean / first rainfall season in the Guianas and latest in the Western Caribbean. A notable exception is the Eastern Caribbean; however, the dates of the RMO means are at the start of the wetter season, not the rainy season, as this region experiences substantial rainfall throughout the year. The Guianas experience a second rainfall season in the Fall; therefore, its second mean onset is later than the other sub-regions' mean onsets.

Table 4.3: Comparison of Onset Means (and Standard Deviations) of different Methods

REGION / ONSET DATE	This Method Relative Meteorological Onset	Liebmann and Marengo (2001)	Bombardi et al. (2017)	Dunning et al (2016/) / Bombardi et al. (2020)

Northwestern Caribbean	May 14th (13 Days)	June 22nd (104 Days)	April 14th (26 Days)	May 19th (35 Days)
Western Caribbean	May 23rd (13 Days)	June 28th (119 Days)	April 25th (30 days)	June 18th (109 Days)
Central Caribbean	April 23rd (18 Days)	August 2nd (138 Days)	April 2nd (22 Days)	May 27th (98 Days)
Eastern Caribbean	May 9th (30 days)	August 1st (107 Days)	April 21st (39 Days)	June 28th (69 Days)
Guianas First Season	April 17th (20 Days)	X	X	April 25th (26 Days)
Guianas Second Season	October 25th (14 Days)	X	X	December 31st (31 Days)

The evolution of the RMO across the 5 sub-regions, shown in Table 4.3, is similar with the evolution of the start of the ERS / first rainfall season found in Chapter 2. Hence, the estimates of ERS start dates using the RMO are consistent with that dynamical view of the rainfall climatology over the Caribbean. When applying the method from Liebmann and Marengo (2001), the climatological onsets are identified further into the rainfall season. This is because Liebmann and Marengo (2001) uses the entire calendar year which includes the post-rainfall dry season. Including the post-rainfall dry season when calculating accumulated precipitation anomalies can cause the minimum of S(n), and consequently the onset, to occur well after the wet season. Several methods attempt to fix this issue. Bombardi et al. (2017) use the derivative of S(n) and determine onset as the first day where the dS(n)/dt changes from negative to positive and is positive for 4 consecutive days. When using the Bombardi et al. (2017) method, however, the mean onset begins well before the start of the climatological wet season in the Caribbean (Chapter 2). This is due to

transient activity occurring in the Caribbean prior to the rainfall season, which induces multiple days of rainfall that satisfy the criteria in Bombardi et al. (2017). Unless modified, the Liebmann and Marengo (2001) and Bombardi et al. (2017) methods are configured for unimodal regimes alone; therefore, onsets and demises in the Guianas could not be calculated under these methods. Additional adaptations of the method from Liebmann and Marengo (2001) include the methods from D16 and B20, both of which calculate the start and end of the hydrological cycle (d_s, d_e) first, and then to determine the year-to-year variability for unimodal patterns they set t_0 as d_s – N to d_e + N, where N is 45 days (B20), and 50 days (D16). For bimodal patterns, t_0 is d_{s1} – N to d_{e1} + N for the first rainfall season and d_{s2} – N to $d_{e\2}$ + N for the second rainfall season, where N is 20 days (D16). This reduces the chances of finding the onset after the demise, or the demise before the onset. The mean onset in the Northwestern Caribbean and first rainfall season in the Guianas using their method is comparable with this study, though the interannual variability of the onsets show the present method to have onsets that are earlier than D16/B20 (Fig. 4.5a,c). The mean onset in the Western (Fig. 4.5b), Central (Fig. 4.5d), and Eastern Caribbean (Fig. 4.5e), and second rainfall season in the Guianas (Fig. 4.5f) are earlier in the present method than in D16/B20.

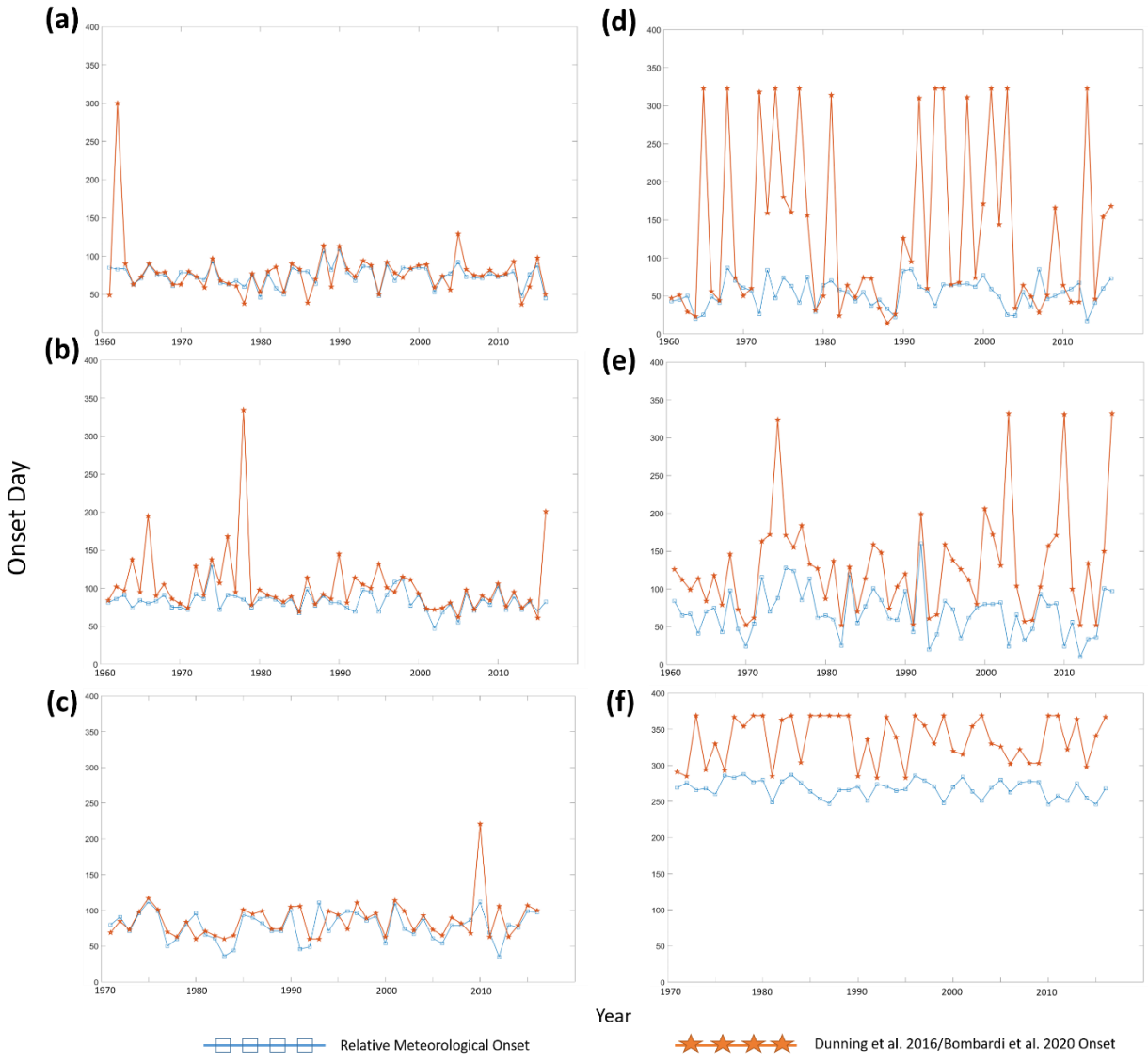

Figure 4.5: Regional station averaged onset dates from 1960/70-2015 in the (a) Northwestern Caribbean, (b) Western Caribbean, (c) Guianas first rainfall season, (d) Central Caribbean, (e) Eastern Caribbean, and (f) Guianas second rainfall season using several methods. Blue squares denote the relative meteorological onset. The orange stars denote onset dates replicating the Dunning et al. 2016 or Bombardi et al. 2020 method.

A closer examination of several cases in the Caribbean helps explain the onset date differences between the present method and D16/B20 method. In the 1974 rainfall cycle in the Northwestern Caribbean (Fig. 4.6a), the minimum of S(n) is the same between the present method and the D16/B20 method. This implies that differences in the definition of the time period used to

calculate the mean threshold and accumulated rainfall between methods did not affect the date of the S(n) minimum. However, D16 and B20 solely use the date of the S(n) minimum to define the onset. The minimum of S(n), which is where previous methods deem the onset of the rainfall cycle, is not the start of the rainfall season in all cases, but rather when rainfall reaches the calculated seasonal yearly threshold or the calendar year climatological threshold. As a result, portions of the rainfall season are missed. The present method mitigates this limitation by not defining the onset as the minimum of S(n), but defines the onset based on the candidate onset that is associated with the minimum of S(n). This difference largely explains why the Northwestern Caribbean onset dates are earlier in the present method than in D16/B20. The Guianas first rainfall season (e.g., Fig. 4.6d) show similar differences between onsets that are largely attributed to how S(n) is utilized to find the onset. In the Eastern Caribbean, the onsets in the present method are several weeks to months earlier than in D16/B20. Since the transition of the less-wet to wet seasons in the Eastern Caribbean is gradual (e.g., Fig 4.6b), the minimum of S(n), regardless of the time period or mean threshold parameter used, is usually well into the wet season. Hence, the large difference between the onset dates in the Eastern Caribbean is predominantly due to placing the onset as the minimum of S(n) vs. utilizing the minimum of S(n) as a benchmark to find the onset.

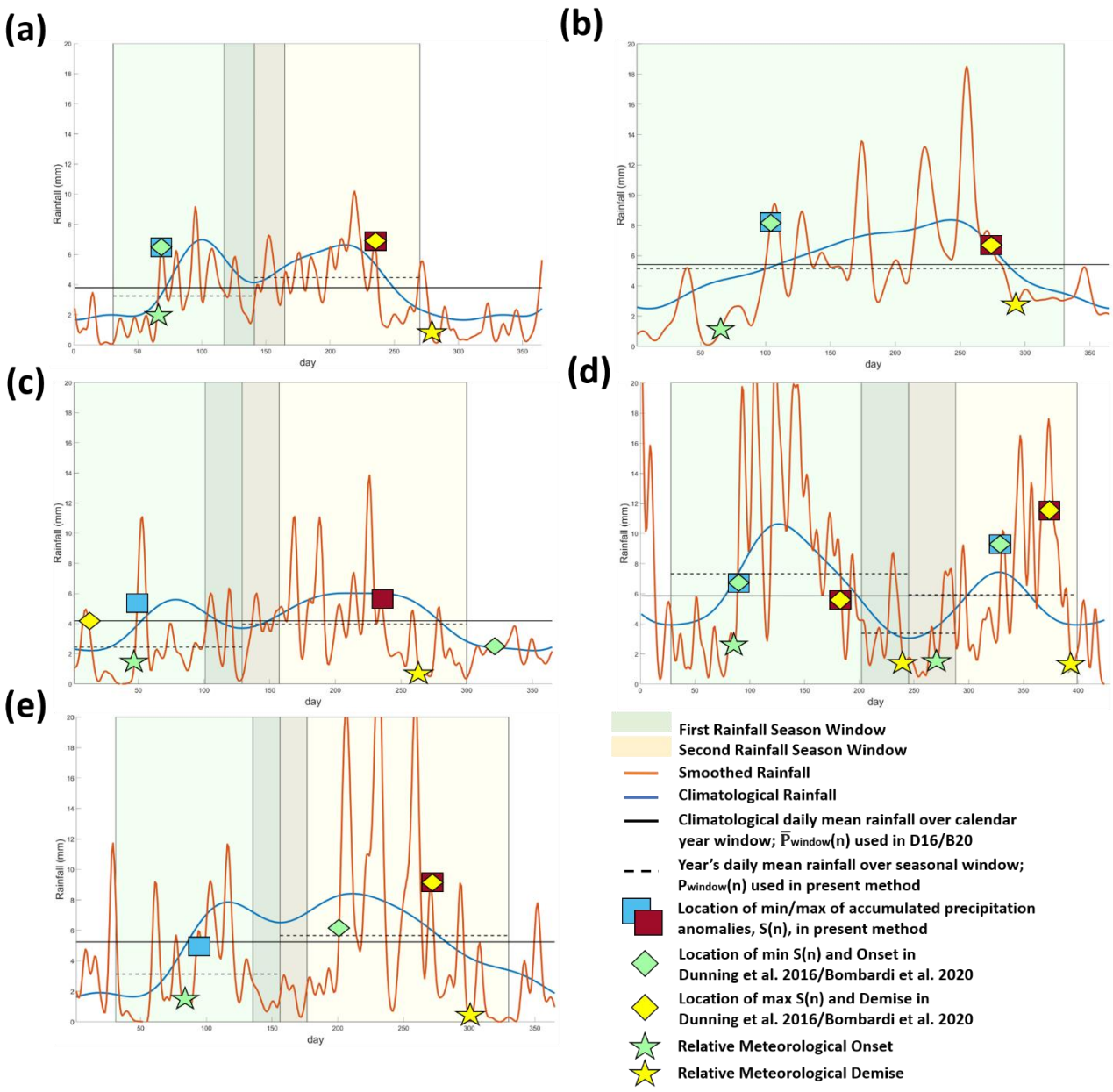

Figure 4.6: (a) is similar to Fig. 4.3c, but for the year 1974 over the Northwestern Caribbean. Similar analysis is applied to other sub-regions of the Caribbean: (b) Eastern Caribbean in 2003, (c) Central Caribbean in 1975, and (e) Western Caribbean in 2015. (d) is similar to Fig 4.4c., but for the year 1997 over the Guianas

In some cases and sub-regions, the window and mean threshold parameters also contribute to differences in onset dates between methods. The 1975 rainfall cycle in the Central Caribbean (Fig. 6c), and 2015 rainfall cycle in the Western Caribbean (Fig. 4.6e), experienced a weaker than

normal ERS and a normal LRS. The D16/B20 missed the onset seen in the ERS (Fig. 6e) or placed the onset as d_e + N (Fig. 4.6d). Using the ERS window with ERS mean thresholds for the given year, the present method captured onsets in the weaker than normal ERS for both sub-regions. As noted in Chapters 2 and 3, the ERS is shorter in duration than the LRS, and the variabilities of the ERS and LRS are independent of each other. When applying a mean threshold that is based on the climatology of the entire hydrological cycle, the mean threshold is biased towards the season with a larger amount of rainfall. Hence, the accumulated precipitation anomalies miss the ERS, resulting in onsets that are either during the LRS, or post-rainfall dry season, especially during dry ERS years. Similar findings are seen in the Guianas, where its second rainfall season is shorter in duration and less in magnitude than its first rainfall season. A climatological mean threshold skews the second onset further into the second rainfall season (e.g., Fig. 4.6d). The S(n) for the second rainfall season in the present method finds onsets that are typically where the transition between the intermittent dry period and second rainfall season are seen. Alongside differences in selecting the minimum of S(n) as the onset, the time and window parameter differences explain why the mean onset standard deviations of D16 and B20 are larger than those estimated in this study, and highlights how previous methods may not capture the transition of the rainfall season(s) in 1) years where the magnitude of the rainfall season is significantly less than its climatology, and 2) sub-regions with non-symmetrical rainfall cycles.

The methodology is replicated for each station in order to determine whether sub-regional RMO dates are representative of their respective stations, and to better compare the station precipitation climatologies in Chapter 2. All sub-region RMO means using station-averaged daily data reflect their corresponding stations' RMO mean. The evolution of the RMO means across the 41 stations in the Caribbean/Guianas closely resembles the evolution of the start of the rainfall

cycle found in Chapter 2 (Fig. 4.7a). The Central Caribbean, Northern Antilles, and Guianas experience its onset first, with dates ranging from early-April to early May. Onset dates migrate westward onto the Northwestern Caribbean, where a SE-to-NW evolution of its onset dates is seen ranging from early May (e.g. Jamaica) to late May (e.g. Florida Keys). The Western Caribbean experiences its onset dates last, with dates ranging from late-May to mid-June. The findings follow the dynamical evolution of the ERS across the Caribbean, where convergence by the North Atlantic Subtropical High (NASH) initiates rainfall over the Central Caribbean and Northern Lesser Antilles and progresses northwestward into the Northwestern Caribbean and in the Western Caribbean in conjunction with convergence from the northward migrating Eastern Pacific Intertropical Convergence Zone (ITCZ) (Chapter 2). The Central and Southern Lesser Antilles also experience later onsets – ranging from mid-May to mid-June. Convergence that starts from NASH does not reach the Central and Southern Lesser Antilles; therefore, the Eastern Caribbean experiences its onset later via convergence from the northward migrating Atlantic ITCZ during the boreal summer (Chapter 2). Before the boreal summer, the Atlantic ITCZ is over the Guianas, which is why the Guianas experience its first rainfall season earlier than most of the other sub-regions. The second onset means in the Guianas also resemble its regional mean onset date (not shown) and is in mid-October as a result of the Atlantic ITCZ migrating southward from the Eastern Caribbean.

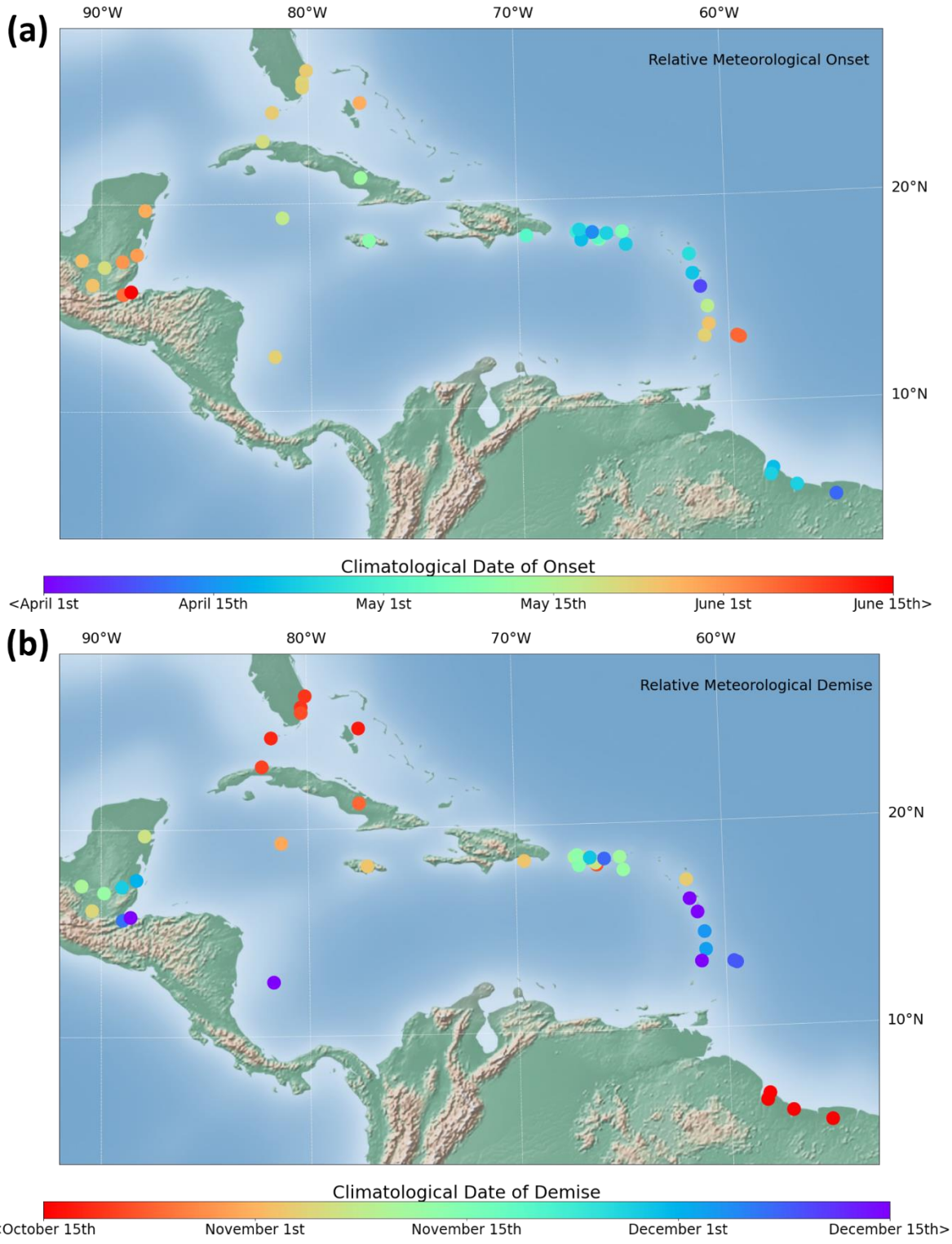

Figure 4.7: Climatological Relative Meteorological Onset (top) and Demise (bottom) dates across stations in the Caribbean.

Nearly all correlations between rainfall amounts/dynamical indices and onsets are weaker and statistically non-significant with RMOs than onsets from D16/B20 (Table 4.4). The contrast is due to how each is calculated. RMOs are independent of the climatology since the mean threshold used to determine S(n) is based on each year's rainfall. Under D16 and B20, the mean threshold to calculate S(n) is based on the climatology; the mean threshold is building the rainfall amount vs. timing relationship into the methodology by investigating anomalous precipitation respective to the mean normal. To better compare with D16 and B20 onsets, onsets that are determined by the climatological mean threshold are calculated using the present method. These onsets will be called the absolute meteorological onsets. The absolute meteorological onset follows the same steps as the RMO except: (1) when calculating $S_{window}(n)$, P_{window} becomes $\overline{P}_{window}$ or the precipitation from the climatology averaged over the seasonal window, and (2) when determining the absolute meteorological onset, the candidate onset must be within the R^{th} percentile of the magnitude of the climatology over the seasonal window.

Generally, absolute onsets have a similar or stronger relationship with the known atmospheric/oceanic modes of variation that shape the regional climatology and variability of ERS rainfall in the region than D16/B20 onsets. All sub-regions have high negative correlations between first seasonal rainfall totals and onset dates. The winter-time North Atlantic Oscillation (NAO) has moderate positive correlations with onset dates for all sub-regions except the Northwestern Caribbean. Moderate negative and positive correlations are seen across the Central Caribbean, Eastern Caribbean, and to an extent Guianas' first rainfall season between onsets and southern Tropical North Atlantic ERS SSTs and SLPs, respectively. ERS zonal 925hPa winds over the Caribbean Sea, or the Caribbean Low-Level Jet (CLLJ), has negative correlations with onset dates across the Western, Central and Eastern Caribbean. The meridional component of 925hPa

winds during the ERS in the Caribbean Sea and during the first rainfall season in the North South American Coastline have moderate to high negative correlations with onset dates across the Northwestern Caribbean and Guianas, respectively. The winter-time NAO is the main driver of ERS variability; the winter-time NAO induces a persistent anomalous SST and SLP pattern over the southern Tropical North Atlantic and Caribbean Sea that affects the ERS across the Caribbean (Chapter 3). During a winter-time positive-NAO, cold SSTs and above-normal SLP are seen over the southern Tropical North Atlantic and persist into the ERS. Alongside stronger easterlies, the anomalous signals weaken moisture convergence over the Caribbean basin and result in a weaker-than normal ERS (Chapter 3). Given the strong inverse relationship between absolute or D16/B20 onsets and ERS/first rainfall season totals, the winter-time NAO induced anomalous SST/SLP pattern is likely responsible for the variability of these onset dates (e.g., positive winter-time NAO = later-than-normal ERS absolute onset). However, since RMOs are not statistically significant with most indices, the findings from the correlations suggest the variability of the rainfall seasons are consequences of changes to rainfall seasons' magnitude rather than changes to rainfall seasons' timing.

The start of the second rainfall season in the Guianas is in the fall, which is also where the demise of the LRS is seen over the Caribbean; therefore, atmospheric/oceanic indices that are known to impact tropical Atlantic rainfall LRS variability are investigated. Onset dates for the second rainfall season are negatively highly correlated with its seasonal rainfall totals. Although weak, some positive correlations are seen between summertime El Niño–Southern Oscillation (ENSO) / Eastern Pacific SSTs and second onset dates.

Table 4.4: Correlations between various atmospheric/oceanic indices and onset dates (first two columns) and demise dates (last two columns) from 1979-2015. Information on indices can be found in Table 4.2. Bold denotes significance at the 95th percentile using a 2-sided t test.

REGION	INDEX	ONSET			INDEX	DEMISE		
NORTHWESTERN CARIBBEAN		REL ONSET	ABS ONSET	DUN./BOM. ONSET		REL DEMISE	ABS DEMISE	DUN./BOM. DEMISE
	ERS TOTALS	-.2652	**-.6575**	**-.3460**	LRS TOTALS	.1487	**.7131**	**.5218**
	NAO	.0659	.1822	.0983	ENSO (JJA)	.1141	**-.3819**	.0537
	STNA SST	.0723	-.0343	.1779	EEP SST	.1234	**-.4558**	-.0457
	STNA SLP	-.1221	.0699	-.1264	EEP SLP	-.0787	**.6031**	.0782
	CLLJ	.1004	-.1245	.0974	CLLJ	-.0105	**.5788**	.1589
	CSv925	**-.3593**	**-.6073**	**-.5087**	CSv925	.1654	.1994	.1913
	CSV925dir	.0540	.1886	.0110	CSV925dir	.0561	**-.5533**	-.1320
WESTERN CARIBBEAN		REL ONSET	ABS ONSET	DUN./BOM. ONSET		REL DEMISE	ABS DEMISE	DUN./BOM. DEMISE
	ERS TOTALS	-.1603	**-.6855**	**-.5099**	LRS TOTALS	-.0606	**.5927**	**.4726**
	NAO	-.0713	**.3148**	**.3485**	ENSO (JJA)	.1134	-.0488	-.0173
	STNA SST	.1786	-.1946	-.2458	EEP SST	.1159	.0463	-.1031
	STNA SLP	-.3094	.0917	.1897	EEP SLP	-.0917	-.0515	.1615
	CLLJ	.1413	**-.3247**	**-.3702**	CLLJ	-.1685	-.1023	.0286
	CSv925	.3034	.0439	-0.047	CSv925	-.006	.0880	.1464
	CSV925dir	-.1043	.2559	.2769	CSV925dir	.1707	.1202	-.0283
CENTRAL CARIBBEAN		REL ONSET	ABS ONSET	DUN./BOM. ONSET		REL DEMISE	ABS DEMISE	DUN./BOM. DEMISE
	ERS TOTALS	-.3150	**-.7481**	**-.6039**	LRS TOTALS	-.0294	**.8219**	**.6472**
	NAO	.1767	**.4682**	**.4107**	ENSO (JJA)	.1323	**-.4291**	**-.4245**
	STNA SST	-.0616	**-.4821**	**-.3428**	EEP SST	.0667	**-.3915**	**-.4127**
	STNA SLP	.2897	**.4322**	**.3421**	EEP SLP	-.0191	**.4349**	.3001
	CLLJ	-.2476	**-.5031**	**-.4900**	CLLJ	-.1886	**.7005**	**.4048**
	CSv925	-.2853	.0052	.0874	CSv925	-.1913	.0445	-.1411
	CSV925dir	.3172	**.6045**	**.4542**	CSV925dir	.1856	**-.5852**	-.2858
EASTERN CARIBBEAN		REL ONSET	ABS ONSET	DUN./BOM. ONSET		REL DEMISE	ABS DEMISE	DUN./BOM. DEMISE
	ERS TOTALS	**-.6944**	**-.7551**	**-.5201**	LRS TOTALS	.2728	**.6367**	**.5209**
	NAO	.1728	**.4193**	.2781	ENSO (JJA)	.0269	-.2862	-.2671
	STNA SST	**-.4257**	**-.4130**	-.2825	EEP SST	-.0551	-.2837	-.3050
	STNA SLP	.3106	**.3936**	.2942	EEP SLP	-.0189	.2162	.1924
	CLLJ	-.3120	**-.4680**	**-.4566**	CLLJ	-.0370	.1388	.2844
	CSv925	**.3383**	.1673	-.0418	CSv925	-.1250	-.1247	-.2369
	CSV925dir	**.4140**	**.5673**	**.4396**	CSV925dir	.0473	-.1175	-.2796
GUIANAS		REL ONSET	ABS ONSET	DUN./BOM. ONSET		REL DEMISE	ABS DEMISE	DUN./BOM. DEMISE

(FIRST SEASON)	RFS1 TOTALS	-.2426	**-.5917**	**-.5917**	RFS1 TOTALS	.3598	**.4877**	**.3777**
	NAO	.1822	**.3400**	.1549	ENSO (JJA)	-.0728	-.1745	-.1741
	STNA SST	-.2787	-.2683	-.2108	EEP SST	-.0368	-.2446	-.3137
	STNA SLP	.2333	**.3512**	.2618	EEP SLP	-.0273	.1966	.2731
	NSAM u925	-.1076	-.0897	-.2311	NSAM u925	.0062	.0107	.0396
	NSAM v925	**-.3983**	**-.5741**	**-.4841**	NSAM v925	.1368	**-.3347**	**-.3340**
		REL ONSET	ABS ONSET	DUN./BOM. ONSET		REL DEMISE	ABS DEMISE	DUN./BOM. DEMISE
GUIANAS (SECOND SEASON)	RFS2 TOTALS	-.2753	**-.6369**	**-.7301**	RFS2 TOTALS	.4613	**.8635**	**.8141**
	ENSO (JJA)	.0513	.1954	.0205	ENSO (SON)	.0404	-.2542	-.1948
	EEP SST	.0522	.2401	.1251	EEP SST	.0540	-.2865	-.2481
	EEP SLP	-.0285	-.1638	-.2255	EEP SLP	-.0905	.2510	.2475
	NSAM u925	**.3424**	-.0382	-.1262	NSAM u925	.0068	.0575	.2233
	NSAM v925	-.0681	.0711	.1326	NSAM v925	-.1317	-.0438	-.1254

4.4.2 Demise Climatology and Variability

The spread between Liebmann and Marengo (2001), Bombardi et al. (2017), and the present method on the mean of the demise for all years across each of the four sub-regions in the Caribbean and Guianas is smaller than the spread of onsets (Table 4.5). The opposite is found between D16/B20 and the present method. The regional RMD mean dates mostly follow the NW to SE progression of the demise of the rainfall season in the Caribbean: the Northwestern Caribbean demise is first, followed by the Western and Central Caribbean, and then the Eastern Caribbean and Guianas' second rainfall season (Chapter 2). The exception is the first rainfall season in the Guianas where its demise is the earliest than the other sub-regions.

When applying the method from Liebmann and Marengo (2001), the mean demise dates are earlier than the climatological transition from wet-to-dry seasons (Chapter 2), as a result of years with abnormally dry rainfall seasons that cause the maximum of S(n) to be the first date of

the calendar year (not shown).

Table 4.5: Comparison of Demise Means (and Standard Deviations) of different Methods

REGION / DEMISE DATE	This Method Relative Meteorological Demise	Liebmann and Marengo (2001)	Bombardi et al. (2017)	Dunning et al. (2016) / Bombardi et al. (2020)
Northwestern Caribbean	November 9th (17 Days)	October 24th (37 Days)	June 9th (16 Days)	October 27th (24 Days)
Western Caribbean	November 24th (26 Days)	October 10th (113 Days)	June 4th (20 Days)	November 5th (75 Days)
Central Caribbean	November 25th (19 Days)	September 16th (116 Days)	May 10th (13 Days)	September 18th (112 Days)
Eastern Caribbean	December 9th (30 Days)	September 6th (131 Days)	June 17th (9 Days)	October 29th (81 Days)
Guianas First Season	September 24th (29 Days)	X	X	August 6th (24 Days)
Guianas Second Season	+1 January 20th (29 Days)	X	X	December 23rd (32 Days)

Bombardi et al. (2017) also shows a demise that is too early, largely because there are multiple years in Caribbean sub-regions that have breaks in their rainfall season that satisfy the criteria set in their method to determine demise. The mean demise dates from D16 and B20 are closer to this study's, yet are also earlier than the climatological wet-to-dry season transition found in Chapter 2. This is due to several reasons. First, D16 and B20 set the demise as the maximum of S(n), but this does not accurately depict the end of the rainfall season, as the date of the maximum of S(n) is when rainfall is below the seasonal yearly or climatological mean threshold. This can limit the length of the rainfall season or inaccurately depict the demise by not including portions

of the rainfall season that have gradual demises or intermittent rainfall that is post-peak of the rainfall season (e.g., Fig. 4.6). The 1974 Northwestern Caribbean (Fig. 4.6a), 1997 Guianas (Fig. 4.6d) and 2015 Western Caribbean (Fig. 4.6e) rainfall cycles all show the maximum date of S(n) to be the same in the present method and D16/B20 methods, which means that the time period and window parameters did not affect the maximum date of S(n). However, the present method utilizing the candidate demise dates finds demises that are located during the transition from wet-to-dry season, and includes post-rainfall season peak intermittent rainfall or rainfall that is gradually decreasing from the date of the maximum of S(n). Second, in years where the rainfall season is anomalously dry, using a mean threshold based on the climatology, as D16 and B20 use, can skew the demise to be d_s – N or before the onset because the accumulated precipitation anomalies will be negative throughout the year and the maximum of S(n) would be at the startdate. Third, using a window that encompasses the entire hydrological cycle, as D16 and B20 use, can skew the demise date if the rainfall season is non-symmetrical or if components of the rainfall season (e.g. ERS and LRS) are independent of one another. Setting the window as the entire hydrological year when one season is anomalously dry and the other is not, or vice versa, can skew the S(n) calculation and cause the demise to be d_s – N or before the onset. For example, the 1975 Central Caribbean rainfall cycle (Fig. 4.6c) has the demise using the method D16 and B20 near d_s – N. Since the ERS was anomalously dry that year, using a mean threshold based on the climatology and calculating S(n) over the entire hydrological cycle caused the maximum of S(n) to be near ds – N. The present method found the demise during the wet-to-dry season transition using the LRS window and mean threshold relative to that year's LRS. These three reasons explain why the standard deviations of the mean demise dates are larger in D16 and B20 than in the present

method (Table 4.5), and how demise dates in the present method are later than in D16 and B20 (Fig. 4.8).

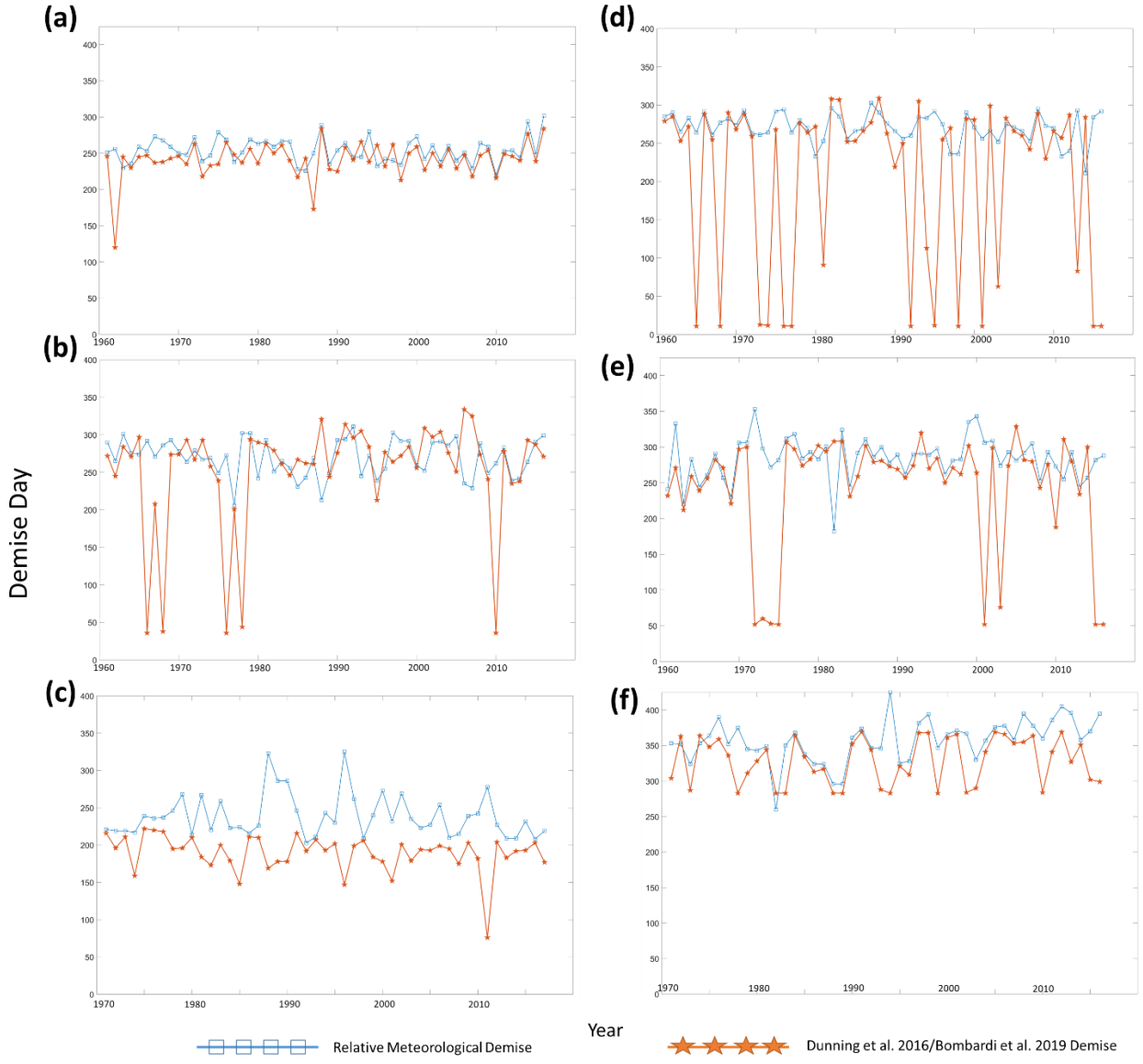

Figure 4.8: same as Fig. 4.5 but for demise dates.

The evolution of the RMD means across stations in the Caribbean match the evolution of the regional RMD means and resembles the dynamical evolution of the end of the rainfall cycle across the Caribbean (Fig. 4.7b). Generally, the evolution of the RMD means follows a NW-to-SE pattern. The demise of the rainfall cycle in the Caribbean begins in the northwestern corridor, with

RMD means between mid-October (e.g. Nassau, Bahamas) to early November (e.g. Worthy Park, Jamaica). The RMD dates migrate southeastward onto the Central Caribbean, with RMD means ranging from late October (e.g. Guaynama, Puerto Rico) to mid-November (e.g. Ensenada, Puerto Rico). In Chapter 2, the earliest climatological demise of the rainfall season IS in the Northwestern Caribbean and later the Central Caribbean. This is due to divergence from NASH and transience from the continental United States that infiltrates the Northwestern Caribbean and progresses into the Central Caribbean during the LRS (Chapter 2). The western Caribbean experiences a large range of demise dates, with inland stations experiencing early-November RMD dates and coastal stations experiencing late-November to December RMD dates. Chapter 2 finds the Western Caribbean during the LRS influenced by convergence from the jet exit region of the Caribbean Low-Level Jet (CLLJ; Amador 1998) and by the Eastern Pacific ITCZ (Chapter 2), which during the LRS slowly migrates southward. It is likely that the later RMD demise dates seen on coastal stations of the Western Caribbean are a result of lingering convergence seen from these dynamical features. The Eastern Caribbean experiences the latest RMD dates out of any Caribbean region, ranging from early to mid-December. The finding resembles the climatological end of the rainfall season across the Eastern Caribbean from the slowly southward migrating Atlantic ITCZ that influences the region during the LRS (Chapter 2). In the Guianas, both the first (Fig. 4.7b) and second (not shown) RMD means are a result of the migration of the Atlantic ITCZ (Chapter 2). The Atlantic ITCZ migrates away from the Guianas by August/September and migrates northward into the Eastern Caribbean to provide the Eastern Caribbean with its rainfall peak during its rainfall season. The second demise is when the Atlantic ITCZ moves south of the Guianas during the winter.

Similarly with onsets, absolute demises have a comparable or stronger relationship with the atmospheric/oceanic modes of variation that shape the Fall portion of the rainfall season than D16/B20 demises, and relative demises have non-significant and weak correlations with the atmospheric/oceanic modes of variation (Table 4.4). All sub-regions have high positive correlations between seasonal rainfall totals and demise dates. ENSO and Eastern Pacific SSTs during the rainfall seasons are negatively correlated with demise dates in the Northwestern, Central, and Eastern Caribbean, and Guianas. Eastern Pacific SLP and CLLJ during the LRS are positively correlated with demise dates in the Northwestern Caribbean, Central Caribbean, and to a lesser extent Eastern Caribbean. In the Guianas, both rainfall season demises have a positive correlation, though weak, with Eastern Pacific SLP, and the first rainfall season demise is negatively correlated with the meridional component of the 925hPa winds across Northern South America. Central Caribbean and Northwestern Caribbean demise dates are negatively correlated with 925hPa wind direction. ENSO is the main driver of LRS variability; the onset of ENSO during the Summer and Fall induces an anomalous see-saw SLP pattern between the Eastern Pacific and Caribbean basins through an ENSO atmospheric bridge (Giannini et al. 2000) that affects the LRS across the Caribbean (Chapter 3). During a warm ENSO, cold SSTs and above-normal SLP are seen over the Caribbean Basin during the LRS, which results in stronger easterlies and weaker moisture convergence over the Caribbean (Chapter 3). Given the strong mutual relationship between absolute or D16/B20 demises and LRS totals, the ENSO induced see-saw SLP pattern is likely responsible for the variability of the Caribbean demise dates. For the Guianas, the first rainfall season demise falls during the LRS; therefore, the effect of ENSO on the Caribbean likely affects the Guianas similarly. Since the second rainfall season of the Guianas is during the winter-time, it is likely the mature-phase of ENSO impacts the demise dates during the second rainfall

season. The correlation differences between demises that are based on a climatological mean threshold such as the absolute and D16/B20 demises vs. demises that are not based on a climatological mean threshold such as the RMDs suggests the variability of the rainfall seasons are a consequence of changes to the rainfall seasons' magnitude rather than changes to the rainfall seasons' timing.

4.4.3 Intermittent Dry Period Characteristics

Table 4.6 highlights the relationship between intermittent dry period characteristics and atmospheric/oceanic indices for sub-regions with intermittent dry periods. In the Caribbean, most sub-regions have statistically significant correlations between magnitude or duration of the intermittent dry period and seasonal rainfall totals, the winter-time NAO, summertime ENSO, southern Tropical North Atlantic SST and SLP during the intermittent dry period, and Caribbean Sea zonal and meridional components of the 925hPa winds during the intermittent dry period. There are some notable sub-regional differences. For example, the Western Caribbean and Central Caribbean have higher correlations between their intermittent dry period characteristics and ERS totals / winter-time NAO than LRS totals / summertime ENSO. For these sub-regions, the variability of the intermittent dry period may be more associated with variability of the ERS than LRS. For example, the Central Caribbean experiences little to no ERS during dry ERS years (Chapter 3), which results in a longer and more intense intermittent dry period. The correlations between the intermittent dry period characteristics and various indices suggest that above-normal magnitude and below-normal duration of the intermittent dry period are associated with 1) above-normal ERS and LRS, 2) a preceding winter-time negative NAO and summertime cold ENSO state, 3) warmer SSTs and above-normal SLP over the southern Tropical North Atlantic, and 4) anomalous westerlies. Since the variabilities of the ERS and LRS are driven by the Southern

Tropical North Atlantic persistent SST/SLP anomalous signal induced by the preceding winter-time NAO and the summertime onset of ENSO, respectively, the variability of the intermittent dry period in the Caribbean is likely driven by competing interactions of the anomalous signals induced by both preceding winter-time NAO and summertime ENSO over the region.

In the Guianas, seasonal rainfall totals, summertime ENSO, and Eastern Pacific SST and SLP are correlated with statistical significance with its intermittent dry period characteristics. The intermittent dry period of the Guianas is during the onset of ENSO in the Fall; therefore, the effects of ENSO on the Caribbean in the Fall similarly affect the Guianas as ENSO displaces the Atlantic ITCZ (Chapter 3).

Correlations between RMOs and intermittent dry period characteristics are small and insignificant for most of the Caribbean, with the exception being moderately negative correlation between Central Caribbean RMDs and magnitude of the intermittent dry period, and moderately positive correlation between the RMD and dry period duration. The lack of correlations between timing characteristics and intermittent dry period characteristics for most of the Caribbean suggest that changes in the timing of the onset and demise may not impact or be impacted by changes in the intermittent dry period, but rather changes in the magnitude of the rainfall season as suggested by the correlation between rainfall amount and intermittent dry period characteristics.

Table 4.6: Correlations between Intermittent Dry Period Magnitude or Duration and several atmospheric/oceanic indices and rainfall characteristics from 1979-2015. Information on indices/characteristics can be found in Table 4.2. Bold denotes significance at the 95th percentile using a 2-sided t test.

REGION	INDEX	INTERMITTENT DRY PERIOD CHARACTERISTIC	
		MAGNITUDE	DURATION
NORTHWESTERN CARIBBEAN	ERS TOTALS	**.3786**	-.2502
	LRS TOTALS	**.3816**	**-.3248**
	Relative Onset	.1552	-.1953

	Relative Demise	.0419	-.0448
	NAO	**-.3300**	**.3117**
	ENSO (JJA)	**-.3490**	**.4053**
	STNA SST	**.4456**	**-.3227**
	STNA SLP	**-.4244**	.2811
	CLLJ	**.5484**	**-.5398**
	CSv925	.2550	-.1494
WESTERN CARIBBEAN		MAGNITUDE	DURATION
	ERS TOTALS	**.5067**	**-.4424**
	LRS TOTALS	**.3300**	**-.3861**
	Relative Onset	.1740	-.1869
	Relative Demise	-.1768	.2168
	NAO (JFM)	**-.4759**	**.4723**
	ENSO (JJA)	**-.3214**	.1793
	STNA SST	**.3294**	**-.3831**
	STNA SLP	.0049	.0287
	CLLJ	.1408	-.1210
	CSv925	.2292	-.2894
CENTRAL CARIBBEAN		MAGNTIUDE	DURATION
	ERS TOTALS	**.7026**	**-.6313**
	LRS TOTALS	**.4649**	**-.4157**
	Relative Onset	-.0041	-.0031
	Relative Demise	**-.4217**	**.3426**
	NAO	**-.5855**	**.4956**
	ENSO (JJA)	**-.3257**	**.3684**
	STNA SST	**.7531**	**-.7122**
	STNA SLP	**-.6202**	**.5381**
	CLLJ	**.6815**	**-.6676**
	CSv925	**.4983**	**-.4298**
GUIANAS		MAGNITUDE	DURATION
	RFS1 TOTALS	**.3110**	-.2229
	RFS2 TOTALS	**.5914**	**-.5496**
	RFS2 Relative Onset	-.0668	.2010

	RFS1 Relative Demise	-.0882	.0822
	NAO	-.0894	.0151
	ENSO (JJA)	**-.3397**	**.3236**
	EEP SST	**-.4111**	**.3925**
	EEP SLP	**.3434**	**-.3689**
	NSAM u925	.1216	-.1317
	NSAM v925	.1268	-.1824

4.5 Adaptability of the Method to an Agronomical Context

The method can also be adapted to investigate agronomical onsets and demises. An example summary of the thresholds used for the agronomical context, in addition to the meteorological contexts, can be found in Table 4.7. Of the studies that investigate agronomical onsets, there are two criteria that are universal: a crop-related mm-threshold, and a criterion to check for the persistence of rainfall above that threshold. Both of these criteria are incorporated into the present method, but their values can be inputted by the user. The agronomical mm threshold is typically based on the soil water requirements of the crops of interest, which may consider rates of evapotranspiration in a given region. For example, Moron and Robertson (2014) used a 5-mm threshold based on evapotranspiration rates in India which can be 4-7 mm/day during their rainfall season (Bandyopadhyay et al. 2009). Marteau et al. (2009) used a 5-mm total over a 7-day period as the threshold to determine a dry spell. Note that the agronomical mm-threshold is not the inflection point mm-threshold that is in the present method. Although it is not required, it is recommended to have the agronomical mm-threshold be at equal to or greater than the inflection point mm threshold because inflection points are the basis for determining candidate onsets and demises. Hence, if the agronomical mm-threshold is less than the inflection point threshold, one could miss inflection points that would otherwise satisfy the agronomical mm threshold.

Table 4.7: A summary of the user-input/calculated thresholds used to calculate temporal characteristics of the annual rainfall cycle in the Northwestern Caribbean. Note that these thresholds can and should be changed by the end-user over their area of study.

	User Thresholds				
Characteristic	Onset mm	Demise mm	# of days for Rate of Change	mm/day	
Onset Candidate Inflection Point	1 mm	N/A	10 days	.102 mm/day	
Demise Candidate Inflection Point	N/A	1 mm	N/A	N/A	
	Agronomical Onset mm Threshold	Agronomical Demise mm Threshold	Consecutive Days of Wet/Dry Spell	# of days out	% of days between # days out above/below mm threshold
Agronomical False/Real Onsets	2 mm	N/A	9 days	30 days	50%
Agronomical False/Real Demises	N/A	1 mm	9 days	15 days	50%
	Climatological $P_{window}(n)$	Annual $P_{window}(n)$	R^{th} Percentile of $P_{window}(n)$	Min of $S_{window}(n)$	Max of $S_{window}(n)$
Abs. Met. Onset	Climatological $P_{ERS}(n)$	N/A	33^{rd}	Yes	N/A
Rel. Met. Onset	N/A	Annual $P_{ERS}(n)$	33^{rd}	Yes	N/A
Abs. Met. Demise	Climatological $P_{LRS}(n)$	N/A	10^{th}	N/A	Yes
Rel. Met. Demise	N/A	Annual $P_{LRS}(n)$	10^{th}	N/A	Yes

The criterion for persistence of rainfall below and above the agronomical mm-threshold is used to determine any false agronomical onsets and demises, respectively. Using the raw daily data, a false agronomical onset is determined if the candidate onset meets one of the following user inputs: (1) Dry spell of length "C" consecutive days are below the agronomical mm threshold; or, (2) the total number of days between the candidate onset date and "N" days out that are below the agronomical mm-threshold is no more than X% of the total number of days between the candidate onset and "N" days out. A typical "C" value is 5 to 10 days (e.g., Diop, 1996; Moron and Robertson, 2014), and a typical "N" days out is 15 to 30 days (Moron and Robertson, 2014), depending on whether one looks for dry spells or wet spells. The X% of the total number of days is a new criterion, and it mitigates the issue of dealing with years where there is not persistent rainfall above the agronomical mm threshold, even if there were consecutive days that produced

rainfall above **the threshold.**

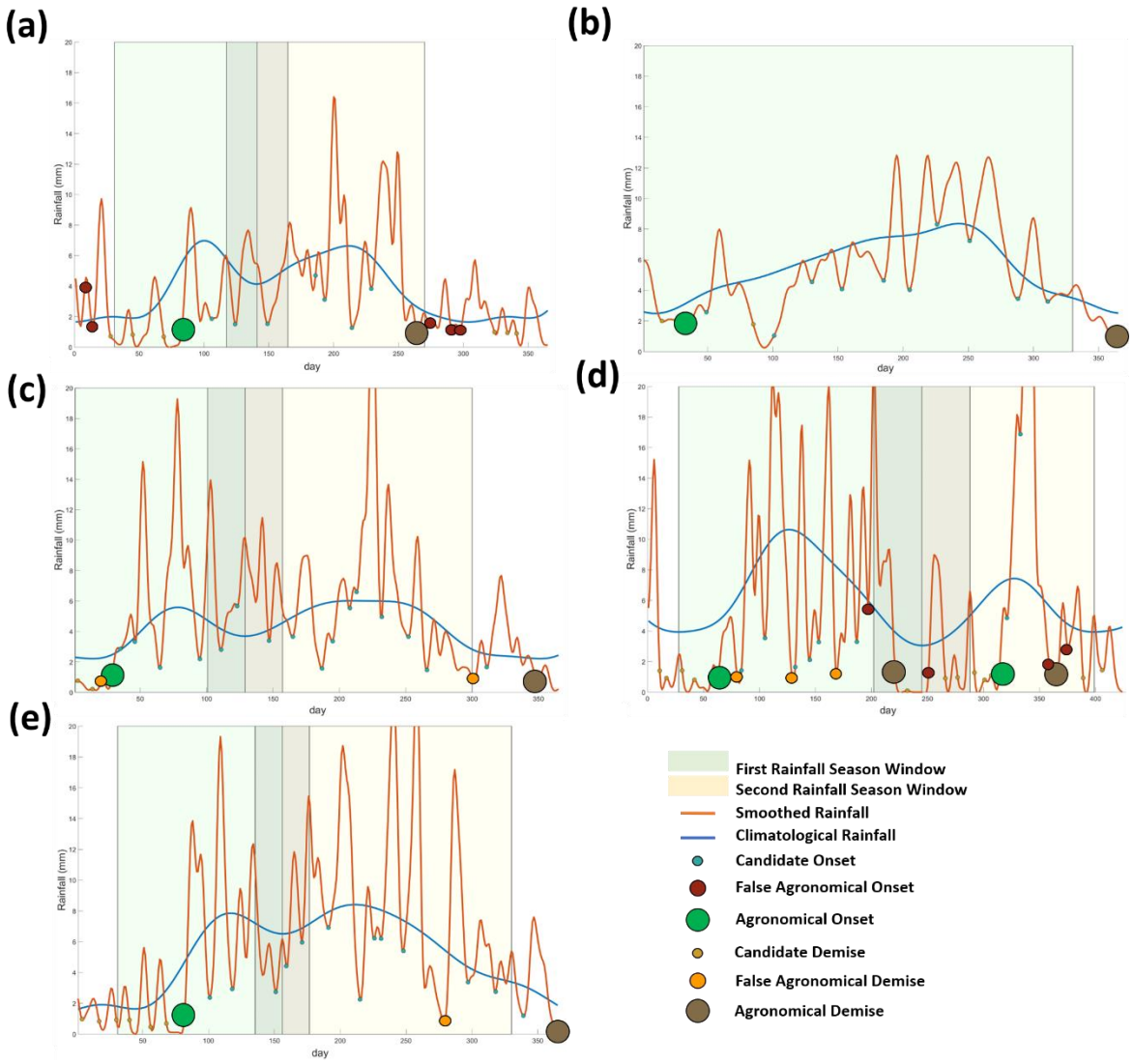

Figure 4.9: Agronomical onsets and demises for (a) Northwestern Caribbean in 1998, (b) Eastern Caribbean in 1987, (c) Central Caribbean in 1976, (d) Guianas in 1971, and (e) Western Caribbean in 2013

A value of 50-60% is recommended, as it provides at least half of the window to have rainfall above the agronomical mm threshold; however, the value can be changed according to the crop of interest, or other agronomical criteria. Similarly, the false agronomical onsets are filtered out and the agronomical onset is the earliest candidate onset after the start of the window. The

false agronomical demises are filtered out and the agronomical demise is the earliest candidate demise after the peak of rainfall within the window.

Illustration of the onset and demise calculations for the agricultural context (Fig. 4.9) uses an onset agronomical threshold of 2mm and a demise agronomical threshold of 1 mm, for the entire Caribbean. A daily rainfall value of 1-2 mm is generally the minimum of rainfall in the annual climatological cycle across the Caribbean sub-regions. In the Guianas, the thresholds are 3mm for onset and 1.5 mm for demise, as the minimums of their annual rainfall cycle is typically between 1.5 and 3mm. For the persistence check, a dry and wet spell of length 9 days, with 30 days out of the onset candidate, and 15 days out of the candidate demise are used to check for false onsets and demises. The method delineates false and actual agronomical onsets and demises under the values used. For example, the Northwestern experienced multiple false agronomical onsets because there were multiple dry spells which did not meet the requirements for the agronomical onset until the start of the ERS (Fig. 4.9a). The Guianas experienced multiple false demises due to intermittent rainfall throughout the first rainfall season (Fig. 4.9d). The ability to delineate false versus true agronomical onsets and demises is valuable for end-users such as farmers and forecasters when determining whether pre- or post-monsoon or transient activity is likely to produce a false wet signal, which helps avoid preparing for the spring growing season too soon or finishing the fall harvest season too early (Marteau et al. 2009; Osorio and Galiano, 2012).

4.6 Discussion

The present method has several advantages, such as the ability to distinguish unimodal dual maxima patterns and calculate its temporal and intermittent dry period characteristics. Previous methods classify regions with unimodal dual maxima patterns as unimodal patterns, because the intermittent dry period between the rainfall maximums is not distinguishable. However, unimodal

dual maxima patterns are a distinct rainfall cycle mode: the pattern appears unimodal, but the sets of dynamical mechanisms and climate drivers influencing each rainfall maximum can be different. Classifying unimodal dual maxima patterns as solely unimodal 1) limits the ability to calculate its intermittent dry period characteristics, and 2) implies that the variabilities of onsets and demises are similar to one another, which may not be the case. This is seen in some sub-regions of the Caribbean, where the ERS and LRS of the rainfall cycle are independent of each other because they are influenced by two separate and largely independent climate drivers and sets of dynamical mechanisms (Chapter 3). The present method is able to classify unimodal dual maxima patterns by distinguishing the climatological behavior of its intermittent dry period, and consequently, configure how temporal and intermittent dry period characteristics are calculated under this modality.

Detecting candidate onset and demise dates through the usage of inflection points that are related to the troughs and peaks of the annual rainfall season provide several gains. The candidate onset and demise dates can be used to determine both meteorological and agronomical onsets and demises, hence the method is universally applicable for both contexts. In the meteorological context, using candidate onsets and demises to find the onset and demise that relates to the minimum or maximum of the accumulated precipitation anomalies, or S(n), addresses the main limitation when using the Liebmann and Marengo (2001), as the min and max of S(n) can miss portions of the rainfall season that has intermittent or light rainfall before or after the main portion of the rainfall season.

The present method incorporates time and seasonal window parameters which have numerous benefits and mitigates limitations seen in previous methods. As most studies deal with unimodal or monsoonal rainfall regimes, they use the annual cycle as a whole to investigate

temporal characteristics. However, not all regions experience rainfall regimes that are unimodal, and the characteristics between non-unimodal regimes differ between its multiple rainfall seasons. Methods that have dealt with non-unimodal regimes do not consider regions that experience different modalities year-to-year, a limitation D16 acknowledges. This method mitigates these limitations by establishing seasonal windows that are determined by the modality of the climatological rainfall cycle, and setting the analysis based on each window. This characterizes temporal characteristics that pertain to each window, and prevents biases, as showcased in the Caribbean. Furthermore, the intermittent dry period window offers a novel way to characterize subtle and distinct intermittent dry periods. The intermittent dry period characteristics this method offers (magnitude and duration) can be used regardless of whether the intermittent dry period is distinct or not, and is a way to investigate its variability and relationship with atmospheric/oceanic modes of variability and other rainfall characteristics.

Specific to the Caribbean, some important implications are found when using the present method. In Gouirand et al. 2020, Caribbean-wide mean winter-to-summer and summer-to-winter dates, which resemble the onset and demise of the rainfall season, are May 13th and October 26th, respectively. However, this study finds that there are many stations and sub-regions with onsets and demise dates that are well before or after the Caribbean-wide mean onset and demise dates found in Gouirand et al. (2020). The sub-regional differences are attributed to how the dynamical mechanisms that shape the regional rainfall climate of the Caribbean evolve differently in space and time across each of the sub-regions (Chapter 2; Chapter 3). Using the present method, the findings from this study emphasizes the importance of investigating the Caribbean on a sub-regional scale. Anderson et al. (2019) and García-Franco et al. (2021) did not detect a MSD across the Western Caribbean under their methodologies, and consequently, did not calculate

characteristics of the MSD in this region; however, the present method does show the MSD, though subtle, across the Caribbean coastlines of Belize, Guatemala, Nicaragua and San Andrés. Because their methods used gridded datasets, the no MSD detection could be due to coastal grid points that incorporate some ocean, which, as was found in Chapter 2, can mask the magnitude of the subtle MSD. The newly-founded/stronger relationships between several atmospheric/oceanic modes of variability and onsets/demises/intermittent dry period characteristics across all sub-regions found in the present method are valuable for diagnosis and prediction of these rainfall characteristics. There are also sub-regional differences between which atmospheric/oceanic modes of variation have a strong relationship with onsets, demises, and characteristics of the intermittent dry period. Investigating the prediction of the associated dynamical mechanisms and rainfall characteristics in the Caribbean and tailoring subseasonal-to-seasonal rainfall forecasts on a sub-regional scale may enhance the prediction of the Caribbean rainfall cycle.

4.7 Conclusion

In this chapter, a novel approach to determine temporal and intermittent dry period characteristics of unimodal, unimodal dual maxima, and bimodal rainfall patterns are proposed and showcased using rainfall station data in the Caribbean. The method first classifies the modality of the climatological rainfall cycle through its intermittent dry period in order to set seasonal windows and time parameters for the yearly analysis. Then information on rainfall and the rate of change of rainfall in the yearly analysis is utilized in order to determine dates of candidate onsets and demises. The method is shown under two lenses: a meteorological context by adapting the Liebmann and Marengo (2001), D16, and B20 methods, and an agronomical context. The method addresses limitations and challenges from previous methods such as 1) the ability to distinguish unimodal dual maxima rainfall patterns and calculate its characteristics, 2) calculate characteristics

of subtle and distinct intermittent dry periods, 3) dealing with years that have abnormally dry rainfall seasons, and 4) dealing with false meteorological and agronomical onsets and demises. As temporal and intermittent dry period characteristics are important variables of the rainfall cycle for numerous stakeholders such as agriculture and water management (Boyard-Micheau et al. 2013; Anderson et al. 2019), the method provides a way to investigate the variability and change of the growing and harvesting seasons.

Specific to the Caribbean, the following conclusions are made:

1) Generally, onsets and demises that are calculated using yearly mean thresholds are not correlated with rainfall amounts associated with either the ERS or LRS, nor the dynamical mechanisms that shape each rainfall season. However, onsets and demises that are calculated using a climatological mean threshold are correlated with rainfall amounts associated with either the ERS or LRS and the dynamical mechanisms that shape each rainfall season. This difference suggests that the variability of the rainfall seasons is influenced by changes in the magnitude of the rainfall seasons, rather than shifts in rainfall season timing.

2) The MSD characteristics are correlated with rainfall amounts and with dynamical mechanisms that shape the ERS and LRS, but not with onsets and demises that are calculated using yearly mean thresholds. This suggests a relationship exists between the magnitude of the rainfall seasons and the strength and duration of the MSD, and the MSD in the Caribbean is influenced by dynamical changes from both the ERS and LRS.

This chapter has important implications for other rainfall modalities, prediction, modeling capabilities, and the understanding of the variability of rainfall across timescales. A few regions yield rainfall cycles with other rainfall modalities such as trimodal patterns (Herrmann and Mohr,

2011; Seregina et al. 2018; B20); the method could be applied to investigate trimodal or other multi-modal patterns that experience a variety of subtle and distinct intermittent dry periods. Although time filtering in the method limits computation of the onsets and demises in real-time, year-to-year onsets and demises can be utilized to investigate their relationship with dynamical mechanisms or weather types that are known to influence the annual rainfall cycle. The usage of seasonal windows can be utilized to investigate intraseasonal variability, by assessing how the season evolves between its beginning and end stages. Other rainfall characteristics, such as the intensity or frequency of wet and dry days, wet-spells, dry-spells, and extreme wet days, can be calculated with the usage of seasonal windows. The ability to assess characteristics of the intermittent dry period can also advance in the understanding of its variability, what dynamical mechanisms shape it, and how it influences the rainfall seasons. This method can also be utilized under a modeling diagnostic framework. For example, the method can be used in models in order to determine their ability in simulating the observed behavior of the temporal and intermittent dry period characteristics of rainfall, and consequently detect biases in models in order to improve representation of observed physical mechanisms related to rainfall characteristics, through a process-based diagnostic approach such as the one reported by Muñoz et al (2017). Finally, the method provides the ability to predict these agronomically-relevant rainfall characteristics, and understand which dynamical mechanisms and climate drivers could be used to predict them; this is what will be explored in Chapter 5 of the thesis.

Part III

Seasonal Prediction of the Caribbean Rainfall Cycle

Chapter 5: Seasonal Prediction of the Caribbean Rainfall Cycle

Note: A modified version of this chapter is under review in Climate Services (2021)[4]

5.1 Introduction

Chapters 2 and 3 presented an improved and comprehensive sub-regional characterization of the Caribbean rainfall cycle. In Chapter 4, sub-regional S2S characteristics for the Caribbean were calculated using a method that is able to accurately characterize the complexities of the rainfall cycle. Naturally, the results from Chapters 2 thru 4 provide a seamless framework to explore the prediction of seasonal rainfall characteristics.

Further motivation to explore rainfall prediction in the Caribbean basin stems from the current lack of investigating the seasonal prediction of rainfall, especially on a sub-regional scale. Gouirand et al. (2020) explored prediction of onsets and demises using weather-types of low-level winds, but treated the Caribbean as only one homogenous region when calculating onsets and demises. Krishnamurthy et al. (2018) conducted a dynamical model forecast skill assessment for the Caribbean, but solely to investigate forecast skill of summer rainfall totals. Other studies investigated prediction of seasonal rainfall characteristics in only a portion of the Caribbean basin, specifically the Caribbean side of Central America during the ERS (Maldonado et al. 2016a; Alfaro et al. 2017; Alfaro et al. 2018) or MSD (Maldonado et al. 2016b).

These Caribbean studies, in addition to most prediction studies that investigate rainfall in other parts of the world, use statistical models based on canonical correlation analysis (CCA; Mason and Baddour, 2008; Tippet et al 2008) to investigate prediction of rainfall characteristics with local and remote dynamical mechanisms and climate drivers using observational datasets

[4]Martinez C., Muñoz Á., Goddard L., Kushnir Y., Ting M., 2021: Seasonal Prediction of the Caribbean Rainfall Cycle. Clim. Serv. *Under Review*

and/or retrospective forecasts from general circulation models (GCMs) (e.g., Tippett and Barnston 2008; Barnston and Tippett 2017). CCA has been applied in the Caribbean (Krishnamurthy et al. 2018), and in neighboring regions such as Central America (Maldonado et al. 2013; Alfaro et al. 2017; Maldonado et al. 2016a,b; Alfaro et al. 2018) and Northern South America (Recalde-Coronel et al. 2014; Muñoz et al., 2016; Fernandes et al. 2020) to investigate relationships between atmospheric/oceanic fields and rainfall characteristics. These studies found multiple fields, such as moisture fluxes (Muñoz et al. 2016; Alfaro et al. 2018; Fernandes et al. 2020), that better predict various rainfall characteristics than variables that are commonly used, such as SSTs or teleconnection indices. In addition, tropical and non-tropical studies using CCA have found that the frequency of wet days was more skillfully predicted than the commonly used seasonal rainfall totals (Robertson et al. 2009; Verbist et al. 2010; Maldonado et al. 2013; Muñoz et al. 2015, 2016a, 2016b; Alfaro et al. 2018; Fernandes et al. 2020). The seasonal forecasts of rainfall characteristics via CCA in these studies were found skillful several months ahead of the target month or season. Such skillful lead time forecasts could improve decision making, agricultural planning, and weather/water risk management.

However, most Caribbean studies, and studies outside of the Caribbean, used CCA under a limited scope. Some studies used CCA with only observations and did not utilize hindcasts from GCMs (Maldonado et al. 2016a; Maldonado et al. 2016b; Alfaro et al. 2017), or they used observations but only hindcasts from one regional dynamical model or a GCM (Muñoz et al. 2016; Alfaro et al. 2018; Fernandes et al. 2020) to investigate the prediction of rainfall characteristics. Generally, a suite of models provides higher skill than using a single model (Goddard et al. 2001; Kar et al. 2011; Muñoz et al., 2020; Kelley et al. 2020; WMO, 2020).

Using the methodology to calculate S2S characteristics from Chapter 4, this chapter seeks to identify potential atmospheric and oceanic variables that could be used for seasonal forecasting of each Caribbean sub-region, based on the variables that are key to the climate drivers and dynamical mechanisms found in Chapters 2 and 3.

Chapter 5 is structured as follows. Section 5.2 and 5.3 describe the data and methods used, respectively. Section 5.4.1, 5.4.2, and 5.4.3, looks at the forecast skill metrics and spatial patterns from the CCA for ERS, LRS, and MSD characteristics, respectively. Section 5.5 discusses the results, and concluding remarks and implications from the results are found in section 5.6. Supplemental Information for this chapter is found in Section 5.7.

5.2 Data

A summary of the variables that will be forecasted (predictands) and those used to forecast (predictors) are described in this section. In this study, two types of predictors are investigated: those from observations, and those from dynamical GCM predictions. Data from 1982-2015 is selected for all variables, as it was the common period for which all predictands and predictors data are available. As an example, Fig. 5.1 shows the datasets, predictors, and predictands used for ERS characteristics.

5.2.1 Predictands

The daily station rainfall dataset described in Chapter 2, Section 2, is utilized here. However, stations in the Guianas and Trinidad and Tobago are omitted as they experience a lagged rainfall cycle that does not conform to the typical ERS, MSD, and LRS, seen in the rest of the Caribbean (Chapter 2). Additional daily rainfall stations from San Andrés and Nicaragua are included in this Chapter and are obtained from CIMH/NOAA GHCN. Additional daily rainfall station data provided by INSIVUMEH are also used. A total of 41 stations are used. Station

information can be found in Table 5.1. Five predictands are explored in this study: the frequency of wet days during the ERS, frequency of wet days during the LRS, intensity of wet days during the ERS, intensity of wet days during the LRS, and magnitude of the MSD. The calculations of the predictands are presented in the methodology section.

Table 5.1: List of rainfall regions, and their corresponding stations used in the study. Station ID, station name, and location in latitude and longitude.

Region	(ID) Station Name	Latitude	Longitude
Northwestern Caribbean	(1) Nassau, Bahamas	25	− 77.5
	(2) Georgetown, Cayman	19.3	− 81.3
	(3) Camaguey, Cuba	21.24	− 77.51
	(4) La Habana, Cuba	23.1	− 82.21
	(5) Worthy Park, Jamaica	18.143	− 77.149
	(6) Ft. Lauderdale, USA	26.1	− 80.28
	(7) Key West, USA	24.55	− 81.75
	(8) Miami Intl. AP., USA	25.82	− 80.28
	(9) Palm Beach, USA	26.68	− 80.08
Central Caribbean / Northern Lesser Antilles	(10) BC Bird Intl. AP, Antigua/	17.135	− 61.791
	(11) Santo Domingo, DR	18.25	− 69.58
	(12) Henry E. Rohlsen AP., St. Croix	17.7	− 64.81
	(13) Cyril E. King, St. Thomas	18.33	− 64.97
	(14) Colosso, USPR	18.381	− 67.157
	(15) Dora Bora, USPR	18.336	− 66.667
	(16) Ensenada, USPR	17.973	− 66.946
	(17) Guaynama, USPR	17.978	− 66.087
	(18) Jajome Alto, USPR	18.072	− 66.143
	(19) Mora Camp, USPR	18.474	− 67.029
	(20) Paraiso, USPR	18.265	− 65.721
	(21) Morovis N., USPR	18.334	− 66.408

Central and Southern Lesser Antilles (or Eastern Caribbean)	(22) CIMH, Barbados	13.148	− 59.624
	(23) Grantley A. Intl. AP., Barbados	13.08	− 59.485
	(24) DCAP, Dominica	15.547	− 61.2993
	(25) Guadeloupe	16.2	− 61.66
	(26) Intl. AP., Martinique	14.59	− 60.99
	(27) Hewanorra, St. Lucia	13.737	− 60.952
	(28) Dumbarton, St. Vincent	13.18	− 61.17
Western Caribbean	(29) CFarm, Belize	17.2	− 89
	(30) Intl. AP., Belize	17.53	− 88.3
	(31) Felipe, Mexico	19.7	-87.9
	(32) Flores, Guatemala	16.915	-89.865
	(33) Las Vegas, Guatemala	15.600	-88.967
	(34) Puerto Barrios, Guatemala	15.737	-88.591
	(35) Belmopan, Belize	17.25	-88.7
	(36) Melinda, Belize	16.983	-88.316
Western Caribbean 2	(37) San Andres, Colombia	12.583	-81.717
	(38) Apto El Embrujo, Colombia	13.35	-81.35
	(39) San Felipe, Colombia	13.35	-81.83
	(40) Empoislas, Colombia	12.53	-81.71
	(41) Puerto Cabezas, Nicaragua	14.04	-83.375

5.2.2 Predictors

Five candidate predictors are chosen for the analysis: SST, SLP, zonal wind at 850hPa (u850), vertically integrated mean flow zonal flux (UQ), and vertically integrated mean flow meridional flux (VQ). The candidate predictors are chosen because of their relationship with the dynamical mechanisms seen in Chapters 2 and 3 that impact the Caribbean rainfall cycle. Although the CLLJ is maximized at 925hPa, and thus zonal winds at 925hPa would be a better predictor

than that at 850hPa, zonal wind data at 925hPa was not readily available outside of the modeling centers, hence the nearest available level to 925hPa is used.

5.2.2.1 Observed Predictors

For obtaining candidate predictors from observations, the European Centre for Medium-Range Weather Forecasts Interim Reanalysis (ERA-Interim) (Dee et al. 2011) is used. For this study, we used a spatial resolution of 0.75° by 0.75° (1.0° by 1.0° for the vertically integrated moisture fluxes), a 6-hourly temporal resolution from 1982 to 2015, and 26 pressure levels. Monthly means of each observed candidate predictor from March through August are calculated and used.

5.2.2.2 Model-based Predictors

Retrospective forecasts, or hindcasts, from five operational models from the North American Multimodel Ensemble (NMME; Table 5.2) (Kirtman et al. 2014) are used for each candidate predictor in order to investigate the potential for real-time prediction with each predictand. NMME data was obtained via http://iridl.ldeo.columbia.edu/SOURCES/.Models/.NMME/ and https://www.earthsystemgrid.org/search.html?Project=NMME. All model hindcasts have been regridded to a 1.0° by 1.0° spatial resolution. Monthly mean fields are used. Information regarding the number of realizations for each model and availability of each candidate predictor in each model can be found in Table 5.2. For each NMME model, individual ensemble members were averaged in order to obtain the ensemble mean. Forecasts initialized in March through August are used.

Table 5.2: Five NMME models used for this study were downloaded from the IRI data library or the Earth System Grid. N/A denotes data that was not available or missing at the time when this study was conducted

Model	Group	Realizations	SST	SLP	u850	UQ	VQ
CMC-CanCM4i (Lin et al. 2020)	Canadian Center for Climate Modeling and Analysis	10	X	X	X	X	X
COLA-RSMAS-CCSM4 (Meehl et al. 2012)	University Corporation for Atmospheric Research	10	X	X	X	X	X
GEM-NEMO (Smith et al. 2018)	Recherche en Prévision Numérique	10	X	X	X	N/A	N/A
NASA-GEOS-5 (Ham et al. 2014)	NASA Goddard	10	X	N/A	N/A	N/A	N/A
NCEP-CFSv2 (Saha et al. 2014)	National Center for Environmental Prediction	24	X	X	X	X	X

5.3 Methodology

To illustrate the forecast methodology, a summary schematic for forecasting seasonal ERS characteristics is provided (Fig. 5.1).

Predictands are calculated from the daily rainfall station data. First, stations are grouped by sub-region based on the classified Caribbean sub-regions from Chapter 2 (Table 5.1); however, Nicaraguan and San Andrés stations are separated from the rest of the Western Caribbean stations because the interannual variability across the Nicaraguan coastline and San Andrés is slightly different from the rest of the Western Caribbean (Chapter 3). A wet day is considered a day with a rainfall amount greater than 1 mm, which is a common threshold to determine wet days in the Caribbean (Chapter 4).

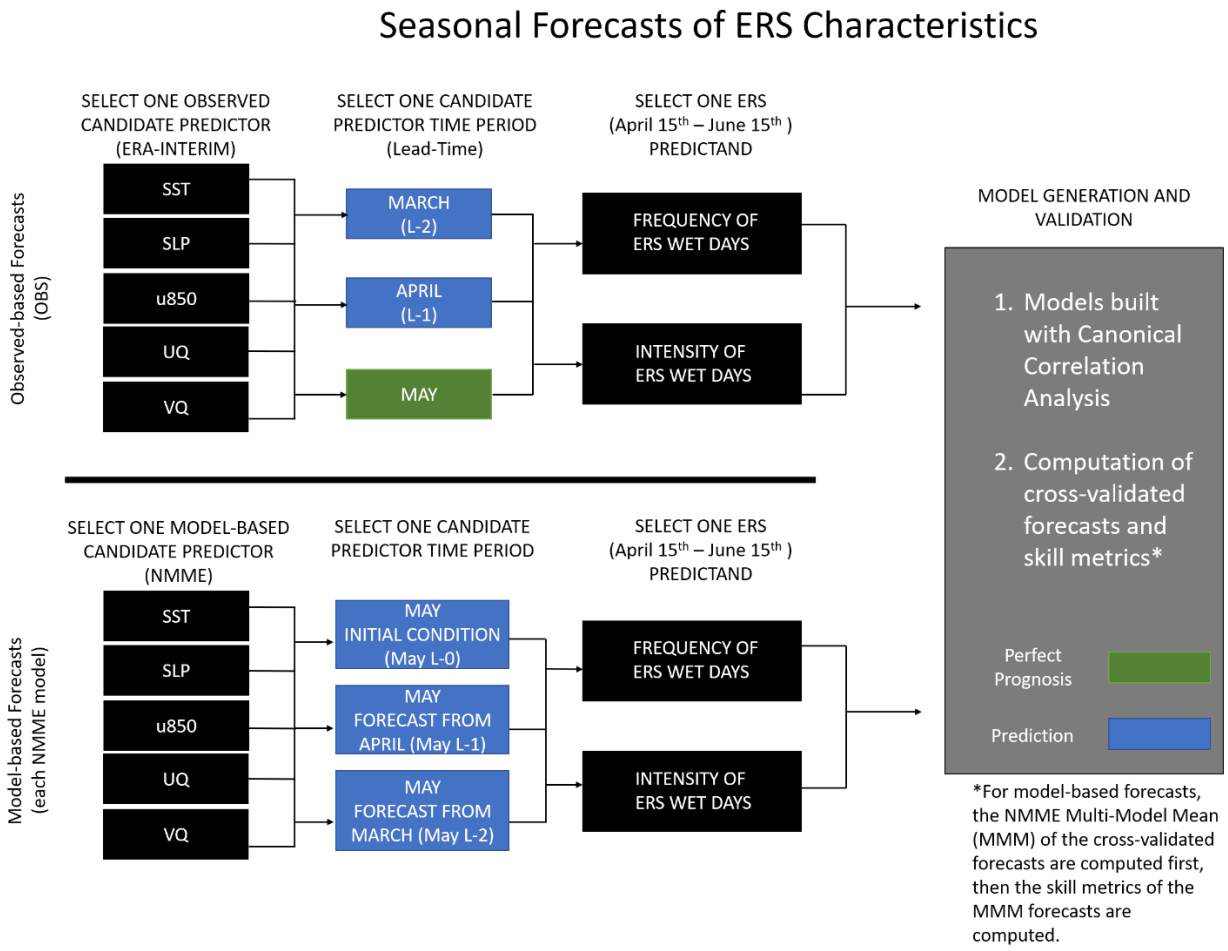

Figure 5.1: Summary of the methodology using the Early-Rainfall Season as an example. The schematic is an adaptation of Fig. 1 from Muñoz et al. 2016.

For most of the Caribbean, the start of the ERS is in May. The exception is in the Central Caribbean where the start of the ERS is in April (Chapter 2; Chapter 4). Therefore, a seasonal window of the ERS (April 15th to June 15th) is used with the target month being May in order to address the earlier start in the Central Caribbean, while following the general start of the ERS in the Caribbean. A seasonal window of the LRS (August 15th to October 31st; target month: August) is used in order to address the different temporal LRS characteristics found in each sub-region (Chapter 2; Chapter 4). For both the ERS and LRS, the number of wet days and the average amount of rainfall per wet day during those seasons are calculated for each station. Although the Eastern Caribbean has a unimodal rainfall cycle with no MSD, rainfall during the ERS in the Eastern

Caribbean transitions between the less wet season to more wet season, and the LRS is typically when the Eastern Caribbean receives the most rainfall; therefore, ERS and LRS predictands are calculated for this region. For each station in the Northwestern, Central, Western 1 and Western 2 Caribbean, the yearly MSD magnitude that is calculated in Chapter 4 is used. Generally, the MSD window is between Late-June and Early-August; therefore, the target month for the analysis is June or July depending on the sub-region. Finally, the observed ERS, MSD, and LRS rainfall characteristics are calculated for each year over each sub-region by averaging the stations' characteristics across the sub-region.

Several steps are done prior to computing the CCA between candidate predictors and predictands. First, the predictands are transformed into a normal distribution by converting the original data to ranks and expressing these ranks as percentiles of the empirical distribution (Mason et al. 2021). Second, the domains of the predictors are determined. Several spatial domains were explored in order to maximize skill between the predictors and predictands while noting the different spatial domains of the dynamical mechanisms and climate drivers that distinctly affect each season of the Caribbean rainfall cycle (Chapter 2; Chapter 3). In this study, the predictor domain selected for investigating ERS and MSD predictands is 7°N-40°N, 100°W-30°W, and for LRS predictands the predictor domain selected is 0°N-40°N, 150°W-20°W. Third, the candidate predictor fields and predictands are pre-filtered through empirical orthogonal function (EOF) analysis in order to reduce noise and decrease the chance of spurious relationships between variables in the CCA (Graham et al. 1987a, b; Barnett et al. 1988; Mason and Baddour, 2008, Tippet et al. 2008). For the predictors, up to10 EOF are selected. For the predictands, up to 5 EOFs are selected for the ERS and LRS, and 4 EOFs are selected for the MSD (the Eastern Caribbean is omitted). In each case, the time series, or principal components (PCs) corresponding to these EOFs

are used in the CCA. The number of CCA time series corresponds to the minimum number of PCs between both variables; therefore, a maximum of 5 (4 for the MSD) CCA time series are available in each CCA model.

The CCA calculates linear combinations of predictor and predictand EOFs, using a linear, multivariate regression model, to produce the combination pairs that maximize their mutual correlation (Graham et al. 1987a, b; Barnett et al. 1988; Mason and Baddour, 2008, Tippet et al., 2008). The skill of each CCA model is evaluated through cross-validation in order to avoid artificial skill (Barnston and Van den Dool, 1993; Mason and Baddour, 2008). A cross validation window of 5 years is used, such that five consecutive years are held out at a time and the middle year of the window is predicted (Mason and Stephenson, 2008). This procedure is repeated until all years in the dataset are forecasted. All cross-validated CCA model outputs that are used in this study are deterministic, meaning there are no uncertainty estimates retained. The term multi-model mean (MMM) will be used here to refer to the NMME ensemble average of deterministic cross-validated CCA model outputs.

The CCA model outputs are classified as either perfect prognosis or prediction. When the observed predictor is taken simultaneously with the predictand, we will refer to the skill between the observations and the CCA model outputs as ‘perfect prognosis’. This is because the observed predictor is simultaneous with the predictand, and thus the predictor field is as accurate as possible. Consequently, the forecast skill is assumed to be at its highest value for this method and model construction. However, since monthly means are used to forecast seasonal characteristics (e.g., May predictors and ERS predictands) this is a near-perfect prognosis. For prior months, the observation-based CCA model outputs (forecasts), are classified as OBS predictions. The target and prior months of the model-based forecasts are classified as MMM predictions. For OBS and

MMM predictions, lead times of 1 month (L-1) and 2 months (L-2) are investigated. For example, OBS L-1 prediction denotes the CCA model output using observed predictors that are 1 month ahead of the target month (e.g., OBS May L-1 prediction uses observed predictors from April). MMM L-1 prediction denotes the CCA model output using NMME target month forecasts of the predictors that were initiated 1 month prior (e.g., MMM May L-1 prediction uses NMME forecasted predictor fields for May that were initiated in April). For MMM prediction, the target month is designated as L-0.

Association and discrimination metrics are used to evaluate the skill of the CCA model deterministic cross-validated forecasts for each sub-region's perfect-prognosis and prediction: Spearman ranked correlation coefficient (Wilks 2011), and the relative operating characteristics (ROC; Mason 2003). The latter is used to determine how well the forecast discriminates above-normal, near-normal, and below-normal values. Areas under the ROC curve (Mason 2003) are computed for below-normal (ROC-B) and above-normal (ROC-A) categories. Values are from 0 to 1 and values greater than 0.5 denote positive skill. Tests for statistical significance of the correlations at the 95th percentile are computed by using a resampling method (500 times).

All CCA calculations and skill metric calculations were conducted using the International Research Institute for Climate and Society (IRI) Climate Predictability Tool (CPT) version 17.4.1 (Mason et al. 2021). CPT is currently being used across Central America and the Caribbean for real-time seasonal climate prediction (Maldonado et al. 2013; Alfaro et al. 2018). It is a convenient and relatively simple tool to produce statistical seasonal prediction models (Muñoz et al. 2010; Maldonado et al. 2013; Recalde-Coronel et al. 2014; Esquivel et al. 2018; Giannini et al. 2020).

5.4 Results

There are some generalized findings for the skill of predicting rainfall characteristics for all seasons of the Caribbean rainfall cycle. First, correlations, ROC-A, and ROC-B were higher for the MMM than most if not all of the individual NMME models for a given candidate predictor-predictand pair; therefore, only the results from the MMM will be shown. Second, when correlations are greater than 0.32, which is also the correlation of statistical significance at the 95th percentile, ROC-A and ROC-B are above 0.6, which denotes positive discriminative skill. Third, the first CCA mode for the L-1 and L-2 MMM have similar spatial patterns and canonical correlations to those for L-0; therefore, these are not shown (See Supplementary Information). In a few cases, MMM prediction under the target month is higher than the perfect prognosis. But most of these differences are not statistically significant, and could be attributed to noise in the observations and systematic errors in ERA-Interim. Note: "observations" and "forecasts" refer to observations and forecasts of the predictand.

5.4.1 Early-Rainy Season

There are statistically significant correlations between observations and forecasts of wet days in the Caribbean during the ERS. There are also sub-regional differences in the details of which model configurations yield the best predictions of the frequency of wet days, and how far in advance these predictions can be made skillfully (Figure 5.2).

For most regions, perfect prognosis of the frequency of wet days is skillful in May, which is generally the start of the ERS and where most of the ERS' rainfall occurs. Some exception is in the Western 1 Caribbean with only weak, insignificant correlations between the observations and SST-, SLP-, and u850-based forecasts, the Western 2 Caribbean with significant correlations only

between the observations and UQ- and VQ-based forecasts, and in the Northwestern Caribbean with non-significant correlations between observations and SST-based forecasts.

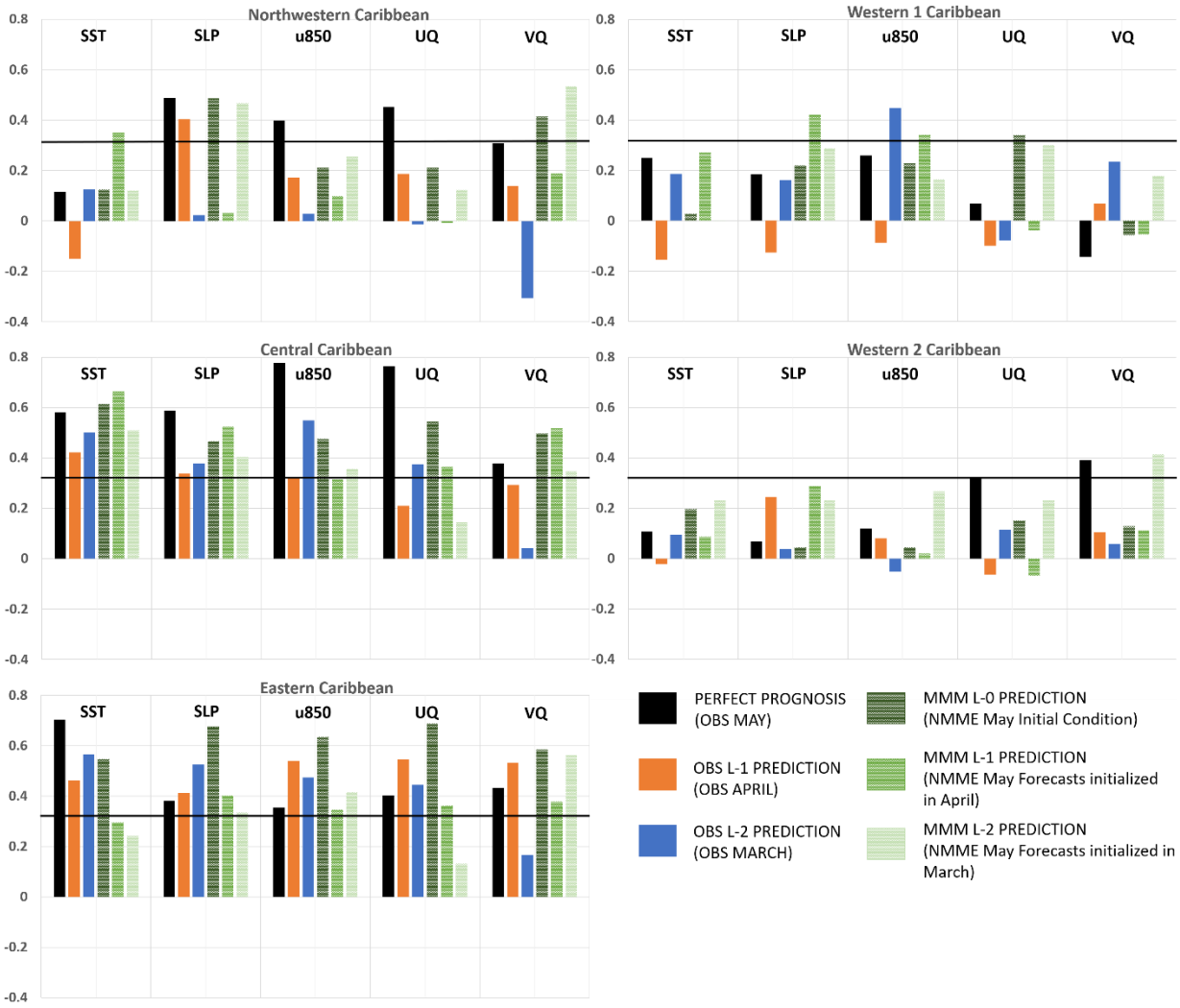

Figure 5.2: Cross-validated sub-region OBS and MMM Spearman correlations between 1982-2015 observed and forecasted frequency of wet ERS days, computed via CCA over 7°N-40°N, 100°W-30°W using observed and model-based sea-surface temperatures, sea-level pressure, zonal winds at 850hPa, vertically integrated zonal and meridional moisture fluxes as predictors. Spearman correlations are calculated for preceding months and monthly lead times of May. Values above the black line denote statistical significance at the 95th percentile.

Nonetheless, the perfect-prognosis from most of the observed predictors demonstrates a significant association for the perfect prognosis of the frequency of wet days. When investigating earlier months, which could potentially serve as predictions, the forecasts are skillful in some sub-regions.

For example, the Central and Eastern Caribbean have significant correlations between observations and forecasts from March and April that are comparable with those seen in the perfect prognosis. The Western 1 and 2 Caribbean do not show skill when using observed predictors in March or April. In the Northwestern Caribbean, only forecasts when using SLP-based predictors in April are correlated significantly with observations.

MMM predictions are comparable with the perfect prognosis (Fig. 5.2). Significant correlations are found between observations and all MMM L-0 forecasts in the Central and Eastern Caribbean, and for the VQ- and SLP-based MMM L-0 forecasts in the Northwestern Caribbean. All L-1 and most of L-2 forecasts from MMM-based predictors have significant correlations with observations in the Central and Eastern Caribbean. In the Northwestern Caribbean, skillful forecasts vary when using L-1 and L-2 for SLP-, SST-, and VQ-based predictors. There are some skillful forecasts in the Western Caribbean when using MMM SLP and UQ under L-1 and L-2; otherwise, the Western Caribbean has no forecast skill. Overall, the comparable results between the MMM prediction and the perfect prognosis suggest the model effectively evolves the predictor fields in the region.

The spatial loadings of the first CCA modes of the OBS and MMM are shown in Figure 5.3. All first CCA modes show high canonical correlations, indicating the canonical patterns are robust. The SST OBS (Fig. 5.3a) and MMM (Fig. 5.3b) spatial loadings are similar and show a dipole SST pattern with a negative loading over the Western, Central, and Eastern Caribbean and a positive loading over the Northwestern Caribbean. The regional loadings are companion to the SST spatial loadings (e.g., Northwestern Caribbean box shows positive loadings and is over the SST spatial positive loading).

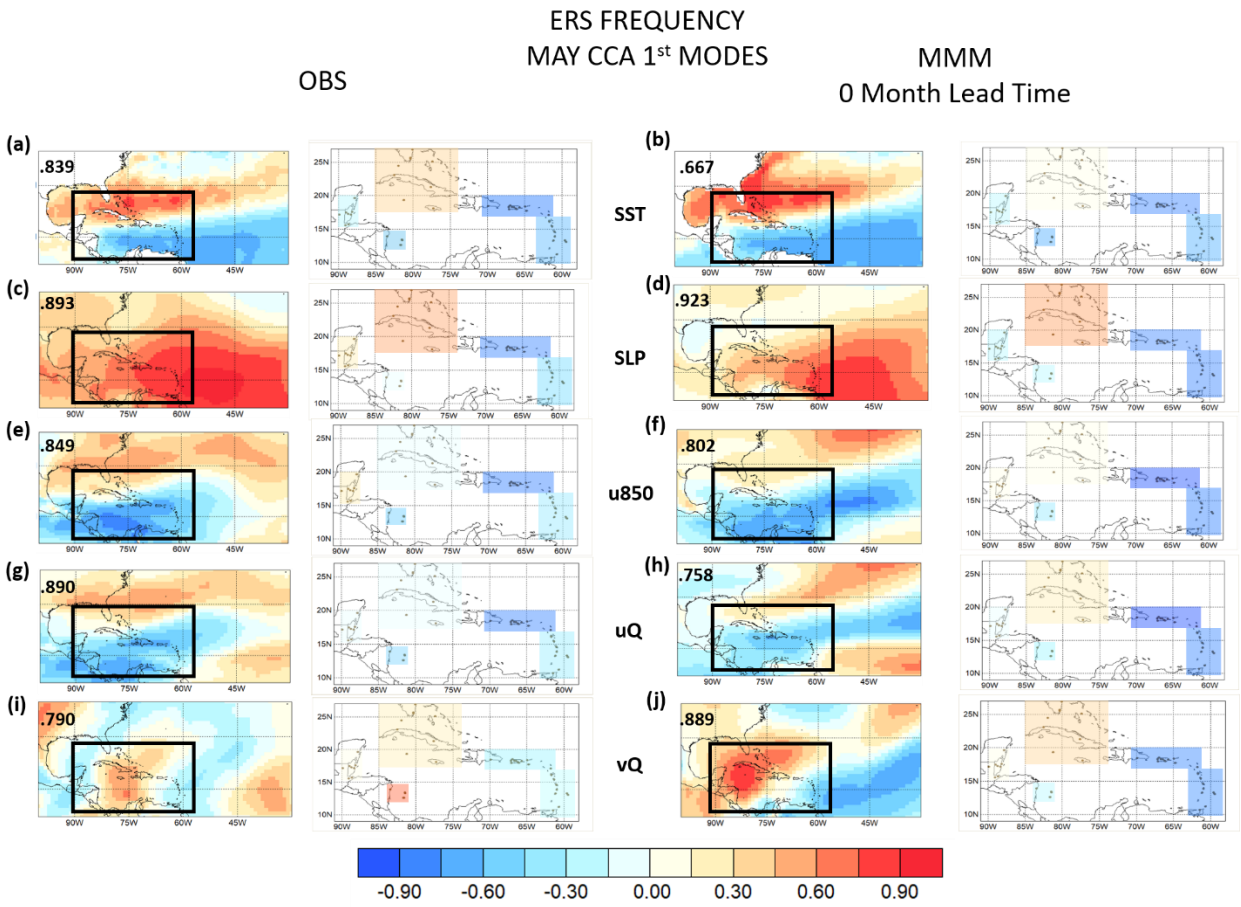

Figure 5.3: Canonical patterns of the first CCA mode using OBS (left) and MMM L-0 (right) for May. Spatial loadings (columns 1 and 3) are from predictors: SST (a,b), SLP (c,d), u850 (e,f), UQ (g,h), and VQ (i,j). Regional loadings (columns 2 and 4) are from the predictand: station-averaged frequency of wet ERS days from each sub-region. Canonical correlations of the first CCA mode are shown on the top left of their spatial loading. The black box denotes the Caribbean (5°N-27°N and 58°-90°W)

For example, if the negative and positive SST loadings were cold and warm SST anomalies, respectively, the number of ERS wet days in the Western, Eastern, and Central Caribbean regions would be below-normal, and in the Northwestern Caribbean, above-normal. The opposite would be true if the positive and negative SST loadings were warm and cold SST anomalies, respectfully.

The May SST (Fig. 5.3a,b) and SLP (Fig. 5.3c,d) CCA models yield spatial patterns that resemble the NAO-SST/SLP persistence signal, and help explain the sub-regional differences found in the correlations. The SST and SLP spatial patterns resemble the May SST and SLP composites of dry minus wet years for ERS (Fig. 3.2b,g). These ERS SST and SLP signals are

induced by the preceding winter NAO that then persist into the ERS. However, the NAO-SST/SLP persistence signal is centered over the Central and Eastern Caribbean in May and the preceding months. As a result, the anomalous SST signal over the Northwestern Caribbean is weak, but the anomalous SST signal over the Central and Eastern Pacific is much larger and persists though the season, and the anomalous SLP signal is centered over the Central and Eastern Caribbean. Therefore, the NAO-SST/SLP persistence signal explains why 1) the Central and Eastern Caribbean experiences consistently significant forecast skill for the frequency of ERS wet days at lead times of up to two months when using SST and SLP and 2) the Northwestern and Western Caribbean experience poor forecast skill using SSTs for all prediction lead times.

Similarly, to the SST and SLP spatial loadings, the u850 (Fig. 5.3e,f), UQ (Fig. 5.3g,h), and VQ (Fig. 5.3i,j) spatial loadings resemble those from the May zonal wind and mean flow moisture flux composites of dry minus wet ERS years (Fig. 3.4a). During years with a dry ERS, the anomalous NAO-SST/SLP persistence signal expands NASH in the Caribbean in May. NASH stretches its western flank further into the Caribbean Sea, displaces the Eastern Pacific and Atlantic ITCZ south, and strengthens the CLLJ. This induces a mean flow (UQ and VQ) convergence/divergence couplet over the Caribbean, where in years with dry ERS', convergence is seen over the Northwestern Caribbean by the western flank of NASH, and in the Western Caribbean by NASH and the exit region of the CLLJ. Meanwhile, near the entrance region of the CLLJ, increased subsidence and enhanced trade winds causes anomalous divergence over the Eastern and Central Caribbean. The CCA UQ and VQ findings suggest that the anomalous convergence over the Northwestern Caribbean in May is largely due to changes in the VQ component of the mean flow. That anomalous convergence seen in May in dry minus wet ERS years is not present in June (Fig. 3.4b). In addition, the first CCA modes of April VQ (not shown)

in ERA-Interim and in MMM L-0 through L-2 do not show the positive VQ spatial loading that is seen in May. Unlike the anomalous SST and SLP patterns, and to some extent the low-level wind and UQ fields, the anomalous VQ field from Fig. 3.4 over the Northwestern and Western Caribbean is visible in May alone. This explains why forecasts for the Northwestern Caribbean using VQ are only skillful in May. There are differences in the location of the positive VQ spatial loading in MMM L-0, L-1, and L-2 (Supplementary Information, Section 5.7) which may explain why the correlations between VQ-model-based forecasts and observations vary in the MMM.

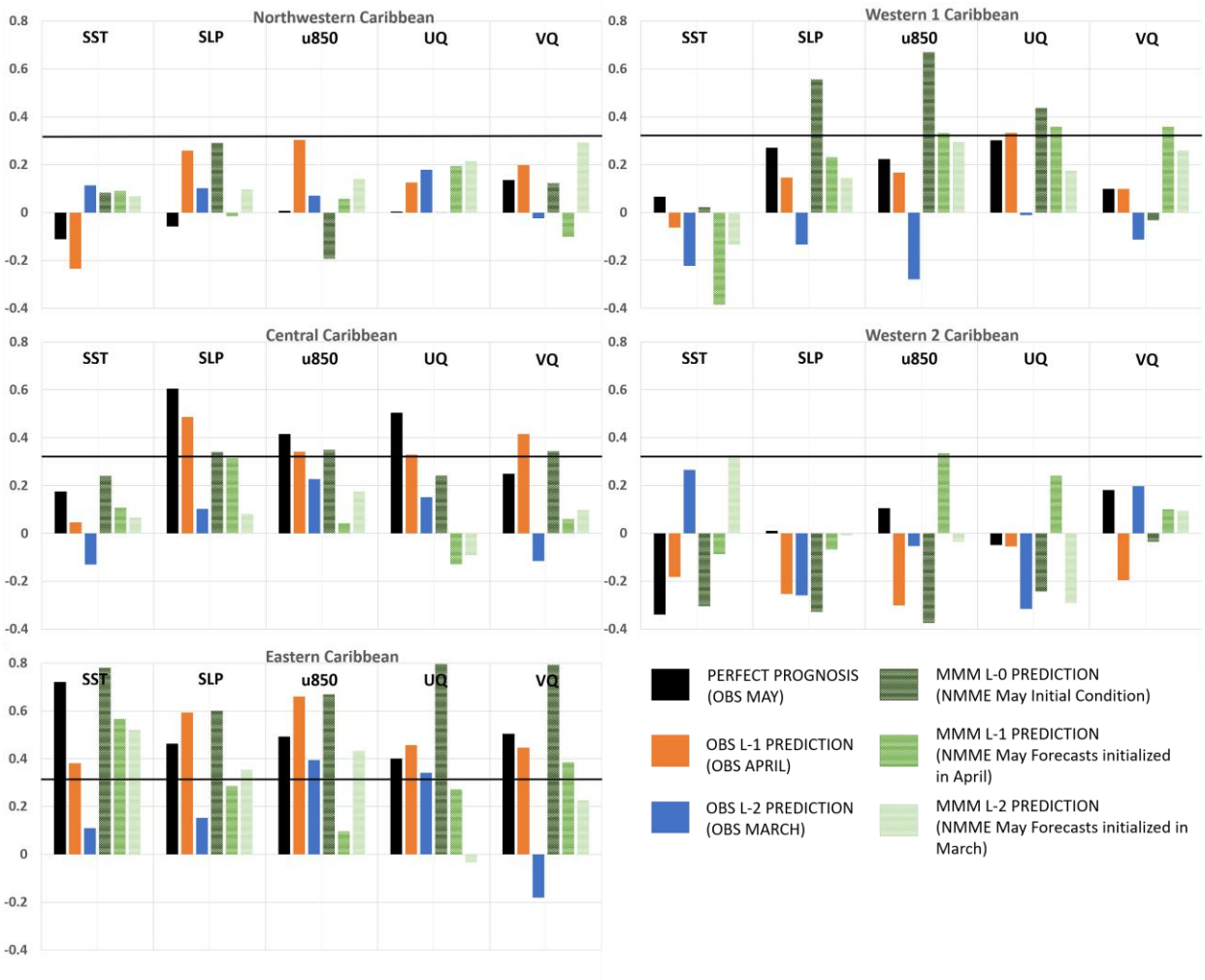

Figure 5.4: Same as Figure 5.2 but for the intensity of wet ERS days

Nonetheless, moisture fluxes provide forecast skill in the Northwestern and Western Caribbean regions that most other candidate predictors do not provide.

Spatial patterns of the first CCA mode of the intensity of wet days in the Caribbean (Figure 5.5) and frequency of wet days are similar; however, correlations between observations and forecasts of the intensity of wet days (Figure 5.4) are weaker than correlations for the frequency of wet days. Positive loadings in the wet-day intensity SLP spatial loading (Fig. 5.5c, d) extend further into the Caribbean than in the wet-day frequency SLP spatial loading, and the wet-day intensity VQ spatial loading (Fig. 5.5i, j) is shifted further west than the wet-day frequency VQ spatial loading. Forecasts of the intensity of wet days are skillful in the Central and Eastern Caribbean using most April and May observed predictors. March UQ, and VQ-based OBS predictors also produce skillful forecasts.

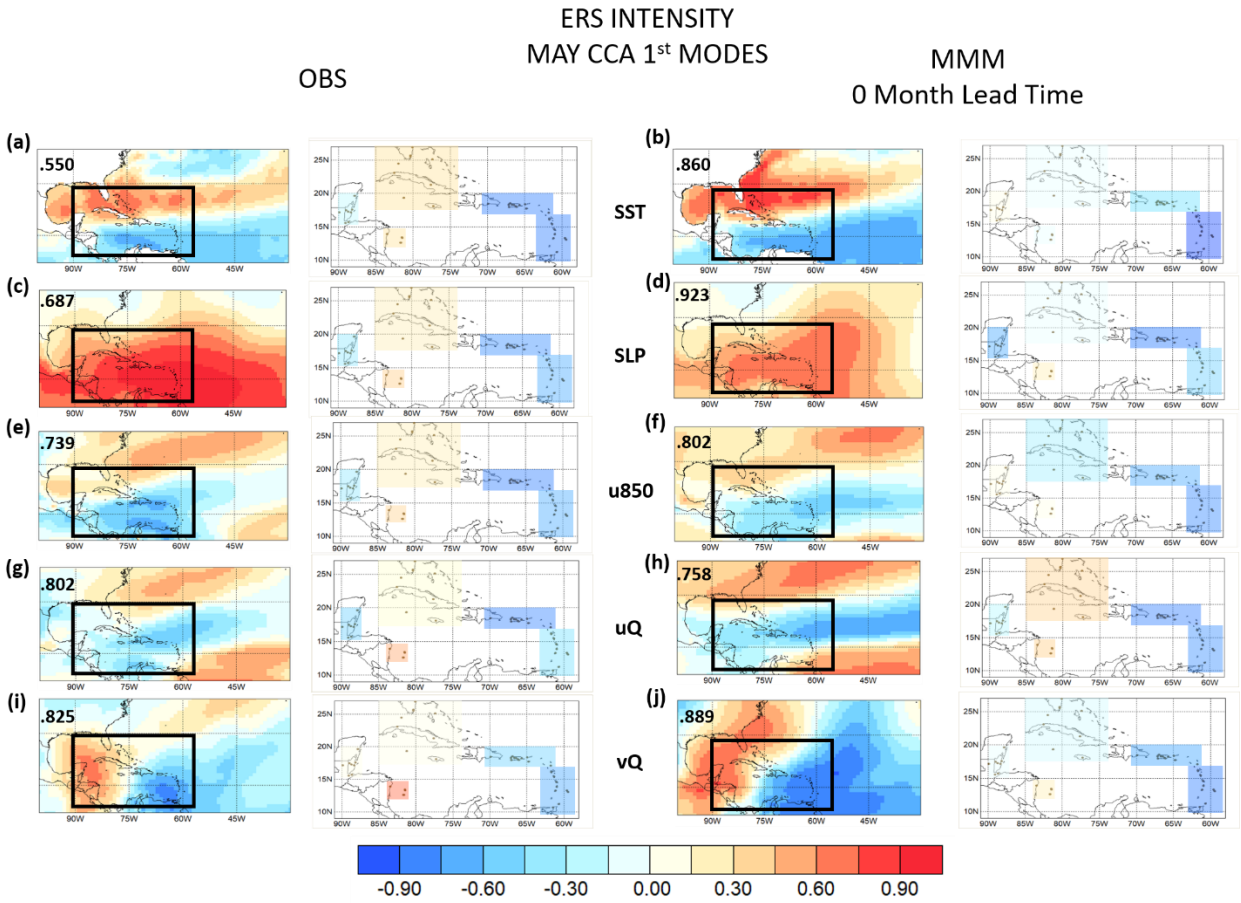

Figure 5.5: same as Figure 5.3 but for the intensity of wet ERS days

The Eastern Caribbean is the only sub-region that shows consistent skillful model-based forecasts for most initial conditions and lead-times.

With the exception of UQ in the Western 1 Caribbean, the Northwestern and Western Caribbean do not show significant skillful forecasts when using OBS predictors. The Western 1 Caribbean is the only sub-region with higher correlations for intensity than frequency of wet days, primarily with forecasts using SLP, u850, and UQ MMM predictors. Since the CCA spatial loadings of wet-day intensity are similar to wet-day frequency, the interpretation of the Chapter 3 findings to explain the sub-regional differences of predictor-predictand skill and climate dynamics of the frequency of wet days are also applied for the intensity of wet days.

5.4.2 Late-Rainy Season

Perfect prognosis of the frequency (Fig. 5.6) and intensity (Fig. 5.7) of wet days using August, the target month and start of the LRS across the Caribbean, is skillful with statistical significance, with sub-regional differences on which predictor-based forecast has the most skill and which predictand is better forecasted. For the intensity of wet days, all perfect-prognosis are significantly correlated with observations in the Northwestern, Central, and Eastern Caribbean and insignificantly correlated with observations in the Western Caribbean. There are similar findings for the frequency of wet days; however, correlations are weaker than those for the intensity of wet days in the Northwestern, Central, and Eastern Caribbean, and stronger than those for the intensity of wet days in the Western Caribbean.

OBS L-1 and L-2 predictions are also skillful for both predictands in the Caribbean, with similar sub-regional differences as those found in the perfect prognosis. The Northwestern, Central, and Eastern Caribbean exhibit skill forecasts using June and July predictors for the intensity of wet days. For the frequency of wet days, skill forecasts using June and July predictors

are significant but weaker than intensity of wet days in the Central Caribbean, and weaker and in some cases insignificant than the intensity of wet days for the Northwestern and Eastern Caribbean. Unlike these sub-regions, the Western Caribbean exhibits stronger and, in some cases, significant June and July observed-based forecast skill for the frequency of wet days than the intensity of wet days.

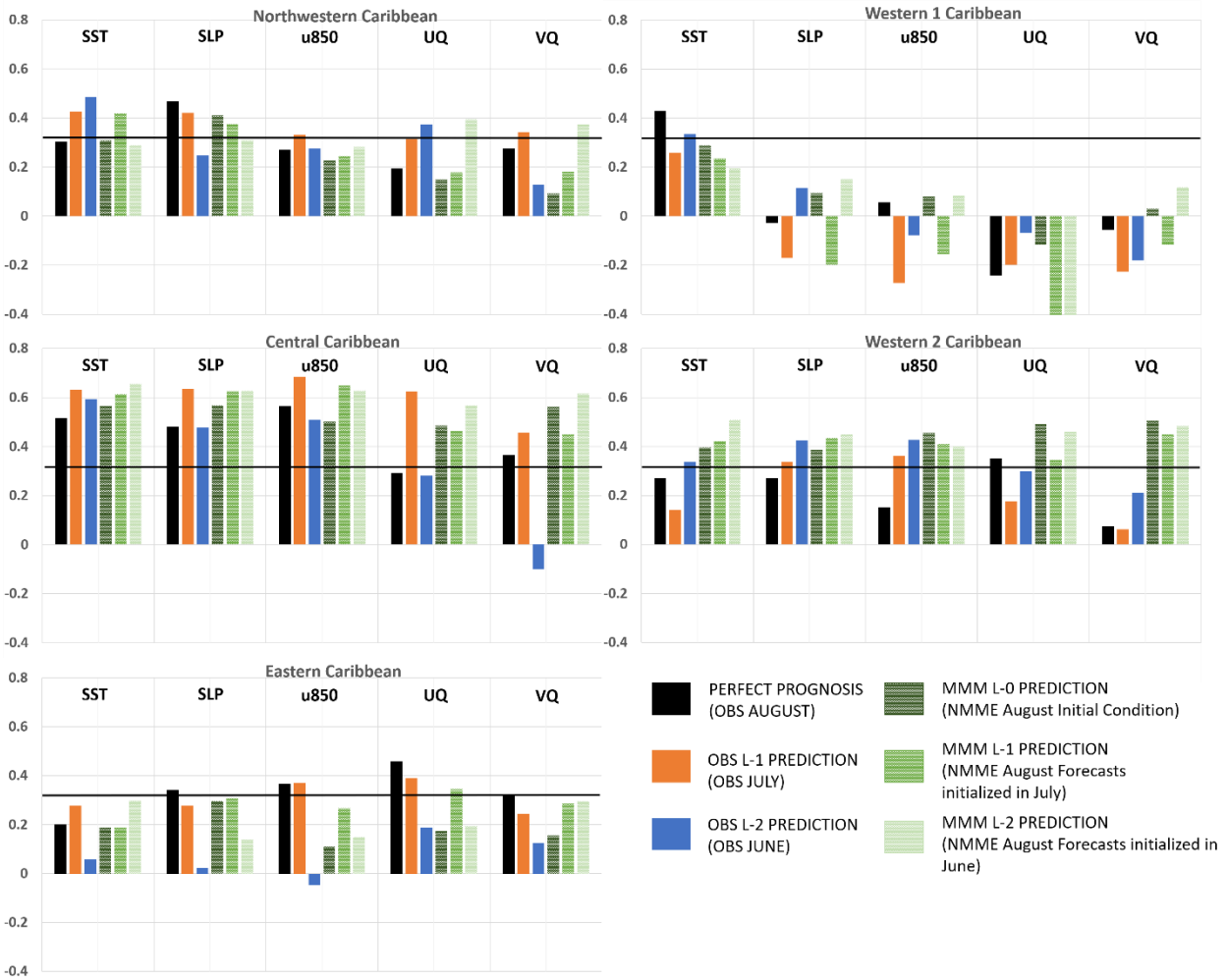

Figure 5.6: Cross-validated sub-region OBS and MMM Spearman correlations between 1982-2015 observed and forecasted frequency of wet LRS days via CCA over 40°N-0°N, 150°W-20°W using observed and model-based sea-surface temperatures, sea-level pressure, zonal winds at 850hPa, vertically integrated zonal and meridional moisture fluxes as predictors. Spearman correlations are calculated for preceding months and monthly lead times of August. Values above the black line denote statistical significance at the 95th percentile.

MMM predictions of the intensity and frequency of LRS wet days are comparable with perfect prognosis of both predictands, and with similar sub-regional differences as those from OBS. MMM prediction of wet LRS intensity is more skillful than prediction of wet LRS frequency for the Northwestern, Eastern, and Central Caribbean. The opposite is found for the Western Caribbean.

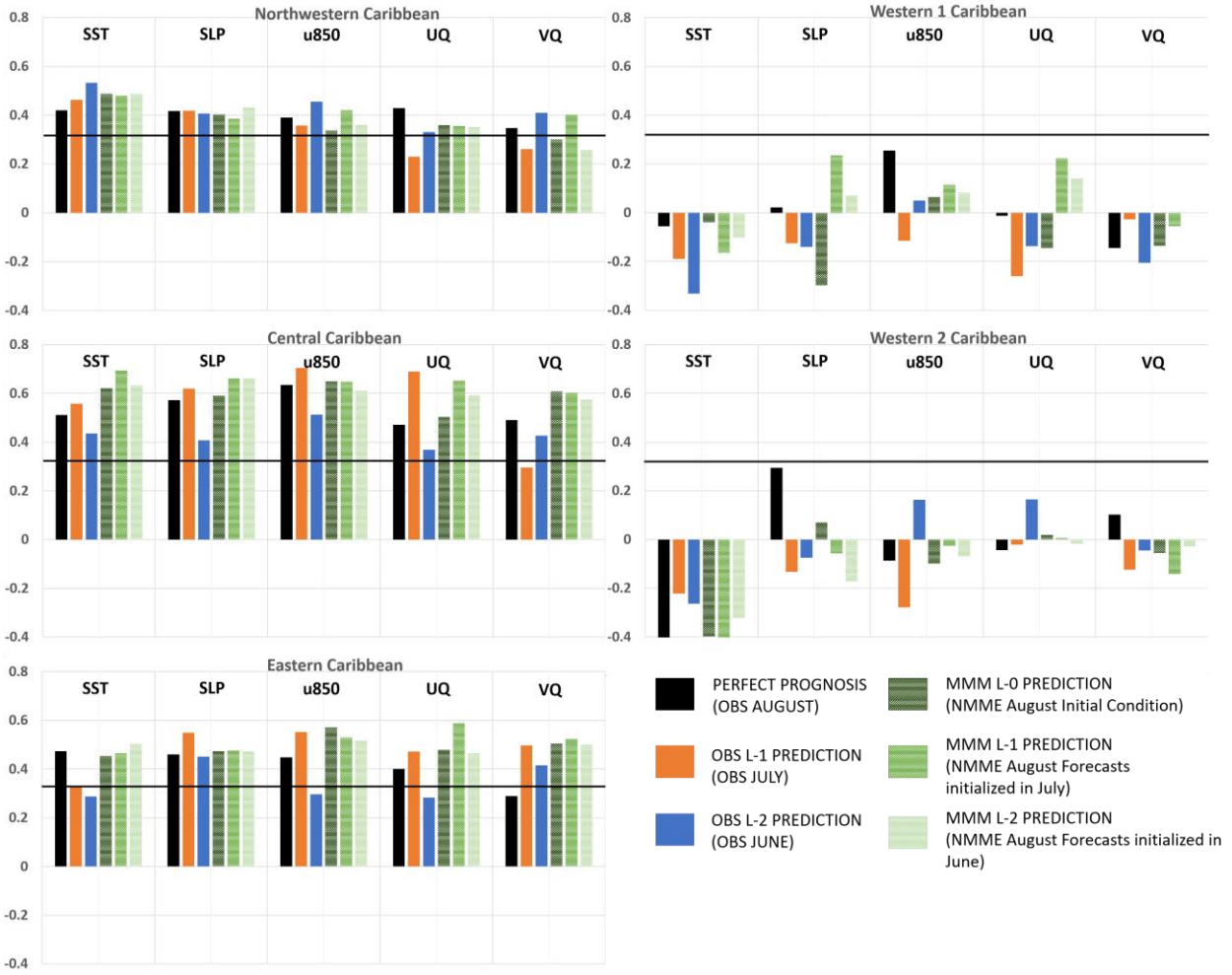

Figure 5.7: same as Figure 5.6 but for the intensity of wet LRS days.

The OBS and MMM first CCA modes for August wet day frequency (Fig. 5.8) and intensity (Fig. 5.9) are similar, with some sub-regional differences. First CCA modes of SSTs in wet-day frequency (Fig. 5.8a, b) and intensity (Fig. 5.9a, b) show a dipole pattern, with negative

loadings over the Caribbean basin and positive loadings over the Eastern Pacific. There is a dipole SLP pattern in the first CCA modes of wet-day frequency (Fig. 5.8c, d) and intensity (Fig. 5.9c,d), with positive loadings over the Caribbean basin and negative loadings over most of the Eastern Pacific. The regional loadings in the Northwestern, Central, and Eastern Caribbean are negative; therefore, the regional loadings are companion to the SSTs spatial loadings and inverted to the SLP spatial loading. If the negative SST and positive SLP spatial loadings are anomalous cold SSTs and anomalous high-pressure, respectively, these sub-regions would experience fewer wet days with less intense wet day rainfall. u850 (Fig. 5.8e,f; Fig. 5.9e,f), UQ (Fig. 5.8g,h; Fig. 5.9g,h), and VQ (Fig. 5.8i,j; Fig. 5.9i,j) show a positive relationship between spatial loadings and Northwestern, Central, and Eastern Caribbean regional loadings.

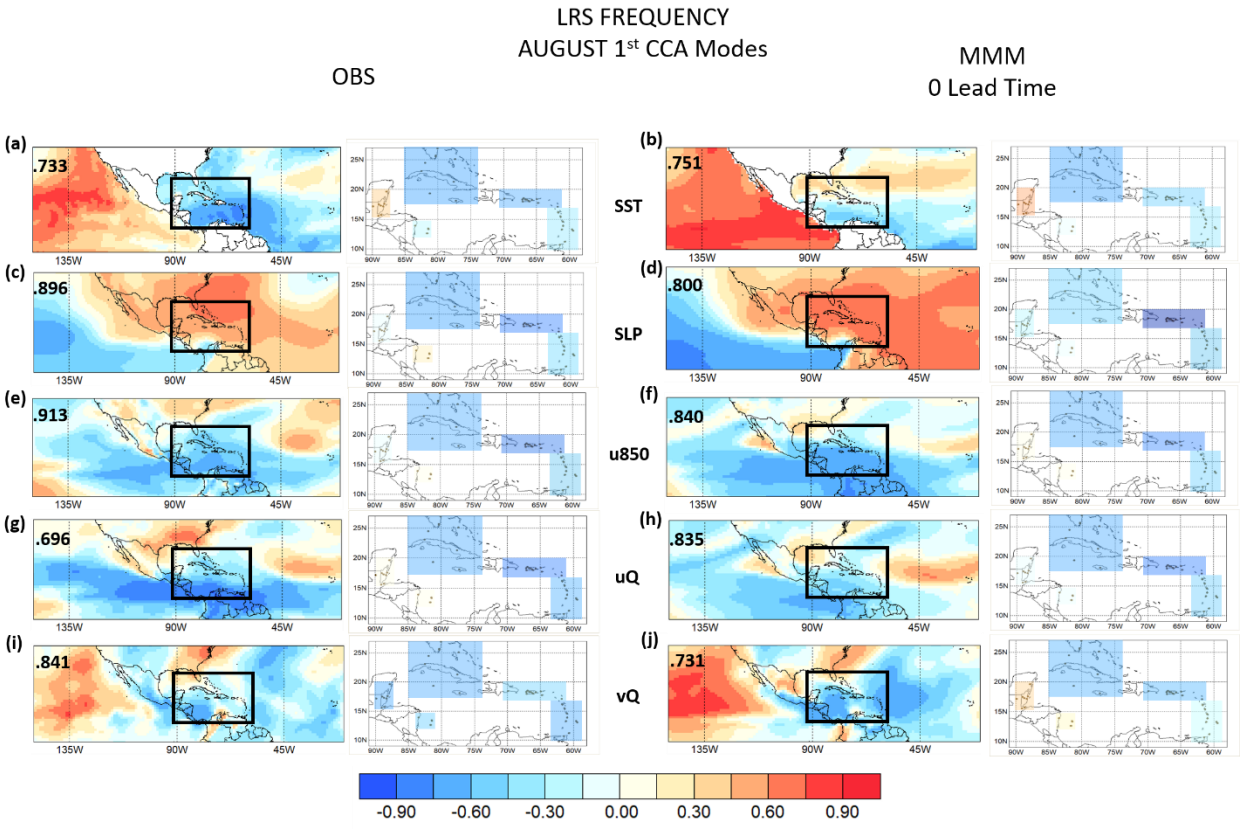

Figure 5.8: same as Figure 5.3 but for the frequency of wet LRS days, the month of August, and spatial loadings are over a larger domain

If the u850, UQ, and VQ spatial loadings imply anomalous easterlies, anomalous zonal divergence, and anomalous meridional divergence, respectfully, the Northwestern, Central, and Eastern Caribbean would experience fewer wet days with less intense rainfall during those wet days. For the frequency of LRS wet days, the regional loadings in the Western 1 and 2 Caribbean from most candidate predictors are weak compared to other sub-regions, which explains why their forecast skill levels fall below significance. However, most regional loadings for the intensity of LRS wet days in the Western 1 and 2 sub-regions are similar with the regional loadings seen across other sub-regions and explains how some forecasts are skillful in the Western Caribbean.

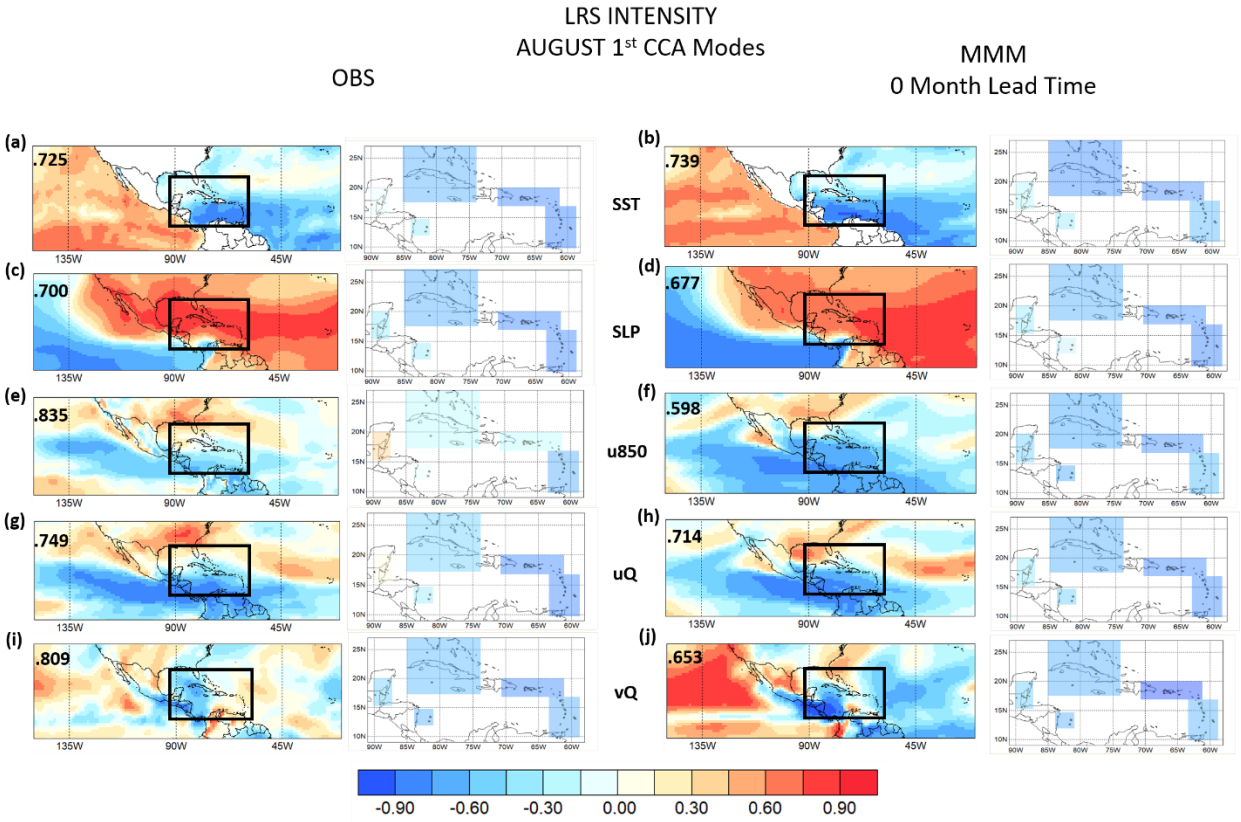

Figure 5.9 same as Figure 5.3 but for the intensity of wet LRS days, the month of August, and spatial loadings are over a larger domain

The spatial loadings of the first CCA modes of frequency and intensity of wet days resemble the spatial composites of the MSD and LRS during dry minus wet LRS years (Fig. 3.5;

3.6), which stem from the summertime onset of ENSO. In Chapter 3, ENSO indices during the summertime are significantly and negatively correlated with Caribbean-wide LRS anomalies. An anomalous SST and SLP response in the TNA (Curtis and Hastenrath 1995; Poveda and Mesa 1997) emerges through an ENSO atmospheric bridge (Giannini et al. 2000). Under an El Niño state, the ENSO atmospheric bridge produces an anomalous anti-cyclonic circulation that intensifies NASH in the Caribbean and produces an anomalous cyclonic circulation in the Eastern Pacific Basin. This induces a low-level wind and moisture circulation that is fluxed from the Caribbean and onto the Eastern Pacific, resulting in enhanced easterlies, subsidence, intensification of the CLLJ, southern displacement of the Eastern Pacific and Atlantic ITCZ, and moisture divergence across most of the Caribbean. The u850, UQ, and VQ spatial loadings in this analysis show the anomalous flux of winds and moisture fluxes that is centered over Central America and Northern South America. The spatial loadings similarly reflect the spatial composites of the mean flow moisture flux during MSD and September dry minus wet LRS years (Fig. 3.6,a,b). Some anomalous convergence over the Western Caribbean is seen under dry LRS years and is related to zonal convergence by the intensification of the exit jet region of the CLLJ (Hidalgo et al. 2015; M19). This explains why most regional loadings and correlations between observations and forecasts over the Western 1 and 2 Caribbean are weak and vary with each candidate predictor, as the Western Caribbean experiences competing dynamical mechanisms that either suppress or enhance convergence in the region (Hidalgo et al. 2015; Chapter 2; Chapter 3).

5.4.3 Mid-Summer Drought

All sub-regions for most earlier months of July and monthly lead times of June/July have statistically significant correlations between observations and forecasts of the magnitude of the MSD (Figure 5.10). In the Western and Northwestern Caribbean regions the MSD typically starts

in July; therefore, the target month is July. In the Central Caribbean, the MSD typically is in June; therefore, the target month is June.

Under perfect prognosis, there are significant correlations between observations and forecasts; however, there are sub-regional differences. The Western 1 and 2 Caribbean show significant correlations between observations and perfect prognosis. Although weaker than the perfect prognosis, there are also significant correlations between observations and OBS L-1 predictions in these sub-regions. In the Central Caribbean, there are positive correlations between observations and perfect prognosis; however, only SST-, SLP, and VQ-based forecasts are significant. In the Northwestern Caribbean, only July SST-based forecasts are significantly correlated with observations.

Some-regions also show skillful OBS L-1 and L-2 predictions. The Western and Central Caribbean have significant correlations between their observations and May OBS forecasts. SST-, SLP- and u850-based forecasts are consistently skillful in these sub-regions.

MMM predictions are skillful and are similar to the perfect prognosis. All MMM L-0 and L-1 forecasts are significantly correlated with observations in the Western 1 and 2 Caribbean regions. In the Northwestern Caribbean, most MMM L-1 predictors are significantly correlated with observations; however, there are some differences notably between VQ and UQ MMM vs. OBS predictions. In the Central Caribbean, all MMM L-1 predictions are significantly correlated with observations. Notable forecasts that show persistent skill in the Caribbean are from SST, SLP, and VQ. All Western Caribbean July and Central Caribbean June forecasts that were initiated in May/June and April/May, respectively, are significantly correlated with observations. In the Northwestern Caribbean, MMM L-1 and L-2 VQ, UQ, and u850-based forecasts show some significant correlations between observations and forecasts.

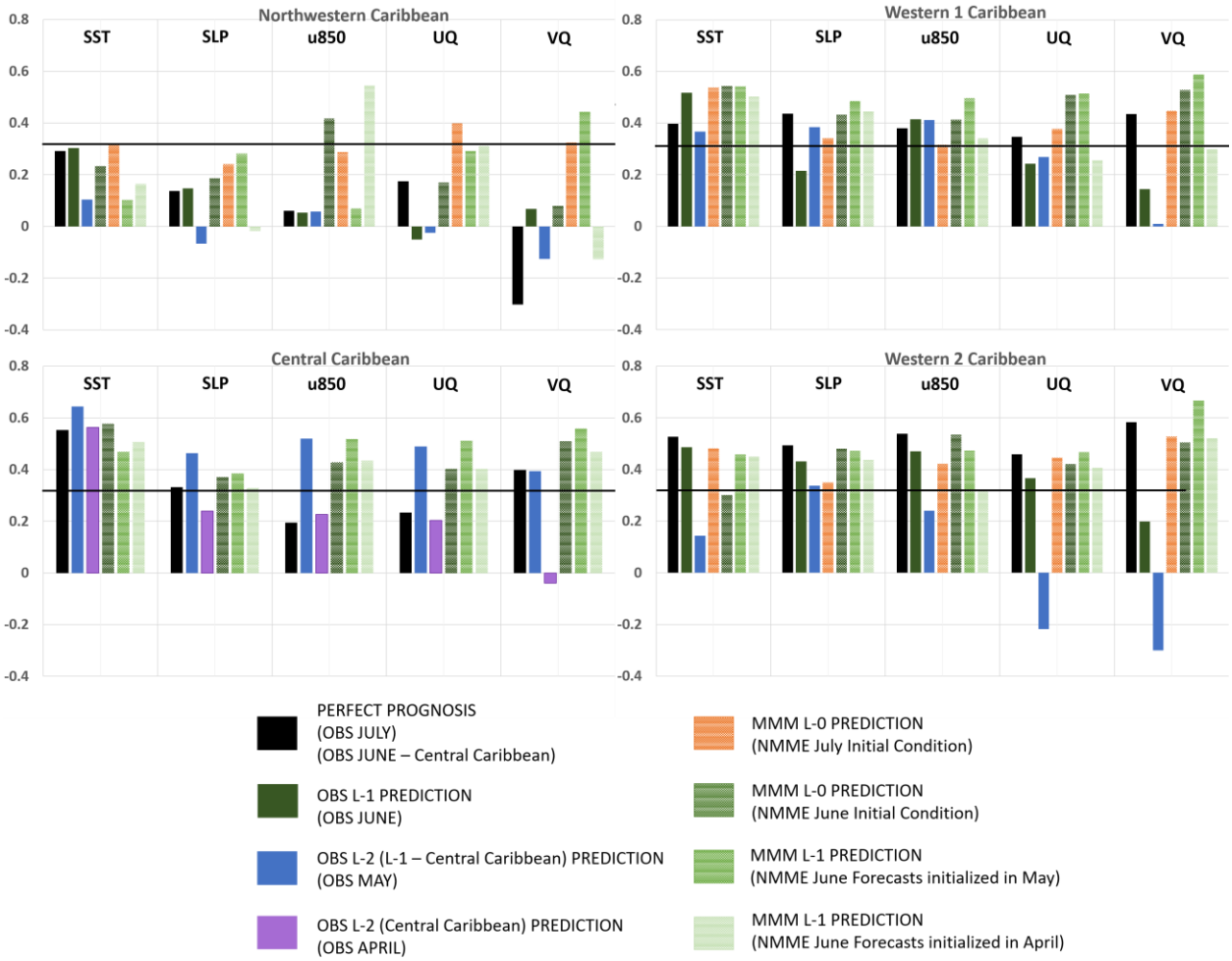

Figure 5.10: Cross-validated sub-region OBS and MMM Spearman correlations between 1982-2015 observed and forecasted magnitude of the MSD that were computed via CCA over 40°N-7°N, 100°W-30°W using observed and model-based sea-surface temperatures, sea-level pressure, zonal winds at 850hPa, vertically integrated zonal and meridional moisture fluxes as predictors. Spearman correlations are calculated for preceding months of July and monthly lead times of June/July. Values above the black line denote statistical significance at the 95th percentile.

The first OBS and MMM CCA modes are similar and the relationship between each spatial and regional loading are positive for most sub-regions (Fig. 5.11). Spatial loadings are negative for SST (Fig. 5.11a,b), and VQ (Fig. 5.11i,j) and positive for SLP (Fig. 5.11c,d) over the Caribbean basin. Regional loadings for all sub-regions are negative.

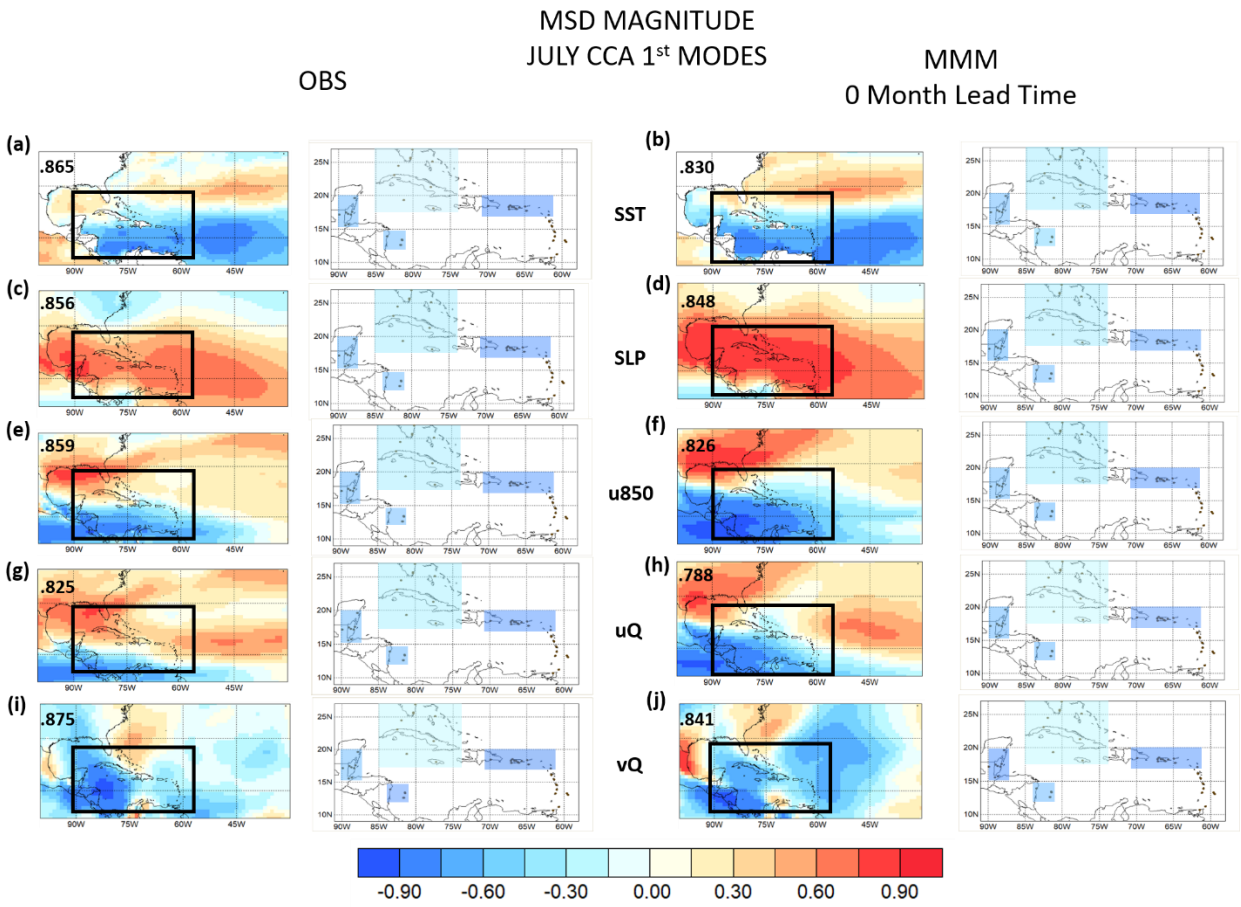

Figure 5.11: same as Figure 5.3 but for the magnitude of the MSD, the month of July, and the Eastern Caribbean is excluded.

Therefore, if the negative regional loadings denote less magnitude of rainfall during the MSD, which means a stronger MSD, the negative spatial loadings in the Caribbean basin would be anomalously cold SSTs, high-pressure, and meridional divergence. There is some exception in the Northwestern Caribbean, where some areas at and north of Cuba experience positive spatial loadings for SSTs, and VQ. Negative spatial loadings in u850 (Fig. 5.11e,f) and UQ (Fig. 5.11g,h) are seen in Central America and portions of the Caribbean basin; therefore, in the Western Caribbean sub-regions, stronger easterlies and zonal divergence are associated with a stronger MSD. In the Northwestern and Central Caribbean regions however, there are some differences between u850 and UQ OBS (Fig. 5.11e,g) and MMM (Fig. 5.11f,h). UQ and u850 in OBS show

positive spatial loadings over the Northwestern Caribbean and portions of the Central Caribbean whereas UQ and u850 in MMM show weak negative loadings over these sub-regions. If the negative spatial loadings in UQ and u850 across Central America denote stronger easterlies and anomalous zonal divergence, respectfully, the positive spatial loadings across the Northwestern and portions of the Central Caribbean denote anomalous westerlies and zonal convergence. The MMM SLP positive loading is centered over the Northwestern and Central Caribbean, whereas the OBS SLP positive loading center is to the south of these sub-regions. If the positive SLP loading is anomalous high-pressure, these sub-regions would experience anomalous westerlies from the northern flank of the anomalous high under OBS and MMM; however, the magnitude of the anomaly would be stronger under OBS and weaker under MMM. The intersection of the negative and positive spatial loadings for most July candidate predictors in the Northwestern Caribbean explains the weaker regional loadings, and weak/non-statistically significant correlations between observations and forecasts in the Northwestern Caribbean compared to the other sub-regions. The negative spatial loadings of the July moisture fluxes and u850 are strongest across the Western Caribbean, which may explain why the correlations between observations and forecasts are highest over the Western Caribbean compared to the other sub-regions.

The Central Caribbean would experience a similar relationship between the predictors and magnitude of the MSD as the other sub-regions; however, their MSD is primarily in June. First CCA modes of the magnitude of the MSD in OBS and MMM were investigated using June candidate predictors (not shown). Compared to July, the negative spatial loadings of June u850 and UQ extend further into the Central Caribbean, which results in a similar positive relationship between candidate predictors and MSD predictand in the Western Caribbean. The westward shift of the low-level wind and UQ negative loadings between June and July spatial loadings are

similarly seen with SLP. This hints at how the MSD starts over the Central Caribbean and then shifts into the Western Caribbean between June and July, as found in other studies (e.g., Curtis and Gamble, 2007; Gamble et al. 2007), and why Central Caribbean correlations between observations and forecasts are significant in June.

The spatial modes of the first CCA modes in June (not shown) and July (Fig. 5.11) for all candidate predictors have similarities with May and August CCA spatial modes from the ERS (Fig. 5.3; 5.5) and LRS (Fig. 5.8; 5.9), and the MSD composites for both ERS and LRS dry minus wet years (Fig. 3.2; Fig. 3.4-6). Both MSD CCA June and ERS CCA May spatial loadings show SLP, u850, and UQ spatial patterns that are shifted east compared to their MSD July and LRS August patterns, and SST negative loadings that are stronger than their MSD July and LRS August patterns. Negative SLP spatial loadings also strengthen over the Eastern Pacific between MSD June and July, increasing the resemblance of the LRS August CCA SLP spatial loading dipole. Remnants of the NAO SST-SLP persistence signal are seen in MSD of dry minus wet ERS years (Fig. 3.2d,i) and the dipole SLP pattern between the Eastern Pacific and Caribbean basins are seen in MSD of dry minus wet LRS years (Fig. 3.5i). As the ERS and LRS CCA spatial loadings in this study resemble the M20 ERS and LRS composites that are a consequence of the NAO-SST persistence signal and summertime onset of ENSO, respectively, the findings of the MSD June and July CCA spatial loadings suggest that the MSD June and July CCA spatial loadings are a result of the decaying NAO-SST/SLP persistence signal and the summertime onset of ENSO.

The transition between the decay of the NAO-SST/SLP persistence pattern and the summertime onset of ENSO is clearly seen in the transition of the MSD VQ spatial loadings between June and July. The ERS May CCA VQ positive spatial loadings over the Northwestern Caribbean and Western Caribbean, which is induced by changes in the western flank of NASH

from the anomalous NAO SST/SLP persistence signal, is seen in the MSD June CCA spatial loadings, but not in the MSD July CCA spatial loadings. Instead, MSD July CCA VQ spatial loadings show negative loadings over Central America and the Northwestern Caribbean that resemble the LRS August VQ CCA negative loadings, where moisture and the low-level wind field are fluxed through Central America via the ENSO atmospheric bridge.

5.5 Discussion

The dynamical mechanisms and climate drivers that shape each seasonal component of the Caribbean rainfall cycle (Chapter 2 and 3) are consistently shown in the CCA model outputs. These are responsible for the skillful seasonal prediction of rainfall characteristics over the Caribbean, and explain sub-regional differences in skill. Skillful forecasts are consistently found for the Central and Eastern Caribbean regions, whereas forecasts are skillful only for certain predictands in the Northwestern and Western Caribbean regions. The winter-time NAO SST-SLP persistence signal and the SLP signal induced by ENSO are primarily centered over the Central and Eastern Caribbean sub-regions during the ERS and LRS, respectively. The winter-time NAO SST-SLP persistence signal and SLP signal induced by ENSO impact the sets of dynamical mechanisms (e.g., NASH, ITCZ, and TNA SSTs) in these two sub-regions such that the dynamical mechanisms produce anomalous divergence, or convergence in concert. However, in the Northwestern and Western Caribbean, the winter-time NAO and ENSO induced anomalous signals result in some dynamical mechanisms to produce anomalous convergence, and other dynamical mechanisms to produce anomalous divergence (e.g., winter-time positive NAO phase induces anomalous ERS divergence from cold SSTs and enhanced subsidence, and anomalous ERS convergence from the intensification of orographic lifting from the stronger-than-normal exit-jet region of the CLLJ). Furthermore, many of the dynamical mechanisms in the Northwestern and Western Caribbean

evolve sub-monthly, which may not be captured using monthly predictor fields (e.g., evolution of the western flank of NASH convergence during the ERS). This may explain why forecasts of the ERS characteristics are not as skillful as forecasts of LRS characteristics in the Caribbean, since the dynamical mechanisms during the LRS exhibit monthly or longer evolutions that are captured when using monthly predictor fields.

Whether the intensity or frequency of wet days is a better metric to forecast depends on the sub-region and rainfall season. For the ERS, the frequency of wet days is easier to predict than intensity of wet days. The same can be said for the LRS frequency of wet days across the Central and Western Caribbean; however, the intensity of wet days is better forecasted than frequency of wet days in the Eastern and to a lesser degree the Northwestern Caribbean. The Eastern Caribbean has a unimodal rainfall cycle that is separated by its wet season and its wetter season. The wettest portion of its wetter season is during the LRS and since the region is chronically wet, it's likely that the 1 mm threshold to define a wet day is too low to distinguish changes in the wetter season. Nonetheless, the frequency of wet days across the Caribbean is generally better forecasted than intensity of wet days, which is a similar finding from studies that used these metrics across other tropical regions near the Caribbean (Muñoz et al. 2016; Alfaro et al. 2018; Fernandes et al. 2020).

Skillful forecasts are normally obtained when using the MMM as it generally outperforms the individual models of the NMME. The MMM results confirm how a suite of models does better than using any one model (Goddard et al. 2001; Kar et al. 2011; Kelley et al. 2020; Muñoz et al., 2020; WMO, 2020).

There are several implications and advantages from investigating the perfect prognosis and prediction of various rainfall characteristics in the Caribbean when utilizing a wide-range of candidate predictors. Figure 5.12 emphasizes the following implications and advantages.

1. In many cases, a candidate predictor is not necessarily a good predictor of a given rainfall characteristic for all sub-regions. For example, VQ is a good predictor of the frequency of ERS wet days in the Caribbean except in Western 1 Caribbean (Fig. 5.12a); SLP is a good predictor of the intensity of ERS wet days in the Caribbean except in Western 2 Caribbean (Fig. 5.12b), and UQ is only a good predictor of the frequency of LRS wet days in the Central, Western 2, and Eastern Caribbean (Fig 5.12c). Furthermore, station climatologies of the various predictands (Fig. 5.12) demonstrate how rainfall characteristics are not uniform in the Caribbean. The sub-regional differences emphasize the importance of investigating seasonal forecasts of Caribbean rainfall characteristics on a sub-regional scale.

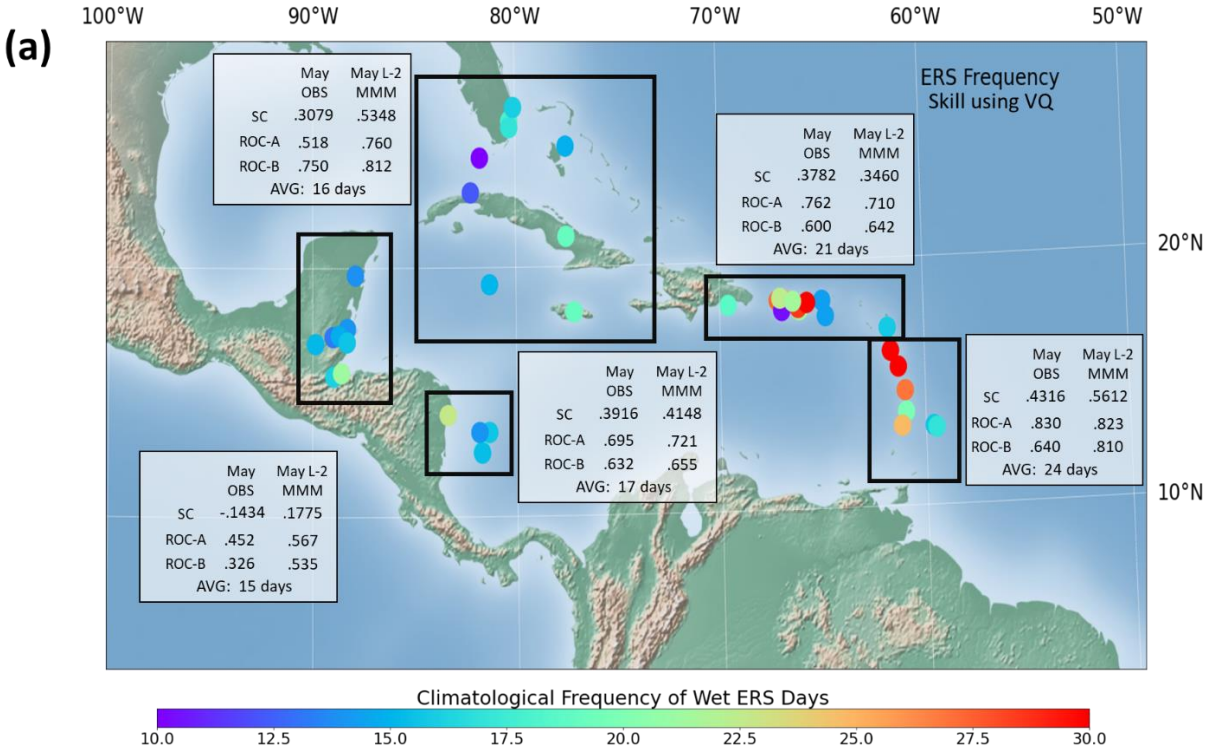

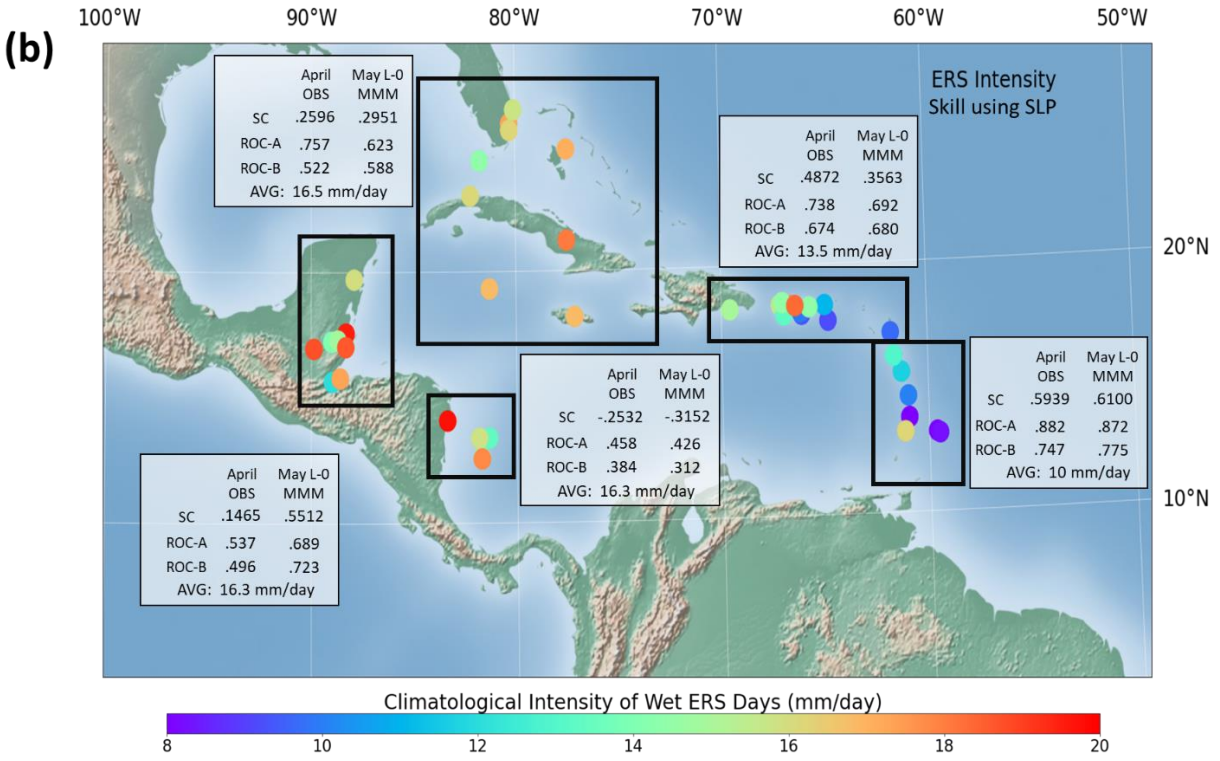
(b)
100°W
90°W
80°W
70°W
60°W
50°W
20°N
10°N
ERS Intensity
Skill using SLP
April OBS | May L-0 MMM
SC .2596 .2951
ROC-A .757 .623
ROC-B .522 .588
AVG: 16.5 mm/day
April OBS | May L-0 MMM
SC .4872 .3563
ROC-A .738 .692
ROC-B .674 .680
AVG: 13.5 mm/day
April OBS | May L-0 MMM
SC .5939 .6100
ROC-A .882 .872
ROC-B .747 .775
AVG: 10 mm/day
April OBS | May L-0 MMM
SC -.2532 -.3152
ROC-A .458 .426
ROC-B .384 .312
AVG: 16.3 mm/day
April OBS | May L-0 MMM
SC .1465 .5512
ROC-A .537 .689
ROC-B .496 .723
AVG: 16.3 mm/day
Climatological Intensity of Wet ERS Days (mm/day)
8 10 12 14 16 18 20

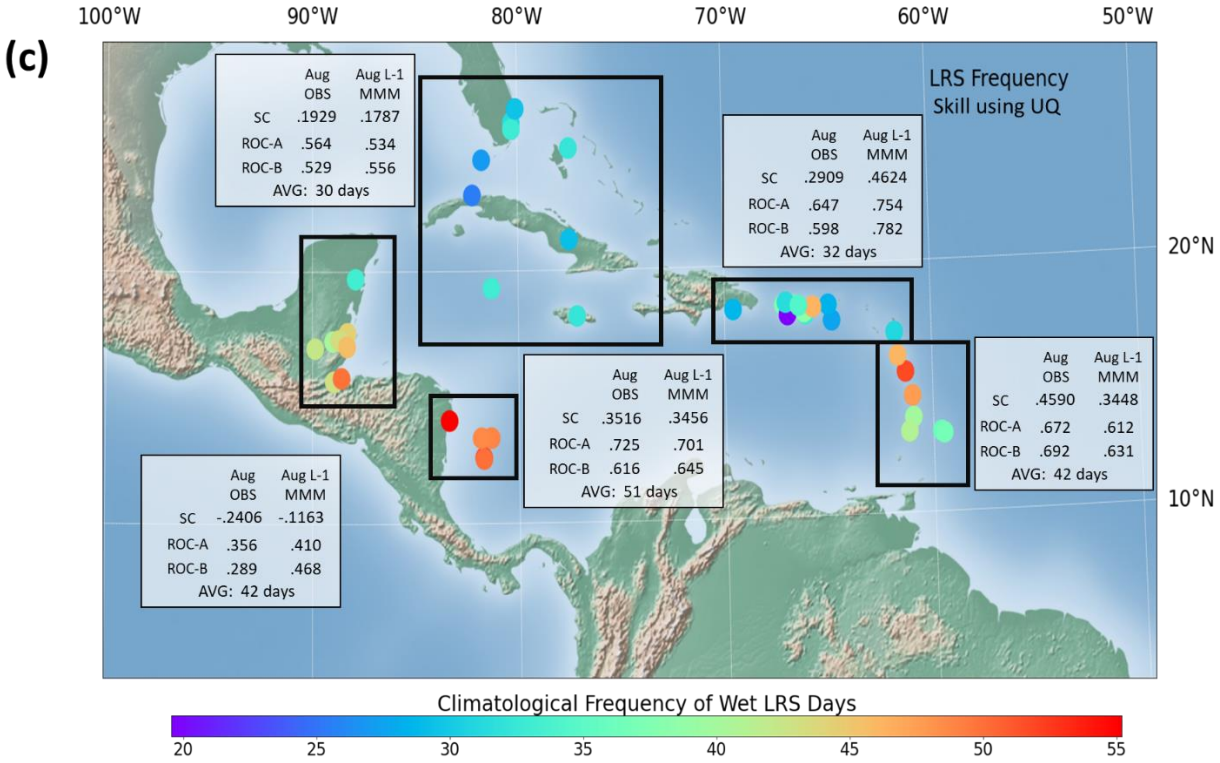
(c)
100°W
90°W
80°W
70°W
60°W
50°W
20°N
10°N
LRS Frequency
Skill using UQ
Aug OBS | Aug L-1 MMM
SC .1929 .1787
ROC-A .564 .534
ROC-B .529 .556
AVG: 30 days
Aug OBS | Aug L-1 MMM
SC .2909 .4624
ROC-A .647 .754
ROC-B .598 .782
AVG: 32 days
Aug OBS | Aug L-1 MMM
SC .4590 .3448
ROC-A .672 .612
ROC-B .692 .631
AVG: 42 days
Aug OBS | Aug L-1 MMM
SC .3516 .3456
ROC-A .725 .701
ROC-B .616 .645
AVG: 51 days
Aug OBS | Aug L-1 MMM
SC -.2406 -.1163
ROC-A .356 .410
ROC-B .289 .468
AVG: 42 days
Climatological Frequency of Wet LRS Days
20 25 30 35 40 45 50 55

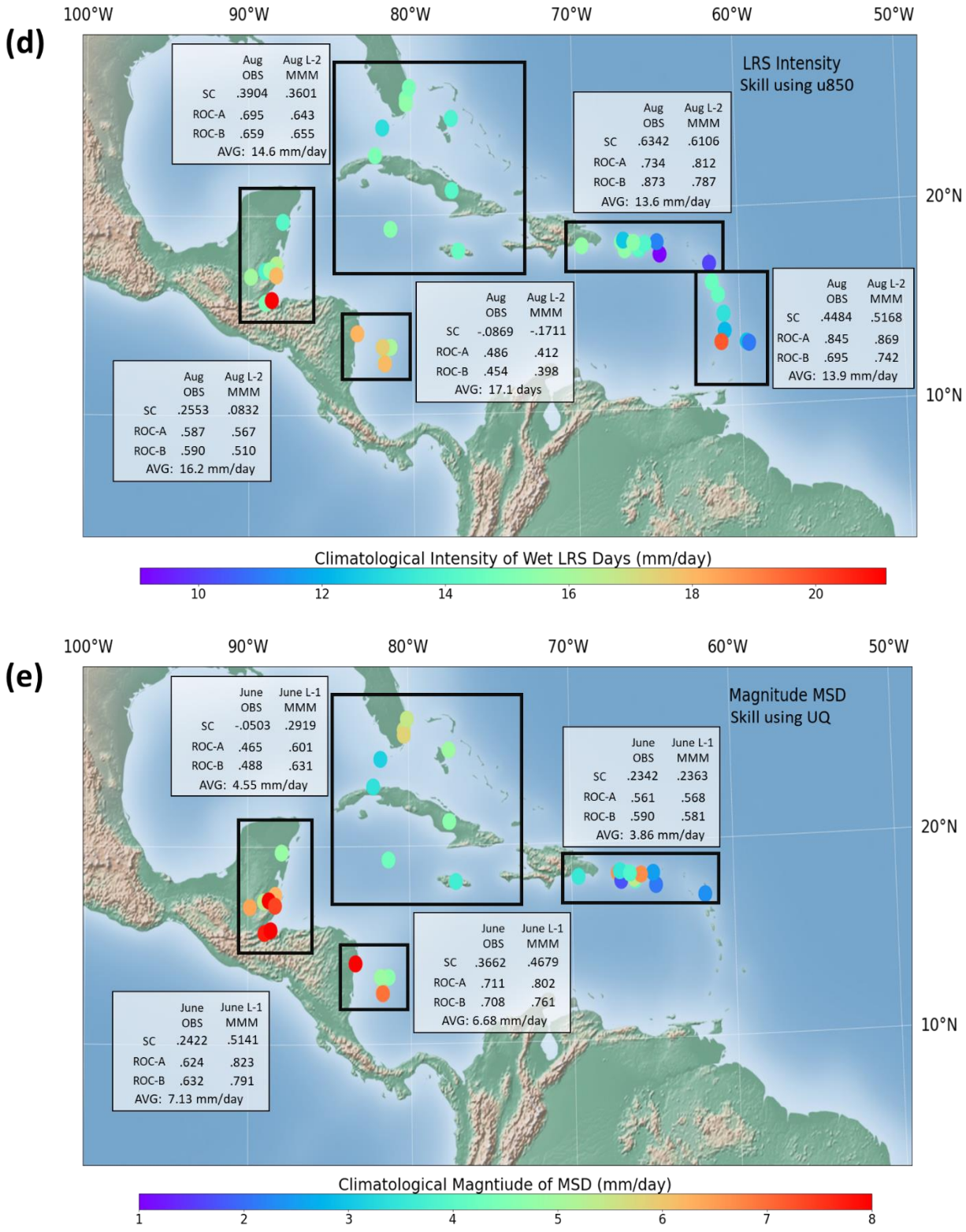

Figure 5.12: Station predictand climatologies (colors) and select forecast skill metrics (light blue box) between Caribbean sub-region (black box) predictands and select predictors. Predictands are (a) Frequency of wet ERS days, (b) Intensity of wet ERS days, (c) Frequency

of LRS days, (d) Intensity of wet LRS days, and (e) Magnitude of the MSD. Select predictors are VQ (a), SLP (b), UQ (c,e), and u850 (d). 'SC' denotes Spearman correlation. ROC-A and ROC-B denote the area under Relative Operating Characteristics for Above-Normal and Below-Normal, respectively. 'AVG' denotes the station-averaged predictand for each sub-region.

2. Skillful forecasts of these characteristics can be made up to 2 months ahead of the season for many of the regions. Forecasts from the MMM at L-1 and L-2 show skill that is comparable with those from OBS (e.g., Fig. 5.12a,c,d,e). The ability to utilize forecasts from models like the NMME, which typically predict one or more seasons into the future, is a significant advantage of using GCMs over observational datasets when producing seasonal forecasts with sufficient lead time, and consequently, ample time for decision making (e.g., proper preparation for growing and harvesting seasons, minimizing food insecurity and water shortages, early humanitarian intervention from inclement hydro-meteorological disasters)

3. UQ and VQ are advantageous to use from GCMs, as they are complex variables that are not readily available from real-time observational monitoring. In some sub-regions and for some predictands, UQ and VQ have the highest forecast skill compared to that from other candidate predictors. MMM UQ and VQ L-0 through L-2 does show comparable skill with perfect prognosis (e.g., Fig 5.12a,c,e); therefore, using models like those within the NMME could be used to produce seasonal forecasts of Caribbean rainfall characteristics using UQ and VQ with substantial time before the target month or season begins.

5.6 Conclusions

Skillful forecasts of agronomically and economically-relevant ERS, MSD, and LRS rainfall characteristics across five sub-regions of the Caribbean using observations from ERA-Interim and dynamical model outputs from the NMME are produced using several candidate predictors that are relevant to the climate dynamics of the Caribbean. For the ERS, forecast skill of the frequency of wet days is higher than the intensity of wet days for most sub-regions of the Caribbean. For the LRS, forecast skill of the intensity of wet days is higher than the frequency of wet days for most sub-regions of the Caribbean. Predictors such as SLP, u850, UQ, and VQ show forecast skill that is comparable, if not better, than SSTs, which is the traditional predictor used to forecast seasonal rainfall characteristics. Generally, forecast skill can be achieved at least a month or two ahead of the target month for all ERS, MSD, and LRS characteristics.

The relationship between predictor-predictand pairs can be attributed to changes in the dynamical mechanisms from the NAO-SST/SLP persistence signal and summertime onset of ENSO for the ERS and LRS, respectively. Spatial patterns from the first CCA modes of the ERS and LRS resemble composites between dry and wet ERS and LRS cases (Chapter 3), which found the winter NAO and its induction of persistent anomalous SST and SLP and summertime onset of ENSO and its see-saw SLP pattern between the Eastern Pacific and Caribbean basins to be responsible for each rainfall seasons' interannual variability. CCA spatial patterns of the MSD bears some resemblance to both the ERS composites and the LRS composites (Chapter 3), which suggests the MSD is influenced by the decay of the NAO-SST/SLP persistence signal and emergence of the summertime onset of ENSO.

There are multiple sub-regional differences as to which CCA model configuration achieves skill. Generally, the Central and Eastern Caribbean regions have consistently significant skill for

all predictions, whereas the Northwestern and Western Caribbean experiences varying levels of skill. The sub-regional differences are largely due to the fact that the sets of local-to-large scale dynamical mechanisms that influence the Northwestern and Western Caribbean, respectively, are larger and more complex than the respective sets that influence the Central and Eastern Caribbean. Additionally, monthly predictor fields may not fully capture the sub-monthly evolution of some dynamical mechanisms seen in the Northwestern and Western Caribbean.

The results from Chapter 5 suggest ways for improving seasonal forecasts of rainfall in the Caribbean that can be readily applied in climate services across the region. Predictor fields from observations and most of the models from the NMME are continuously updated and freely available to use. CIMH, which hosts the Caribbean Regional Climate Center (RCC) and produces the Caribbean Regional Climate Outlook Forum (CariCOF), National Meteorological Services in the Caribbean, and Regional Climate Outlook Forums in Central America can use the prediction framework from this chapter to produce seasonal forecasts of ERS, MSD, and LRS characteristics in the Caribbean. Since each Caribbean sub-region has a different set of skillful model configurations, climate services can delineate the Caribbean into its classified sub-regions and tailor seasonal forecasts based on skillful CCA models that are developed for each sub-region. The NAO and its SST/SLP persistence signal has yet to be utilized to produce seasonal rainfall forecasts, especially in the ERS where it is the primary climate driver of ERS interannual variability. Hence, there is potential to enhance the prediction of the ERS by investigating observed winter-NAO indices and consequently, SST and SLP anomalies across the southern North Atlantic and Caribbean basin.

Finally, Chapter 5 provides a framework to investigate other seasonal rainfall characteristics and motivates an investigation of the sub-seasonal prediction of the Caribbean

rainfall cycle. The frequency of extreme wet and dry days, which provide some indication of flood and drought events, have been investigated in other tropical regions and found skillful (Muñoz et al. 2016; Alfaro et al. 2018). Statistical model predictions of these characterics over the ERS, MSD, and LRS could be investigated to determine what small-to-large scale dynamical mechanisms provide skill and explain the variability of these characteristics. Temporal characteristics (e.g., onset, duration, demise) of the rainfall cycle are more useful than rainfall amount for some farmers (Marengo et al. 2001; Ingram et al. 2002), as changes to the start and end of the rainfall cycle heavily affect agricultural planning (Camberlin and Diop 2003; Diaconescu et al. 2014; Obarein and Amanambu 2019). Temporal characteristics were explored in this Chapter; however, forecast skills of these characteristics were relatively poor across the Caribbean when using monthly predictor fields. As noted in Chapter 4, sub-regional onsets and demises in the Caribbean display sub-monthly variability; therefore, forecast skill of these characteristics may be improved under a sub-seasonal lens. A sub-seasonal prediction study may also improve forecast skill across the Northwestern and Western Caribbean for the rainfall characteristics addressed in this study. Due to the sub-monthly evolution of the western flank of NASH convergence band and dynamics, sub-seasonal prediction of the moisture fluxes in May may provide better prediction of ERS characteristics in the Northwestern and Western Caribbean. Overall, the comprehensive and refined understanding of sub-regional seasonal prediction of rainfall in the Caribbean from this chapter provides 1) various possible ways of improving current forecast information across the Caribbean basin and Central America, 2) a better understanding of the seasonal dynamical mechanisms and climate drivers that influence agronomically and economically-relevant rainfall characteristics in the region, and 3) the potential to enhance decision making (e.g., agricultural

planning, and water and food risk management) regarding inclement seasonal hydro-meteorological hazards.

5.7 Supplemental Information

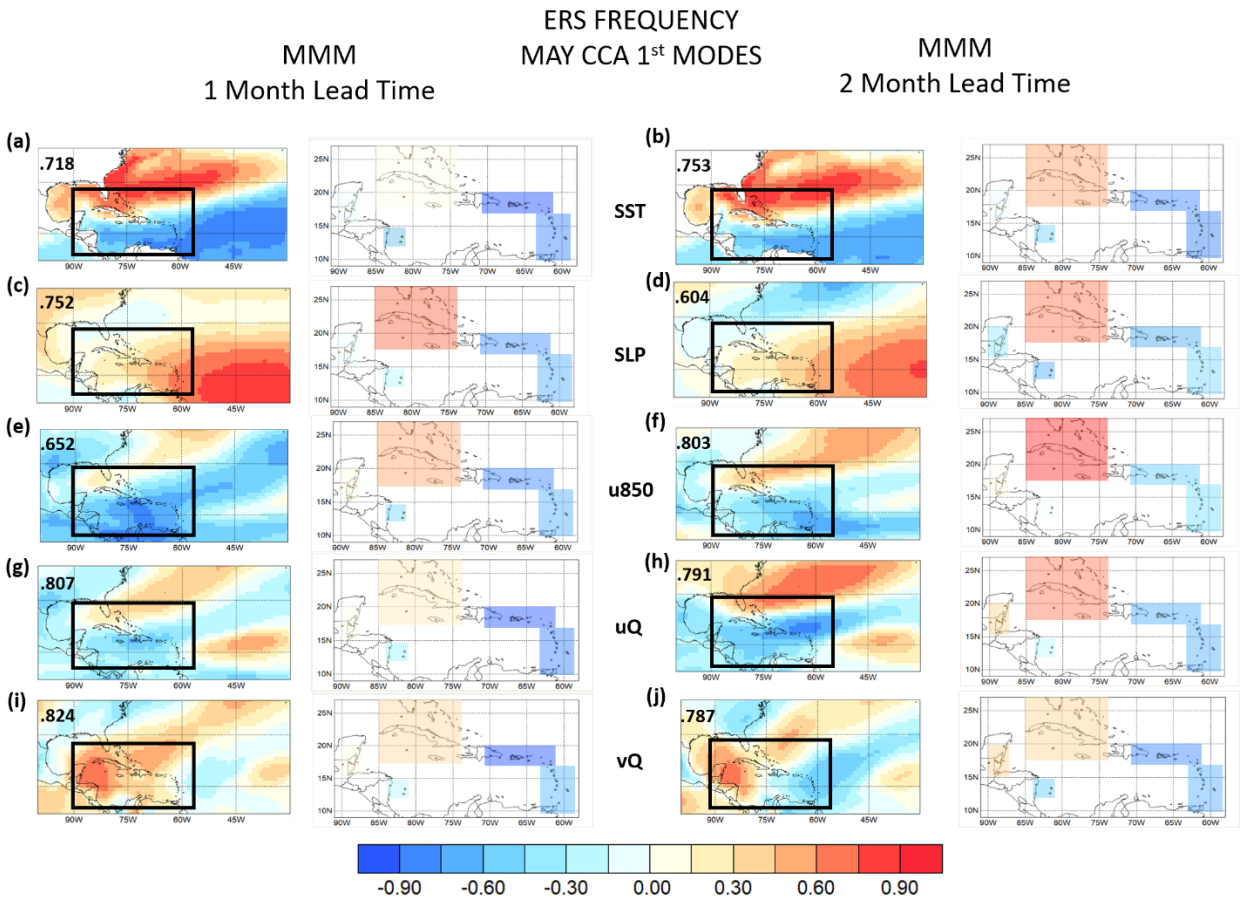

Figure 5.13: Canonical patterns of the first CCA mode using MMM L-1 (left) and L-2 of the NMME (right) for May. Spatial loadings (columns 1 and 3) are from predictors: SST (a,b), SLP (b,c), u850 (e,f), UQ (g,h), and VQ (i,j). Regional loadings (columns 2 and 4) are from the predictand: station-averaged frequency of wet ERS days from each sub-region. Canonical correlations of the first CCA mode are shown on the top left of their spatial loading.

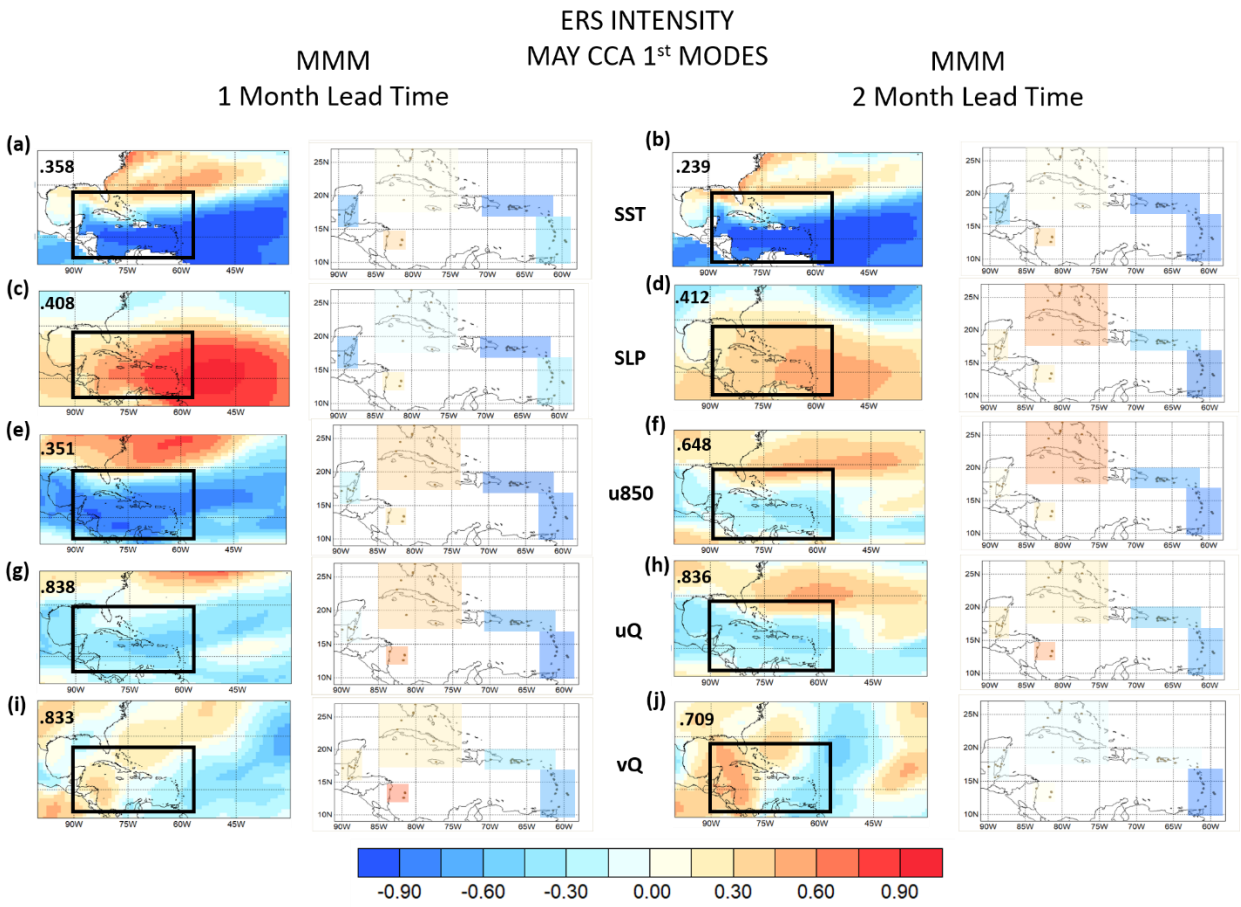

Figure 5.14: same as Figure 5.13 but for the predictand: intensity of wet LRS days

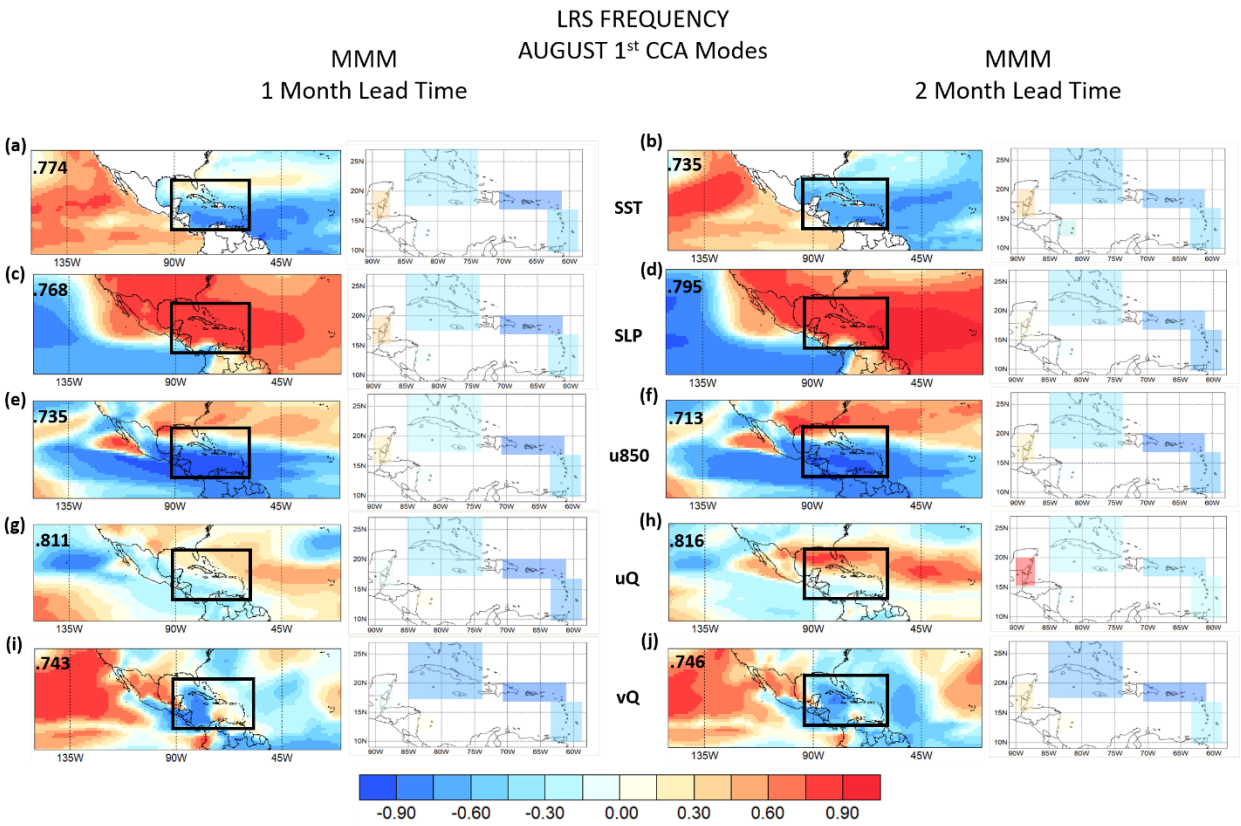

Figure 5.15: same as Figure 5.13 but for the predictand: frequency of wet LRS days, the month of August, and spatial loadings are over a larger domain.

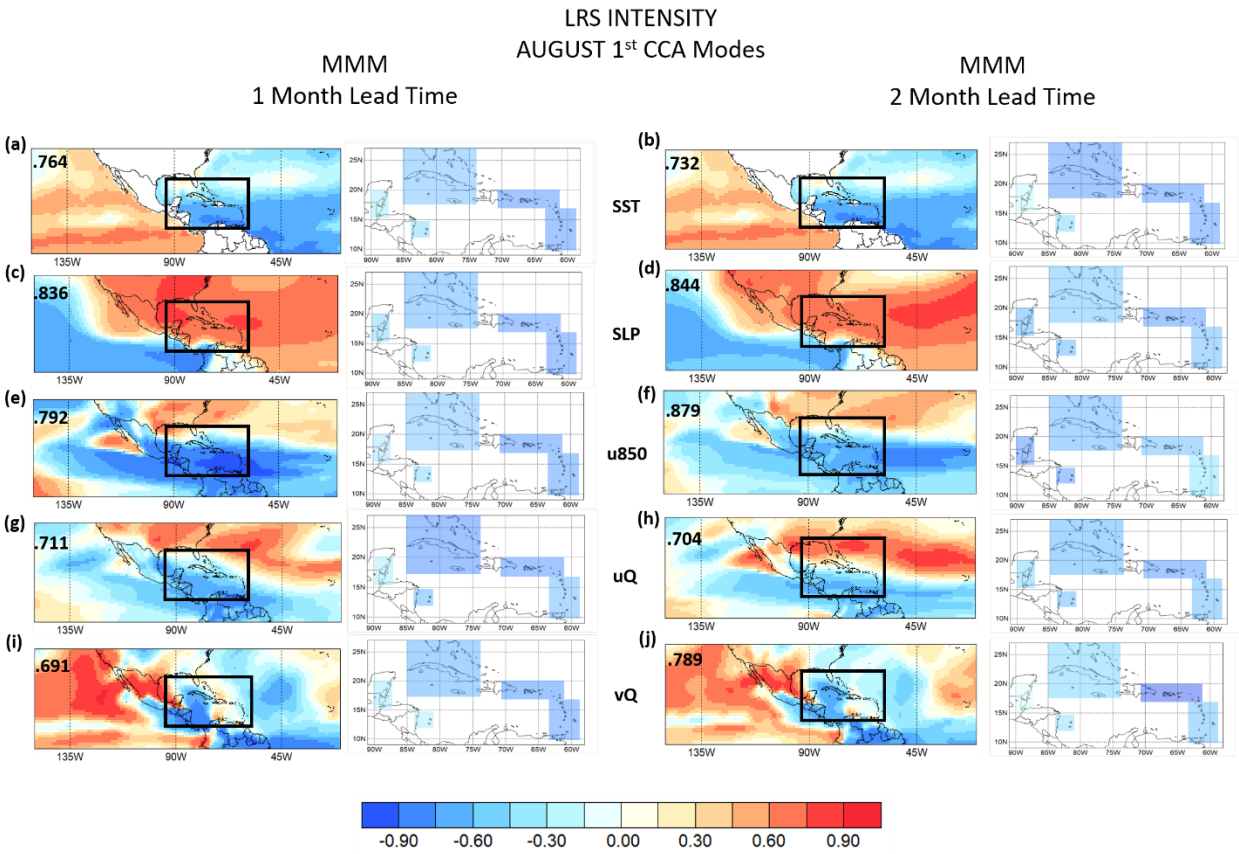

Figure 5.16: same as Figure 5.13 but for the predictand: magnitude of the MSD, the month of July, and the Eastern Caribbean is excluded.

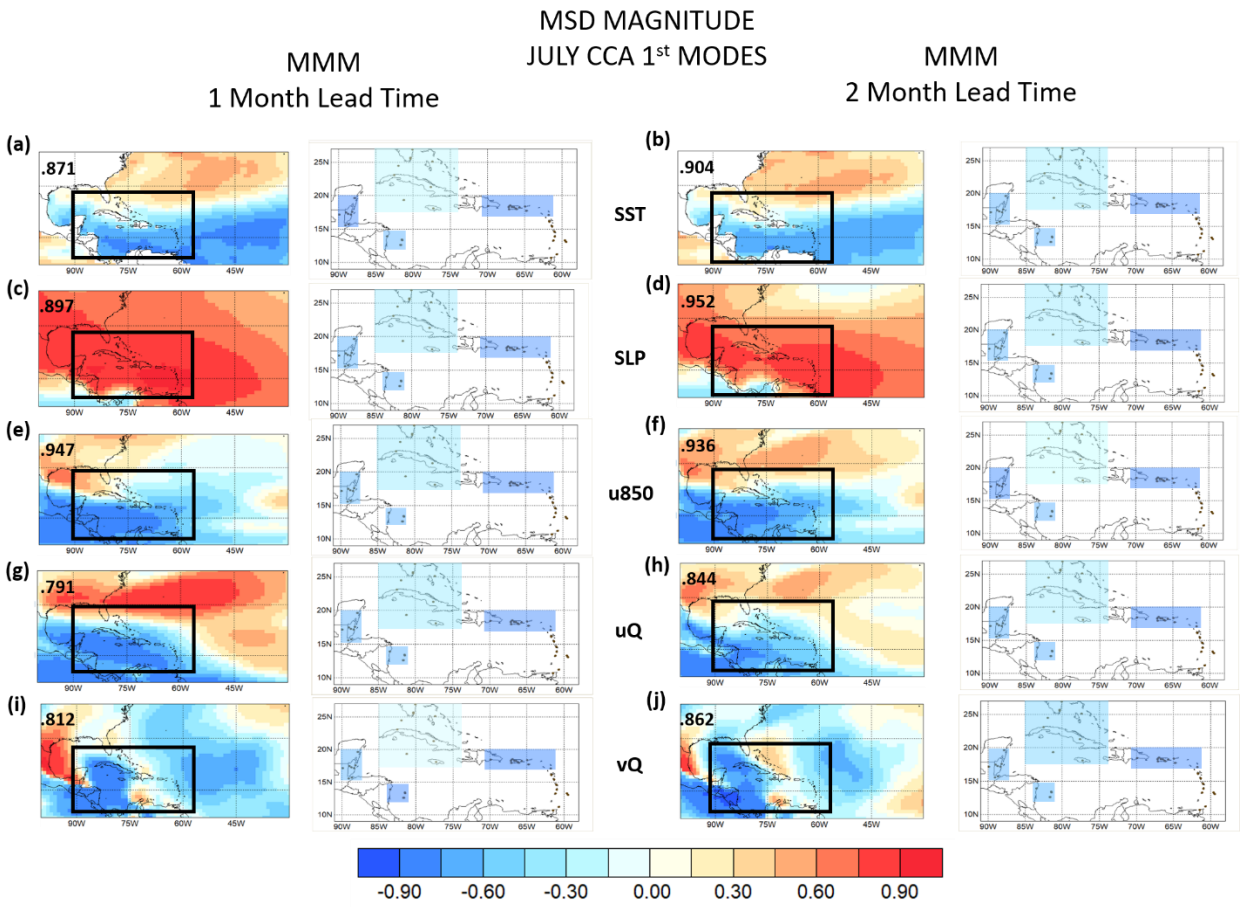

Figure 5.17: same as Figure 5.13 but for the predictand: frequency of wet LRS days, the month of August, and spatial loadings are over a larger domain.

Conclusions

Chapter 6: Conclusions

The Caribbean rainfall cycle is a vital factor in the socieoeconomic stability of the Caribbean basin. As this region is subject to changes to the rainfall cycle, many stakeholders (e.g., agriculture, health, water management) turn to their local weather or climate service for reliable forecasts of rainfall. The success of these forecasts is dependent on effectively characterizing the climate dynamics of the region. A comprehensive understanding of the seasonal climatology, variability, characteristics, and prediction of the Caribbean rainfall cycle on a sub-regional scale is produced in this thesis. The work is completed through observations, reanalysis, and global climate model outputs under a temporally and spatially fine lens.

First, an observational understanding of the seasonal climatology and variability of the Caribbean rainfall cycle is described (Chapter 2 and 3). In Chapters 2 and 3, daily rain gauge data from the CIMH and the NOAA GHCN is used to investigate regional variations of the Caribbean rainfall cycle at a higher temporal resolution than what was provided in previous studies. In Chapter 2, a principal component analysis using pentad climatologies of the rain gauge data and a total moisture budget analysis using ERA-Interim Reanalysis were conducted to distinguish sub-regional characteristics of the seasonal climatological rainfall cycle and delineate the role small-to-large scale dynamical processes influence the cycle. The main results found that mass convergence from the NASH, the Eastern Pacific ITCZ, and the Atlantic ITCZ, are the dominating drivers of precipitation in the Caribbean. The AWP and CLLJ modify the extent of moisture convergence from these three main facilitators. The interactions of these dynamical processes produce the seasonal components of the Caribbean rainfall cycle: the WDS, the ERS, the MSD, and the LRS. The analysis found five-sub-regions, each with a unique set of dynamical processes that produces its own climatological annual cycle. The expansion and contraction of the western

flank of NASH generates the subtle bimodal pattern of the precipitation annual cycle in the Northwestern Caribbean, Central Caribbean, and with the Eastern Pacific ITCZ the Western Caribbean. The analysis identifies the Atlantic ITCZ as the major source of precipitation for the central and southern Lesser Antilles, which is responsible for these areas' unimodal rainfall pattern. The Atlantic ITCZ is also the major source of precipitation in Trinidad and Tobago and the Guianas; the Atlantic ITCZ moves over this region twice every year which results in its bimodal rainfall pattern.

Chapter 3 then expands on the findings from Chapter 2 by investigating the interannual variability of the Caribbean rainfall cycle and associated dynamical mechanisms. Using the rain gauge data, the wettest and driest Caribbean-wide ERS and LRS years are selected in order to create spatial composites of SSTs and SLPs, and the mean flow component of the moisture budget. The main results showed that the ERS and LRS variability are impacted in distinctly different ways by two unique and largely independent, dominant large-scale phenomena: the NAO and the ENSO, respectively. Specifically, the interannual variability of the ERS is dominated by persistent anomalous SSTs due to a WES feedback, initiated by the preceding winter NAO. The interannual variability of the LRS is dominated by ENSO and an associated seasonal SLP see-saw between the Eastern Pacific and Caribbean basin/tropical Atlantic.

Chapters 2 and 3 illustrate the complexities of the Caribbean rainfall cycle and provides an explanation for why existing methodologies that calculate S2S characteristics, such as onset, demise and relative dry periods between rainfall seasons like the MSD, are unsuitable to use for a region with complex rainfall patterns like the Caribbean. Chapter 4 describes the calculation of sub-regional S2S characteristics in the Caribbean by proposing a novel and comprehensive method that deals with multifaceted rainfall patterns. This approach consists of three steps: (1) create the

annual cycle climatology of rainfall and classify its modality by the presence or absence of intermittent dry period(s), (2) identify seasonal windows of the rainfall cycle based on its climatological modality, (3) calculate yearly intermittent dry period characteristics and calculate temporal rainfall characteristics for each year using information on daily rainfall amount and the concurrent rate of change. The method may be utilized under a meteorological or agronomical lens and to delineate false meteorological and agronomical onsets and demises. When applying the method to calculate S2S characteristics in the Caribbean, meteorological onsets and demises that are calculated via each year's ERS and LRS mean thresholds effectively characterize the seasonal evolution of mean onsets and demises in the Caribbean. The year-to-year variability of MSD characteristics, and onsets and demises that are calculated by climatological ERS and LRS mean thresholds resemble the variability of seasonal rainfall totals in the Caribbean and are statistically significantly correlated with the identified dynamical processes that impact each seasonal component of the rainfall cycle.

With a complete observational understanding of the climate dynamics and rainfall patterns in the Caribbean (Chapters 2 and 3), and a methodology to calculate S2S Caribbean rainfall characteristics (Chapter 4), the seasonal prediction of relevant rainfall characteristics in the region is investigated. In Chapter 5, the forecast skill (Spearman Correlation and Relative Operating Characteristics) from statistical model outputs via canonical correlation analysis is assessed for station-averaged sub-regional frequency and intensity of the ERS and LRS wet days and magnitude of the MSD. Predictor fields are taken from the ERA-Interim and North American Multi-Model Ensemble (NMME). For the ERS, forecast skill of the frequency of wet days is generally higher than the intensity of wet days for most sub-regions of the Caribbean. For the LRS, forecast skill of the intensity of wet days is generally higher than the frequency of wet days for

most sub-regions of the Caribbean. Numerous predictors such as SLP, u850, UQ, and VQ show forecast skill that is as good as, if not better, than SSTs, which is the most-commonly used predictor to forecast seasonal rainfall characteristics. Generally, forecast skill can be achieved at least a month or two ahead of the target month for all ERS, MSD, and LRS characteristics. Furthermore, the Central and Eastern Caribbean regions have consistently significant skill for all CCA model configurations, whereas the Northwestern and Western Caribbean experiences varying levels of skill. The sub-regional differences and consistently significant skill across lead times up to at least two months can be attributed to changes in the dynamical mechanisms from the NAO-SST/SLP persistence signal and summertime onset of ENSO for the ERS and LRS, respectively. The spatial pattern of anomalies during the MSD bear resemblance to both the ERS and LRS spatial patterns.

These findings, in summary, produce a comprehensive illustration of the Caribbean hydrological cycle, an observational framework that has numerous implications and benefits for stakeholders in this region and the broader scientific community. Specific to the Caribbean, this thesis provides 1) a better understanding of the seasonal dynamical mechanisms and climate drivers that influence agronomically and economically-relevant rainfall characteristics in the Caribbean, and 2) various possible ways of improving current operational forecasting across the region. The main findings highlight the importance of utilizing temporally and spatially fine resolutions across datasets and analyses, and the significance of investigating the Caribbean across each sub-region and seasonal component of the rainfall cycle. A similar framework can be utilized for modeling. Simulating the observed climate dynamics and sub-regional Caribbean rainfall characteristics in models can be done to detect biases in models and consequently improve representation of the Earth climate system. The work from this thesis can be adapted into a modeling framework to investigate future changes to the Caribbean rainfall cycle and its dynamical

mechanisms. Caribbean rainfall does exhibit temporal variabilities that were not explored in this thesis, such as decadal, or multi-decadal. There are also some rainfall characteristics, like onset and demise, that only exhibit subseasonal variability. Prediction of the Caribbean rainfall cycle and the role dynamical mechanisms and climate drivers have in shaping this cycle may also be investigated under these time scales. There are other regions that are indirectly affected by the climate dynamics of the Caribbean (e.g., the Southeastern United States); therefore, the findings from this thesis could improve the understanding of teleconnections between the Caribbean climate system and other regional climate systems. Finally, a significant motivation for this thesis arose from an understanding of the negative impact inhabitants of the Caribbean experience from hydro-meteorological disasters and changes to the rainfall cycle. One can hope that these findings enhance decision making and resiliency from future climate, climate variability, hydro-meteorological disasters, and other weather/climate risks.

References

Agudelo, P., C. Hoyos, J. Curry, and P. Webster, 2011: Probabilistic discrimination between large-scale environments of intensifying and decaying African easterly waves. *Climate Dynamics*, **36**, 1379–1401.

Alfaro E. J., X. Chourio, Á. G. Muñoz, and S. J. Mason, 2017: Improved seasonal prediction skill of rainfall for the Primera season in Central America. *Int J Climatol.* https://doi.org/10.1002/JOC.5366

Alfaro, E. J., X. Chourio, Á. G. Muñoz, and S. J. Mason, 2018: Improved seasonal prediction skill of rainfall for the Primera season in Central America. *Int. J. Climatol.*, **38**, e255–e268, https://doi.org/10.1002/joc.5366.

Allen, T. L., B. E. Mapes, 2017: The late spring Caribbean rain-belt: climatology and dynamics. *Int J Climatol*., **37**, 4981–4993.

Amador, J. A., 1998: A climatic feature of the tropical Americas: the trade wind easterly jet. *Top Meteor. Oceanogr*., **5**(2), 1–13.

Amador, J. A., 2008: The intra-Americas sea low-level jet. *NY Acad. Sci.* **1146**(1), 153-188. doi: 10.1196/annals.1446.012

Amador, J. A., V. O. Magaña, and J. B. Perez, 2000: The low level jet and ´convective activity in the Caribbean. Preprints 24th Conference in Hurricanes and Tropical Meteorology. *American Meteorological* Society: Fort Lauderdale, FL; 114–115.

Anderson, T. G., K. J. Anchukaitis, D. Pons, and M. Taylor, 2019: Multiscale trends and precipitation extremes in the central american midsummer drought. *Environmental Research Letters* **14**, 124016.

Angeles, M. E., González J. E., N. D. Ramírez-Beltrán, C. A. Tepley, and D. E. Comarazaour, 2010: Origins of the Caribbean rainfall bimodal behavior. *J. Geophys. Res.,* **115**(D11), D11106.

Ayarzagüena, B., S. Ineson, N. J. Dunstone, M. P. Baldwin, and A. A. Scaife, 2018: Intraseasonal effects of El Niño-Southern oscillation on North Atlantic climate. *Journal of Climate*, **31**(21).

Bandyopadhyay, A., A. Bhadra, N.S. Raghuwanshi, and R. Singh, 2009: Temporal trends in estimates of reference evapotranspiration over India. *J. Hydrol.* Eng., **14** (5), 508-515.

Barnett, T., N. Graham, M. Cane, S. Zebiak, S. Dolan, J. O'Brien, and D. Legler, 1988: On the prediction of the El Nino of 1986-1987. *Science*, **241**(4862), 192–196. https://doi.org/10.1126/science.241.4862.192

Barnston, A. G., and R. E. Livezey, 1987: Classification, seasonality and persistence of low-frequency atmospheric circulation patterns. *Mon. Wea. Rev*., **115**, 1083–1126, https://doi.org/10.1175/1520-0493(1987)115<1083:CSAPOL>2.0.CO;2

Barnston, A. G., and M. K. Tippett, 2017: Do statistical pattern corrections improve seasonal climate predictions in the North American Multimodel Ensemble models? *Journal of Climate*, **30**, 8335– 8355. https://doi.org/10.1175/JCLI-D-17-0054.1.

Bellante, L. 2019: Double exposure, dispossession, and farmer resistance in the cornfields of Chiapas, Mexico, PhD thesis, The University of Arizona.

Berrisford, P., P. Kållberg, S. Kobayashi, D. Dee, S. Uppala, A. J. Simmons, P. Poli, and H. Sato 2011: Atmospheric conservation properties in ERA-Interim. *Q.J.R. Meteorol. Soc.,* **137**: 1381-1399.

Berrisford, P., and Coauthors, 2011: The ERA-Interim archive version 2.0. European Centre for Medium-Range Weather Forecasts ERA *Rep*. 1, 23.

Bjerknes, J. 1964: Atlantic air–sea interaction. *Adv Geophys*, **10**:1–82

Bladé, I., M. Newman, M. A. Alexander, and J. D. Scott, 2008: The late fall extratropical response to ENSO: Sensitivity to coupling and convection in the tropical west Pacific. *J. Climate*, **21**, 6101–6118, https://doi.org/10.1175/2008JCLI1612.1.

Bombardi, R. J. and L. M. V Carvalho, 2008: Variability of the monsoon regime over the Brazilian savanna: the present climate and projections for a 2xCO2 scenario using the MIROC model. *Revista Brasileira de Meteorologia*, **23**(1), 58–72.

Bombardi, R. J. and L. M. V Carvalho, 2009: IPCC global coupled model simulations of the South America monsoon system. Climate Dynamics, **33**(7–8), 893–916.

Bombardi, R. J., K.V. Pegion, J.L. Kinter, B.A. Cash, and J. M. Adams, 2017: Sub-seasonal predictability of the onset and demise of the rainy season over monsoonal regions. *Frontiers in Earth Science*, **5**. https://doi.org/10.3389/feart.2017.00014.

Bombardi, R. J., V. Moron, and J.S. Goodnight 2020: Detection, variability, and predictability of monsoon onset and withdrawal dates: A review. *Int. J. Climato.*, **40**:641–667.

Bovolo, C. I., R. Pereira, G. Parkin, C. Kilsby, and T. Wagner, 2012: Fine-scale regional climate patterns in the Guianas, tropical South America, based on observations and reanalysis data. *Int. J. Climatol*., **32**: 1665-1689

Boyard-Micheau, J., P. Camberlin, N. Philippon, and V. Moron, 2013: Regional-scale rainy season onset detection: A new approach based on multivariate analysis, *J. Clim.*, **26**(22), 8916– 8928.

Brubaker, K. L., A. Entekhabi, and P.S. Eagleson, 1993: Estimation of continental precipitation recycling. *J Clim* **6**(6), 1077–1089.

Burpee, R. W. 1972: The origin and structure of easterly waves in the lower troposphere of North Africa. *Journal of the Atmospheric Sciences* **29**, 77–90.

Cai, W., and Coauthors, 2014: Increasing frequency of extreme El Niño events due to greenhouse warming. *Nat. Climate Change*, **4**, 111–116, doi:https://doi.org/10.1038/nclimate2100.

Camberlin, P., and M. Diop, 2003: Application of daily rainfall principal component analysis to the assessment of the rainy season characteristics in Senegal. *Climate Res.*, **23**, 159–169.

Camberlin, P., V. Moron, R. E. Okoola, N. Philippon, and W. Gitau, 2009: Components of rainy seasons' variability in equatorial East Africa: Onset, cessation, rainfall frequency and intensity, *Theor. Appl. Climatol*., **98**(3–4), 237–249, doi:10.1007/s00704-009-0113-1.

Carlson, T. N., and J. M. Prospero, 1972: The large-scale movement of Saharan air outbreaks over the northern equatorial Atlantic. *Journal of Applied Meteorology*, **11**(2), 283–297.

Carvalho, L.M.V., C. Jones, F. Cannon, J. Norris, 2016: Intraseasonal-to-interannual variability of the Indian monsoon identified with the large-scale index for the Indian monsoon system (LIMS). *Journal of Climate*, **29**(8), 2941–2962.

Cayan, D.R. (1992): Latent and sensible heat flux anomalies over the Northern Oceans: Driving the sea surface temperature, *J. Phys. Ocean.* **22**, 859–881.

Chang, P., L. Ji, H. Li, 1997: A decadal climate variation in the tropical Atlantic Ocean from thermodynamic air–sea interactions. *Nature*, **385**, 516–518

Chen, A. A., and M. A. Taylor, 2002: Investigating the link between early season Caribbean rainfall and the El Niño +1 year. *International Journal of Climatology* **22**: 87–106

Chiang, J. C. H., and D. J. Vimont, 2004: Analogous meridional modes of atmosphere-ocean variability in the tropical Pacific and tropical Atlantic. *J. Climate*,**17**(21), 4143–4158.

Cook, B. I., and B. M. Buckley, 2009: Objective determination of monsoon season onset, withdrawal, and length. *Journal of Geophysical Research*, **114**(D23), D23109.

Cook, K. H., E. K. Vizy, 2010: Hydrodynamics of the Caribbean low level jet and its relationship to precipitation. *J Clim.* **23**:1477–1494.

Curtis, S, and D. W. Gamble. 2007: Regional variations of the Caribbean mid-summer drought. *Theor. Appl. Climatol.* **94**(1–2): 25–34.

Curtis, S., and S. Hastenrath, 1995: Forcing of anomalous sea surface temperature evolution in the tropical Atlantic during Pacific warm events. *J. Geophys. Res*., **100**(15), 835–15 847.

Czaja, A., P. Van der Vaart, P, and J. Marshall, 2002: Diagnostic study of the role of remote forcing in tropical Atlantic variability. *J. Clim*. **15**, 3280–3290.

Davis, R. E., B. P. Hayden, D. A. Gay, W. L. Phillips, and G. V. Jones, 1997: The North Atlantic subtropical anticyclone. *J. Climate,* **10**, 728–744.

Dee, D., and Coauthors, 2011: The ERA-Interim reanalysis: Configuration and performance of the data assimilation system. *Q. J. R. Meteorological Soc.* **137**, 553–597

Diaconescu, E. P., P. Gachon, J. Scinocca, and R. Laprise, 2015: Evaluation of daily precipitation statistics and monsoon onset/retreatover western Sahel in multiple data sets. *Climate Dynamics*, **45**(5–6), 1325–1354.

DiMego, G. J., L. F. Bosart, and G. W. Enderson, 1976: An examination of the frequency and mean conditions surrounding frontal incursions into the Gulf of Mexico and Caribbean Sea. *Mon. Wea. Rev.,***104**, 709–718.

Diop, M., 1996: A propos de la durée de la saison des pluies au Sénégal. *Sécheresse* **7**, 7–15

doi: 10.1175/1520-0442(2000)013<2845:COAOCV>2.0.CO;2

Dong, B., R. T. Sutton, and T. Woollings, 2011: Changes of interannual NAO variability in response to greenhouse gases forcing. *Clim. Dynam*., **37**, 1621–1641.

Drosdowsky, W., 1996: Variability of the Australian summer monsoon at Darwin: 1957–1992. *J. Climate*, **9**, 85–96.

Dunion, J. P., 2011: Rewriting the climatology of the tropical North Atlantic and Caribbean Sea atmosphere. *Journal of Climate*, **24**(3), 893–908.

Dunning, C.M., E.C.L. Black, and R.P. Allan, 2016: The onset and cessation of seasonal rainfall over Africa. *Journal of Geophysical Research-Atmospheres*, **121**(19), 11,405–11,424.

Durán-Quesada, A. M., M. Reboita, and L. Gimeno, 2012: Precipitation in tropical America and the associated sources of moisture: a short review, *Hydrological Sciences Journal*, **57**:4, 612-624.

Durán-Quesada, A. M., L. Gimeno, J. A. Amador, and R. Nieto, 2010: Moisture sources for Central America: Identification of moisture sources using a Lagrangian analysis technique, *J. Geophys. Res.*, **115**, D05103

Eichhorn A., J. Bader, 2017: Impact of tropical Atlantic sea-surface temperature biases on the simulated atmospheric circulation and precipitation over the Atlantic region: an ECHAM6 model study. *Clim Dyn* **49**, 2061–2075

Enfield, D. B., and E. J. Alfaro, 1999: The dependence of Caribbean rainfall on the interaction of the tropical Atlantic and Pacific Oceans, *J. Clim*., **12**, 2093–2103.

Esquivel, A., L. Llanos-Herrera, D. Agudelo, S. D. Prager, K. Fernandes, A. Rojas, J. J. Valencia, and J. Ramirez-Villegas, 2018: Predictability of seasonal precipitation across

major crop growing areas in Colombia. *Climate Serv.*, **12**, 36–47, https://doi.org/10.1016/j.cliser.2018.09.001.

Fasullo, J., and P. J. Webster, 2003: A hydrological definition of Indian monsoon onset and withdrawal. *Journal of Climate*, **16**(19), 3200–3211.

Fereday, D. R., J. R. Knight, A. A. Scaife, C. K. Folland, and A. Philipp 2008: Cluster analysis of North Atlantic–European circulation types and links with tropical Pacific sea surface temperatures. *J. Climate*, **21**, 3687–3703, https://doi.org/10.1175/2007JCLI1875.1

Fernandes K., A.G. Muñoz, J. Ramirez-Villegas, D. Agudelo, L. Llanos-Herrera, A. Esquivel, J. Rodriguez-Espinoza, and S.D. Prager 2020: Improving Seasonal precipitation forecasts for agriculture in the Orinoquía Region of Colombia. *Weather Forecast*., **35**. 437-449, 10.1175/WAF-D-19-0122.1

Fitzpatrick, R. G. J., C. L. Bain, P. Knippertz, J. H. Marsham, and D. J. Parker, 2015: The west African monsoon onset: a concise comparison of definitions. *Journal of Climate*, **28**(22), 8673–8694.

Food and Agriculture Organization of the United Nations (FAO), 2016: Situation report: dry corridor in Central America. FAO.

Gamble, D. W., D. B. Parnell, and S. Curtis, 2007: Spatial variability of the Caribbean mid-summer drought and relation to North Atlantic high circulation. *Int. J. Climatol.* **28**(3): 343–350.

García Serrano, J., C. Cassou, H. Douville, A. Giannini, and F. J. Doblas-Reyes, 2017: Revisiting the ENSO teleconnection to the tropical North Atlantic. Journal of Climate, **30**(17), 6945–6957.

García, S. R., and M. T. Kayano, 2009: Determination of the onset dates of the rainy season in Central Amazon with equatorially antisymmetric outgoing longwave radiation. Theoretical and Applied Climatology, **97**(3–4), 361–372.

García-Franco, J. L., S. Osprey, and L. J. Gray 2021: A wavelet transform method to determine monsoon onset and retreat from precipitation time-series. *Int. J. Climatol*. 1– 23. https://doi.org/10.1002/joc.7130

George, S. E., and M. A. Saunders 2001: North Atlantic Oscillation impact on tropical north Atlantic winter atmospheric variability, *Geophys. Res. Lett*., **28**, 1015–1018.

Giannini, A., J. C. H. Chiang, M. A. Cane, Y. Kushnir, and R. Seager, 2001b: The ENSO teleconnection to the tropical Atlantic Ocean: Contributions of the remote and local SSTs to rainfall variability in the tropical Americas. *J. Climate*, **14**, 4530–4544

Giannini, A., M. A. Cane, and Y. Kushnir 2001a: Interdecadal Changes in the ENSO Teleconnection to the Caribbean Region and the North Atlantic Oscillation, *J. Clim.*, **14**, 2867–2879

Giannini, A., Y. Kushnir, and M. A. Cane, 2000: Interannual variability of Caribbean rainfall, ENSO, and the Atlantic Ocean. *J. Climate*, **13**, 297–311.

Giannini, A., Y. Kushnir, and M. A. Cane, 2001c: Seasonality in the impact of ENSO and the North Atlantic High on Caribbean Rainfall, Phys. Chem. Earth (B), **28**(2), 143–147.

Goddard, L. and Coauthors, 2020: *Climate Services Ecosystems in times of COVID-19*. World Meteorological Organization. https://public.wmo.int/en/resources/bulletin/climate-services-ecosystems-times-of-covid-19.

Goddard, L., S. Mason, S. Zebiak, C. Ropelewski, R. Basher, and M. Cane, 2001: Current approaches to seasonal to interannual climate predictions. Int. J. Climatol., 21: 1111-1152. https://doi.org/10.1002/joc.636

Gouirand, I., M.R. Jury, and B. Sing, 2012: An analysis of low- and high-frequency summer climate variability around the Caribbean Antilles, *J. Clim.*, **25**, 3942-3952

Gouirand, I., V. Moron, and B. Sing, 2020: Seasonal atmospheric transitions in the Caribbean basin and Central America. *Clim. Dyn.* **55**, 1809–1828. https://doi.org/10.1007/s00382-020-05356-6

Gouirand, I., V. Moron, and B. Sing, 2020: Seasonal atmospheric transitions in the Caribbean basin and Central America. *Clim. Dyn.* **55**, 1809–1828. https://doi.org/10.1007/s00382-020-05356-6

Graham, N. E., J. Michaelsen, T. P. Barnett 1987a: An investigation of the El Niño-southern oscillation cycle with statistical models 1. Predictor Field Characteristics. *Journal of Geophysical Research*, **92**(C13), 14,251–14,270.

Graham, N. E., J. Michaelsen, T. P. Barnett, 1987b: An investigation of the El Niño-southern oscillation cycle with statistical models 2. Model Results. *Journal of Geophysical Research*, **92**(7), 14,271– 14,289.

Ham, Y. G., M. M. Rienecker, M. J. Suarez, and Coauthors, 2014: Decadal prediction skill in the GEOS-5 forecast system. *Clim. Dyn.*, **42,** 1–20 https://doi.org/10.1007/s00382-013-1858-x

Hamada, J. I., M. D. Yamanaka, J. Matsumoto, S. Fukao, P. A. Winarso, T. Sribimawati, 2002: Spatial and temporal variations of the rainy season over Indonesia and their link to ENSO. *J. of the Meteorological Society of Japan*, **80**: 285–310.

Hastenrath, S., 2002: The intertropical convergence zone of the eastern Pacific revisited, *Int. J. Climatol.*, **22**, 347–356

Hellin, J., R. Cox, and S. López-Ridaura, 2017: Maize diversity, market access, and poverty reduction in the Western Highlands of Guatemala. *Mt. Res. Dev*. **37**, 188–98

Henderson-Sellers, A., and P. J. Robinson, 1986: *Contemporary Climatology*. New York: Longman.

Hernández Ayala, J. J. 2019: Atmospheric teleconnections and their effects on the annual and seasonal rainfall climatology of Puerto Rico. *Theor. Appl. Climatol*. 2019: https://doi.org/10.1007/s00704-019-02774-3

Herrera E, V. Magaña, E. Caetano, 2015: Air–sea interactions and dynamical processes associated with the midsummer drought. *Int. J. Climatol.* **35**, 1569–1578

Herrera, D., and T. Ault, 2017: Insights from a new high-resolution drought atlas for the Caribbean spanning 1950 to 2016. *Journal of Climate*, **30**(19), 7801–7825. https://doi.org/10.1175/JCLI-D-16-0838.1

Herrera, E., V. Magaña, and E. Caetano, 2015: Air–sea interactions and dynamical processes associated with the midsummer drought. *Int. J. Climatol.*, **35:** 1569-1578.

Herrmann, S. M., and K. I. Mohr, 2011: A continental-scale classification of rainfall seasonality regimes in Africa based on gridded precipitation and land surface temperature products. *J. Appl. Meteor. Climatol*., **50**, 2504–2513.

Hidalgo, H. G., A. M. Durán-Quesada, J. A. Amador, E. J. Alfaro, 2015: The Caribbean Low-Level Jet, the Intertropical Convergence Zone and precipitation patterns in the Intra-Americas Sea: a proposed dynamical mechanism. *Geografiska Annaler*, Series A: *Physical Geography*, **97**, 41–59.

Hu Z. Z., A. Kumar, B. Huang, 2011: Persistent atmospheric and oceanic anomalies in the North Atlantic from summer 2009 to summer 2010. *J. Clim.* **24**(22), 5812–5830. https://doi.org/10.1175/2011JCLI4213.1

Huang, B., P. W. Thorne, and Coauthors, 2017: Extended Reconstructed Sea Surface Temperature version 5 (ERSSTv5), Upgrades, validations, and intercomparisons. *J. Climate*, doi: 10.1175/JCLI-D-16-0836.1

Huang, H.-P. R. Seager, Y. Kushnir (2005): The 1976/77 transition in precipitation over the Americas and the influence of tropical sea surface temperature. *Climate Dynamics*, **24**, pp. 721-740

Hurrell J. W., Y. Kushnir, M. Visbeck, G. Ottersen, (2003): An overview of the North Atlantic Oscillation. *AGU Geophysical Monograph*, **134**, 1–35

Ineson, S., and A. A. Scaife, 2009: The role of the stratosphere in the European climate response to El Niño. Nat. Geosci., **2**, 32–36, https://doi.org/10.1038/ngeo381.

Ingram, K.T., M.C. Roncoli, and P.H. Kirshen, 2002: Opportunities and constraints for farmers of west Africa to use seasonal precipitation forecasts with Burkina Faso as a case study. Agric. Syst.,**74**(3): 331–349.

Inoue, M., I. C. Handoh, and G. R. Bigg, 2002: Bimodal distribution of tropical cyclogenesis in the Caribbean: Characteristics and environmental factors. *J. Climate*, **15**, 2897–2905.

Jiménez-Esteve, B., and D. I. V. Domeisen, 2018: The tropospheric pathway of the ENSO–North Atlantic teleconnection. *J. Climate*, **31**, 4563–4584, https://doi.org/10.1175/JCLI-D-17-0716.1.

Jin, F. J., and A. Zangvil, 2010: Relationship between moisture budget components over the eastern Mediterranean, *Int. J. Climatol.*, **30**(5), 733–742,

Joseph, P.V., K. P. Sooraj, and C.K. Rajan, 2006: The summer monsoon onset process over South Asia and an objective method for the date of monsoon onset over Kerala. International Journal of Climatology, **26**(13), 1871–1893.

Jury, M., B. A. Malmgren, and A. Winter, (2007): Sub-regional precipitation climate of the Caribbean and relationships with ENSO and NAO. *J. of Geophys. Res.*, **112**, D16107.

Kalnay, E., and Coauthors, 1999: The NCEP/NCAR 40-year reanalysis project. *Bull. Am. Meteorol. Soc*. **77**, 437–472.

Kaplan, A., M. Cane, Y. Kushnir, A. Clement, M. Blumenthal, and B. Rajagopalan, 1998: Analyses of global sea surface temperature 1856-1991, *Journal of Geophysical Research*, **103**, 18,567-18,589

Kar S. C., N. Acharya, U. C. Mohanty, M. A. Kulkarni, 2011. Skill of mean of distribution of monthly rainfall over India during July using multi-model ensemble schemes. *Int. J. Clim.* DOI: 10.1002/joc.2334.

Karnauskas, K.B., R. Seager, A. Giannini, and A. J. Busalacchi, 2013: A simple mechanism for the climatological midsummer drought along the Pacific coast of Central America. Atmósfera 26:261–281. https://doi.org/10.1016/S0187-6236(13)71075-0

Kelley, C., N. Acharya, C. Montes, and T. J. Krupnik, Md. A. Mannan, and S. M. Q. Hassan, 2020: Exploring the predictability of within-season rainfall statistics of the Bangladesh monsoon using North American Multimodel Ensemble outputs. *Theor. Appl. Climatol.*, **141**, 495–508, https://doi.org/10.1007/s00704-020-03202-7.

King, M. P., I. Herceg-Bulic´, F. Kucharski, and N. Keenlyside, 2018: Interannual tropical Pacific sea surface temperature anomalies teleconnection to Northern Hemisphere

atmosphere in November. *Climate Dyn*., **50**, 1881–1899, https:// doi.org/10.1007/s00382-017-3727-5.

Kirtman, B. P., and Coauthors, 2014: The North American multimodel ensemble: Phase-1: Seasonal to interannual prediction; phase-2 toward developing intraseasonal prediction. *Bull. Amer. Meteor. Soc.*, **95**, 585–601,

Krishnamurthy, L., Á. G. Muñoz, G. A. Vecchi, R. Msadek, A. T. Wittenberg, B. Stern, R. Gudgel, and F. Zeng, 2018: Assessment of summer rainfall forecast skill in the Intra-Americas in GFDL high and low-resolution models. *Climate Dyn.*, **52**, 1–18, https://doi.org/10.1007/S00382-018-4234-Z.

Kushnir, Y., 1994: Interdecadal variations in North Atlantic sea surface temperature and associated atmospheric conditions. *J. Climate*, **7**, 141–157.

Kushnir, Y., W. A. Robinson, P. Chang, and A. W. Robertson, 2006: The physical basis for predicting Atlantic sector seasonal-to-interannual climate variability, *J. Clim*., **19**, 5949–5970.

Kushnir, Y., W. A. Robinson, I. Bladé, N. M. J. Hall, S. Peng, and R. Sutton, 2002: Atmospheric GCM response to extratropical SST anomalies: Synthesis and evaluation. *J. Climate*, **15,** 2233–2256.

Lewsey, C., G. Cid, and E. Kruse. 2004: Assessing Climate Change Impacts on Coastal Infrastructure in the Eastern Caribbean. *Marine Policy*, **28**:393-409.

Li, W. and R. Fu, 2004: Transition of the large-scale atmospheric and land surface conditions from the dry to the wet season over Amazonia as diagnosed by the ECMWF re-analysis. *Journal of Climate*, **17**(13), 2637–2651.

Liebmann, B., and J. A. Marengo, 2001: Interannual variability of the rainy season and rainfall in the Brazilian Amazon Basin. *Journal of Climate*, **14**(22), 4308–4318.

Liebmann, B., I. Bladé, G. N. Kiladis, L. M. V. Carvalho, G. B. Senay, D. Allured, S. Leroux, and C. Funk, 2012: Seasonality of African precipitation from 1996 to 2009. *Journal of Climate*, **25**(12), 4304–4322.

Liebmann, B., S. J. Camargo, A. Seth, J. A. Marengo, L. M. V. Carvalho, D. Allured, R. Fu, and C. S. Vera, 2007: Onset and end of the rainy season in South America in observations and the ECHAM 4.5 atmospheric general circulation model. *Journal of Climate*, **20**(10),2037–2050.

Lin, H., and Coauthors, 2019: The Canadian seasonal to interannual prediction system version 2. (CanSIPSv2).

Madden, R., and P. Julian, 1971: Detection of a 40–50 day oscillation in zonal wind in the tropical Pacific. *J. Atmos. Sci*., **28**, 702–708.

Magaña, V, J. A. Amador, and S. Medina, 1999: The midsummer drought over Mexico and Central America. *J. Clim.* **12**(6): 1577–1588.

Maldonado, T., E. Alfaro, and H. Hidalgo. 2018: Revision of the main drivers and variability of Central America Climate and seasonal forecast systems. *Revista de biologia tropical*. **66**.

Maldonado, T., A. Rutgersson, E. Alfaro, J. Amador, and B. Claremar 2016a: Interannual variability of the midsummer drought in Central America and the connection with sea surface temperatures. *Adv. Geosci.* **42**:35–50. https://doi.org/10.5194/adgeo-42-35-2016

Maldonado, T., E. Alfaro, A. Rutgersson, J. A. Amador, 2016b: The early rainy season in Central America: the role of the tropical North Atlantic SSTs. *Int J Climatol*. https://doi.org/10.1002/joc.4958

Maldonado, T., E. Alfaro, B. Fallas-López, and L. Alvarado, 2013: Seasonal prediction of extreme precipitation events and frequency of rainy days over Costa Rica, Central America, using Canonical Correlation Analysis. *Adv. Geosci.*, **33**, 41–52, https://doi.org/10.5194/adgeo-33-41-2013.

Malmgren, B. A., A. Winter, D. Chen, 1998: El Niño Southern oscillation and North Atlantic oscillation control of climate in Puerto Rico. *Journal of Climate* **12**(4): 977–985.

Mapes, B. E., P. Liu, and N. Buenning, 2005: Indian monsoon onset and the Americas midsummer drought: Out-of-equilibrium responses to smooth seasonal forcing. *J. Climate*, **18,** 1109–1115.

Marengo, J. A., B. Liebmann, V. E. Kousky, N. P. Filizola, and I. C. Wainer, 2001: Onset and End of the Rainy Season in the Brazilian Amazon Basin. *J. Climate*, **14**, 833–852, https://doi.org/10.1175/1520-0442(2001)014<0833:OAEOTR>2.0.CO;2.

Marshall, J., Y. Kushnir, D. Battisti, P. Chang A. Czaja, R. Dickson, J. Hurrell, M. McCartney, R. Saravanan, and M. Visbeck 2001: North Atlantic climate variability, phenomena, impacts and mechanisms. *Int. J. Climatol*., **21**, 1863-1898

Marteau R., V. Moron, N. Philippon, 2009: Spatial coherence of monsoon onset over Western and Central Sahel (1950–2000). *Journal of Climate*, **22**, 1313–1324.

Martin E. R., C. Schumacher, 2011: Modulation of Caribbean precipitation by the Madden–Julian oscillation. *J. Clim*. **24**:813–824

Martinez, C., L. Goddard L, Y. Kushnir, and M. Ting, 2019: Seasonal climatology and dynamical mechanisms of rainfall in the Caribbean. *Clim. Dyn.*, **53**, 825-846 https://doi.org/10.1007/s00382-019-04616-4

Martinez, C., Y. Kushnir, L. Goddard, and M. Ting, 2020: Interannual variability of the early and late-rainy seasons in the Caribbean. *Clim. Dyn.*, **55**, 1563–1583 https://doi.org/10.1007/s00382-020-05341-z

Martinez, C., Á. Muñoz, L. Goddard L, Y. Kushnir, and M. Ting, 2021a: An Adaptive Approach to Quantify Weather-within-Climate Rainfall Characteristics. *Clim. Dyn.* Under Review.

Martinez, C., Á. Muñoz, L. Goddard L, Y. Kushnir, and M. Ting, 2021b: Seasonal Prediction of the Caribbean Rainfall Cycle. *Clim. Serv.* Under Review

Mason S. J., and O. Baddour, 2008: Statistical Modelling. In: Troccoli A., Harrison M., Anderson D.L.T., Mason S.J. (eds) Seasonal Climate: Forecasting and Managing Risk. NATO Science Series, vol 82. Springer, Dordrecht. https://doi.org/10.1007/978-1-4020-6992-5_7

Mason, S., M. Tippet, L. Song, and Á. Muñoz, 2021: Climate Predictability Tool version 17.4.1. Columbia University Academic Commons. https://doi.org/10.7916/d8-z7qf-4z45

Mason, I. B., 2003: Binary events. *Forecast Verification: A Practitioner's Guide in Atmospheric Science,* I. T. Jolliffe and D. B. Stephenson, Eds., John Wiley, 37–76.

Mason, S. J. and D. B. Stephenson, 2008: *How do we know whether seasonal climate forecasts are any good?* Berlin: Springer.

Meehl, G. A., and Coauthors, 2012: Climate system response to external forcings and climate change projections in CCSM4. *J. Climate*,**25,** 3661–3683.

Misra, V., A. Bhardwaj, and A. Mishra, 2017: Local onset and demise of the Indian summer monsoon. *Climate Dynamics*, **51**, 1609–1622.

Misra, V., H. Li, M. Kozar, 2014: The precursors in the Intra-Americas Seas to seasonal climate variations over North America *J. Geophys. Res. (Oceans),* **119** (5), 2938-2948

Mitchell, T., and J. M. Wallace, 1992: The annual cycle in equatorial convection and sea surface temperature. *J. Climate*, **5**, 1140–1156.

Moron V., A. W. Robertson, L. Wang , 2019: Chapter 3 - weather within climate: sub-seasonal predictability of tropical daily rainfall characteristics. In: Robertson A. W., F. Vitart (Eds.), Sub-Seasonal to Seasonal Prediction. *Elsevier*, 47–64

Moron V., I. Gouirand, M. Taylor, 2015: Weather types across the Caribbean basin and their relationship with rainfall and sea-surface temperatures. *Clim. Dyn.* **47**: 601–621

Moron, V., A. W. Robertson, and R. Boer, 2009: Spatial coherence and seasonal predictability of monsoon onset over Indonesia. *Journal of Climate*, **22**(3), 840–850.

Moron, V., and A. W. Robertson 2014: Interannual variability in Indian summer monsoon rainfall onset date at local scale, Int. J. Climatol., **34**, 1050–1061.

Moron, V., and I. Gouirand, 2003: Seasonal modulation of the ENSO relationship with sea level pressure anomalies over the North Atlantic in October–March 1873–1996. *Int. J. Climatol*., **23**, 143–155, https://doi.org/10.1002/joc.868.

Mote, T. L., C. A. Ramseyer, and P.W. Miller, 2017: The Saharan Air Layer as an early rainfall season suppressant in the eastern Caribbean: The 2015 Puerto Rico drought. *Journal of Geophysical Research: Atmospheres,* **122**, 10,966–10,982.

Mugo R., J. Ininda, and R. Okoola, 2016: Inter Annual Variability of Onset and Cessation of the Long Rains in Kenya. *J. Meteorol. Relat. Sci*., **9**, 30–47.

Muñoz, Á. G, and Coauthors, 2015: 'Cross-time scale interactions and rainfall extreme events in southeastern South America for the austral summer. Part I: Potential predictors', *Journal of Climate*, **28**(19), 7894–7913. doi: 10.1175/JCLI-D-14-00693.1

Muñoz, Á. G., and Coauthors, 2016b: 'Cross-time scale interactions and rainfall extreme events in southeastern south america for the austral summer. Part II: Predictive skill', *Journal of Climate*, **29**(16), 5915–5934. doi: 10.1175/JCLI-D-15-0699.1.

Muñoz, Á. G., and Coauthors (2017), A Weather-Type-Based Cross-Time-Scale Diagnostic Framework for Coupled Circulation Models, *Journal of Climate*, **30**(22), 8951–8972. doi: 10.1175/JCLI-D-17-0115.1.

Muñoz, Á. G., X. Chourio, A. Rivière-Cinnamond, M. A. Diuk-Wasser, P. A. Kache, E. A. Mordecai, L. Harrington, and M. C. Thomson, 2020: AeDES: a next-generation monitoring and forecasting system for environmental suitability of Aedes-borne disease transmission. *Scientific reports*, **10**(1), 12640. https://doi.org/10.1038/s41598-020-69625-4

Muñoz, E., A. J. Busalacchi, S. Nigam, and A. Ruiz-Barradas, 2008: Winter and summer structure of the Caribbean low-level jet. *J. Clim*. **21**(6): 1260–1276.

Muñoz, Á. G., and Coauthors, 2010: An environmental watch system for the Andean countries: El Observatorio Andino. *Bull. Amer. Meteor. Soc.*, **91**, 1645–1652, https://doi.org/10.1175/2010BAMS2958.1.

Muñoz, Á. G., J. Díaz-Lobatón, X. Chourio, and M. Stock, 2016a: Seasonal prediction of lightning activity in North Western Venezuela: Large-scale versus local drivers. *Atmos. Res.*, **172–173**, 147–162,

Nandargi, S., and S.S. Mulye, 2012: Relationships between rainy days, mean daily intensity, and seasonal rainfall over the Koyna catchment during 1961–2005. J. Sci. World, https://doi.org/10.1100/2012/894313

National Oceanic and Atmospheric Administration (NOAA) the Climate Global Hazards, (2005): “State of the Climate Global Hazards” National Climatic Data Center, July 2005. Accessed from http://www.ncdc.noaa.gov/sotc/hazards/2005/jul.

National Oceanic and Atmospheric Administration (NOAA) the Climate Global Hazards, (2005): “State of the Climate Global Hazards” National Climatic Data Center, July 2005. Accessed from http://www.ncdc.noaa.gov/sotc/hazards/2005/jul.

Nicholls, N., J. L. McBride, and R. J. Ormerod, 1982: On predicting the onset of the Australian wet season at Darwin. Mon. Wea. Rev., 110, 14–17.

Nieto-Ferreira, R. and T. M. Rickenbach, 2011: Regionality of monsoon onset in South America: a three-stage conceptual model. International Journal of Climatology, **31**(9), 1309–1321.

Obarein, O. A. and A. C. Amanambu, 2019: Rainfall timing: variation, characteristics, coherence, and interrelationships in Nigeria. Theoretical and Applied Climatology, **137**, 2607–2621.

Office of Disaster Preparedness and Emergency Management (ODPEM)., (2010): "133 Communities Impacted by Nicole." *Jamaica Observer*, October 2, 2010. Accessed from http://www.jamaicaobserver.com/news/133-communities- impacted-by-Nicole

Office of Disaster Preparedness and Emergency Management (ODPEM)., (2010): "133 Communities Impacted by Nicole." *Jamaica Observer*, October 2, 2010. Accessed from http://www.jamaicaobserver.com/news/133-communities- impacted-by-Nicole

Pomposi, C., Y. Kushnir, and A. Giannini, (2015): Moisture budget analysis of SST-driven decadal Sahel precipitation variability in the twentieth century. *Clim. Dyn.* **44**, 3303–3321.

Pons D, M. J. Taylor, D. Griffin, E. J. Castellanos, and K. J. Anchukaitis, 2016: On the production of climate information in the high mountain forests of Guatemala *Ann. Am. Assoc. Geogr.* **107** 323–35

Poveda G, and O. J. Mesa, 1997: Feedbacks between hydrological processes in tropical South America and large-scale ocean–atmospheric phenomena. *J Climate* **10**, 2690–2702

Poveda G, and O. J. Mesa, 2000: On the existence of Lloro (the rainiest locality on Earth): enhanced ocean-land-atmosphere interaction by a low level jet. *Geophys. Res. Lett.* **27**(11): 1675–1678.

Recalde-Coronel, G. C., A. G. Barnston, and Á. G. Muñoz, 2014: Predictability of December–April rainfall in coastal and Andean Ecuador. *J. Appl. Meteor. Climatol.*, **53**, 1471–1493, https://doi.org/10.1175/JAMC-D-13-0133.1.

Reding P. J., 1992: The Central American Cold Surge: an observational analysis of the deep southward penetration of North America Cold Fronts. MSc. thesis, Department of Meteorology, Texas A&M University

Reynolds, R.W., N.A. Rayner, T.M. Smith, D.C. Stokes, and W. Wang, 2002: An Improved In Situ and Satellite SST Analysis for Climate. *J. Climate*, **15**, 1609-1625.

Robertson, A. W., V. Moron, and Y. Swarinoto, 2009: Seasonal predictability of daily rainfall statistics over Indramayu district, Indonesia. *Int. J. Climatol.*, **29**, 1449–1462, https://doi.org/10.1002/joc.1816.

Rodriguez-Vera, G., R. Romero-Centeno, C.L. Castro, and V.M. Castro, 2019: Coupled Interannual Variability of Wind and Sea Surface Temperature in the Caribbean Sea and the Gulf of Mexico. *J. Climate*, **32**, 4263–4280, https://doi.org/10.1175/JCLI-D-18-0573.1

Rudloff, W., 1981: World-Climates, with Tables of Climatic Data and Practical Suggestions. Wissenschaftliche Verlagsgesellschaft mbH Stuttgart.

Ryu, J.-H., K. Hayhoe, 2013: Understanding the sources of Caribbean precipitation biases in CMIP3 and CMIP5 simulations. *Clim. Dyn.* **42**(11–12), 3233–3252

Sáenz, F., and A. M. Durán-Quesada, 2015: A climatology of low level wind regimes over Central America using a weather type classification approach. *Front. Earth Sci*., **3**, 3-15.

Saha, S., and Coauthors, 2014: The NCEP Climate Forecast System version 2. *J. Climate*, 27, 2185–2208, https://doi.org/10.1175/JCLI-D-12-00823.1.

Schultz, D. M., W. E. Bracken, and L. F. Bosart, 1998: Planetary- and synoptic-scale signatures associated with Central American Cold Surges. *Mon. Wea. Rev*. **126**, 5–27

Seager, R, N. Henderson, 2013: Diagnostic computation of moisture budgets in the ERA-interim reanalysis with reference to analysis of CMIP-archived atmospheric model data. *J Cim* **26**:7876–7901

Seager, R., and Coauthors 2000: Causes of Atlantic Ocean climate variability between 1958 and 1998. *J. Clim.* **13**, 2845–2862.

Seager, R., N. Naik, G., and A. Vecchi, 2010: Thermodynamic and dynamic mechanisms for large-scale changes in the hydrological cycle in response to global warming. *J Clim* **23**:4651–4668

Seregina, L. S., A. H. Fink, R. van der Linden, N. A. Elagib, and J. G. Pinto, 2018: A new and flexible rainy season definition: validation for the greater horn of Africa and application to rainfall trends. *International Journal of Climatology*, **39**, 989–1012.

Servain, J. 1991: Simple climatic indices for the tropical Atlantic ocean and some applications, *J. Geophys. Res.*, **96**, 15,137 – 15,146, doi:10.1029/91JC01046.

Shaw, B. (1987): An analysis of the rainfall regimes on the coastal region of Guyana. *Journal of Climatology*, **7**, 291–302.

Silva, V., and V.E. Kousky 2012: The South American Monsoon System: Climatology and Variability, Modern Climatology, Dr Shih-Yu Wang (Ed.) ISBN: 978-953-51-0095-9, InTech.

Simpson, M.C., D. Scott, D. M. Harrison, and Coauthors 2010: Quantification and Magnitude of Losses and Damages Resulting from the Impacts of Climate Change: Modelling the Transformational Impacts and Costs of Sea Level Rise in the Caribbean (Full Document). Barbados, West Indies: United Nations Development Program (UNDP).

Smith, G. C., and Coauthors, 2018: Impact of coupling with an ice-ocean model on global medium-range NWP forecast skill. *Mon. Wea. Rev.*, **146**, 1157–1180, https://doi.org/10.1175/MWR-D-17-0157.1.

Spence, J. M., M. A. Taylor, and A. A. Chen. 2004: The Effect of Concurrent Seasurface Temperature Anomalies in the Tropical Pacific and Atlantic on Caribbean Rainfall. *International Journal of Climatology* **24**,1531-1541, doi: 10.1002/joc.1068.

Stephenson, T. S., and Coauthors, (2014): Changes in extreme temperature and precipitation in the Caribbean region, 1961–2010. *Int. J. Climatol.* **34**, 2957–2971, doi: 10.1002/joc.3889.

Taylor M. A., and E. J. Alfaro, 2005: Central America and the Caribbean, Climate of. In: Oliver J.E. (eds) *Encyclopedia of World Climatology*. Encyclopedia of Earth Sciences Series. Springer, Dordrecht

Taylor, M. A., D. B. Enfield, and A. A. Chen, 2002: Influence of the tropical Atlantic versus the tropical Pacific on Caribbean rainfall. *J. Geophys. Res*., **93**, 485–498,

Taylor, M. A., T. S. Stephenson, A. Chen., and K. Stephenson, 2012: CLIMATE CHANGE AND THE CARIBBEAN: REVIEW AND RESPONSE. *Caribbean Studies,* **40**(2), 169-200.

Tippett M. K., DelSole T., Mason S. J., Barnston A.G., 2008: Regression-based methods for finding coupled patterns. *Journal of Climate,* **21**:4384–4398. doi: 10.1175/2008JCLI2150.1

Tippett, M. K., and A. G. Barnston, 2008: Skill of multimodel ENSO probability forecasts. *Mon. Wea. Rev.*.

Toma V, and P. Webster, 2010: Oscillations of the intertropical convergence zone and the genesis of easterly waves. part I: diagnostics and theory. *Climate Dynamics* **34**: 587–604, doi:10.1007/s00382-009-0584-x.

Torres-Valcárcel A. R., 2018: Teleconnections between ENSO and rainfall and drought in Puerto Rico. *Int J Climatol* **38**, 1190–1204. https:// doi.org/10.1002/joc.5444

Trenberth, K. E., and C. J. Guillemot, 1995: Evaluation of the global atmospheric moisture budget as seen from analysis. *J Clim* **8**:2255–2272

United Nations Office for the Coordination of Humanitarian 880 Affairs (OCHA), (2015): Drought in Central America in 2015 (as for October 6, 2015).

United Nations Office for the Coordination of Humanitarian 880 Affairs (OCHA), (2016): Humanitarian bulletin: Haiti, June 2016, **62**, 5-6.

United Nations Office for the Coordination of Humanitarian 880 Affairs (OCHA), (2015): Drought in Central America in 2015 (as for October 6, 2015).

United Nations Office for the Coordination of Humanitarian 880 Affairs (OCHA), (2016): Humanitarian bulletin: Haiti, June 2016, **62**, 5-6.

Vaughan, C., S. Dessai, 2014: Climate services for society: origins, institutional arrangements, and design elements for an evaluation framework. WIREs. *Clim. Change,* **5**, 587–603. https://doi.org/10.1002/wcc.290

Verbist, K., A. W. Robertson, W. M. Cornelis, and D. Gabriels, 2010: Seasonal predictability of daily rainfall characteristics in central northern Chile for dry-land management. *J. Appl. Meteor. Climatol.*, **49**, 1938–1955, https://doi.org/10.1175/2010JAMC2372.1.

Waliser, D. E., C. Gautier, 1993: A satellite-derived climatology of the ITCZ. *J. Climat.,* **6**, 2162–2174

Wang B., and LinHo, 2002: Rainy season of the Asian–Pacific summer monsoon. *Journal of Climate*, **15**(4), 386–398.

Wang, B., 1994: Climatic regimes of tropical convection and rainfall. *J. Climate,* **7**, 1109–1118.

Wang, C, D. B. Enfield, S.-K. Lee, and C. W. Landsea, 2006: Influences of the Atlantic warm pool on Western Hemisphere summer rainfall and Atlantic hurricanes. *J. Climate*, **19**, 3011– 3028

Wang, C. S.-K. Lee, and D. B. Enfield, 2008: Climate response to anomalously large and small Atlantic warm pools during the summer. *J. Climate*, **21**, 2437–2450.

Wang, C., 2001: Atlantic climate variability and its associated atmospheric circulation cells. *J Clim* **15**(13), 1516–1536

Wang, C., 2007: Variability of the Caribbean low-level jet and its relations to climate. *Climate Dyn*., **29**, 411–422

Wang, C., and S.-K. Lee, 2007: Atlantic warm pool, Caribbean low-level jet, and their potential impact on Atlantic hurricanes. *Geophys Res Lett* **34**:L02703

Wang, C., D. B. Enfield, 2001: The tropical Western Hemisphere warm pool. *Geophysical Research Letters*, **28**, 1635–1638.

Wang, C., S.-K. Lee, and C. Mechoso, 2010: Interhemispheric influence of the Atlantic Warm Pool on the Southeastern Pacific. *J.Clim.* **23**:404–418.

Webster, P.J. and S. Yang, (1992) Monsoon and Enso: selectively interactive systems. Quarterly *Journal of the Royal Meteorological Society*, **118**(507), 877–926.

Weisberg, R. H., 1996: On the evolution of SST over the PACS region, *Abstracts of 76 th AMS Annual Meeting*, Atlanta, Georgia, *Amer. Meteor. Soc.*, 378.

Wilks, D. S. 2011: *Statistical methods in the atmospheric sciences*. Academic Press.

World Meteorological Organization, "Guidance on Operational Practices for Objective Seasonal Forecasting". Kumar, A., J.P. Ceron, C. Coelho, L. Ferranti, R. Graham, D. Jones, W. Merryfield, Á.G. Muñoz, S. Pai, E. Rodríguez. Guidance prepared under the auspices of the World Meteorological Organization Commission for Climatology (CCI) and Commission for Basic Systems (CBS). 2020

Wu, R., and B. Kirtman, 2011: Caribbean Sea rainfall variability during the rainy season and relationship to the equatorial Pacific and tropical Atlantic SST. *Clim. Dyn.* **37**(7–8), 1533–1550

Xie, S. P., and S. G. H. Philander, 1994: A coupled ocean–atmosphere model of relevance to the ITCZ in the eastern Pacific. *Tellus A*, **46**(4), 340–350.

Zhang, C. 2001: Double ITCZs, *J. Geophys. Res.*, **106**(D11), 11785–11792.